

Benchmarks of Fuel Burnup and Material Activation Computational Tools Against Experimental Data for Research Reactors

Results of a Coordinated Research Project



IAEA

International Atomic Energy Agency

BENCHMARKS OF FUEL BURNUP
AND MATERIAL ACTIVATION
COMPUTATIONAL TOOLS AGAINST
EXPERIMENTAL DATA FOR
RESEARCH REACTORS

The following States are Members of the International Atomic Energy Agency:

AFGHANISTAN	GEORGIA	OMAN
ALBANIA	GERMANY	PAKISTAN
ALGERIA	GHANA	PALAU
ANGOLA	GREECE	PANAMA
ANTIGUA AND BARBUDA	GRENADA	PAPUA NEW GUINEA
ARGENTINA	GUATEMALA	PARAGUAY
ARMENIA	GUYANA	PERU
AUSTRALIA	HAITI	PHILIPPINES
AUSTRIA	HOLY SEE	POLAND
AZERBAIJAN	HONDURAS	PORTUGAL
BAHAMAS	HUNGARY	QATAR
BAHRAIN	ICELAND	REPUBLIC OF MOLDOVA
BANGLADESH	INDIA	ROMANIA
BARBADOS	INDONESIA	RUSSIAN FEDERATION
BELARUS	IRAN, ISLAMIC REPUBLIC OF	RWANDA
BELGIUM	IRAQ	SAINT LUCIA
BELIZE	IRELAND	SAINT VINCENT AND
BENIN	ISRAEL	THE GRENADINES
BOLIVIA, PLURINATIONAL STATE OF	ITALY	SAMOA
BOSNIA AND HERZEGOVINA	JAMAICA	SAN MARINO
BOTSWANA	JAPAN	SAUDI ARABIA
BRAZIL	JORDAN	SENEGAL
BRUNEI DARUSSALAM	KAZAKHSTAN	SERBIA
BULGARIA	KENYA	SEYCHELLES
BURKINA FASO	KOREA, REPUBLIC OF	SIERRA LEONE
BURUNDI	KUWAIT	SINGAPORE
CAMBODIA	KYRGYZSTAN	SLOVAKIA
CAMEROON	LAO PEOPLE'S DEMOCRATIC REPUBLIC	SLOVENIA
CANADA	LATVIA	SOUTH AFRICA
CENTRAL AFRICAN REPUBLIC	LEBANON	SPAIN
CHAD	LESOTHO	SRI LANKA
CHILE	LIBERIA	SUDAN
CHINA	LIBYA	SWEDEN
COLOMBIA	LIECHTENSTEIN	SWITZERLAND
COMOROS	LITHUANIA	SYRIAN ARAB REPUBLIC
CONGO	LUXEMBOURG	TAJIKISTAN
COSTA RICA	MADAGASCAR	THAILAND
CÔTE D'IVOIRE	MALAWI	TOGO
CROATIA	MALAYSIA	TRINIDAD AND TOBAGO
CUBA	MALI	TUNISIA
CYPRUS	MALTA	TURKEY
CZECH REPUBLIC	MARSHALL ISLANDS	TURKMENISTAN
DEMOCRATIC REPUBLIC OF THE CONGO	MAURITANIA	UGANDA
DENMARK	MAURITIUS	UKRAINE
DJIBOUTI	MEXICO	UNITED ARAB EMIRATES
DOMINICA	MONACO	UNITED KINGDOM OF GREAT BRITAIN AND
DOMINICAN REPUBLIC	MONGOLIA	NORTHERN IRELAND
ECUADOR	MONTENEGRO	UNITED REPUBLIC OF TANZANIA
EGYPT	MOROCCO	UNITED STATES OF AMERICA
EL SALVADOR	MOZAMBIQUE	URUGUAY
ERITREA	MYANMAR	UZBEKISTAN
ESTONIA	NAMIBIA	VANUATU
ESWATINI	NEPAL	VENEZUELA, BOLIVARIAN REPUBLIC OF
ETHIOPIA	NETHERLANDS	VIET NAM
FIJI	NEW ZEALAND	YEMEN
FINLAND	NICARAGUA	ZAMBIA
FRANCE	NIGER	ZIMBABWE
GABON	NIGERIA	
	NORTH MACEDONIA	
	NORWAY	

The Agency's Statute was approved on 23 October 1956 by the Conference on the Statute of the IAEA held at United Nations Headquarters, New York; it entered into force on 29 July 1957. The Headquarters of the Agency are situated in Vienna. Its principal objective is "to accelerate and enlarge the contribution of atomic energy to peace, health and prosperity throughout the world".

IAEA-TECDOC-1992

BENCHMARKS OF FUEL BURNUP
AND MATERIAL ACTIVATION
COMPUTATIONAL TOOLS AGAINST
EXPERIMENTAL DATA FOR
RESEARCH REACTORS

RESULTS OF A COORDINATED RESEARCH PROJECT

INTERNATIONAL ATOMIC ENERGY AGENCY
VIENNA, 2022

COPYRIGHT NOTICE

All IAEA scientific and technical publications are protected by the terms of the Universal Copyright Convention as adopted in 1952 (Berne) and as revised in 1972 (Paris). The copyright has since been extended by the World Intellectual Property Organization (Geneva) to include electronic and virtual intellectual property. Permission to use whole or parts of texts contained in IAEA publications in printed or electronic form must be obtained and is usually subject to royalty agreements. Proposals for non-commercial reproductions and translations are welcomed and considered on a case-by-case basis. Enquiries should be addressed to the IAEA Publishing Section at:

Marketing and Sales Unit, Publishing Section
International Atomic Energy Agency
Vienna International Centre
PO Box 100
1400 Vienna, Austria
fax: +43 1 26007 22529
tel.: +43 1 2600 22417
email: sales.publications@iaea.org
www.iaea.org/publications

For further information on this publication, please contact:

Physics Section
International Atomic Energy Agency
Vienna International Centre
PO Box 100
1400 Vienna, Austria
Email: Official.Mail@iaea.org

© IAEA, 2022
Printed by the IAEA in Austria
March 2022

IAEA Library Cataloguing in Publication Data

Names: International Atomic Energy Agency.
Title: Benchmarks of fuel burnup and material activation computational tools against experimental data for research reactors / International Atomic Energy Agency.
Description: Vienna : International Atomic Energy Agency, 2022. | Series: IAEA TECDOC series, ISSN 1011-4289 ; no. 1992 | Includes bibliographical references.
Identifiers: IAEAL 22-01481 | ISBN 978-92-0-101322-4 (paperback : alk. paper) | ISBN 978-92-0-101222-7 (pdf)
Subjects: LCSH: Nuclear reactors — Research. | Nuclear reactors — Computer programs. | Fuel burnup (Nuclear engineering).

FOREWORD

Research reactors are powerful tools that contribute to scientific and technological progress worldwide. They are used for research and development in a wide variety of fields, in capacity building in nuclear science and technology, to produce radioisotopes crucial for medical and industrial applications, to support the development of national nuclear infrastructure, and in many other research and industrial applications for the benefit of humanity.

The design, safe operation and effective utilization of research reactors and their associated experiments rely on understanding the complex physical processes that take place during steady state operation and transient conditions. One crucial contribution to this understanding is the detailed simulation of those processes using dedicated computer codes. Recent progress in computer technology and numerical methods has led to a substantial increase in the sophistication and complexity of the computer codes used. While correct application of these methods and codes is essential, their validation is not an easy task. As a number of the validated codes used for research reactors were originally developed for nuclear power plant simulations, there was a recognized need to perform a similar qualification process in the case of research reactors by benchmarking the codes against experimental data.

To address this need, the IAEA designed and implemented a coordinated research project (CRP) entitled Benchmarks of Computational Tools against Experimental Data on Fuel Burnup and Material Activation for Utilization, Operation and Safety Analysis of Research Reactors, carried out from 2015 to 2020. The overall objective of this CRP was to increase the knowledge and expertise of Member States in the area of numerical analysis to improve the design, operation, utilization, safety and decommissioning of research reactors. The CRP included research groups from 11 Member States and focused on developing benchmark specifications (reactor descriptions and experimental data) for nine research reactors with different designs, power levels and utilization activities. Multicycle core depletion analysis benchmarks focused on fuel depletion for the core lifetime and included experiments that cannot be accurately modelled without performing neutronics and burnup analysis for multiple cycles of reactor operation. Target or sample activation, fuelled experiments and structural material activation benchmarks focused on the irradiation of in-core and ex-core samples, experiments involving fissile materials and activation of structural materials. In this category, the focus was on experiments that can be modelled without analysis of full core depletion. The IAEA published the benchmark specifications in Technical Reports Series No. 480, Research Reactor Benchmarking Database: Facility Specification and Experimental Data.

The present publication provides information on, and compiles the results of, the benchmark studies performed by the CRP participants for all benchmark specifications developed during the CRP, as well as conclusions on the benchmark specifications, modelling approaches, computer codes used and user effects. The supplementary files available on-line present individual benchmark contributions

The IAEA is grateful to the experts who contributed their input and expertise, provided data, shared the results of their calculations and agreed to make these results available to the research reactor community through this publication. The IAEA officers responsible for this publication were N. Pessoa Barradas of the Division of Physical and Chemical Sciences, F. Marshall and S. Geupel of the Division of Nuclear Fuel Cycle and Waste Technology, and A.M. Shokr and F. Naseer of the Division of Nuclear Installation Safety.

EDITORIAL NOTE

This publication has been prepared from the original material as submitted by the contributors and has not been edited by the editorial staff of the IAEA. The views expressed remain the responsibility of the contributors and do not necessarily represent the views of the IAEA or its Member States.

Neither the IAEA nor its Member States assume any responsibility for consequences which may arise from the use of this publication. This publication does not address questions of responsibility, legal or otherwise, for acts or omissions on the part of any person.

The use of particular designations of countries or territories does not imply any judgement by the publisher, the IAEA, as to the legal status of such countries or territories, of their authorities and institutions or of the delimitation of their boundaries.

The mention of names of specific companies or products (whether or not indicated as registered) does not imply any intention to infringe proprietary rights, nor should it be construed as an endorsement or recommendation on the part of the IAEA.

The authors are responsible for having obtained the necessary permission for the IAEA to reproduce, translate or use material from sources already protected by copyrights.

The IAEA has no responsibility for the persistence or accuracy of URLs for external or third party Internet web sites referred to in this publication and does not guarantee that any content on such web sites is, or will remain, accurate or appropriate.

CONTENTS

1. INTRODUCTION	1
1.1. BACKGROUND	1
1.2. OBJECTIVE	2
1.3. SCOPE.....	2
1.4. STRUCTURE	3
2. COORDINATED RESEARCH PROJECT DESCRIPTION	4
2.1. PROJECT SUMMARY	4
2.2. PROJECT MEETING SUMMARY	4
2.2.1. First Research Coordination Meeting: 13–17 April 2015	4
2.2.2. Second Research Coordination Meeting: 18–22 July 2016.....	5
2.2.3. First Technical Meeting: 16–20 October 2017	6
2.2.4. Consultancy Meeting to Prepare for the Third RCM: 26–28 June 2018	8
2.2.5. Third Research Coordination Meeting: 27–31 August 2018.....	8
2.2.6. Consultancy Meeting: 6–9 May 2019.....	9
2.2.7. Second Technical Meeting: 2–6 September 2019	9
2.2.8. Consultancy Meeting: 19–21 February 2020.....	11
2.2.9. Consultancy Meeting: 17–19 November 2020	12
2.3. SUMMARY OF THE CALCULATIONS	12
3. RESULTS OF THE COORDINATED RESEARCH PROJECT	16
3.1. BENCHMARKED FACILITIES AND EXPERIMENTS	16
3.1.1. Open Pool Australian Lightwater (OPAL) Reactor.....	16
3.1.2. Atominstut (ATI) TRIGA Mark II	17
3.1.3. Experimental Training Research Reactor 2 (ETRR-2).....	18
3.1.4. Institute for Nuclear Research TRIGA 14 MW	19
3.1.5. IPEN/MB-01 Critical Facility.....	19
3.1.6. Israel Research Reactor 1 (IRR-1).....	20
3.1.7. Jožef Stefan Institute (JSI) TRIGA Mark II	21
3.1.8. South African Fundamental Atomic Research Installation 1 (SAFARI-1)..	21
3.1.9. Thai Research Reactor-1/Modification 1 (TRR-1/M1)	22
3.2. DESCRIPTION OF CODES	23
3.2.1. AUS98	23
3.2.2. COCONEUT.....	24
3.2.3. CONDOR, CITVAP	24
3.2.4. DARWIN2	26
3.2.5. DRAGON	26
3.2.6. MUTZAV	27
3.2.7. FISPACT-II	27
3.2.8. SCALE/KENO-VI.....	27
3.2.9. MCNP	28
3.2.10. MERCURE6	29
3.2.11. ORIGEN	29
3.2.12. OSCAR-5.....	29
3.2.13. SCALE 6.1/ORIGEN	31
3.2.14. Serpent 2	31
3.2.15. TRIPOLI-4.....	32
3.2.16. MVP.....	32

3.2.17. WIMS-D4	32
3.3. NUCLEAR DATA LIBRARIES	32
3.4. SUMMARY OF RESULTS	33
3.4.1. ANSTO-1	33
3.4.2. ANSTO-2	34
3.4.3. ANSTO-3	34
3.4.4. ATI-1	35
3.4.5. ATI-2	35
3.4.6. EAEA-1	36
3.4.7. EAEA-2	36
3.4.8. INR-1	37
3.4.9. IPEN-1	37
3.4.10. IRR-1	38
3.4.11. JSI-1	38
3.4.12. NECSA-1	39
3.4.13. NECSA-2	39
3.4.14. TINT	40
4. CONCLUSIONS	41
4.1. THE BENCHMARK SPECIFICATIONS	41
4.2. CODES, MODELLING APPROACHES AND RESULTS.....	41
4.3. SUMMARY AND OUTLOOK.....	45
REFERENCES.....	47
ANNEX I BENCHMARK CONSOLIDATED RESULTS AGAINST EXPERIMENTAL DATA FROM ANSTO-1	50
ANNEX II BENCHMARK CONSOLIDATED RESULTS AGAINST EXPERIMENTAL DATA FROM ANSTO-2	80
ANNEX III BENCHMARK CONSOLIDATED RESULTS AGAINST EXPERIMENTAL DATA FROM ANSTO-3	97
ANNEX IV BENCHMARK CONSOLIDATED RESULTS AGAINST EXPERIMENTAL DATA FROM ATI-1	107
ANNEX V BENCHMARK CONSOLIDATED RESULTS AGAINST EXPERIMENTAL DATA FROM ATI-2	126
ANNEX VI BENCHMARK CONSOLIDATED RESULTS AGAINST EXPERIMENTAL DATA FROM EAEA-1	137
ANNEX VII BENCHMARK CONSOLIDATED RESULTS AGAINST EXPERIMENTAL DATA FROM EAEA-2	147
ANNEX VIII BENCHMARK CONSOLIDATED RESULTS AGAINST EXPERIMENTAL DATA FROM INR-1	156
ANNEX IX BENCHMARK CONSOLIDATED RESULTS AGAINST EXPERIMENTAL DATA FROM IPEN/MB-01	168
ANNEX X BENCHMARK CONSOLIDATED RESULTS AGAINST EXPERIMENTAL DATA FROM IRR-1	180
ANNEX XI BENCHMARK CONSOLIDATED RESULTS AGAINST EXPERIMENTAL DATA FROM JSI-1.....	194

ANNEX XII BENCHMARK CONSOLIDATED RESULTS AGAINST EXPERIMENTAL DATA FROM NECSA-1 AND NECSA-2	226
ANNEX XIII BENCHMARK CONSOLIDATED RESULTS AGAINST EXPERIMENTAL DATA FROM TINT	249
ANNEX XIV SUPPLEMENTARY FILES	259
LIST OF ABBREVIATIONS	262
CONTRIBUTORS TO DRAFTING AND REVIEW	264

1. INTRODUCTION

1.1. BACKGROUND

With progress in computer technology and numerical methods, capabilities of computer codes have been substantially enhanced. The recent development of these methods and tools allows for better simulation of the complex processes taking place during the routine operation and transient conditions of research reactors. Correct application of these methods and codes is essential to improve design, operation, utilization and safety aspects of research reactors and associated experiments. However, the validation process of computational codes is not an easy task. In order to demonstrate the quality of these computational methods and codes, it is important to benchmark them against experimental data as part of assessing the validity of their application to the design, operation and safety analysis of research reactors.

The International Atomic Energy Agency (IAEA) implemented from 2015 to 2020 the Coordinated Research Project (CRP) T12029 titled “Benchmarks of Computational Tools against Experimental Data on Fuel Burnup and Material Activation for Utilization, Operation and Safety Analysis of Research Reactors”, with the participation of 12 institutions from 12 Member States. This CRP, jointly conducted by the Division of Nuclear Installation Safety (NSNI), the Division of Nuclear Fuel Cycle and Waste Technology (NEFW) and the Division of Nuclear Applications (NAPC), follows CRP J71013 “Innovative Methods in Research Reactor Analysis: Benchmark against Experimental Data on Neutronics and Thermohydraulic Computational Methods and Tools for Operation and Safety Analysis of Research Reactors”, completed in 2013 with the development of nine benchmarks for nine research reactors, in the areas of neutronic and thermohydraulics. The benchmark specifications developed under CRP J71013 were published in the First Edition of Technical Reports Series No. 480 [1], and the CRP results were published in IAEA-TECDOC-1879, Benchmarking against Experimental Data of Neutronics and Thermohydraulic Computational Methods and Tools for Operation and Safety Analysis of Research Reactors [2].

CRP T12029 was dedicated to collecting available experimental data and using these data to benchmark the computational methods and tools used for fuel burnup, in particular in multicycle depletion analysis and material and target activation calculations for research reactors. The overall objective of this CRP was to encourage international cooperation and foster exchange of information and expertise in numerical analysis to improve the design, operation, utilization, safety and decommissioning of research reactors.

The expected research outputs of the CRP were:

- A database of experimental results, measurements and associated facility specifications that is useful for supporting verification and validation of burnup and activation computer codes;
- A publication on the final results of the benchmark studies comparing the experimental and computational results on fuel burnup and material activation, including identification of open issues for future research and development activities.

Twelve Member States participated in the CRP and the primary focus was on gathering experimental data. The benchmarks were presented in the areas of:

- Multicycle core depletion analysis;
- Target and/or sample activation and fuelled experiments (including activation of structural components).

A secondary focus was to perform a set of preliminary analyses to assess the quality of the benchmark data and extract initial conclusions on the applicability of codes to the various experiments.

1.2. OBJECTIVE

The main objective of this publication is to provide the final consolidated results of the benchmark studies performed by the participants of the CRP. From the consolidated results of various codes applied to a range of research reactor experimental cases in the broad areas of multicycle core burnup and of materials activation, it is possible to gauge the applicability and relevance of the codes and methodologies to the benchmarks considered, to note the sensitivity of calculation results to modelling choices, to collate a set of modelling approaches and results in support of training and qualification of code users and analysts and to support validation activities of codes, methodologies and models for the areas that are addressed in this CRP.

This publication is intended as an information resource for use by operating organizations, researchers, regulatory bodies, reactor designers, technical support organizations and other parties involved with research reactors and interested in benchmarking the computer codes and models they use for research reactor operation, safety analysis and utilization.

1.3. SCOPE

The scope of this publication is the benchmark analysis performed by the CRP participants for the benchmark specifications introduced in the Second Edition of Technical Reports Series No. 480 [3], which cover fuel burnup and material activation for research reactors with a range of designs, power levels, operating regimes and experiment facilities.

The results obtained by the individual CRP participants are consolidated for each benchmark, in order to draw specific conclusions on the benchmark specifications, modelling approaches, and, when possible, user effects and computer codes used.

The publication also describes the activities during the CRP and the conclusions of the CRP participants based on the analysis results.

In the context of this publication, the term ‘benchmark specification’ means the well defined facility geometric and material specification, as well as associated experiments with corresponding measured and operational data as described in Ref. [3]. Uncertainties in specification and data were limited, therefore the scope of this CRP could not include the performance of comprehensive uncertainty analyses.

1.4. STRUCTURE

Following this introductory section, Section 2 gives an overview of the CRP and summarizes the work completed during the CRP related to modelling fuel burnup and material activation for research reactors using computer codes. Section 3 contains three sub-sections that cover benchmark and experiments, short descriptions of the codes used by the CRP participants and a summary of results obtained by the participants for each benchmark specification. Section 4 presents the conclusions of the CRP, as well as specific conclusions on the benchmark specifications, modelling approaches, user effects, computer codes used and results. This publication also includes 13 annexes which provide the consolidated results of the benchmarks performed by the CRP participants for each benchmark specification. A 14th annex, given in the supplementary files on-line, includes detailed individual reports of each CRP participant on the codes and models used, as well as the results obtained for their benchmark analyses.

The structure described above is intended to provide the user with a logical progression from the general information and conclusions in Sections 2, 3 and 4, to the more detailed information and calculation results in the Annexes and individual reports of the CRP participants (contained in the supplementary files on-line). This gives the user of this publication a means to identify the work done during the CRP that may be relevant to their particular needs and then obtain the detailed results and conclusions most applicable to their own benchmark activities.

2. COORDINATED RESEARCH PROJECT DESCRIPTION

2.1. PROJECT SUMMARY

Experimental data were obtained across a wide range of research reactor designs for fuel burnup calculations and material/target activation and utilization and operation of research reactors. The data were compiled into the benchmark specifications that consist of facility specifications, experiment descriptions and corresponding experiment data for nine research reactors. Each benchmark specification was provided in a way to serve as a stand-alone resource to perform independent benchmarks by interested institutions worldwide.

Overall, the specific research outcomes of the CRP were:

- Transferred knowledge through increased cooperation in the area of research reactor numerical analysis, including design, safety analysis, operation and utilization;
- Enhanced capabilities of the CRP participants in performing numerical analysis and safety assessment of research reactors;
- Collected sets of experimental data of fuel burnup and material/target activation and compiled a comprehensive database useful for performing benchmarks;
- Benchmarked fuel burnup and material/target activation computer codes against experimental results;
- Proposals for future research and development activities involving research reactors and the codes used in modelling them.

2.2. PROJECT MEETING SUMMARY

This section summarizes the meetings that were held in the course of the CRP. Overall, there were three research coordination meetings (RCMs), two technical meetings and four consultancy meetings.

2.2.1. First research coordination meeting: 13–17 April 2015

The focus of the first meeting was to assess the range and quality of data available for benchmarking. The preference was for a range of benchmarks for a range of different reactor designs to maximize the impact of the results from the CRP. Considerations took into account the outcomes and learnings from the previous CRP J71013. The participants made brief presentations of their respective facilities. The meeting considered the outcomes and lessons learned from the previous CRP J71013. The first year of CRP T12029 would focus on the gathering of experimental data from potential data providers.

Discussions focussed on development of prescribed formats with regard to data submissions. The neutronic full-core submissions would follow the neutronic template set during CRP J71013 and a draft template was developed for the material/target activation data. It was decided that the data would be submitted in stages in order to verify and improve the quality of the submissions.

A detailed plan for the first year was agreed on, including the standard and detail of the benchmark data to be submitted.

2.2.1.1. Summary of the meeting conclusions and suggestions

The first RCM resulted in the following conclusions and suggestions:

- The CRP is valuable to the research reactor community and will significantly support validation of burnup and activation codes used for research reactor analysis.
- The participants highlighted the importance of the inclusion of appropriate uncertainties in the provided experimental data.
- Submissions were received spanning the entire intended range of activation analysis, fuelled experiments, multicycle analysis, gamma ray spectrometry and mass spectrometry.
- It was confirmed that the expected primary outputs will be achieved from this CRP. The first will be a database of relevant experimental data and facility descriptions. The second will be a publication describing the results of the code benchmarking activities.
- For the multicycle depletion experiments, the focus would be on experimental data which contains fuel burnup measurements. For material/target activation, the focus would be on data useable for benchmarking activation codes. Data providers are also encouraged to supply neutronic specifications for those who intend to calculate flux/spectrum independently.
- To ensure the quality of the planned benchmark database, submissions of experimental benchmark documentation are planned in a phased approach: submissions of facility and experimental description; submission of experimental data; submission of own preliminary analysis; and independent CRP member review.
- To ensure consistency with the publications that resulted from CRP J71013 [1, 2], the data should follow prescribed submission templates. A basic design of each template was prepared, which was then finalized by the data providers during the first year of the CRP.

2.2.2. Second research coordination meeting: 18–22 July 2016

An overview of the CRP and the intended focus was provided at the beginning of the meeting. It was noted that the CRP is progressing well and that effective communication had been ongoing between data providers, reviewers and the IAEA.

During the meeting, the participants updated the action matrix, which captures the various submissions and the intended overall action plan to improve the data submission. A matrix of participants' contributions versus the benchmarks was created to check that each benchmark will have a sufficient number of participants performing calculations and that all participants had committed to perform calculations for at least the minimum number of benchmarks.

The format of the data submissions and individual country reports were discussed. Moreover, it was agreed that the individual country reports will include all benchmark cases analysed by the country.

2.2.2.1. Summary of the meeting conclusions and suggestions

The second RCM resulted in the following conclusions and suggestions:

- It was again confirmed that the two primary outputs foreseen for this CRP were achievable. The first would be a database of relevant experimental data and facility descriptions. The second would be a publication describing the results of the code benchmarking activities.
- The current state of submissions by data providers, as captured in the action matrix, represented an acceptable quantity of benchmarks and covered a wide range of research reactors and experiments.
- Coverage of participants per benchmark was assessed and adjusted to ensure that at least three participants were committed to provide contributions for each benchmark. Further, it was confirmed that all participants adhered to the minimum of two contributions per participant. Contributions were categorized as ‘commitment’ or ‘tentative’, and a detailed schedule for submission of each individual country report was agreed with participants.
- Data providers would act as consolidators of the individual benchmark contributions for their respective benchmark(s). Data providers would develop result submission spreadsheet templates for each experimental case for use by the benchmark participants. Furthermore, data providers were automatically benchmark participants for their own data submissions.
- The structure and content of the individual country benchmark reports, consolidator reports and overall CRP results publication were developed and agreed upon in the form of tables of contents for these reports. Benchmark participants and consolidators were advised to follow these tables of contents to the greatest extent practicable.
- It was agreed that no publication would include the information produced for the CRP without appropriate consultation with the relevant CRP participants and the IAEA, and in some cases publications might not be allowed due to contractual and copyright issues.
- The process for additional CRP partners to join as observers and their privileges for accessing and using the benchmark specifications and experimental data was also discussed and agreed. They would have full access to data like other participants.

2.2.3. First technical meeting: 16–20 October 2017

The meeting had participants from both the CRP and from organizations not involved in the CRP. Its objective was to review the results of the benchmarks that had been completed to the date of the meeting. Participants were asked to present recent results from research reactor modelling benchmarking studies, including best practices and lessons learned, and to provide feedback on the results presented by the other participants. In addition, participants were also asked to provide feedback on the status of the benchmark specifications and data.

In the beginning of the meeting, the participants summarized the progress and importance of the CRP. In particular, the challenges facing the research reactor community with spent fuel management and decommissioning were emphasized, as well as the role computational tools play in addressing these challenges.

During the meeting, the participants were divided into groups according to their primary interest regarding the benchmark, and then into three groups according to their primary function of code

developer, reactor analyst, or reactor experimentalist. Each group presented challenges and lessons learned while performing the benchmarks.

It was noted that some benchmark specifications available under the CRP were identified as of particularly high standard and, as such, could be useful for code verification and validation. The value of considering propagation of statistical uncertainties through burnup was discussed and it was agreed that it will be considered in the case of Monte Carlo depletion analysis. Furthermore, it was acknowledged that a better and more frequent interaction between code developers and code users would be beneficial to both parties.

2.2.3.1. Summary of the meeting conclusions and suggestions

The first technical meeting resulted in the following conclusions and suggestions:

- Work performed by attending institutions in the area of multicycle depletion and activation was presented. This included both progress against the set milestones of the ongoing CRP related to this meeting, as well as analyses conducted by various organizations not participating in the CRP.
- It was noted that some benchmark specifications available under the CRP have been identified as of particularly high standard and as such could be useful for code verification and validation. The meeting also noted that additional data were available from organizations not participating in the CRP, and considered whether this could be included in the CRP. Some benchmark specifications that were being developed under the CRP were incomplete and it was considered valuable to finalize these and make them available to the research reactor community through the planned IAEA publication of the benchmark specifications.
- It was suggested that research reactor analysts performing multicycle depletion analysis use the benchmark specifications available in Technical Reports Series No. 480 to first perform “snapshot neutronic analysis” to gain some confidence in the model prior to performing the complete multicycle depletion analysis.
- The use and strengths and weaknesses of various Monte Carlo and deterministic methods to perform multicycle depletion analysis was discussed. Although Monte Carlo methods are very accurate in principle, some adaptation is often needed prior to applying these to cycle-follow type analysis. The IAEA publications resulting from the CRP would provide the experience of the participants in making such adaptations.
- The value of considering the propagation of statistical uncertainties through burnup was discussed and it was agreed that it would be considered in the case of Monte Carlo depletion analysis, in particular when finer spatial zones are employed for depletion tracking.
- It was considered valuable to establish a coordinated research activity for propagation of uncertainties (from various sources such as cross-sections, material specifications and dimensions) for calculations relevant to research reactor analysis. Such international benchmark activities were ongoing for light water reactors and high temperature reactors at the time of the meeting, and could add value to the toolsets for research reactor analysis.
- It was noted that there are several approaches to licensing research reactors and their experiment facilities, and these approaches involve computational analysis and simulations to different degrees. However, in all cases, codes and models related to safety need verification and validation following a defined process. At the date of the meeting, widely different methods were in use and there was a need to develop standard

guidelines for supporting Member States in establishing requirements for verification and validation of software and models for safety analysis in research reactor applications.

- It was observed that code validation would benefit from data from experiments designed and commissioned specifically for validation, rather than trying to fit existing data to this purpose.
- In the case of benchmark specifications where the neutron spectrum is available, it needs to be clearly stated how it was obtained and if any spectrum adjustment was applied, including the details.
- It was noted that better and more frequent interaction between code developers and code users would be beneficial to both parties, and organizing activities to facilitate these interactions could be considered.
- From the different operating regimes and associated analysis conducted on these benchmarks, it was observed that quite accurate burnup estimations (and plutonium production) can be obtained based on accumulated irradiation history, without detailed core-follow modelling. However, for the prediction of reactivity and flux distribution modelling, more detail in the reactor operational data is needed.
- The definition and relevance of approaches in considering fuel burnup limits were discussed as an important driving factor for the meeting and associated CRP, as the accuracy of codes employed for such purposes would influence the margins employed when designing fuel management and core loading strategies.

2.2.4. Consultancy meeting to prepare for the third RCM: 26–28 June 2018

The consultancy meeting was planned to prepare for the third and final RCM. During the meeting, the benchmark participation matrix was updated according to the current status of each participant. It was noted that some of the tentative commitments by the participants would have to be removed due to limitation in the resources available.

On the final day of the consultancy meeting, the participation matrix and the action matrix were finalized by the participants who attended the meeting. Issues that corresponded to countries not present were to be addressed by email. The major problems concerned data that had not been submitted, which had to be ready for use by the participant countries by the beginning of the third RCM at the latest. If the countries were not able to provide usable results, the action matrix was to be updated

Moreover, it was discussed that, for the end of the CRP, there should be a better in-depth understanding of the differences in the calculated results caused by user defined variables and the applicability of in-house and commercial codes corresponding to the operation and specification of the research reactor.

2.2.5. Third research coordination meeting: 27–31 August 2018

The participants recognized the need to extract as much benefit from the benchmark, as well as the value of the benchmark set as a training and development tool.

During the meeting, the action matrix was updated and modified to display the final commitments of each participant during the final phase of the project. A deadline of October 2018 was chosen for the participants that have submitted results to the consolidators, to finalize any simulation and provide their individual report. Furthermore, a deadline of January 2019 was chosen for the participants who had not submitted any results to the consolidators.

The last day of the meeting began with a discussion on the conclusions of the meeting. Possible future activities, which include technical meetings and regional workshops, were also discussed. The following items summarize the conclusions of the meeting:

- The CRP provided a valuable opportunity for experts in the research reactor community to come together and share experience, lessons learned and practises applied at their facilities.
- The established database of experiments and associated analyses represented a comprehensive collection of research reactor benchmarks that benefit the research reactor community.
- Good agreement was observed between submitted results for the benchmarks. Specifically, most benchmarks exhibited reasonable agreement between calculational and experimental results and the overall trends in calculated parameters were similar.
- It was suggested that a set of tables be developed that summarize the benchmark exercises in terms of areas of application, nature of experiment, physical phenomena and modelling methodologies used. This will assist end users in navigating the CRP report depending on their specific need or interest.
- The benchmarks and results collected in the CRP have a clear benefit to the research reactor community. From the various contributors, there were examples of how the set was used to support code validation as a training and skills development tool, as well as motivation for developers to improve their computational methods and tools.

2.2.6. Consultancy meeting: 6–9 May 2019

The consultancy meeting was planned to review the consolidated reports and determine if there were any incomplete items that CRP participants needed to submit, and to compile the existing text and consolidated reports into a first draft of the planned publication, intended as the main output of the CRP.

During the meeting, the publication was discussed by the participants and the existing text was reviewed. Several sections were revised during the meeting, based on the group discussions and conclusions. A common approach for the different sections of the text was defined, including a general approach for the structure of each section, for the presentation of codes, concepts, information in tables and figures and terminology. The publishing requirements at the IAEA, including copyright, text originality, figures and tables were presented.

It was noted that a number of consolidated reports remained incomplete at the time of the meeting. An action plan was developed for completing outstanding sections of the publication, including drafting and editing.

2.2.7. Second technical meeting: 2–6 September 2019

The meeting had participants from both the CRP and from organizations not involved in the CRP. Its objectives were: (a) to review the results of the computational benchmarking activities completed under the CRP; (b) to enable Member States not participating in the CRP to share their research reactor computational benchmark information with others in the research reactor community; and (c) to share knowledge related to best practices and lessons learned. In addition, participants were also asked to provide feedback on the status of the benchmark specifications and data.

The first three days were dedicated to presentations and discussions by the participants on their experiences with and results of benchmarks of computational tools and methods.

During the meeting, the participants were divided into three working groups according to their primary interest in multicycle burnup, material activation analysis, or CRP participation. One group was tasked with reviewing the CRP publication input and progress, while the other two groups dealt with the identification of good practices identified, knowledge gaps and proposals for future work. Each working group developed a presentation to document their discussions, including successes, challenges and lessons learned performing benchmarks, and these were discussed in a final plenary session.

2.2.7.1. Summary of the meeting conclusions and suggestions

The second technical meeting resulted in the following conclusions and suggestions:

- The set of benchmarks and associated analysis results included in the recently completed CRP on fuel burnup and activation was presented and discussed. The participants agreed that the body of knowledge captured during the CRP provides a valuable resource to the research reactor community and that the IAEA could consider allowing further expansion of this set in the future.
- It was noted that many of the participants used the benchmarks as a basis for validating codes and methods, as well as the training and development of users. Participants agreed that the benchmark set is a valuable asset to assist in qualifying their calculational procedures and the people performing the analysis.
- Many participants commented that some of the experimental procedures described in the benchmark specifications could be used to improve and standardize the way they perform similar measurements at their home institutions.
- More focused training activities using the material developed in this and the previous CRP could be considered. These activities are envisaged to go beyond basic usage and cover the entire modelling process, from engineering and physics input data processing, to interpretation of the final results. The regional workshops were identified as a good vehicle for such training activities.
- All participants agreed that there are sufficient calculational tools available to perform fuel depletion and material activation analysis. However, many participants expressed concern that access to these codes are being restricted and that alternatives need to be explored. It was noted that many alternatives with similar capabilities do exist. It was agreed that the various mechanisms on how Member States can gain access to codes needed to be captured in the meeting report or the final CRP report.
- Many participants used customized, internally developed systems to combine various analysis codes. It was agreed that, as with input data, code output standards would be developed to better facilitate the transfer of data between codes.
- It was agreed by all meeting participants that what constitutes accurate or correct results depends on the application. A consensus was reached that the benchmarks developed in the CRP, together with the results collected, provide a reasonable indication of the level of accuracy that can be achieved when calculating various parameters related to material activation and fuel depletion, using current, state of the art codes and methods.
- A number of meeting participants, who did not participate in the CRP, indicated that they have relevant experimental data available. These participants were encouraged to share their data for the benefit of the entire research reactor community.
- All participants agreed that the effect of input uncertainties on final results is not well quantified. It could be valuable to establish a coordinated research activity for

propagation of uncertainties (from various sources such as cross-sections, material specifications and engineering specifications) for calculations relevant to research reactor analysis. Within this context, it would be valuable to receive input from the nuclear power reactor community, as the benchmarking of uncertainty propagation is well established there.

- It was noted that a number of routine safety calculations related to material activation, such as heating calculations of irradiation targets and the long-term activation of structural material, were not well covered by the available benchmarks. It would be valuable if additional experimental data could be sought in these areas.
- The benchmarks developed in this CRP (T12029) and the previous one (J71013) provide an excellent opportunity to monitor how calculational tools and methods develop over time to meet the various challenges posed by the problems that were in the scope of these benchmarks. Some coordinated effort to revisit these problems from time to time might be a useful vehicle to communicate how tools are evolving and the current state of the art in research reactor modelling. In particular, modern approaches such as uncertainty propagation for reactor analysis, or coupled neutronic and thermohydraulic safety analysis, are recent trends which could effectively be evaluated on some of the already defined benchmark problems.

2.2.8. Consultancy meeting: 19–21 February 2020

Before the meeting, all the consolidated reports were reviewed by one of the CRP participants, Ms Marcella Cagnazzo, with particular focus on consistency in technical content, presentation, concepts and terminology. During the meeting, the consolidated reports were revised, paying particular attention to the review comments. The main text of the CRP report was also reviewed, and the participants made comments on issues still to be addressed. Comments pertaining to the whole report and related to the actions necessary to complete the report were compiled and an action plan was developed. The development of the Second Edition of Technical Reports Series No. 480 [3] was discussed.

The following comments on the publication and proposed actions to complete it were made:

- Each contributor was prompted to submit electronic copies of the following documents to the IAEA and grant the IAEA permission to use the information provided in that documents:
 - Facility description;
 - Benchmark definition, with measurement data;
 - Country report;
 - Consolidated report.
- The facility description and benchmark definitions would either be added to a revision of Ref. [1] or included in the supplementary files to be electronically available from the IAEA publication web site. The participants supported a revision of the existing publication.
- Benchmark consolidators need to respond to review comments and provide suggested conclusions.
- The publication would be subject to technical editorial review by the IAEA. Consistency in referencing the country reports, in nomenclature of benchmark and facility name, codes and data libraries was to be ensured. The terminology on error, uncertainty, deviation and difference was to be clarified by the participants.

- The Conclusions Section was deemed to need still extensive work, including:
 - All consolidators were to review their reports, considering the information desired to be in the overall conclusions, and enhance the individual benchmark conclusions. In order to mention a conclusion in the main body of the CRP report, it needs to be mentioned in the consolidated reports.
 - Section 4.1 of the Conclusions on benchmark specifications was to be revised. Each benchmark owner or consolidator would determine the information to include in the proposed table. A preamble discussion of the table, including considerations on the “introductory” or “advanced” characteristics of each benchmark or other criteria, would be developed.
 - Section 4.2 of the Conclusions would merge the information for modelling and for the codes, but it was decided that extensive discussion of user effects was not appropriate, because the project was not structured to collect user effects. All consolidators would fill out the table in Section 4.2.

2.2.9. Consultancy meeting: 17–19 November 2020

Prior to the consultancy meeting, the IAEA project officers followed up on the action plan developed in the consultancy meeting held in February 2020. This led to a revised draft of the publication, including consolidated reports revised by the consolidators according to the review previously made. This draft was shared in advance with all the meeting participants. During the meeting, the participants reviewed and revised the publication and provided further input, leading to a revised draft. The participants devised an action plan to finalize the publication, which was then strictly adhered to.

2.3. SUMMARY OF THE CALCULATIONS

Table 1 presents a summary of the calculations made for the benchmarks addressed in the CRP. The criteria for selection were, besides being within the scope of the CRP, that the experimental data and facility specification were of sufficiently high quality and that each benchmark specification was modelled by at least two CRP participants.

The table lists, for each benchmark, the name and country of the originating research reactor, the name of the benchmark experiment, the type of benchmark and the contributors to each benchmark. For each contributor, the table also includes the number of different methodologies used for the given benchmark and the codes used. The number of individual calculations made for each benchmark varied from two calculations made by two participants up to nine calculations made by four participants. In total, 53 calculations were made, addressing 14 benchmarks originating from nine research reactors.

A wealth of different computer codes was used. The participant from Argentina submitted 14 calculations for eight different benchmarks, for which it used CITVAP [4], CONDOR [5, 6], FISPACT-II [7, 8], KENO-VI [9], MCNP5 [10, 11], ORIGEN [12], SCALE6.1 [13] and Serpent 2 [14, 15]. The participant from Australia submitted five calculations for four different benchmarks, for which it used AUS98 [16], CITVAP, CONDOR, MCNP5, ORIGEN and Serpent 2. The participant from Austria submitted two calculations for two different benchmarks, for which it used MCNP6 [10, 17] and Serpent 2. The participant from Brazil submitted one calculation for one benchmark, for which it used MCNP5 and SCALE. The participant from Egypt submitted three calculations for two different benchmarks, for which it

used CITVAP, MCNPX v2.7 [10, 18], WIMS [19, 20] and an analytical model. The participant from France submitted six calculations for two different benchmarks, for which it used COCONEUT2.0 [21], DARWIN2 [22], MCNP6, MERCURE6 [23, 24] and TRIPOLI-4 [25, 26]. The participant from Israel submitted two calculations for two different benchmarks, for which it used DRAGON4.1.0 [27], MCNP4b [10, 28] and MUTZAV [29]. The participant from Romania submitted two calculations for two different benchmarks, for which it used MCNPX v2.6 [10, 30] and MCNPX v2.7. The participant from Slovenia submitted four calculations for four different benchmarks, for which it used FISPACT-II and MCNP6. The participant from South Africa submitted 11 calculations for seven different benchmarks, for which it used MCNP6, OSCAR-5 [31], MGRAC (the OSCAR nodal diffusion core solver) [31] and Serpent 2. The participant from Thailand submitted three calculations for two different benchmarks, for which it used MCNPX v2.6 and MVP [32]. Some of these codes, such as MCNP, have sub-versions within the main version quoted. These were not considered sufficiently significant to be mentioned in Table 1, but are given in the consolidated reports for each benchmark (see Annexes I to XIII). A description of each code is given in Section 3.2.

The type of experiment addressed by each benchmark is also noted in Table 1. In all cases, these fall in the two main categories of (i) multicycle core and fuel element burnup and (ii) activation of irradiated materials, which were in the scope of the CRP.

TABLE 1. SUMMARY OF BENCHMARK CALCULATIONS

Reactor	Country	Benchmark name	Type of experiment	Benchmark contributors	Number of methodologies	Codes used
OPAL	Australia	ANSTO-1	Multicycle burnup	Argentina	2	CONDOR, CITVAP, Serpent 2
				Australia	2	CONDOR, CITVAP, Serpent 2
		France	3	COONEUT2.0, TRIPOLI-4		
		South Africa	2	OSCAR-5/MGRAC, OSCAR-5/Serpent 2		
ANSTO-2	Structure material activation	Argentina	1	MCNP5, SCALE6.1/ORIGEN		
		Australia	1	MCNP5, ORIGEN		
		France	3	MCNP6, DARWIN2, TRIPOLI-4, MERCURE6		
ANSTO-3	Activation of Au grains	Argentina	2	CONDOR, CITVAP		
		Australia	1	MCNP5		
		Slovenia	1	MCNP6		
ATI	Austria	ATI-1	Fuel element burnup	Austria	1	MCNP6, Serpent 2
				Thailand	1	MCNPX v2.6
ATI-2	Austria	ATI-2	Foil activation	Austria	1	Serpent 2
				Slovenia	1	MCNP6, FISPACT-II
ETR-2	Egypt	EAEA-1	Fuel element burnup	Argentina	1	CONDOR, CITVAP
				Egypt	1	WIMS, CITVAP
		Israel	1	MUTZAV/MCNP4b, DRAGON4.1.0		
		South Africa	2	OSCAR-5/MGRAC, OSCAR-5/Serpent 2		
EAEA-2	Austria	$^{134}\text{Cs}/^{137}\text{Cs}$ activity ratio in LEU targets	Australia	1	AUS98	
			Egypt	2	Analytical model, MCNPX v2.7	
TRIGA 14 MW	Romania	INR-1	Fuel element burnup	Romania	1	MCNPX v2.6
				South Africa	2	OSCAR-5/MGRAC, OSCAR-5/Serpent 2

TABLE 1. SUMMARY OF BENCHMARK CALCULATIONS (cont.)

Reactor	Country	Experiment name	Type of experiment	Benchmark contributors	Number of methodologies	Codes used
IPEN/ MB-01	Brazil	IPEN/ MB-01	^{99}Mo activation	Argentina	4	Serpent 2, CONDOR, CITVAP, SCALE/KENO-VI, MCNP5
				Brazil	1	MCNP5, SCALE
				Slovenia	1	MCNP6, FISPACT-II
				South Africa	1	OSCAR-5/MCNP6, OSCAR-5/Serpent 2
IRR-1	Israel	IRR-1	Multicycle burnup	Israel	1	MUTZAV/MCNP4b, DRAGON4.1.0
				South Africa	1	OSCAR-5/MGRAC, OSCAR-5/Serpent 2
JSI TRIGA Mark II	Slovenia	JSI-1	Foil activation	Argentina	1	MCNP5, FISPACT-II
				Slovenia	1	MCNP6
SAFARI-1	South Africa	NECSA-1	Multicycle burnup	Argentina	2	MCNP5, CONDOR, CITVAP
				South Africa	2	OSCAR-5/MGRAC, OSCAR-5/Serpent 2
				Romania	1	MCNPX v2.7
				South Africa	1	OSCAR-5/MGRAC, OSCAR-5/Serpent 2
TRR-1/M1	Thailand	TINT	Multicycle burnup	Argentina	1	CONDOR, CITVAP
				Thailand	2	MVP, MCNPX v2.6

3. RESULTS OF THE COORDINATED RESEARCH PROJECT

This section presents the facilities and experiments that were benchmarked, the codes that were used to benchmark them and the consolidated results of the benchmark analyses.

Table 1 provides guidance on the type of experiments that each benchmark addresses. Detailed information about each benchmark is given in the consolidated reports provided in the Annexes of this publication. The full facility specifications of the benchmarks are provided in the Second Edition of Technical Reports Series No. 480, Research Reactor Benchmarking Database: Facility Specification and Experimental Data [3], which also contains the experimental data, in most cases given in spreadsheets, as well as spreadsheet templates for inputting simulation results. For some of the benchmarks, Ref. [3] also contains input files for specific codes used.

The following sections give an overview of the individual facilities and the experimental data provided for this CRP.

3.1. BENCHMARKED FACILITIES AND EXPERIMENTS

3.1.1. Open Pool Australian Lightwater (OPAL) Reactor

The Open Pool Australian Lightwater (OPAL) reactor is a 20 MW pool-type nuclear multipurpose research reactor that first went critical in August 2006 and commenced full power operation later in November 2006 at the Australian Nuclear Science and Technology Organisation (ANSTO) Research Establishment at Lucas Heights, located in South Sydney, Australia. OPAL's main uses are:

- Irradiation of target materials to produce radioisotopes for medical and industrial applications;
- Research in the field of materials science using neutron beams and associated instruments;
- Analysis of minerals and samples using neutron activation techniques and delayed neutron activation techniques;
- Irradiation of silicon ingots, termed neutron transmutation doping, for use in the manufacture of electronic semiconductor devices.

The reactor has a compact core, cooled and moderated by light water and reflected by heavy water. The fuel is material testing reactor (MTR) plate type with U_3Si_2 meat and aluminium as clad. All irradiation and beam facilities are located outside the core and within the heavy water reflector vessel. The vessel is located at the bottom of a deep open pool for easy access, shielding and natural circulation cooling during shutdown. The following experiments were provided for benchmarking purposes:

- Burnup: The ANSTO-1 benchmark provides operational data including power as a function of time over cycles 7 to 13, control rod positions at those times, coolant temperatures, heavy water purity and refuelling strategy. The core for cycle 7 contains only fresh fuel and so the core state is well defined and ideal for a burnup calculation. The burnup of fuel is assessed by the calculated core reactivity. In addition, the fuel contains cadmium wires as burnable poison and the burnup of this material is also important in the calculation.

- Activation: The ANSTO-2 benchmark provides dose survey results during replacement of a primary beam shutter for one of the cold neutron beam ports. The data provided in the specification includes operational details, material compositions for the relevant shutter components and decay periods following reactor shutdown. This allows the analyst to calculate the activation of the various components and identify the important radioisotopes. The dose measurements, along with the geometry and locations of the components, are provided to allow calculation of the dose due to the photon source term from the activation calculation.
- Activation: The ANSTO-3 benchmark provides details of a gold grain irradiation performed in one of the pneumatic irradiation facilities. Analysts that want to model the entire reactor, can calculate the flux in the gold grains and directly calculate the activity at the provided calibration time. All details of the target and facility are provided to allow a high-fidelity model. Alternatively, a calculated spectrum at the outer boundary of the irradiation facility is provided to use either directly or in a simplified model of the facility, for activation of the gold grains to compare with the measured activity.

3.1.2. Atominstitut (ATI) TRIGA Mark II

The Atominstitut (ATI) reactor of the TU Wien (Austria) is a pool-type TRIGA (Training, Research, Isotopes, General Atomics) MARK II reactor, moderated and cooled by light water. The reactor is licensed for 250 kW steady state and up to 250 MW pulse operation. The fuel is made of a uniform mixture of uranium (8.5 wt%, enriched 19.95 wt% in ^{235}U), hydrogen (1.6 wt%) and zirconium (89.9 wt%). This composition gives to the fuel a strong moderating property that is a function of the fuel temperature; it decreases when the fuel temperature increases. Because of this behaviour, the fuel temperature coefficient is strongly negative and TRIGA reactors can also be operated in a pulse mode (i.e. in prompt criticality state).

The core has the geometry of a right cylinder made of 91 locations distributed in 6 concentric rings. These locations can be filled either with fuel elements or other core components, like dummy elements (i.e. graphite elements), control rods, neutron source and irradiation channels.

In the recent years, the reactor was converted from a highly heterogeneous core which included high enriched uranium (HEU) fuel elements, to a full low enriched uranium (LEU) core. As a result, the current core load consists out of 76 stainless steel clad zirconium hydride fuel elements in a cylindrical geometry.

The ATI reactor is equipped with various irradiation facilities inside and outside the reactor core. It incorporates facilities for neutron and gamma irradiation studies as well as for isotopes production, samples activation and students training.

In this benchmark specification, the following experiments were provided for benchmarking purposes:

- Burnup: The ATI-1 benchmark exercise consists of a fuelled experiment conducted at the ATI reactor. Experimental data were obtained through the analysis by axial gamma ray spectrometry of several irradiated fuel elements of known operating history. The measurement purpose was to provide information about fuel composition (e.g. production and depletion of major and minor actinides and fission products) under different irradiation conditions. Additional input data, such as reactor core geometry and configuration, in-core neutron flux spectra and distributions, reactor operating history are provided. The experimental data produced in terms of activity values for the

detected fission products in the fuel elements is available for comparison with calculated results.

- Activation: The ATI-2 benchmark exercise consists of an activation experiment conducted at the ATI reactor. Experimental data were obtained through the irradiation and subsequent analysis by gamma ray spectrometry of fissile and fertile material samples. The purpose of the exercise was to analyse the production and depletion rates of relevant elements in the targets under different irradiation conditions.

3.1.3. Experimental Training Research Reactor 2 (ETRR-2)

The Experimental Training Research Reactor 2 (ETRR-2), also called the Multipurpose Reactor, is located at the INSHAS Nuclear Research Centre (NRC) of the Egyptian Atomic Energy Authority (EAEA) about 60 km from Cairo. The reactor is a 22 MW open-pool type, cooled and moderated with light water and reflected by beryllium and light water. The reactor is designed and manufactured by Investigaciones Aplicadas (INVAP), Applied Research in English, a company in Argentina. The reactor is designed to be used in a wide variety of fields including radioisotope production, neutron physics, materials science and training. The facility was constructed and commissioned through the 1990's with initial criticality on 27 November 1997.

The ETRR-2 core is an array of fuel elements, absorber plates inside guide boxes, double wall core chimney and irradiation boxes. The core chimney has a grid of 30 positions with 6×5 configurations. It is divided into two zones where two guide boxes (for absorber control plate insertion) are placed. The reactor began operation with 29 fuel elements and a fixed position for irradiating cobalt. The reactor core has since been modified to 27 fuel elements to provide two positions for the production of ^{99}Mo from LEU as a main product and ^{131}I as a by-product.

The fuel plates consist of a meat of U_3O_8 powder with an enrichment of 19.7 wt% of ^{235}U , dispersed in an aluminium matrix, with aluminium cladding. The fuel active length is 80 cm and the active width is 6.4 cm with an active thickness of 0.7 mm. The core was loaded with three different types of fuel elements at first loading: (i) fuel element type 1 (~146 g of ^{235}U), (ii) fuel element type 2 (~209 g of ^{235}U) and (iii) standard fuel element type (~404 g of ^{235}U).

The reactor uses six flat plates as a neutron absorber material. There are two Al-6061 guide boxes on the grid with three absorber plates for each guide box, arranged in two parallel groups. The whole control absorber plate assembly consists axially of (from top to bottom): a stainless steel plate called the upper cap, the absorber plate itself, another stainless steel plate called the lower cap and the coupling rod. The core chimney surrounds the core and extends upwards inside the reactor tank. Around the chimney there is an Al-6061 irradiation grid that has locations where reflectors and irradiation boxes can be placed. The beryllium reflectors, which surround the core chimney, are fixed in the innermost positions of the external grid, plus one additional row of grid positions between the chimney and the thermal column.

The ETRR-2 research reactor provided two benchmarks in this CRP:

- Fuel burnup: The EAEA-1 benchmark provides measured burnup data of three ETRR-2 fuel elements. The data are derived from measurements of the concentration of the ^{137}Cs isotope as a fission product. The irradiation histories of the three fuel elements in four core loadings are provided for numerical simulation.
- Burnup – $^{134}\text{Cs}/^{137}\text{Cs}$ activity ratio: The EAEA-2 benchmark aims to provide measured burnup of the LEU targets irradiated at ETRR-2. The measurement in this benchmark

is based on the measurements of the $^{134}\text{Cs}/^{137}\text{Cs}$ activity and mass ratios. The neutron flux calculated using the MCNP5 code is provided with the measurements. The specifications of the targets and time of irradiation are also provided.

3.1.4. Institute for Nuclear Research TRIGA 14 MW

The Training, Research, Isotopes, General Atomics (TRIGA) reactor operated by the Institute for Nuclear Research (INR) in Pitesti, Romania, is a 14 MW open pool type research reactor. It was designed by General Atomics, a US company, in the 1970s, as part of a dual-core facility in which the other reactor core is the TRIGA Annular Core Pulsed Reactor. The two reactors are located at opposite ends of a 10 m deep pool. The concrete shield structure was constructed as an integral part of the building. A hot cell facility was built in proximity as to allow underwater transfer of irradiated fuel.

The active core is made up of 5×5 fuel clusters, eight boron carbide (B_4C) control rods and several in-core experimental locations and is installed in an approximately square grid array with beryllium blocks in the outer zone. Core conversion to LEU was completed in 2006.

The main utilization of the research reactor has been long term testing of nuclear power reactor fuel and structural materials in dedicated irradiation devices. It is also used for neutron physics research and radioisotope production.

The INR-1 benchmark is a power ramp test on a low enriched UO_2 fuel specimen in a natural convection capsule. The purpose is to enable calculation of test fuel burnup during the irradiation campaign, which may also involve burning the TRIGA reactor core. The experimental data provided are: control rods' critical position for a reference fresh core configuration, reactor and capsule operation data, isotopic ratios of uranium at end of irradiation by mass spectrometry.

3.1.5. IPEN/MB-01 Critical facility

The Instituto de Pesquisas Energéticas e Nucleares / Marinha do Brasil - 01 (IPEN/MB-01) reactor (Nuclear and Energy Research Institute / Brazilian Navy in English) is a zero power critical facility especially designed for measurement of a wide variety of reactor physics parameters to be used as benchmark experimental data for checking the calculation methodologies and related nuclear data libraries commonly used in the field of reactor physics. The IPEN/MB-01 reactor reached its first criticality on 9 November 1988 and since then it has been utilized for basic reactor physics research and as an instructional laboratory system.

This facility consists of a 28×26 square array of UO_2 fuel rods, 4.3% enriched in ^{235}U and clad in stainless steel (Type 304) immersed into a light water tank. The control banks are composed of 12 Ag–In–Cd rods and the safety banks of 12 B_4C rods. The pitch of the IPEN/MB-01 reactor was chosen to be close to the optimum moderator ratio (maximum k_∞). This feature favours the neutron thermal energy region events and at the same time provides the isothermal reactivity coefficient of the IPEN/MB-01 reactor core with an inversion point.

The experiments performed at the reactor are the following: critical configurations, buckling and extrapolation length, spectral characteristics, reactivity measurements, temperature reactivity coefficient, kinetic parameters, reaction-rates and power distributions. The criticality portion of the experiments has been documented under the International Criticality Safety

Benchmark Evaluation Project (ICSBEP), while the others are documented under International Reactor Physics Experiment Evaluation (IRPhE) projects.

Besides all these experimental activities, the IPEN/MB-01 reactor is also used as an educational laboratory and additionally provides training courses for reactor operators, as well as undergraduate and graduate courses for the University of São Paulo.

In this benchmark specification, the following experiments were provided for benchmarking purposes:

- Activation: The benchmark exercise aims to determine the activity induced by ^{99}Mo . The activity of $\text{UAl}_x\text{-Al}$ miniplates irradiated in the reflector region of the IPEN/MB-01 reactor, determined through the measurement of the 140.5 keV gamma peak of both ^{99}Mo and $^{99\text{m}}\text{Tc}$, is provided. Additionally, $^{197}\text{Au}(n,\gamma)$ reaction rates data, measured by employing diluted gold foils in the $\text{UAl}_x\text{-Al}$ miniplate irradiation position, is provided.

3.1.6. Israel Research Reactor 1 (IRR-1)

The Israel Research Reactor 1 (IRR-1) is a 5 MW, open-pool, light water reactor. The core is composed of MTR fuel assemblies (FAs), 93% enriched and reflected mostly by graphite elements and partly by light water. The coolant is light water flowing downwards by gravity to an open decay tank located below the reactor pool and pumped back to the pool. The top of the core is about 7.5 m below the pool's water level. The experimental facilities include: six horizontal radial beam-tubes, two tangential beam tubes, two pneumatic sample conveyers (so-called rabbit systems) and several irradiation positions in the reflector.

The IRR-1 reactor is not operated in a fixed cycle and there is no 'equilibrium core'. Therefore, the number of FAs in the core may vary between 24 and 30. The cooling time between cycles is also not fixed and can range between two days and a month. Moreover, between 1975 and 1985, the FAs in the core were gradually replaced from US manufactured FAs to French manufactured FAs.

In this benchmark specification, the following experiments are provided for benchmarking purposes:

- Burnup: The IRR-1 benchmark is related to the burnup of the all-French manufactured FA cores from 1985 to 2017. It provides core specifications, which include detailed descriptions of the rods in the core. Also provided are all the 164 core layouts during that period, with their total MWd and year of irradiation and the initial ^{235}U mass inside each of the fuel assemblies in 1985, based on the best available knowledge (up to few percent). These are needed, as some of the French manufactured FAs were already burned to some degree before 1985, during the ten year period of mixed cores. As for the experimental data, the benchmark provides the following:
 - Total and axial distribution of ^{235}U depletion in nine FAs, measured by rhenium gamma transmission measurement. Five of the analysed FAs were used since 1985, and thus are part of the benchmark experimental data. The measurements on the remaining four FAs were taken, in order to better estimate the uncertainty of the initial burnup in 1985;
 - Total and axial activity distribution of the burnup indicator ^{137}Cs in the nine FAs;

- 27 critical conditions (such as core, height of control rods, beginning of cycle (BOC) and end of cycle (EOC)) throughout the irradiation history from 1985 to 2017.

3.1.7. Jožef Stefan Institute (JSI) TRIGA Mark II

The Jožef Stefan Institute (JSI) TRIGA Mark II reactor is a 250 kW light water reactor with an annular graphite reflector cooled by natural convection. The reactor was built between 1962 and 1966 and achieved first criticality on 31 May 1966.

The reactor core is located at the bottom of a 6.25 m high open tank, 2 m in diameter. In total, there are 91 locations in the core, which can be filled either by standard U–ZrH TRIGA fuel elements or other components like control rods, a neutron source, or irradiation channels. The central channel (CC), consisting of an air-filled aluminium tube, occupies the central ‘A’ position in the reactor core. In the outer ‘F’ fuel element ring of the core, there are five irradiation channels. Two of these are equipped with pneumatic sample transfer systems, namely the pneumatic tube (PT) in the ‘F24’ position and the fast pneumatic transfer system in the ‘F22’ position.

In this benchmark specification, the following experiments are provided for benchmarking purposes:

- The JSI-1 benchmark case is an activation benchmark, based on experimental activation rate data for a set of nuclear reactions, obtained in the framework of several experiments. The benchmark case includes experimental activation rate data for:
 - $^{197}\text{Au}(n,\gamma)$, $^{238}\text{U}(n,\gamma)$, $^{232}\text{Th}(n,\gamma)$, $^{55}\text{Mn}(n,\gamma)$, $^{59}\text{Co}(n,\gamma)$, $^{45}\text{Sc}(n,\gamma)$, $^{58}\text{Fe}(n,\gamma)$, $^{117}\text{Sn}(n,n')$, $^{27}\text{Al}(n,p)$ and $^{27}\text{Al}(n,\alpha)$ reactions in the PT irradiation channel of the JSI TRIGA Mark II reactor for samples irradiated without cover, as well as under cadmium (Cd) and boron nitride (BN) covers;
 - $^{27}\text{Al}(n,\gamma)$, $^{27}\text{Al}(n,p)$, $^{27}\text{Al}(n,\alpha)$ and $^{197}\text{Au}(n,\gamma)$ reactions in the CC and IC40 irradiation channels;
 - $^{197}\text{Au}(n,\gamma)$ reaction in four measurement positions in the reactor core between the fuel elements.

3.1.8. South African Fundamental Atomic Research Installation 1 (SAFARI-1)

The South African Fundamental Atomic Research Installation 1 (SAFARI-1) reactor is a 20 MW tank-in-pool type MTR operated by the South African Nuclear Energy Corporation SOC Ltd. (Necsa) in Pelindaba, South Africa. The reactor core contains MTR type (plate fuel) LEU fuel elements and follower type control rods. The core is reflected by beryllium elements on three sides, with a pool-side facility on the fourth side. Various in-core irradiation facilities are also present.

The SAFARI-1 research reactor is utilized in this benchmark definition to facilitate the comparison of various codes and methods against one another, but also against experimental results. These results primarily include, for numerous cycles, critical conditions, BOC flux-wire mapping experiments, spectral measurements and control rod calibration experiments. During the specified time frame spanned by this benchmark problem, the SAFARI-1 reactor underwent a beryllium reflector element replacement. This activity was accompanied by a series of flux foil measurements, which are additionally included in this benchmark.

The information provided herein reflects, as accurately as attainable, the geometric and material layout of the reactor core for all conditions considered, and thus allows code packages which are able to model high levels of heterogeneity to be fully tested. All scenarios make use of the same core component descriptions, although core layout and configuration may differ between cases. Care is taken to avoid the description of commercially sensitive in-core components. Where such components have a significant impact on core parameters, simplified equivalent definitions are provided.

In particular, the benchmark provides calculational scenarios for:

- The NECSA-1 burnup benchmark exercise: This set of experiments contains two parts:
 - The first describes a BOC SAFARI-1 reactor core for cycle C1211-1 with provided BOC calculated number densities for all fuel elements. All core components are described in Part A and the core layout matching cycle C1211-1 is utilized as a basis. Part A contains the various scenarios, which culminate in BOC experiments for Cu wire activation and control rod calibration experiments.
 - The second describes a SAFARI-1 multicycle (just over a year, C1108-1 to C1211-1) core operational regime. Plant operational data for all mentioned cycles are provided in two formats, namely full detailed plant data system dumps per cycle (power levels, bank positions, MWh, etc.) and a simplified averaged stepwise representation for each cycle. This scenario contains multicycle reactivity, as well as cycle specific Cu wire activation and control rod calibration experiments.
- The NECSA-2 activation benchmark exercise: This case describes an activation experiment relating to the buildup of neutron poisons in beryllium reflector elements in SAFARI-1 over many years of operation, and subsequent experiments to determine the impact of replacing the poisoned elements with fresh beryllium reflectors.

3.1.9. Thai Research Reactor-1/Modification 1 (TRR-1/M1)

The Thai Research Reactor-1/Modification 1 (TRR-1/M1) is essentially a TRIGA Mark III research reactor designed and manufactured by General Atomics. Historically, this reactor was converted from an MTR type reactor in 1977. The nominal power of TRR-1/M1 is 1.3 MW thermal. The core of TRR-1/M1 is submerged in an open pool with a concrete biological shield. The cooling of the core is done by natural circulation of the pool water, which is in turn cooled and purified in external coolant circuits. The TRR-1/M1 experimental facilities include neutron beam tubes, a thermal column with graphite, one rotary specimen rack, a pneumatic transfer system and several in-core and out-of-core irradiation positions. The proposed benchmark for TRR-1/M1 is a multicycle depletion case. In this benchmark, the operation history of over 35 years has been summarized to be used for numerical simulation, using MVP and MCNPX. There are 19 core loadings for the benchmark in total. Three fuel elements were selected to perform gamma ray spectrometry in order to evaluate the fuel burnup.

In this benchmark specification, the following experiments are provided for benchmarking purposes:

- Burnup: In the TRR-1/M1 benchmark calculation, 19 different core loadings are modelled in order to simulate the fuel utilization history. Burnup and control rod positions are modelled according to the fuel loading strategy. The burnup of each fuel is analysed individually one fuel zone per fuel element. In addition, the depletion calculation is at the nominal power of 1 MW. The depletion calculations used both MVP and MCNPX models. The percentage of ^{235}U burned are calculated and compared by

MVP and MCNPX for each fuel element, in accordance with the 19 core loading strategies.

- Activation: TRR-1/M1 benchmark provides calculated values of ^{235}U by MVP and MCNPX in comparison with the measurement values. Three fuel elements were selected to perform gamma ray spectrometry in order to evaluate the fuel burnup. The method for burnup experiment is based on measurement of ^{137}Cs activity since it is linearly proportional to the number of fissions which makes it a good burnup monitor.

3.2. DESCRIPTION OF CODES

Table 1 summarizes the specific codes used by each of the participants in the CRP for each of the benchmarks.

The following sections give a brief description of the codes used by the participants in the CRP. Additional information and details regarding the scope and utilization of the codes in each benchmark can be found in Annexes I–XIII.

3.2.1. AUS98

AUS98 [16] is a collection of modular codes developed at the Australian Nuclear Science and Technology Organisation (ANSTO) to solve a range of problems for systems including fission reactors, fusion blankets and other neutron applications. It includes a 200-group neutron and 37-group photon cross-section library based on the Evaluated Nuclear Data Files (ENDF/B-VI.1). Neutron cross-sections for important nuclides are available for a range of temperatures. The system includes modules for reactor lattice calculations, one-dimensional transport calculations, multidimensional diffusion calculations, cell and whole reactor burnup calculations, as well as flexible editing, plotting and auxiliary data processing programs to assist the analyst. The modules are capable of multi-region resonance shielding, coupled neutron and photon transport, including kinetics and perturbations, energy deposition and fission product inventory calculations within the one code system. The modules and libraries have been benchmarked against a wide range of thermal and fast reactor benchmarks experiments.

A calculation is performed by calling the individual modules in a script that is preprocessed and converted to Fortran for execution. The script not only controls the sequence of calculations (resonance shielding, cross-section homogenization, group collapse, criticality search, burnup and refuelling) but also provides the input to define materials, geometry and power history. A typical reactor calculation sequence begins with the preparation of cross-sections using the MIRANDA module for resonance calculations and either ANAUSN, a 1-dimensional discrete ordinates module, or ICPP, a collision probability module. These cross-sections are then used by the POW3D multidimensional diffusion module for flux and criticality calculations including kinetics if needed. Burnup can be performed using microscopic or macroscopic cross-sections using the modules MICBURN or BURNMAC, respectively. Information is passed between the various modules using data pools for cross-sections, geometry, fluxes and status for isotopic compositions and spatial smearing factors of materials. Results for fluxes and cross-sections can be plotted using the AUSPLOT interactive plotting module that is run as a stand-alone module.

3.2.2. COCONEUT

COre COncEption NEUronic Tool (COCONEUT) [21] is a deterministic code developed by TechnicAtome (previously known as Areva TA), used for calculations during the early stages of research reactor design. COCONEUT is a multigroup transport and diffusion theory code. COCONEUT is meant to speed up calculation time by providing the main parameters of interest in reactor calculation within a few days of CPU time. Two main steps are required to estimate such parameters with COCONEUT which follows the traditional cell and core calculation methodology.

The first step involves cross-section preparation for the specific problem. The starting point is a multigroup cross-section library based on the Joint Evaluated Fission and Fusion File JEFF-3.1.1 [33]. Self-shielding calculations are performed using the Sanchez-Coste method with a collision probability method calculated in 2-D using the 281-group Santamarina Hfaiedh Energy Mesh (commonly known as SHEM) energy mesh [34]. The energy spectrum is calculated for several 2-D patterns (standard assembly geometry, control assembly surrounded by standard assembly). Such cross-section treatment needs to be computed for each element type in the core (standard and control assemblies, reflector blocks, other components).

Cross-sections are then collapsed into a 26-group energy mesh, optimized for the MTR type research reactor energy spectrum. The 281 to 26-group energy condensation is carried out using the method of characteristics (MOC) [35] that enables a treatment of the scattering anisotropy.

To perform 3-D diffusion calculations, an additional step is carried out to homogenize and condense cross-sections into a 4-group energy mesh as a function of burnup (cross-section library creation). First, fuel depletion 26-group calculations with the MOC solver are performed to obtain an optimal energy spectrum for cross-section collapsing. Subsequently, the 26 to 4-group energy condensation is carried out through an equivalence procedure that preserves the reference reaction rates. The second step consists of full core calculations and assessment of core equilibrium states. The main neutronic design parameters are evaluated both in transport with MOC and a 2-D exact description of the core and in diffusion on a 3-D model with a homogenized assembly description.

Probabilistic codes (TRIPOLI-4 [25, 26] and MCNP [10]) are also linked to the COCONEUT scheme via formatted material balance outputs. Stochastic models are used to evaluate accurately the neutronic performance of the reactor, such as neutron flux in reflector, gamma heating and reaction rates. Therefore, the COCONEUT line enables the evaluation of all main reactor performance and safety parameters.

3.2.3. CONDOR, CITVAP

Investigación Aplicada's (INVAP) neutronic calculation line [36, 37] is composed of a combination of in-house developed codes and utilities, together with several nuclear data libraries and well known third-party codes.

The codes available in the calculation line are classified as:

- Production packages: The codes and tools used to produce high quality results regarding the requirements both for design and production (where computational performance constraints have to be satisfied);

- State of the art packages: This refers to the codes that are used for research and development (where computational performance is not mandatory), and also used for verifications of the production codes in novel design requirements or as independent calculation requirements.

The production packages contain mainly the deterministic calculation codes and they are used for facility design. These codes need to be as fast and accurate as possible, including innovative calculation capabilities allowed by the computational package. The state of the art codes contain the Monte Carlo and computational fluid dynamics (CFD) codes, which are mainly used for verification purposes, specific design (when production codes cannot be applied) and research and development activities. These codes need to be as precise and accurate as possible (with a reasonable calculation cost) and have to represent an alternative approach to the problem to be solved.

3.2.3.1. *CONDOR: cell code*

Cell level calculation is a very important step in the calculation of a given reactor. This calculation is carried out with high spatial and energy details to properly model the FAs of the reactor. To perform this calculation, a good transport method is needed, and the collision probabilities method (CPM) in a multigroup scheme is an excellent choice.

CONDOR [5, 6] solves the transport equation in 2-D general geometries using the CPM and the heterogeneous response method. In the latter method, the whole system is divided into space elements, which are coupled to model the whole system, where each individual space element is solved by the CPM.

The subgroup method is used in complicated geometries to calculate the effective resonance for the resonant isotopes. This provides an accurate method for calculating FAs in 2-D, taking into account the heterogeneous character of the FAs. Accordingly, CONDOR can model very complicated geometries, needed for some FAs or components of a reactor, very rapidly and accurately.

In addition, it includes several options to perform state dependent calculations to properly simulate the behaviour of the reactor core. As an example, CONDOR can easily generate the burnup dependent homogenized and condensed effective resonance for the thermohydraulic feedback.

The pre-processing capabilities of CONDOR enable the use of regular expressions to create the necessary geometries in a simple way. These make the input preparation of complicated systems significantly easier. Due to this capability and its computational efficiency, burnup dependent 2-D full core calculations are easily performed.

3.2.3.2. *CITVAP: core code*

Core calculation is the other key step in the calculation of a given reactor. This calculation is carried out with a high spatial volume. The diffusion method is an effective method to efficiently solve the neutron flux.

CITVAP is a code developed from the well known diffusion code CITATION II [38, 39]. CITVAP greatly enhances the capabilities for design and fuel management provided by CITATION II, giving the user an easy-to-use set of free-format keywords that provide a more

intuitive input file. CITVAP can solve the following one-, two- and three-dimensional geometries: rectangular (XYZ), cylindrical (R θ Z), triangular (TZ) and hexagonal (HZ). Furthermore, it has the capability to calculate neutron flux and adjoint flux (useful for the calculation of the kinetic parameters). The main improvements carried out in CITVAP can be divided in two categories:

- From a design point of view:
Several calculation options are available, such as: (i) burnup calculation, (ii) fuel management, (iii) search for equilibrium cores, (iv) control rod movement strategies, (v) Xe and Sm transients (including thermohydraulic feedback), (vi) calculation of feedback coefficients (including power feedback coefficient), etc.
- From a reactor operation point of view:
Several administrative capabilities were added, for example: control rod movement and power changes with the operation time, fuel management with the proper fuel IDs for safeguards inventories, pool storage management, etc.

3.2.4. DARWIN2

DARWIN2 [22] was designed to offer an application range covering the entire nuclear fuel cycle, from uranium enrichment up to radioactive waste storage, via fuel fabrication, use of the fuel elements in the reactor core and spent fuel reprocessing. This code is a modular computer code used to calculate isotopic concentrations under irradiation (burnup and activation) conditions and/or under cooling conditions (decay), and allows the following key parameters, derived from concentrations to be calculated:

- Activity, mass, concentration;
- Neutron production by spontaneous fission and (α , n) reaction;
- Total neutron production and neutron spectrum;
- α , β , γ residual power and power spectra;
- Potential radiotoxicity.

DARWIN consists of two modules, INTERPEP and PEPIN. Neutron spectra are input into the INTERPEP module in addition to material impurities and irradiation history (including decay time). The results obtained as an output of the INTERPEP module are integrated reaction rates over all energy groups. These reaction rates are then used in the PEPIN module in order to determine photon spectra and activity inventory of materials per radionuclide.

3.2.5. DRAGON

The computer code DRAGON (Reactor Cell Calculation System with Burnup) [27] contains a collection of models that can simulate the neutron behaviour of a unit cell or a fuel assembly in a nuclear reactor. It includes all of the functions that characterize a lattice cell code, namely:

- The interpolation of microscopic cross-sections supplied by means of standard libraries;
- Resonance self-shielding calculations in multidimensional geometries;
- Multigroup and multidimensional neutron flux calculations that can take into account neutron leakage;
- Transport-transport or transport-diffusion equivalence calculations, as well as editing of condensed and homogenized nuclear properties for reactor calculations;
- Isotopic depletion calculations.

3.2.6. MUTZAV

MUTZAV [29] was used in Soreq's burnup calculations. It is a coupling between two commercial software packages: MCNP4b [10, 28], used for neutron transport calculation of the full core and DRAGON4.1.0 [27], used to burnup the materials in the meat fuel region. The coupling between MCNP and DRAGON's depletion module was developed using Python scripts:

- The Monte Carlo simulation generates flux in 69 energy groups for each depletion zone. Each zone is then depleted in DRAGON using WLUP (WIMS Library Update Project [20]) into 69 energy group cross-sections and depletion chains, for a total of 91 nuclides (23 actinides, 48 fission products and 20 burnable absorbers).
- The isotopic compositions of each zone in the MCNP core file are updated accordingly and the next Monte Carlo simulation is performed.

This code was first validated against similar research reactors (IAEA Generic MTR [40] and Ohio-State University Research Reactor) by conducting the comparisons code-to-code as well as code-to-experiment.

3.2.7. FISPACT-II

FISPACT-II [7, 8] is an enhanced multi-physics, inventory and source-term code system providing a wide variety of advanced, predictive, spectral and temporal simulation methods, and employing the most up-to-date and complete nuclear data forms for both neutron and charged particle interactions.

FISPACT-II has been developed and is maintained by the United Kingdom Atomic Energy Authority (UKAEA) at Culham. As a comprehensive, modern object-oriented Fortran code, FISPACT-II fully processes all ENDF-6 [41] nuclear data including the complete TENDL data with full covariances files. Code features include self-shielding factors, broad temperature dependence, thin/thick target yields, robust pathway analysis, Monte Carlo sensitivity and uncertainty quantification and propagation using full covariance data.

The latest generation of processing codes PREPRO, NJOY and CALENDF are used to provide the user with the most sophisticated incident-particle nuclear data from the TENDL-2017 [42, 43], HEIR-0.1 [44], ENDF/B-VIII.0 [41], JEFF-3.3 [33], JENDL-4.0 [45, 46] and CENDL-3.1 [47] international libraries, which are complemented with the latest decay and fission yield data, including the most recent GEFY-6.1 [48] data. The maturity of modern, technological nuclear data, including TENDL and GEF, provides truly comprehensive data for all simulation requirements. The result is a multi-physics platform that can accommodate the needs of all nuclear applications including activation, transmutation, depletion, burnup, decays, source definition, full inventories, displacement per atom (dpa), kerma, primary damage spectra, gas/radionuclide production and more.

3.2.8. SCALE/KENO-VI

The SCALE Code System [13] is a widely used modelling and simulation suite for nuclear safety analysis and design that is developed, maintained, tested and managed by the Reactor and Nuclear Systems Division of the Oak Ridge National Laboratory (ORNL). SCALE provides a comprehensive, verified and validated, user-friendly tool set for criticality safety,

reactor and lattice physics, radiation shielding, spent fuel and radioactive source term characterization and sensitivity and uncertainty analysis. Since 1980, regulatory bodies, licensees, technical support organizations and research institutions around the world have used SCALE for criticality safety analysis and design. The criticality safety analysis sequence with KENO-VI [9] (CSAS6) was developed within the SCALE code system to provide automated, problem dependent, cross-section processing followed by calculation of the neutron multiplication factor for the system being modelled using KENO-VI.

KENO-VI is an extension of the KENO Monte Carlo criticality program developed for use in the SCALE system. KENO-VI contains all features currently in KENO V.a, plus a more flexible geometry package known as the SCALE Generalized Geometry Package. The geometry package in KENO-VI is capable of modelling any volume that can be constructed using quadratic equations. The primary purpose of KENO-VI is to determine the effective neutron multiplication factor k_{eff} . Other calculated quantities include lifetime, generation time, energy dependent leakages, energy and region dependent absorptions, fissions, flux densities and fission densities.

Most notable improvements to KENO-VI in this latest release are the capability to perform calculations in the continuous energy mode (as opposed to the traditional multigroup approach) and the capability to calculate angular fluxes and flux moments for later use in sensitivity/uncertainty calculations. KENO-VI maintains all of its capabilities in both continuous energy and multigroup modes. When multigroup parameters are requested in the continuous energy mode, KENO-VI automatically collects appropriate tallies into the predefined or user-specified group structure. In addition, HTML format output is provided that may be viewed interactively in the user's web browser. KENO-VI retains the KENO V.a features such as flexible data input, a scattering model in the cross-sections that includes higher order scattering contributions, a procedure for matching lethargy boundaries between albedos and cross-sections to extend the usefulness of the albedo feature, and restart capabilities. This advanced user-oriented program features a more complex geometry package, simplified data input and efficient use of computer storage. These features allow the user to readily solve large geometrically complex problems whose computer storage requirements and geometric complexity preclude solution by previous versions of KENO.

3.2.9. MCNP

Monte Carlo N-Particle (MCNP) [10, 11, 17, 18, 28, 30] is a general-purpose, continuous energy, generalized geometry, time dependent, coupled neutron/photon/electron Monte Carlo transport code. Historically, the first Los Alamos general-purpose particle transport Monte Carlo code was the Monte Carlo Simulation [10] written in 1963.

Since this date, MCNP has been improved with a series of developments (with different releases of MCNP code versions) making it very versatile and easy to use including:

- A powerful general source, criticality source and surface source;
- Both geometry and output tally plotters;
- A rich collection of variance reduction techniques;
- A flexible tally structure;
- An extensive collection of cross-section data.

Prior to the release of the MCNP5 version in 2003, the MCNP code did not have the capability to perform material depletion and burnup calculations. Since the release of the Monte Carlo N-

Particle eXtended 2.7.0 (MCNPX 2.7.0) version in 2011, it has been updated to include this feature.

MCNPX is compatible with MCNP5, and all standard evaluated nuclear data libraries used by MCNP can be used by MCNPX 2.7.0. Furthermore, data libraries containing particle-interaction can be replaced by physics models if the libraries are not available. The program also includes cross-section measurements, benchmark experiments, deterministic code development and improvements in transmutation code and library tools through the CINDER'90 project [49]. Two years later, MCNP6 was released which provides new options of calculating the point-kinetics parameters: (i) the neutron generation time, (ii) the effective delayed neutron fraction and (iii) Rossi- α factor.

3.2.10. MERCURE6

MERCURE6 [23, 24] is used to design gamma radiation shielding. It is a 3-D stochastic code to integrate straight-line attenuation point kernels. The multigroup gamma calculations performed allow making buildup factor calculations using the Kitazume or CEA (SERMA) method and calculation of scalar flux at calculation points and determination of dose equivalent rates and energy deposits using response functions taken from ICRP 74 [50].

3.2.11. ORIGEN

Oak Ridge Isotope GENERation (ORIGEN) [12] is a point depletion, buildup and decay code that allows various results to be calculated including isotopic activities, isotopic compositions and decay photon spectra as a function of time. It has built-in cross-section data for various reactor designs and fuel burnup states including resonance integrals, and it also includes libraries for decay chains including decay radiations, fission product yields, activation products, actinide production and photon emission data. In addition, changes can be made to parts of the included libraries or instead completely alternate data can be entered. The matrix exponential method is used to solve a large system of coupled, linear first-order ordinary differential equations with constant coefficients that describe the evolution of the various isotopes with time.

3.2.12. OSCAR-5

The Overall System for Calculation of Reactors, Generation 5 (OSCAR-5) [31] system enables multi-code and multi-physics support for research reactor analysis, with the primary aim to allow the use of fit-for-purpose tools in the support of reactor operation. The OSCAR-5 system incorporates a powerful pre- and post-processing system, which maintains a consistent, code-independent model and manages the data passing between target codes.

The main entry point to the system is the construction of a unified, code-independent system model. A detailed model of each assembly type and reactor pool (or reflector) is built using the constructive solid geometry module of the system. Assembly models are combined in an assembly library, from which full-core configurations are constructed. All material properties (e.g. isotopic composition and nominal material state, etc.) are also defined in a code-independent fashion.

The model building process is facilitated in the system via extensive visualization schemes, allowing 2-D and 3-D rendering with multiple filters to isolate the components and materials being considered. This can be done at both component and core level. Macros for the creation

of typical component types, geometry processing and mesh optimization schemes, as well as mesh completion algorithms, assist in the creation and final deployment of the model.

In order to use the model in a target code that can handle detailed geometry, translators are used to write the code specific cell and material cards. These translators are defined once in the system and therefore do not depend on the model. This mechanism also ensures that the model remains consistent when it is exported to multiple codes. Additional translators can be added without modifying the core system, so that new target codes can easily be incorporated.

Detailed assembly and core models cannot be used directly in a nodal diffusion solver, since it requires an additional homogenization step in between. The cOMPoSe (OSCAR Model Preparation System) tool is used to systematically move from the heterogeneous unified description, using point wise cross-section data, to a set of homogenized mixtures with energy condensed to few group representations.

Once a suitable model is prepared, it can be deployed to various analysis applications. The final deployment of an application is once again handled by a set of translators for each target code. This, together with the model, provides a set of inputs for the target code. The neutronic codes currently coupled to the system for the sake of this benchmark are Serpent 2 [14, 15], MCNP6 [10, 17] and MGRAC (the OSCAR-5 nodal diffusion core solver) [31].

3.2.12.1. HEADE

The Heterogeneous Assembly Depletion (HEADE) code is a lattice code which forms part of the OSCAR-5 system.

In HEADE, few group nodal cross-sections are prepared by a neutron transport solver based on a low-order response matrix scheme to couple cells and using the collision probability method within each cell. Typically, the code uses a 172-group nuclear data library, in either WIMS-E or WIMS-D (Winfrith Improved Multi-Group Scheme) [20] format. Standard unit assembly calculations are utilized to determine homogenized diffusion parameters for fuel assemblies, while colourset environments are used to determine control rod, irradiation rig and reflector nodal equivalent parameters. HEADE supports both cylindrical and Cartesian geometry types, as well as allows various symmetry options to be defined. Both eigenvalue as well as fixed source calculations are supported.

HEADE produces a set of multigroup homogenized diffusion parameters for use in the global diffusion calculation. These parameters include assembly averaged cross-sections (the user can control the number and structure of the energy groups), but also a number of advanced equivalence parameters, such as cross-section moments, pin power/flux form factors and discontinuity factors. These parameters allow for features such as cross-section rehomogenization and flux/power reconstruction in the diffusion solver. The user has the option to select any number of isotopes to be treated microscopically, with the remainder lumped into a single macroscopic structural material.

3.2.12.2. MGRAC

The Multi-Group Reactor Analysis Code (MGRAC) [31] is the nodal diffusion solver associated with the OSCAR-5 system. In MGRAC, the calculation of the steady-state neutron flux distribution is based on the solution of the three-dimensional multigroup time-independent diffusion equation by means of a modern transverse-integration nodal method for Cartesian

geometry. This nodal method, which is known as the Multi-Group Analytic Nodal Method, engages an analytic solution to the one-dimensional transverse-integrated multigroup diffusion equation, in order to determine a relationship between node side-average net currents and node-average fluxes. It is subject to only one approximation, namely that of a finite-order polynomial approximation for the transverse leakage inhomogeneous source term in the one-dimensional equation. Various iteration acceleration methods are also available.

MGRAC utilizes a microscopic depletion model. Depletion history tracking in MGRAC involves both fuel exposure and nuclide (an arbitrary number of actinides, fission products and burnable absorbers) inventory tracking. In MGRAC, the depletion tracking mesh (i.e. the exposure mesh) is quite independent of the neutronic mesh.

3.2.13. SCALE 6.1/ORIGEN

SCALE [13] is a code system developed for nuclear design and safety analysis, developed, maintained and managed by ORNL. It provides various codes that address criticality safety, reactor physics, radiation shielding, radioactive source term characterization and sensitivity and uncertainty analysis. In addition, nuclear data libraries and processing tools for multigroup and continuous energy applications are available. ORIGEN [12] is the code within SCALE 6.1 for point depletion, buildup and decay calculations that allow various results to be obtained including isotopic activities, isotopic compositions and decay photon spectra as a function of time. It has built-in cross-section data for various reactor designs and fuel burnup states including resonance integrals. It also contains libraries for decay chains including decay radiations, fission product yields, activation products, actinide production and photon emission data. In addition, transport codes within SCALE can be used to model a user-defined system and the COUPLE code can be applied to calculate problem dependent neutron spectrum weighted cross-sections that are representative of conditions within any given reactor or fuel assembly, and convert these cross-sections into a library that can be used by ORIGEN. The matrix exponential method is used to solve a large system of coupled, linear first-order ordinary differential equations with constant coefficients that describe the evolution of the various isotopes with time.

3.2.14. Serpent 2

Serpent 2 [14, 15] is the second full release of Serpent, a general-purpose continuous energy Monte Carlo particle transport code developed at VTT Technical Research Centre of Finland, which includes burnup capability. It is capable of treating complex three-dimensional geometries, and, similar to MCNP6 [17], it utilizes pointwise energy cross-section libraries for neutron interaction physics. Although originally intended as a simplified reactor physics code, the latest versions of Serpent 2 incorporate numerous additional features making it suitable for full-scale reactor calculations.

Material activation and burnup without the use of external codes has always been a principle feature of the Serpent 2 transport code. Radioactive decay and fission yield data used in the calculation is read from standard ENDF [41] format data libraries. The Bateman equations are solved using an advanced matrix exponential method, with a predictor corrector algorithm to account for flux changes within the depletion step.

The main implementation difference between MCNP6 and Serpent 2 is the use of a faster tracking algorithm, whose drawback is that it makes the track length estimator for flux

unavailable. This is not a problem in regions of high collision density, but makes the flux estimation in small, low collision regions difficult.

3.2.15. TRIPOLI-4

TRIPOLI-4 [25, 26] is a 3-D continuous energy Monte Carlo code, developed by CEA, used for neutron, photon and coupled neutron/photon and charged particle transport using pointwise cross-sections. It can be used to calculate shielding, reactor physics with depletion, criticality safety and nuclear instrumentation for both fusion and fission processes. To enhance the user experience, it can use ROOT [51] to generate geometry information for the model easily and efficiently. A depletion module allows burnup and activation of materials. It supports diverse nuclear data libraries, including JEFF [33], ENDF/B [41], JENDL [45, 46] and FENDL [52].

3.2.16. MVP

The MVP/GMVP code [32] was developed mainly for nuclear reactor core analysis. It implements sufficient capabilities from the viewpoint of the analysis; it has flexible geometrical modelling and supports evaluated nuclear data such as JENDL-3.14, JENDL-3.25 [45, 46] and ENDF/B-VI [41]. MVP employs a fast computational algorithm suitable for recent vector and/or parallel computers. In order to apply it to burnup calculation problems, the MVP-BURN [32] code was developed by implementing an auxiliary code which has a function to calculate buildup and decay of nuclides in irradiated materials (depletion calculation). By using the continuous energy Monte Carlo code, microscopic reaction rates of all nuclides are obtained. Since the depletion calculation is possible if the microscopic reaction rates are given, the coupling of a Monte Carlo code and a depletion calculation code is realized only by implementing an interface program between them. The auxiliary code has the functions of the depletion calculation, file management and interface with MVP. A whole burnup calculation is performed by executing alternately these codes.

3.2.17. WIMS-D4

WIMS-D4 [20] is a cell code for calculations in slab geometry, single fuel rods or fuel rod clusters. It incorporates collision probability or discrete ordinates method used to calculate fluxes in multigroup schemes, with various possible boundary conditions. It incorporates its own nuclear data library (P0 and P1, resonance parameters and burnup information). A post-processor condenses and homogenizes macroscopic cross-sections, and these are then converted to the appropriate format for use in a core code (for example CITVAP).

3.3. NUCLEAR DATA LIBRARIES

The nuclear data libraries used in each calculation have a direct impact on the results obtained. A number of international libraries exist, including the Evaluated Nuclear Data File (ENDF) [41], Joint Evaluated Fission and Fusion (JEFF) Nuclear Data Library [33], Japanese Evaluated Nuclear Data Library (JENDL) [45, 46], TALYS-based evaluated nuclear data library (TENDL) [42, 43], High-Energy Intra-Nuclear Cascade Liège-based Residual nuclear data library (HEIR) [44] and the Chinese Evaluated Nuclear Data Library (CENDL) [47]. Each of these libraries is regularly updated, with new versions being released with unique identification numbers. The latest versions available, at the time the CRP calculations were performed, were ENDF/B-VIII, JEFF-3.3, JENDL-4.0, TENDL-2019, HEIR-0.1 and CENDL-3.1. The

participant from Slovenia also used the International Reactor Dosimetry and Fusion File (IRDFF-v1.05) [53] and the International Reactor Dosimetry File (IRDF-2002) [54].

The libraries used were not considered to be a specific part of the input, i.e. they are not part of the benchmark specification. Each analyst chose specific nuclear data libraries and in some cases also different versions of the libraries. Detailed information on the nuclear data used in each case is provided in the consolidated reports given in the annexes and in the individual reports given in the supplementary material that accompanies this publication.

3.4. SUMMARY OF RESULTS

This section provides a short summary of the results obtained for each benchmark, including the codes used, the level of agreement between results obtained by different participants (including, wherever applicable and possible, reasons for eventual deviations) and the appropriateness of the benchmarks for given applications.

3.4.1. ANSTO-1

Three deterministic and two stochastic codes were used by the four participants to perform the burnup calculations for the OPAL core. Each of these codes involves the analyst making a series of choices regarding construction of the model, such as approximations adopted to represent the actual geometry, discretisation of the burnup regions, time steps in burnup, number of neutron groups, homogenization of material regions, flux solution method and cross-section libraries. The various choices made by the analysts has produced results that differ when compared in detail, but looking at general characteristics and trends, the following observations can be made:

- All participants were able to develop models that provided agreement in the reactivity values to within ± 1000 pcm (excluding data points that may have been influenced by xenon transients).
- Almost all results show an upward trend in reactivity from cycle 7 to cycle 12 (this is not evident in the SFA results).
- Almost all results show an increase in reactivity (a kick-up) at the end of each cycle.
- Two of the participants had an offset at cycle 10 which coincides with the step change in heavy water purity.

The first observation means that all participants were able to develop models that provided sufficient accuracy and precision to reliably predict reactor operation from an operations perspective.

Due to the burnup of the cadmium wires in the fuel assemblies, some participants suggested that the second and third observations may be linked. To investigate this further, all participants performed sensitivity studies on the modelling details of the cadmium wires, increasing the number of axial and radial burnup zones or flux solution within the wires. However, despite the improvement in some results it did not significantly change the observed trends and it was concluded that those strategies would not address the effects observed. This means there is no plausible explanation for the second and third observations.

The fourth observation is specific to the deterministic results of France (FRA) and South Africa (SFA), as well as the stochastic results of FRA and to a lesser degree the stochastic results of

SFA. The deterministic results of FRA (COCONUT) require an adjustment in reactivity due to changes in heavy water purity as the COCONUT model does not explicitly account for the change in purity. The method used to account for this may introduce a bias that results in this offset. The deterministic results for SFA (MGRAC) are based on a model that does not represent the complete heavy water reflector. For this reason, an approximation is adopted to represent the actual reflector. This approximation may introduce a bias when there is a step change in the heavy water purity that is seen as a step change in the core reactivity. It is not clear what is causing the significant step change observed in the stochastic FRA (TRIPOLI-4) results and the smaller (perhaps not significant) change in the stochastic SFA (Serpent 2) results.

It was clear that some of the data provided was not of sufficient detail or accuracy to capture the power levels and the resulting xenon transients that lead to some outlier values. Ignoring these results, it was demonstrated that both the historic deterministic codes and the modern stochastic codes are capable of performing multicycle burnup of both the fuel and burnable cadmium wires within the fuel assemblies to an accuracy sufficient for operational purposes. The accuracy was comparable for both types of codes and all codes employed in this benchmark. In addition, the results demonstrate the applicability of the benchmark data as a practical and complete set of reactor specification and operational data for performing multicycle benchmark calculations.

3.4.2. ANSTO-2

Calculation of dose rates due to activation of reactor structures is an important and necessary capability to support maintenance and installation tasks at reactors. The calculation involves several steps each performed using a different code and model, as well as assumptions, to enable the calculation to be achieved in a simple and practical manner. There were three participants in this benchmark using a total of four different calculation lines with a total of six different codes. The results obtained by the participants indicate that the adopted methodologies and computational models were able to predict the maximum dose rates associated with the benchmark activity. In addition, most of the other results were indicative of the measured dose rates and from a radiological perspective were sufficient to support the installation activities.

The benchmark specification and data are sufficient for any analyst to perform the benchmark and serve as a useful and realistic exercise to benchmark any proposed methodology for activation of reactor structures and subsequent dose rate calculation. The attention of users of the benchmark is drawn to the fact that the measured dose rate at position 8 may not be correct and, thus, may lead to discrepancies with calculated results.

3.4.3. ANSTO-3

Calculation of activities of irradiated materials, in particular for medical radioisotopes, is an important and necessary capability to support utilization of research reactors. This calculation requires accurate data for the target materials, reactor state and irradiation conditions. The ANSTO-3 benchmark provides this data to enable the analyst to verify their calculation tools and methods for such a calculation. There were three participants in this benchmark using five different calculation lines with two different codes to calculate the ^{198}Au activity of irradiated gold grains. The results obtained by the participants indicate that the adopted methodologies and computational models were able to predict the ^{198}Au activity within the required tolerance for four of the five calculations.

The benchmark specification and data are sufficient for any analyst to perform the benchmark and serve as a useful and realistic exercise to benchmark any proposed methodology for irradiation and activation of materials.

3.4.4. ATI-1

Two participants contributed to the ATI-1 benchmark using Monte Carlo computer codes to model the experiment and to compare calculated results to experimental values for each scanned fuel element. Two Monte Carlo codes were selected by the participants; Serpent 2 and MCNPX (version 2.6).

Some simulation simplifications were assumed in the different calculation models: e.g. sometimes the different core configurations during the referenced period were collapsed into a unique one. In all cases, the core configuration at the date of first criticality was set with all fresh fuel elements, even if this does not exactly correspond to the core configuration during the experiment.

For all the fission products compared with experimental data, except ^{137}Cs , the different irradiation history of the fuel elements (previous irradiation) does not affect the results. As expected, for the long half-life nuclide ^{137}Cs , the calculated concentration in those fuel elements that were not inserted fresh at the beginning of the reference period was lower than the experimental concentration.

In conclusion, the comparison showed a good agreement between the Serpent 2 calculation and the measurement results. The MCNPX model produced results that are in general less accurate, compared to measured values. Nevertheless, the results can still be considered consistent among themselves and in consideration of the assumption made as input to the simulation process.

3.4.5. ATI-2

Two participants contributed to the ATI-2 benchmark using Monte Carlo computer codes to model the experiment and calculate results to be compared against experimental values. The ATI-2 benchmark experiment was reproduced with different approaches and different codes (Serpent 2, MCNP, FISPACT) by the participants.

The first approach implied the complete reactor modelling, including the irradiation facility utilized for the experiment, with Serpent 2. In this case, the calculated results show a good agreement with the experimental values for most of the determined activities. In some cases, when the evaluated activities present very low absolute values, a lower precision in the calculated and the experimental data is observed. Nevertheless, the Serpent 2 calculated results are still in fair agreement with the experimental results, but with higher discrepancy.

The second approach involved calculations by means of the combination of MCNP and FISPACT code. In this case, the input data provided within the benchmark specification package (such as the neutron spectrum at the irradiation position) was used in the first step of the calculation. The calculated results show consistency among them, even if they systematically overestimate the experimental values.

3.4.6. EAEA-1

The benchmark is essentially a multicycle depletion case of ETRR-2, which covers the burnup history of four cycles. The fuel burnup was determined from the ^{137}Cs content, obtained via gamma ray spectrometry performed for three selected fuel assemblies. The % ^{235}U burnup of these three fuel elements are available for comparison with numerical simulation. Information like critical control rod position during the reactor operation and axial burnup profile will improve this benchmark.

Four organizations participated in the calculation of the benchmark and two of them with two different methodologies:

- EAEA from Egypt modelled the reactor using a deterministic calculation line based on WIMS and CITVAP codes;
- INS from Israel modelled the reactor using a stochastic calculation code MCNP coupled with the DRAGON code to perform the burnup calculation;
- Necsa from South Africa modelled the reactor using a deterministic (HEADE-MGRAC) and a stochastic (Serpent 2) calculation line. Both methods were integrated into the OSCAR-5 system;
- INVAP from Argentina modelled the reactor using a deterministic calculation line (CONDOR-CITVAP) (additional conceptual comparisons were done using the CONDOR code).

In general, the calculated values agree very well between the participants (standard deviation about 5%) and no significant difference was observed between deterministic and stochastic codes, except for the less depleted fuel assembly (FE022).

The absolute differences with respect to the measured values ranges from about 20% in the less depleted fuel assembly (FE022) to a very good agreement in the most depleted fuel assembly (FE020).

3.4.7. EAEA-2

This benchmark focused on relating the burnup of UAl_x plates irradiated in ETRR-2 to $^{134}\text{Cs}/^{137}\text{Cs}$ activity (or mass) ratio. A sample was collected from irradiated UAl_x plates after dissolving in sodium hydroxide (NaOH) and the $^{134}\text{Cs}/^{137}\text{Cs}$ activity ratio was measured using gamma ray spectrometry. The thermal, epithermal and fast neutron average flux in the LEU plates, as well as the energy dependent flux profile have been calculated using the MCNP5 code and were provided.

Three calculation tools have contributed to this benchmark. The first tool was the MCNPX code, which was used to simulate the reactors and calculate both the actinide and non-actinide inventories in LEU target plates, as well as the $^{134}\text{Cs}/^{137}\text{Cs}$ activity and mass ratios. The data library used was ENDF/B-VII.0. The second tool was the AUS98 neutronic code system. This is a collection of modular codes developed at ANSTO to solve a range of problems for systems including fission reactors, fusion blankets and other neutron applications. It uses a 200-group neutron and 37-group photon cross-section library based on ENDF/B-VI.1. The third tool was an analytical model used to calculate the ^{235}U burnup, as well as the buildup of ^{134}Cs and ^{137}Cs using the neutron flux calculated by the MCNP5 code.

The values of ^{235}U burnup obtained using the three calculation tools were 1.01%, 1.08% and 1.05%. However, the actual ratios calculated differ significantly from these measured values. One source of the discrepancy between the calculations and the measurements is the large uncertainty in the measured ^{134}Cs activity (~30%).

3.4.8. INR-1

The benchmark focused on Romania's TRIGA 14 MW reactor, for which reactivity results on the cold reference core configuration (RCC) at reactor startup are provided, and on an isolated low enriched UO_2 test fuel element irradiated in a pressurized capsule. The irradiation campaign was long enough that calculation of the burnup of the reactor fuel along with that of the test fuel needed to be done, in order to capture the evolution of the power distribution around the capsule. For the test fuel, isotopic ratios of uranium were determined as a result of destructive examinations.

The benchmark was created with the aim to provide all the data needed in an unambiguous manner, so as to allow little or no room for interpretation of the data. That implies making some choices such as: (i) collapsing short lived core configurations, (ii) giving a unique, effective TRIGA fuel temperature for all configurations, (iii) neglecting the reactivity effects of beam tubes, (iv) assuming a unique axial burnup distribution in the core, and (v) the homogenization of bottom and top reflector layers. When data are missing, such as for the initial content of ^{234}U and ^{236}U in the test fuel, a sensitivity study is suggested.

Two organizations participated in the calculation of the benchmark:

- Necsa from South Africa. Necsa constructed a model using the OSCAR-5 system and deployed the Monte Carlo code Serpent 2, as well as the nodal diffusion code MGRAC for neutronic analysis. The model was used directly in Serpent 2, but an additional homogenization step was performed as part of the deployment of MGRAC.
- INR from Romania: the data provider. INR created a model of the reactor and an experiment with MCNPX.

Both participants obtained good results with experimental reactivity and burnup measurements.

As expected, the Monte Carlo codes (MCNPX and Serpent 2) are capable of treating well the isolated test fuel in the context of the TRIGA core. When the fuel element was depleted by the lattice code HEADE by Necsa (surrounded by a homogenized fuel mixture and beryllium reflector on the right), the accuracy of the test pin lattice model was restricted by the capabilities of the code. Generally, a nodal solver is not appropriate for this kind of burnup problem.

3.4.9. IPEN-1

The experiments reveal that the calibrations both for the power and the high purity germanium (HPGe) detectors were fundamental. Furthermore, the quality of the benchmark values is intimately related to the calibration process. The technical analyses of the benchmark results provided by the participants further reveal that state of the art calculation methods and related nuclear data libraries have reached a very high level of quality and sophistication. The agreement of the calculated results to the benchmark values were particularly satisfactory for the ^{99}Mo activity benchmark, which means that the objective designated in the design goals for the target and target positioning in a reactor environment was met. Both stochastic and deterministic methods were employed in the theoretical analyses. Only miniplate number 9

showed a systematic overprediction of the calculated results. The results calculated by different participants, employing the same code and a related nuclear data library, were very similar and showed no clear differences. This is a very promising outcome for the nuclear data community, as it suggests that the cross-section adjustment related to thermal reactors will no longer be a concern in future.

The discrepancy in the $^{197}\text{Au}(n,\gamma)$ reaction rate benchmark values were more severe. Only Argentina provided deterministic results. In fact, a systematic and consistent underprediction of the calculated results was found among all participants. For this reason, the utilization of a 70c cross-section seems to be more appropriate for the $^{197}\text{Au}(n,\gamma)$ reaction rates.

3.4.10. IRR-1

Overall, there is a good agreement between calculations and experimental results. While the agreement is usually up to ~ 1500 pcm for the criticality measurements, it is within the measurement of uncertainty ($\sim 3\%$) for the depletion measurement. For ^{137}Cs activity, the deviations between the experimental and calculation results are somewhat larger (up to 8%), possibly because, as discussed above, the measurement of absolute ^{137}Cs activity for MTR spent FAs is harder to calibrate (to translate from net count rate to activity), while the determination of depletion made via the measurement of transparency to gamma rays from an external source suffered less from this technical issue.

The axial distribution of depletion in the FA was found to be asymmetric. This feature can be explained by the presence of control rods in the upper side ‘pushing’ the power to the lower side of the core.

Sensitivity checks made for the Soreq simulations demonstrated that the depletion distribution is less sensitive to changes in the model (compared with the measurement uncertainty), than criticality calculations. Thus, one cannot use them to validate the very fine details of the model, such as impurities content, small errors in the measured power, etc. Calculations of k_{eff} at measured critical conditions are more sensitive and can detect those inaccuracies in the models relative to the real core.

3.4.11. JSI-1

The benchmark case collects experimental reaction rate measurements and calculations from several experimental campaigns. Calculations of the reaction rates were performed by the JSI using the particle transport code MCNP6 in conjunction with the ENDF/B-VII.1 nuclear data library. The JSI TRIGA activation benchmark case received partial coverage from the Argentinian counterpart INVAP, who performed activation calculations using the FISPACT-II activation code in conjunction with the ENDF/B-VII.1 and TENDL-2014 nuclear data libraries.

The comparison between the experimental and calculated reaction rates provides valuable feedback information, both on the representativeness of the computational model and the quality of the nuclear data. However, due to the numerous input physical quantities required and possible sources of uncertainty or bias, a precise determination of the cause of observed discrepancies for certain reaction rates is generally not straightforward.

The JSI TRIGA benchmark provides clear indications of the nuclear data quality for certain nuclear reactions. For the $^{117}\text{Sn}(n,n')$ reaction, a consistent 50% relative difference is observed between experimental and JSI calculated values using cross-section data from the ENDF/B-

VII.1 nuclear data library. This difference was attributed to inaccurate cross-sections in ENDF/B-VII.1. Considerably better agreement with the experimental data, i.e. relative differences of the order of 10% was observed for the INVAP calculated data using the TENDL-2014 nuclear data library. Consistent disagreement between the experimental and calculated values was observed for the $^{58}\text{Fe}(n,\gamma)$ reaction, which was more pronounced for cadmium and boron nitride covered samples. The observation indicates problems in the nuclear data for the $^{58}\text{Fe}(n,\gamma)$ reaction in the epithermal energy range. Overall, good consistency was observed between the experimental and calculated $^{197}\text{Au}(n,\gamma)$ reaction rates, especially for the experiments performed in the reactor core, this reaction being a standard dosimetry reaction. Systematic differences were observed between experimental and calculated $^{27}\text{Al}(n,\gamma)$ reaction rates, the calculated data being consistent, possibly indicating problems with the cross-section data. The experimental measurements of this reaction rate are challenging on account of the short product half-life of around 2.24 minutes. Limited consistency was observed between the experimental and calculated reaction rate values for the threshold reactions on aluminium ($^{27}\text{Al}(n,p)$ and $^{27}\text{Al}(n,\alpha)$), for which significant conclusions are not possible. A systematic difference between the JSI and INVAP calculated $^{27}\text{Al}(n,\alpha)$ reaction rates using the ENDF/B-VII.1 nuclear data library was noted, the JSI data being more consistent with the experimental data. No clear explanation is evident. Limited consistency was observed for the other measured neutron capture reactions, which does not provide any clear indications.

3.4.12. NECSA-1

The SAFARI-1 benchmark contains two distinct parts: NECSA-1 relates to multicycle depletion modelling, enumerated by Experiments 1 to 3 in the SAFARI-1 consolidated report (see Annex XII); NECSA-2 relates to the activation of beryllium reflector elements and the associated buildup of neutron poisons in the beryllium elements, given as Experiment 4 in the SAFARI-1 consolidated report.

With regard to the multicycle depletion modelling (NECSA-1), the SAFARI-1 benchmark presents a series of experiments to indirectly determine the accuracy of multicycle depletion analysis. In particular, analysis of multicycle reactivity, BOC Cu wire activation in each fuel element and control rod calibration provides indirect measures of fuel depletion. Results exhibited good agreement with experimental data. Multicycle results indicate that after an initial burn-in period (3 to 4 cycles), the reactivity offset from critical settles to a stable level of less than 500 pcm, which is, however, strongly dependent on the approach used in processing plant data. Reactivity results obtained from deterministic and stochastic solutions methods consistently show a notable standard deviation (also order of 500 pcm), which largely originates from the extensive in-core irradiation rig movements during operation, the details of which are not included in the benchmark specifications.

Cycle specific Cu wire activation profiles match the experimental results well, and the analysis presented generally shows total activation errors per core position (over all cycles) to be within 10% and 15%. Good agreement is also found for control rod calibration experiments, but all analyses show a slight overestimation of the control rod worth per rod in all cycles analysed.

3.4.13. NECSA-2

The beryllium reflector poisoning in the SAFARI-1 reactor has been modelled by two participants using different approaches and methods. The effect of the beryllium reflector poisoning on reactivity and neutron flux or activity has also been accounted for through

measurements and calculations. The South African and Romanian participants calculated this benchmark and established comparisons to experimental measurements.

Results between the submissions agree well in terms of the reactivity impact of the accumulated neutron poisons in the beryllium reflectors. However, modelling of spectrum measurements with nickel and cobalt foils by both participants show some notable differences to the measurements, indicating that local poison estimates are less well captured. This is to some extent expected as an approximate operational history is utilized in modelling the poison buildup over many decades; as such, the local movement and operational history of particular beryllium reflector elements might be needed in future versions of the benchmark specification to improve this subset of experiments.

3.4.14. TINT

The benchmark is basically a multicycle depletion case of TRR-1/M1, which covers the burnup history over 35 years. The fuel burnup was determined from the ^{137}Cs content, obtained via gamma ray spectrometry performed for three selected fuel assemblies. The % ^{235}U burnup of these three fuel elements are available for comparison with numerical simulation, together with their axial profile.

Two organizations participated in the calculation of the benchmark, both with two different methodologies.

- TINT from Thailand modelled the reactor using stochastic codes MVP and MCNPX.
- INVAP from Argentina modelled the reactor using a deterministic calculation line CONDOR-CITVAP, additionally using CONDOR code.

In general, the calculated values of all the codes agree quite well with the measured values and most of the results overpredict the experimental value.

However, there are some discrepancies in some of the modelling codes that need further analysis. For example, the Monte Carlo codes do not have axial discretization that allow a proper 3-D burnup calculation or a comparison between the axial profiles provided.

Only one calculation compares the axial profile, showing in general a good agreement, except for the top measurement of one fuel element.

The deterministic codes used as a standard design approach achieved a very good agreement with the data.

4. CONCLUSIONS

4.1. THE BENCHMARK SPECIFICATIONS

The compiled facility and associated experimental descriptions differ greatly in purpose, detail level and complexity. In order to assist the users of this publication in finding the most appropriate benchmark for their purposes, a high level categorization is provided in this section. This categorization is based on the perspective of participants in the CRP after completing modelling of the benchmarks, and serves as a suggested guide to aid navigation of the benchmarks and calculations reported in this publication.

In Table 2, each experiment is listed and categorized into three possible areas of application. Table 3 categorizes the benchmarks in terms of the results obtained in the analysis conducted by the CRP participants.

The first category in Table 2, “Introductory modelling”, indicates whether the experiment is deemed appropriate as a training tool for analysts who are newcomers to this type of benchmark and may only be aware of the basic or introductory capabilities of the codes to be used in its modelling. The benchmarks would allow users to gain initial familiarity with the general features of the applicable codes.

The second category, “Advanced modelling”, implies that the benchmark potentially requires knowledge of more advanced options of the codes and methodologies relevant to this type of benchmark. This category also implies that some additional level of judgement and knowledge might be needed from the analyst in order to correctly interpret the information in the facility and experimental description.

Finally, the third category, “Validation support”, indicates whether the benchmark is believed to exhibit the required level of detail and completeness to be used in more formal code, model or user qualification or validation type activities. In this case, the entries in Table 2 are more descriptive and indicate to which type of analysis this perspective applies. In some cases, only some experimental results are included in this category. This categorization is supported by additional information provided in Table 3, as discussed below.

4.2. CODES, MODELLING APPROACHES AND RESULTS

In general, good agreement was observed between submitted results for the benchmarks. Specifically, most results were within experimental uncertainties where these were available and the overall trends in calculated parameters were quite similar.

For benchmarks that lack direct experimental measurements of fuel depletion, code to code comparisons of calculated depletion parameters can still yield valuable insight into the effect of using different methodologies and assumptions. As such, in addition to the experimental measurements, a selected number of calculated outputs, chosen by the benchmark provider, was included in the result templates.

The work conducted during the CRP included analysis of the provided benchmarks by participants, with the aim to achieve a reasonable level of coverage of all submitted experiments. This analysis work allowed both for a thorough review of the completeness of the benchmarks specifications, as well as a determination of the accuracy and spread with which the combination of different codes, methodologies and users could model them.

TABLE 2. HIGH LEVEL CATEGORIZATION OF BENCHMARK SPECIFICATIONS

Benchmark	Introductory modelling	Advanced modelling	Validation support
ANSTO-1	No	Yes	Reactivity
ANSTO-2	No	Yes	Maximum dose rate only
ANSTO-3	Yes	Yes	Reaction rate
ATI-1	Yes	Yes	Fuelled experiment
ATI-2	Yes	No	Fission products
EAEA-1	Yes	Yes	Burnup
EAEA-2	Yes	No	No
INR-1	No	Yes	Reactivity; fuelled experiment
IPEN/MB-01	No	Yes	Reaction rate; activation
IRR-1	Yes	Yes	Reactivity; ²³⁵ U depletion distribution; fuel ¹³⁷ Cs activity distribution
JSI-1	Yes	No	Reaction rate
NECSA-1	Yes	Yes	Reactivity
NECSA-2	No	Yes	Global poison buildup and reactivity only
TINT	Yes	Yes	Burnup

Table 3 summarizes this information in the form of a brief high level summary of the analysis conducted on each benchmark. Note that the level of coverage of these benchmarks were, in some cases, still somewhat sparse and, therefore, the information in this table has to be interpreted as largely qualitative. Table 3 is largely intended as a guide to aid navigation of the benchmarks and calculations reported in this publication, and the reader is encouraged to refer to the relevant annexes to understand the reasoning behind the entries in this table.

Table 3 indicates the wide range of problem specifications, modelling approaches and applied codes. Each benchmark is described by its overall type and the set of codes used by the various participants which modelled the specific experiment during the CRP. This list simply reflects the work that has been done. It is neither an indication of applicability of the codes, nor does it imply that other codes could not be applied in these cases.

Table 3 also provides information about the typical deviations, both against experiment (Column 5 – “Typical deviation”) as well as between participants (Column 6 – “Typical range between submissions”), that were found in this work. The values given as typical deviations against the experimental results are based on those calculations that were considered to follow the benchmark specifications more closely.

Although results are often benchmark specific, and the reader is advised to consult the individual annexes for the relevant context, some general trends can be observed. The typical

levels of deviation against experiment are valuable from the perspective of safety and utilization analysis, as they provide an indication of the obtainable accuracy, as well as the typical safety margins that have to be applied when performing such analyses. For example, a deviation of 500 pcm in reactivity and 10% in resulting fuel burnup estimates are typical in the case of multicycle depletion analysis, although in some cases better agreement is reached. For activation cases, deviations of approximately 20% in calculated activity is often achieved. In approaching code and model validation related analysis for research reactor applications such estimates could be considered the current state of the art. For most of the benchmark problems considered, it is clear that both deterministic and stochastic methods can effectively be applied to these classes of problems. Results are in general well aligned and, in many cases, applied synergistically.

In Table 3, deviations are also reported in terms of spread in results among benchmark participants. This information can, when read in conjunction with the proposed benchmark categorization in Table 2, assist users of this benchmark set in selecting relevant benchmarks for their own analysis purposes. For example, benchmarks with a narrow spread among participants generally indicate that the benchmark can be successfully modelled with a variety of approaches, whilst a wider spread may indicate that certain methodologies are preferable for such problems. A wider spread may also indicate that experience plays an important part in successfully modelling a given benchmark, preventing it from being utilized as an early stage training vehicle.

It was observed that the user effect, that is, differences of results due to the options users take when performing their calculations, was more evident in cases where there were opportunities for multiple interpretations of input data. Based on individual submissions, it is possible to extract information about the effect of using different data sources, modelling choices and tool chains. However, this CRP did not make a comprehensive analysis of this information, because to address this issue in a systematic way, a dedicated effort would be needed, where a set of benchmarks would be calculated by different users using the same codes and nuclear data libraries.

As mentioned in Section 3.3, the nuclear data libraries were not considered to be a specific part of the input, that is, they were not part of the benchmark specification. Therefore, their effect on the results obtained was not tested in a systematic way. Nevertheless, some participants did test the nuclear data used. The participant from Argentina studied the impact of the nuclear data libraries in the calculated reactivity and in the ^{99}Mo activity for the IPEN/MB-01 benchmark, by using Serpent 2 with the nuclear data libraries ENDF/B-VII.0, ENDF/B-VI.8 and JEFF-3.2. Differences below 500 pcm were obtained for the calculated reactivity and differences below 15% were obtained for the ^{99}Mo activity in ten different miniplates, but around 5% or better in the majority of the cases. In several other cases, they also used CONDOR, which is based on ENDF/B-VI.8 and Serpent 2 with ENDF/B-VII.0 to calculate the same benchmark (see Table 1), also obtaining acceptable differences in the results. In those cases, it was different users that made the calculations with each code, so the differences obtained combine code, user and nuclear data libraries effects. The participant from Israel used the code MUTZAV with ENDF/B-VII and MCNP6.1 with ENDF/B-VIII to calculate, for the IRR-1 benchmark, the reactivity for burnup of a fuel assembly in an infinite lattice, obtaining deviations in the reactivity calculated of up to 400 pcm.

TABLE 3. HIGH LEVEL CATEGORIZATION OF CONDUCTED ANALYSIS

Benchmark	Benchmark type	Codes	Modelling approach used	Typical deviation	Typical range between submissions
ANSTO-1	Multicycle depletion	CONDOR/CITVAP Serpent 2 OSCAR-5 TRIPOLI-4 COCONeut2.0	Monte Carlo Deterministic	Reactivity 500 pcm	Reactivity 500 pcm
ANSTO-2	Activation	MCNP5/SCALE 6-ORIGEN MCNP5/ORIGEN2.0 MCNP6 TRIPOLI-4 DARWIN/MERCURE6	Monte Carlo Deterministic	Maximum dose rate 20% Other dose rates inconsistent	Maximum dose rate 20% Other dose rates inconsistent
ANSTO-3	Activation	CONDOR/CITVAP MCNP	Monte Carlo Deterministic	Activity 10%	Activity 10%
ATI-1	Fuel burnup	Serpent 2 MCNPX	Monte Carlo	Activity 5–15%	Activity 60%
ATI-2	Activation	Serpent 2 MCNP/FISPAC	Monte Carlo Deterministic	Activity 10%	Activity 100%
EAEA-1	Fuel burnup	WIMS/CITVAP CONDOR CONDOR/CITVAP Serpent 2 MGRAC MCNP	Deterministic Monte Carlo	Burnup 10%	Burnup 5%
EAEA-2	$^{134}\text{Cs}/^{137}\text{Cs}$ activity ratio in LEU targets	MCNPX AUS98 Analytical	Monte Carlo Deterministic Analytical	Activity ratio 83%	Activity ratio 5%
INR-1	Test fuel burnup	MCNPX OSCAR-5 Serpent 2 MGRAC	Monte Carlo Deterministic	Reactivity 20–50 pcm	Reactivity 77 pcm Isotopic ratio <1% rel.
IPEN/ MB-01	Reaction rate; Activation	Serpent 2 CONDOR CITVAP SCALE/KENO-VI MCNP5 SCALE MCNP6 FISPACT-II OSCAR-5/MCNP6 OSCAR-5/Serpent 2	Monte Carlo Deterministic	Reaction rate 5% Activity: 5%	Typically 6%
IRR-1	Multicycle depletion	MUTZAV DRAGON4 MCNP4b	Monte Carlo	Reactivity 1500 pcm ^{235}U depletion 2.5% ^{137}Cs activity 8%	Reactivity 1000 pcm ^{235}U depletion 2% ^{137}Cs activity 20%

TABLE 3. HIGH LEVEL CATEGORIZATION OF CONDUCTED ANALYSIS (cont.)

Benchmark	Benchmark Type	Codes	Modelling Approach Used	Typical Deviation	Typical Range Between Submissions
JSI-1	Activation	MCNP6 FISPACT-II	Monte Carlo	Reaction rate 20%	24%, up to 120% in some cases
NECSA-1	Multicycle depletion	OSCAR-5 Serpent 2 MCNP6 CONDOR/CITVAP	Monte Carlo Deterministic	Reactivity 500 pcm	Reactivity 200 pcm
NECSA-2	Activation	OSCAR-5 MCNP6 & MCNPX SCALE6 FISPACT-II	Monte Carlo Deterministic	Reactivity 100 pcm Reaction rates 30%	Reactivity 200 pcm Reaction rates 50%
TINT	Fuel burnup	MVP MCNPX CONDOR, CITVAP	Monte Carlo Deterministic	Burnup 10%	Burnup 6%

ENDF/B-VI.8 and ENDF/B-VII.0 cross-section libraries were used with Serpent 2 in the ANSTO-1 benchmark to investigate the effect of cross-section data using the same Serpent 2 model. Core reactivity was consistently higher using the ENDF/B-VII.0 library with a difference of 530 pcm averaged over critical configurations for seven cycles. This result is consistent with results from benchmarking calculations for various LEU systems, where typically 500 pcm higher values were reported for ENDF/B-VII.0 data compared to ENDF/B-VI.8 [55]. This difference is mainly due to improvements in the ^{238}U cross-section data that is important for thermal LEU systems, which led to higher accuracy of results based on ENDF/B-VII.0 data.

These results indicate that the nuclear data libraries used have an influence in the results obtained, which is not larger than differences obtained with different codes and/or different users and, in the cases mentioned above, are within values considered acceptable for the cases in question. It remains, however, important to consult the relevant consolidated report for each benchmark, given in the Annexes, to understand the factors affecting the spread in results.

4.3. SUMMARY AND OUTLOOK

The CRP provided a valuable opportunity for experts in the research reactor community to come together and share experience, lessons learned and practises applied in benchmarking and modelling activities at their facilities. The database of experiments and associated analyses represent, together with that from the previous CRP, a comprehensive collection of research reactor benchmarks to benefit the research reactor community. Originating from this CRP alone, there were a total of 53 analysis contributions for 14 experimental benchmarks originating from nine different research reactors.

The benchmarks and the results provided in this CRP cover a broad range of operational, utilization and safety related activities relevant for research reactors, addressing multicycle core and fuel element burnup and activation of irradiated materials. All benchmarks were calculated by more than one participant. Also, many participants used more than one calculational tool or

approach to evaluate a single benchmark problem. This ensured a good coverage in terms of codes, methods and modelling methodologies. The results obtained for most of the benchmark problems considered demonstrated that the codes and methods available, both deterministic and stochastic, together with the nuclear data available, yielded results that met usual operational requirements.

Fuel burnup and associated poison buildup or burnup was addressed by several of the benchmarks, and one benchmark includes a well defined core state of completely fresh fuel. This enables analysts to use the results presented here to benchmark and validate their tools, codes and methods for fuel management purposes, critical configuration predictions and fuel optimization. A typical application is often found in cycle and core reload design, as well as for calculation of safety and utilization parameters on a cycle-to-cycle basis.

Several of the benchmarks addressed the activation of targets or foils within the core or ex-core irradiation facilities. These irradiations often involve tight tolerances on activities for either patient doses or for commercial planning. As such, accurate predictions are needed, and for the benchmarks where accurate data were available, these criteria were satisfied by the calculated results.

Several of the benchmarks are of sufficiently high quality and have the level of detail and completeness necessary to be used for validation support of the codes used, specific core and reactor models developed, and to qualify the proficiency of individual code users. With respect to the last point, the benchmarks developed can be used as a training, skills development and capacity building tool in the specific areas that they address, in particular when it is noted that the benchmarks cover a broad range of types of reactors, problems and approaches.

Finally, the participants of the CRP noted that several areas important for research reactor modelling were not explicitly addressed, including some standard features of the codes (such as calculation of feedback coefficients or kinetic parameters) used in support of current safety, operational and utilization needs, as well as advanced effects and modelling capabilities. In particular, they noted that the design, operation and utilization of research reactors involves ever improving calculational methodologies for analysis of reactor physics. As examples of these, the use of best-estimate modelling approaches, combined with the propagation of associated uncertainties, is a particular area that has become standard in calculation methodologies used for nuclear power plants, but one in which much enhancement in research reactor analysis is possible. This is leading to two emerging areas in research reactor modelling that go beyond the state of the art and beyond the type of problems addressed in this publication: firstly, the use of fully coupled neutronic and thermohydraulic analysis schemes, and secondly the propagation of relevant uncertainties and calculation of sensitivities, as applied to such best estimate analysis.

REFERENCES

- [1] INTERNATIONAL ATOMIC ENERGY AGENCY, Research Reactor Benchmarking Database: Facility Specification and Experimental Data, Technical Reports Series No. 480, IAEA, Vienna (2015).
- [2] INTERNATIONAL ATOMIC ENERGY AGENCY, Benchmarking against Experimental Data of Neutronics and Thermohydraulic Computational Methods and Tools for Operation and Safety Analysis of Research Reactors – Results of a Coordinated Research Project, IAEA-TECDOC-1879, IAEA, Vienna (2019).
- [3] INTERNATIONAL ATOMIC ENERGY AGENCY, Research Reactor Benchmarking Database: Facility Specification and Experimental Data, Technical Reports Series No. 480 (Rev. 1), IAEA, Vienna (in preparation).
- [4] VILLARINO, E., LECOT, C., Neutronic calculation code CITVAP 3.1., Proc. IX Encontro Nacional de Fisica de reatores e Termo-hidraulica, Caxambu, Brazil, 25–29 October (1993).
- [5] VILLARINO, E., CONDOR Calculation Package Physor 2002, Proc. International Conference on the New Frontiers of Nuclear Technology: Reactor Physics, Safety and High-Performance Computing, Seoul, Korea (2002).
- [6] VILLARINO, E., CONDOR-CITVAP-MCNP calculation line description, Proc. National Meeting of Reactor Physics and Thermal Hydraulics, Rio de Janeiro, Brazil (2002).
- [7] SUBLET, J.-CH., et al., FISPACT-II: An Advanced Simulation System for Activation, Transmutation and Material Modelling, Nuclear Data Sheets **139** (2017) 77–137.
- [8] UK ATOMIC ENERGY AUTHORITY, The FISPACT-II User Manual (M. Fleming, T. Stainer, M. Gilbert, ed.), Report UKAEA-R(18)001, Abingdon, Oxon (2018).
- [9] BOWMAN, S.M., KENO-VI Primer: A Primer for Criticality Calculations with SCALE/KENO-VI Using GeeWiz, Oak Ridge National Laboratory Report ORNL/TM-2008/069, Oak Ridge, TN (2008).
- [10] JOHNSTON, R.R., A General Monte Carlo Neutronics Code, Los Alamos National Laboratory Report LAMS-2856, Los Alamos, NM (1963).
- [11] X-5 MONTE CARLO TEAM, MCNP – A General Monte Carlo N-Particle Transport Code, Version 5, Los Alamos National Laboratory Report LA-UR-03-1987, Los Alamos, NM (2008).
- [12] OAK RIDGE NATIONAL LABORATORY, ORIGEN 2.0: Isotope generation and depletion code – Matrix exponential method, Oak Ridge National Laboratory Report ORNL-RSIC-CCC 371, Oak Ridge, TN (1980).
- [13] OAK RIDGE NATIONAL LABORATORY, SCALE: A Comprehensive Modeling and Simulation Suite for Nuclear Safety Analysis and Design, Oak Ridge National Laboratory Report ORNL/TM-2005/39, Version 6.1, Oak Ridge, TN (2011).
- [14] LEPPÄNEN, J., Serpent – a Continuous-energy Monte Carlo Reactor Physics Burnup Calculation Code User’s Manual, VTT Technical Research Centre of Finland, 18 June 2015 (2015).
- [15] LEPPÄNEN, J., PUSA, M., VIITANEN, T., VALTAVIRTA, V., KALTIAISENAHO, T., The Serpent Monte Carlo Code: Status, development and applications in 2013, Ann. Nucl. Energy **82** (2015) 142–150.
- [16] ROBINSON, G.S., HARRINGTON, B.V., The 1998 version of the AUS modular neutronics code system, Australian Nuclear Science and Technology Organization ANSTO/E734, Lucas Heights (1998).
- [17] PELOWITZ, D.B., MCNP6 User’s Manual, Version 1.0, Rev. 0, Los Alamos National Laboratory Report LA-CP-13-00634, Los Alamos, NM (2013).

- [18] PELOWITZ, D.B., MCNPX User's Manual, Version 2.7.0, Los Alamos National Laboratory Report LA-CP-11-00438, Los Alamos, NM (2011).
- [19] ASKEW, J.R., FAYERS, F.J., KEMSHELL, P.B., A general description of the lattice code WIMS, *J. Brit. Nucl. Energy Soc.* **5** (1966) 564–585.
- [20] INTERNATIONAL ATOMIC ENERGY AGENCY, WIMS-D Library Update, IAEA, Vienna (2007).
- [21] LACOMBE, J.G., BOURET, C., KOUBBI J., MANIFACIER, L., COCONEUT: Enhancing Neutronic Design for Research Reactors, Proc. RRFM-IGORR Conference 2016, Berlin, Germany, 13–17 March (2016).
- [22] SAN-FELICE, L., ESCHBACH, R., BOURDOT, P., Experimental Validation of the DARWIN2.3 Package for Fuel Cycle Applications, *Nucl. Technol.* **184** (2013) 217–232.
- [23] MERCURE PROJECT TEAM, MERCURE 6.3: User Guide, Commissariat à l'énergie atomique et aux énergies alternatives Technical Report, CEA/DEN/DANS/DM2S/SERMA/LPEC/RT/07-4125/A.
- [24] SUTEAU, C., CHIRON, M., ARNAUD, G., Improvement of Mercure-6's General Formalism for Calculating Gamma-Ray Build-up Factors in Multilayer Shields, *Nucl. Sci. Eng.* **147** (2004) 43–55.
- [25] TRIPOLI-4 PROJECT TEAM, TRIPOLI-4 Version 10 User Guide, Commissariat à l'énergie atomique et aux énergies alternatives Technical Report, CEA/DEN/DANS/DM2S/SERMA/LTSD/RT/15-5928/A.
- [26] DIOP, C.M., et al., TRIPOLI-4: A 3D continuous-energy Monte Carlo transport code, Proc. First International Conference on Physics and Technology of Reactors and Applications (PHYTRA1), Marrakech, Morocco, 14–16 March (2007).
- [27] MARLEAU, G., HÉBERT, A., ROY, R., A user guide for DRAGON version 4, Institut de Génie Nucléaire, Technical Report IGE-294, Montréal (2011).
- [28] BRIESMEISTER, J.F. (Ed.), MCNP – A General Monte Carlo N-Particle Transport Code, Version 4B, Los Alamos National Laboratory Report LA-12625-M, Los Alamos, NM (1997).
- [29] KRAKOVICH, A., NEDER, I., STEINITZ, U., HAZENSHPRUNG, N., Whole-Core Monte-Carlo Simulations and Experimental Measurements of IRR1 Fuel Depletion During More Than Thirty Years of Operation, Proc. PHYSOR 2018, Cancun, Mexico, 22–26 April (2018).
- [30] PELOWITZ, D.B. (Ed.), MCNPX User's Manual, Version 2.6.0, Los Alamos National Laboratory Report LA-CP-07-1473, Los Alamos, NM (2008).
- [31] PRINSLOO, R., et al., Recent developments of the OSCAR calculational system, as applied to selected examples from IAEA research reactor benchmarks, Proc. 18th IGORR Conference, Sydney, Australia, 3–7 December (2017).
- [32] NAGAYA, Y., OKUMURA, K., SAKURAI, T., MORI, T., MVP/GMVP Version 3: General Purpose Monte Carlo Codes for Neutron and Photon Transport Calculations Based on Continuous Energy and Multigroup Methods, Japan Atomic Energy Agency JAEA-Data/Code 2016-018 (2017).
- [33] OECD NUCLEAR ENERGY AGENCY, Joint Evaluated Fission and Fusion (JEFF) Nuclear Data Library, <https://www.oecd-nea.org/dbdata/jeff>
- [34] HFAIEDH, N., SANTAMARINA, A., Determination of the optimized SHEM mesh for transport calculation, Proc. International Topical Meeting on Mathematics and Computation, Supercomputing, Reactor Physics and Nuclear and Biological Applications, Avignon, France, 12–15 September (2005).
- [35] SANTANDREA, S., SANCHEZ, R., Acceleration techniques for the characteristic method in unstructured meshes, *Ann. Nucl. Energy* **29** (2002) 323–352.
- [36] VILLARINO, E., MOCHI, I., SARTORIO, P., INVAP Neutronic Calculation Line, *Mecánica Computacional XXXIII* (2014) 3217–3226.

- [37] VILLARINO, E., ALBERTO, P., ALBORNOZ, F., DOVAL, A., HERGENREDER, D., INVAP Nuclear Engineering Department Calculation Suite, Proc. 39th RERT International Meeting 2018, Edinburgh, Scotland, 4–7 November (2018).
- [38] FOWLER, T.B., VONDY, D.R., Nuclear Core Analysis Code: CITATION, Oak Ridge National Laboratory Report ORNL-TM-2496, Oak Ridge, TN (1969).
- [39] FOWLER, T.B., VONDY, D.R., CUNNINGHAM, G.W., Nuclear Reactor Core Analysis Code CITATION, Oak Ridge National Laboratory Report ORNL-TM-2496 (Rev. 2), Oak Ridge, TN (1971).
- [40] INTERNATIONAL ATOMIC ENERGY AGENCY, Research Reactor Core Conversion from the Use of Highly Enriched Uranium Fuels: Guidebook, IAEA-TECDOC-233, IAEA, Vienna (1980).
- [41] INTERNATIONAL ATOMIC ENERGY AGENCY, Evaluated Nuclear Data File (ENDF), <https://www-nds.iaea.org/exfor/endl.htm>
- [42] KONING, A.J., et al., TENDL: Complete Nuclear Data Library for Innovative Nuclear Science and Technology, Nuclear Data Sheets **155** (2019) 1–55.
- [43] KONING, A.J., ROCHMAN, D., SUBLET, J.-CH., TALYS-based evaluated nuclear data library, https://tendl.web.psi.ch/tendl_2019/tendl2019.html
- [44] FLEMING, M., EASTWOOD, J., STAINER, T., DAVID, J.-C., MANCUSI, D., HEIR: A High-Energy Intra-Nuclear Cascade Liège-based Residual nuclear data library for simulation with FISPACT-II, Nucl. Instrum. Methods Phys. Res., Sect. A **908** (2018) 291–297.
- [45] SHIBATA, K., et al., JENDL-4.0: A New Library for Nuclear Science and Engineering, J. Nucl. Sci. Technol. **48** (2011) 1–30.
- [46] JAPAN ATOMIC ENERGY AGENCY, JENDL – Japanese Evaluated Nuclear Data Library, <https://www.ndc.jaea.go.jp/jendl/jendl.html>
- [47] CHINA NUCLEAR DATA CENTER, CENDL-3.1 – The Chinese Evaluated Nuclear Data Library https://www.oecd-nea.org/dbforms/data/eva/evatapes/cendl_31/
- [48] SCHMIDT, K.-H., JURADO, B., GEF – GEneral Fission model, <https://www.cenbg.in2p3.fr/GEneral-Fission-model>
- [49] WILSON, W.B., et al., A Manual for CINDER’90 Version 07.4 Codes and Data, Los Alamos National Laboratory Report LA-UR-07-8412, Los Alamos, NM (2008).
- [50] INTERNATIONAL COMMISSION ON RADIOLOGICAL PROTECTION, Conversion Coefficients for use in Radiological Protection against External Radiation, ICRP Publication 74, Ann. ICRP 26 (3-4) (1996).
- [51] RADEMAKERS, F., BRUN, R., ROOT: An Object-Oriented Data Analysis Framework, Linux Journal **51** (1998) 6.
- [52] INTERNATIONAL ATOMIC ENERGY AGENCY, Fusion Evaluated Nuclear Data Library (FENDL), <https://www-nds.iaea.org/fendl/>
- [53] INTERNATIONAL ATOMIC ENERGY AGENCY, International Reactor Dosimetry and Fusion File (IRDF) v.1.05, <https://www-nds.iaea.org/IRDFv105/>
- [54] INTERNATIONAL ATOMIC ENERGY AGENCY, International Reactor Dosimetry File 2002 (IRDF-2002), Technical Reports Series No. 452, IAEA, Vienna (2006).
- [55] CHADWICK, M.B., et al., ENDF/B-VII.0: Next Generation Evaluated Nuclear Data Library for Nuclear Science and Technology, Nuclear Data Sheets **107** (2006) 2931–3060.

ANNEX I

BENCHMARK CONSOLIDATED RESULTS AGAINST EXPERIMENTAL DATA FROM ANSTO-1

I-1. INTRODUCTION

The ANSTO-1 benchmark analysis, including the reactor specification and experimental data, is documented in Ref. [I-1]. The benchmark evaluates the capability to perform fuel depletion, which is indirectly assessed using estimates of the core reactivity for critical core configurations. Computer codes and models are an integral part of the safety analyses, utilization and optimization of modern research reactors. At the many nuclear organizations that operate and utilize research reactors, computer codes are used for day-to-day operational support and for safety related parameters of the reactor. This includes a range of deterministic based reactor code systems such as CONDOR-CITVAP [I-2], OSCAR-5 [I-3] and COCONEUT2.0 [I-4] for reactor physics, fuel management and operational optimization. In addition, the Monte Carlo based codes TRIPOLI-4 [I-5] and Serpent 2 [I-6] show promise for being used to follow core burnup and provide detailed three-dimensional representations of the reactor and facilities. All of these codes and methods have a range of capabilities and corresponding limitations. This Annex presents results from the benchmarking of all these codes for the ANSTO-1 benchmark.

I-2. SUMMARY OF THE BENCHMARK SPECIFICATION AND CODES AND MODELS USED

I-2.1. Summary of the benchmark specification

The goal of the benchmark is to perform multicycle burnup of the core and follow the evolution of the core over OPAL (Open Pool Australian Light water reactor) operating cycles 7 to 13 by calculating the core reactivity for the critical configurations provided. To enable the analyst to perform these calculations, the following details were provided as part of the benchmark:

- Detailed reactor specification to allow modelling of the relevant components of the reactor;
- The fuel management strategy for the relevant cycles;
- Operational data including reactor power as a function of time and critical control rod positions at specified times.

The initial core configuration (cycle 7) was a clean core with no burnup and so allows for a well-defined initial core state. The burnup requires burnup of the fuel and associated cadmium wires in the fuel used as burnable poison to manage core reactivity and axial power profile.

I-2.2. Summary of the codes and libraries used

The codes and associated cross-section libraries used to perform the burnup and reactivity calculations are presented in Table I-1. All participants used both deterministic and stochastic based codes to perform the benchmark.

TABLE I-1. CODES AND LIBRARIES USED BY PARTICIPANTS

Participant	Code (library)
Argentina	CONDOR 2.7.01 – CITVAP 3.9.04 (ENDF/B-VII.0) Serpent 2.1.29 (ENDF/B-VI.8 and ENDF/B-VII.0)
Australia	CONDOR 2.55 – CITVAP 3.5 (WIMS69 and HELIOS for Hf) Serpent 2.1.22 (ENDF/B-VII.0)
France	COCONeut2.0 (JEFF-3.1.1) TRIPOLI-4.10 (JEFF-3.1.1)
South Africa	OSCAR-5/MGRAC (JEF-2.2 and ENDF/B-VII.1) OSCAR-5/Serpent 2.1.29 (ENDF/B-VII.1)

I-2.3. Summary of the models used

The models constructed and the assumptions adopted for the various calculations are presented for each of the participants.

I-2.3.1. Argentina (ARG) models

The proposed ARG scheme for the ANSTO-1 benchmark is to develop alternate calculation approaches for burnup calculations that consider diverse paths. The design and calculation for reactor cores includes several steps of increasing complexity and intended accuracy, with each approach relevant to different engineering design stages. As a result, the process is characterized by an increasing level of calculation detail and several steps including, but not limited to:

1. A preliminary estimation of core parameters considering a burnup evolution with all rods out (ARO) and constant (nominal) power.
2. An estimation considering critical control rod positions for burnup evolution with constant power.
3. A detailed estimation considering critical control rod position and burnup evolution at actual power (namely all xenon and samarium transients).
4. A detailed independent verification with alternative methods (usually Monte Carlo based codes).

The increase in detail from step 1 to 4 is usually reflected as increasing calculation time and CPU and memory requirements.

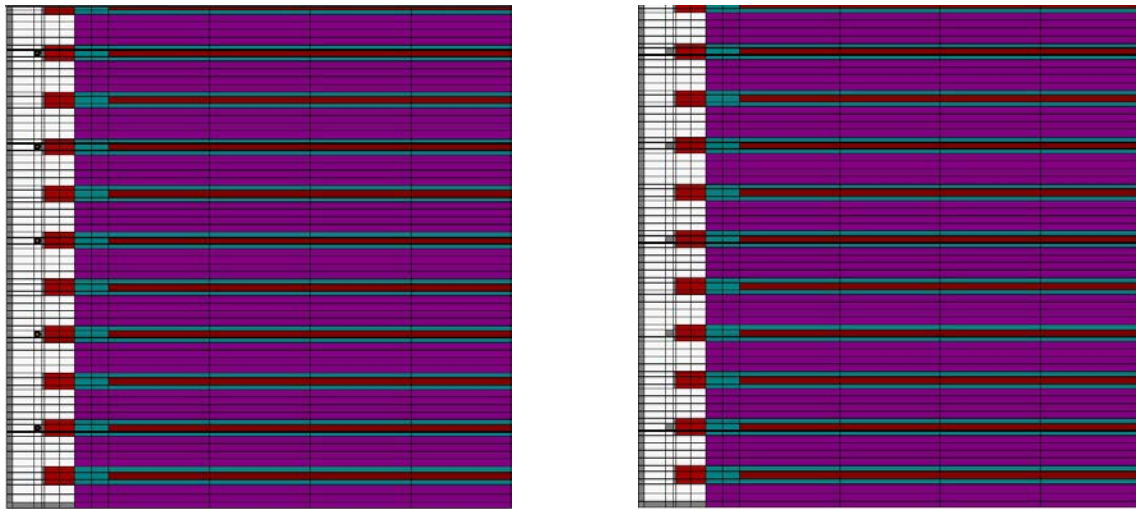
I-2.3.1.1. CONDOR-CITVAP models

The first step involves a series of cell calculations performed using the multigroup heterogeneous response method code CONDOR for the relevant components, to obtain homogenized and condensed few group constants. In the second step, a full 3-D finite difference diffusion model is developed in CITVAP, using the constants obtained in CONDOR for each material zone.

A complete 3-D model was developed considering the data and control rod positions as reported in Ref. [I-1].

Cell models (CONDOR)

The 2-D cell level models were developed in the updated CONDOR 2.7.01, considering both the components inside and outside the core. Examples for CONDOR fuel assembly (FA) models are presented in Fig. I-1.



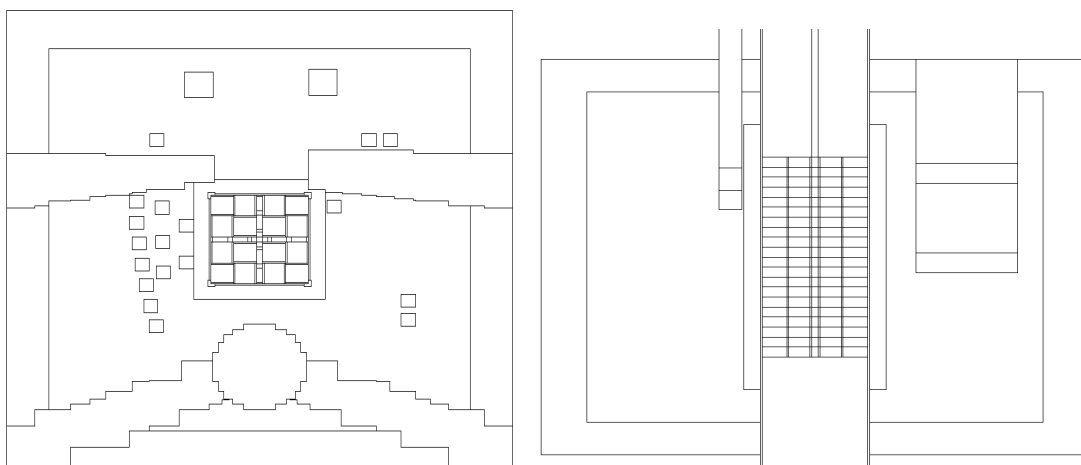
a) Cell model $\frac{1}{4}$ FA with burnable poison

b) Cell model $\frac{1}{4}$ FA without burnable poison

FIG. I-1. CONDOR cell-level models with and without burnable poison. (courtesy of INVAP, Argentina)

Core models (CITVAP)

The 3-D core level models were developed in CITVAP 3.9.04, considering both the components inside and outside the core. These models have been presented in Ref. [1-7], where some minor updates were performed. The homogenized few group parameters obtained from the CONDOR models were inserted in the corresponding CITVAP zone. The revised CITVAP models are presented in Fig. I-2.



a) x-y plot at centre of active length

b) y-z plot at centre of active length

FIG. I-2. CITVAP 3-D core-level models. (courtesy of INVAP, Argentina)

Regarding core burnup, the benchmark specifies the reactor power and the control rod position against time during reactor operation. As has been previously stated, the following approaches were used regarding reactor power and time:

- (a) Full power calculation for burnup with ARO and then critical calculation after burnup.
- (b) Full power calculation at critical burnup.
- (c) Variable power against real time.

In order to deal with approach 1 and 2, the control rod information was processed to simulate the operation of the reactor at full power against full power daytime unit. This approximation does not allow the simulation of the xenon concentrations changes after power transients (mainly after restart), but it is a reasonable approximation for the benchmark analysis.

For all CONDOR-CITVAP cases, the WLUP 69 group nuclear data library was used [I-8] at cell level. Furthermore, the homogenization and condensation procedure considered three energy groups at core level, with the energy limits presented in Table I-2.

TABLE I-2. CONDENSATION ENERGY LIMITS FOR CITVAP CALCULATION

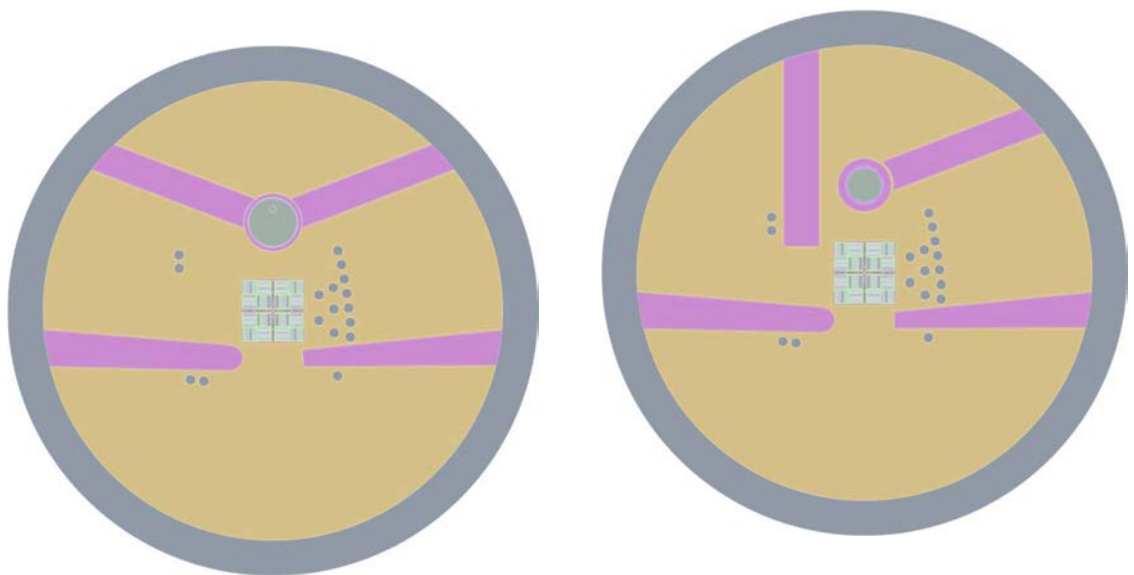
Group	Lower limit [MeV]	Upper limit [MeV]
1	0.821	10 (from library)
2	0.625E-6	0.821
3	0	0.625E-6

I-2.3.1.2. Serpent model

A complete 3-D model was developed in Serpent, considering data and control rod positions as reported in Ref. [I-1]. A highly detailed geometry was adopted including:

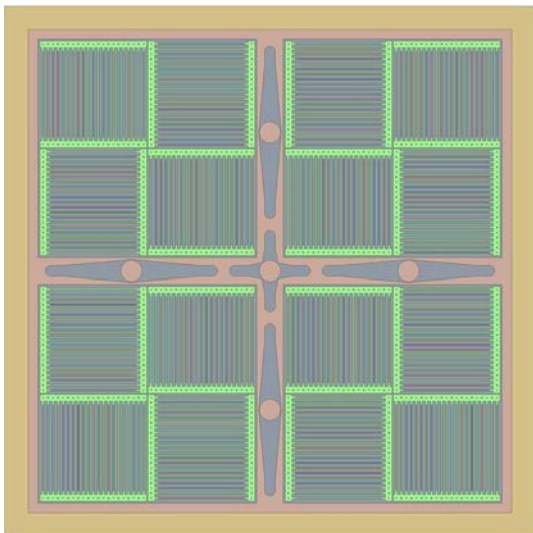
- (a) A full 3-D core model, where each fuel assembly was considered independently. Ten axial zones and individual materials were considered for each fuel plate (meat zone). Furthermore, for those fuel assemblies with cadmium wires (burnable poisons), independent materials were considered, with five axial zones and four radial divisions. This scheme results in up to 9760 materials to be evolved in burnup cases.
- (b) All main structural components, such as the core chimney and the reflector vessel.
- (c) The detailed control rods, including the plate-type CR1 to CR4 and the cross-type regulating CR5.
- (d) The most relevant experimental devices present in the reflector vessel, such as bulk irradiation positions, thermal beams and cold beams. Furthermore, a simplified model for the cold neutron source was included.

The main model features are presented in Fig. I-3. Burnup was performed with the ARO configuration and then critical configuration calculations were performed for the reactivity evaluation.

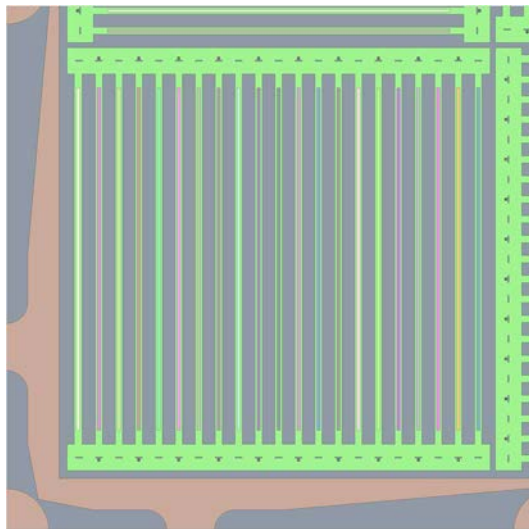


a) Full x-y plot at centre of active length

b) Full x-y plot 5 cm below centre of active length



c) Core detail x-y plot at centre of active length



d) Fuel detail x-y cut. Materials can be appreciated

FIG. I-3. Various details of the Serpent model. (courtesy of INVAP, Argentina)

I-2.3.2. Australia (AUL) models

I-2.3.2.1. CONDOR-CITVAP models

The starting point for the neutronic calculations was a 69 group nuclear data library based on the WIMS library and data from the HELIOS library. Cell calculations were performed using CONDOR for the fuel assemblies, control rods, other core components and irradiation facilities. A 3-group (thermal, epithermal and fast) cross-section library was developed using the various cell models. A one quarter two-dimensional model of a fuel assembly is shown in Fig. I-4. It indicates the detail represented in the CONDOR model used for cross-section preparation including the fuel meat, clad, coolant, side plate and cadmium burnable wires.

The whole reactor CITVAP model was optimized for quick run times and contains about 3.1 million mesh points. The detail in the model is indicated in the horizontal cross-section in Fig. I-5. The model is three-dimensional.

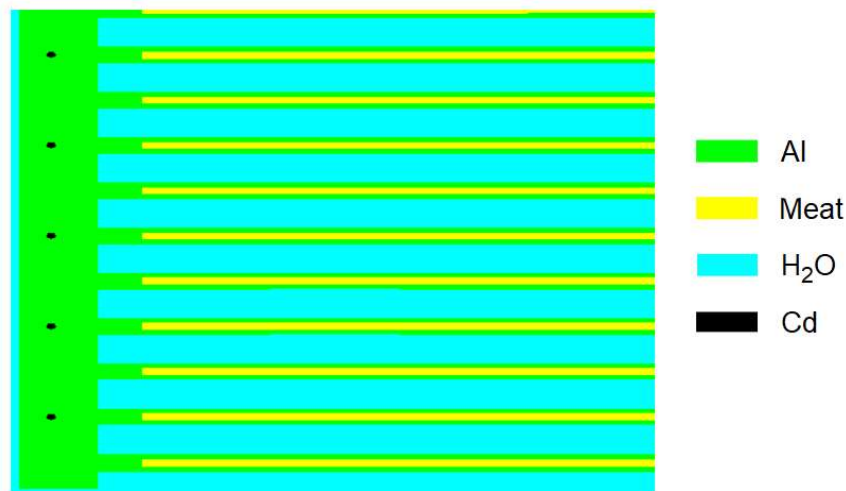


FIG. I-4. CONDOR cell model of one quarter of a fuel assembly. (courtesy of ANSTO, Australia)

Some important and noteworthy features of the reactor model include:

- (a) Separate representation of fuel plate-coolant region and side plate region in fuel assemblies. This allows accurate calculation of the respective fluxes and spectrum for each region which can vary significantly across a fuel assembly.
- (b) Explicit representation of all irradiation facilities close to the core. This allows accurate calculation of the overall core reactivity and any asymmetric power tilt in the core.
- (c) Explicit representation of beam facilities including the cold neutron source. These large regions of effective void have a significant effect on the core reactivity and core power distribution. The helium inside the beam tubes was represented by 10% density heavy water to facilitate convergence of the diffusion solution and account for the reactivity and power tilt effects. It will not provide reliable fluxes within the beam tubes as they will be highly directional and require discrete ordinates or other methods but will reproduce the global effects.
- (d) The use of different heavy water cross-sections depending on distance from core. Three sets of cross-sections were obtained by condensing over the relevant neutron spectrum at three regions in the reflector. This is important for the slowing down of neutrons within the reflector region and contribution to core reactivity.
- (e) The detailed structure above and below the core, specifically the core grid and the upper fuel assembly zone were not modelled. Instead these regions were modelled as simply light water. This will produce local artefacts but have only a slight impact on the global parameters of interest here.

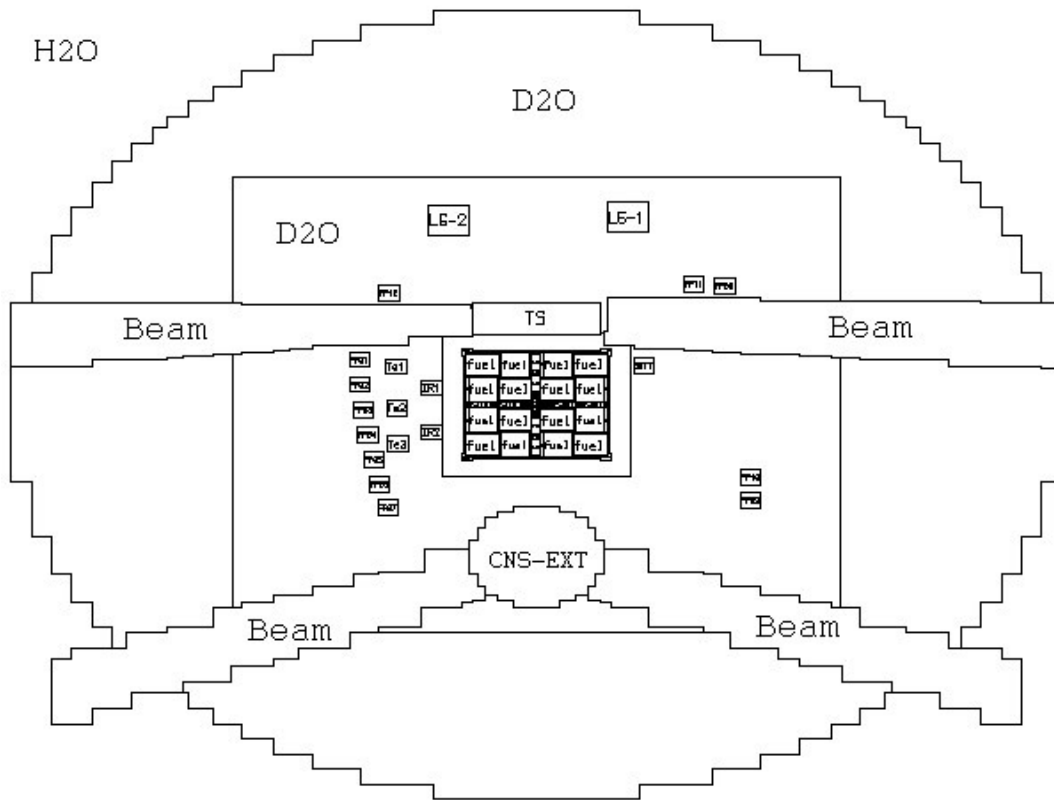


FIG. I-5. Radial cross-section of CITVAP reactor model at core centreline. (courtesy of ANSTO, Australia)

I-2.3.2.2. Serpent model

The model used in Serpent was comprised of the core, chimney, heavy water reflector, near-core facilities and 30 cm thickness of light water around the reflector vessel. Each component is explicitly modelled. For the fuel assembly, for example, each fuel plate with explicit cladding, fuel meat, side plates, inlet nozzle and the cadmium wires was represented. Each simulation was run with 64 000 neutrons/cycle for 1000 cycles with 100 inactive cycles. A typical uncertainty for k_{eff} was ± 0.00012 . To allow for efficient manipulation of the input and output files and to automate some processes, such as control rod positions, an Excel spreadsheet was used to build the model and manage the various input files. Figures I-6 and I-7 show radial and axial views from the Serpent model used in this work at the core centreline. Although all facilities present in the reactor were included in the model, only facilities that were provided as part of the benchmarking were actually implemented. The other facilities were flooded with heavy water so effectively were not present, to be consistent with the benchmark specification [I-1].

Each fuel assembly was burnt with 10 material axial zones and the cadmium wires were burnt in groups of 5 (4 groups per fuel assembly) in 5 axial zones and 5 radial regions, resulting in a total of 1760 burnable materials.

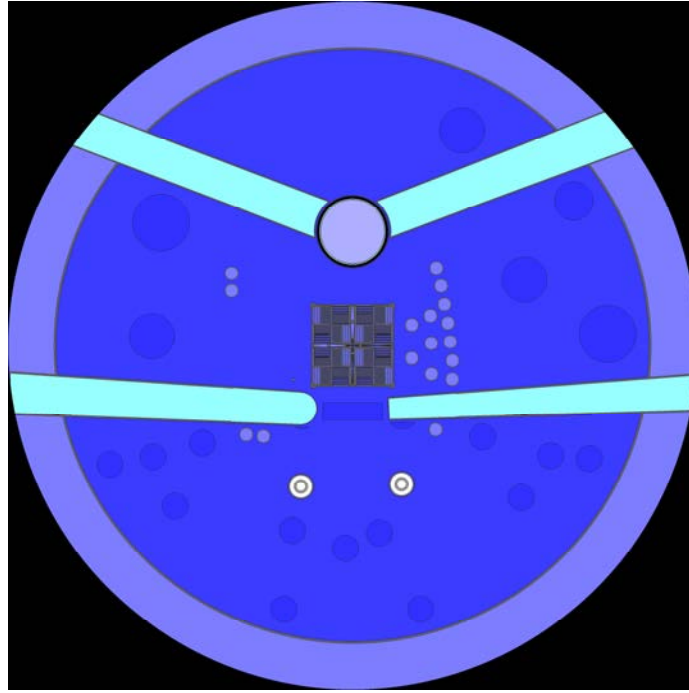


FIG. I-6. Radial cross-section of Serpent reactor model at core centreline. (courtesy of ANSTO, Australia)

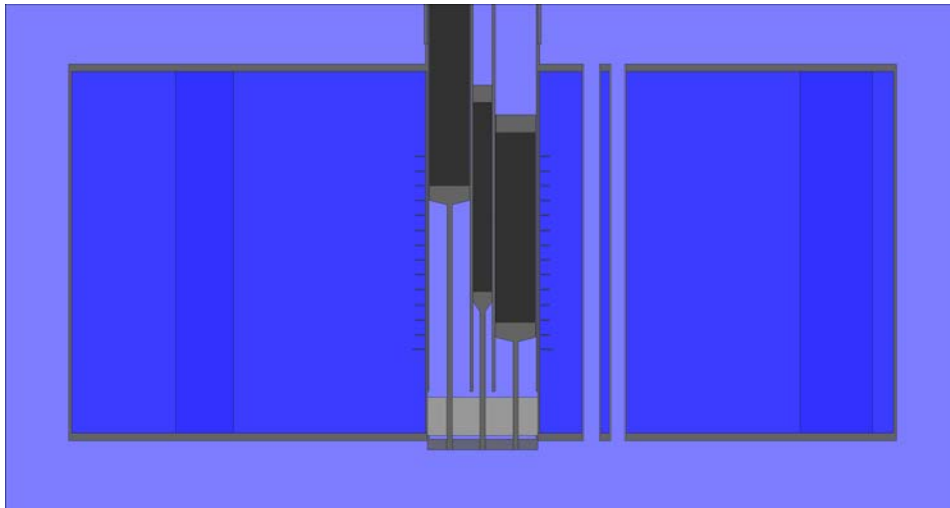


FIG. I-7. Axial cross-section of Serpent reactor model at core centreline. (courtesy of ANSTO, Australia)

I-2.3.3. France (FRA) models

I-2.3.3.1. COCONEUT

COCONEUT uses SILENE as a geometry interface. It is user-friendly and enables a quick generation of 2-D or 3-D cylindrical and Cartesian features together in variable meshes. It leads to geometries which are quite close to reality (see Fig. I-8). In this case, however, no beam tubes were modelled for simplicity reasons (see Fig. I-9). This leads to a bias in calculations that will be discussed along with the results.

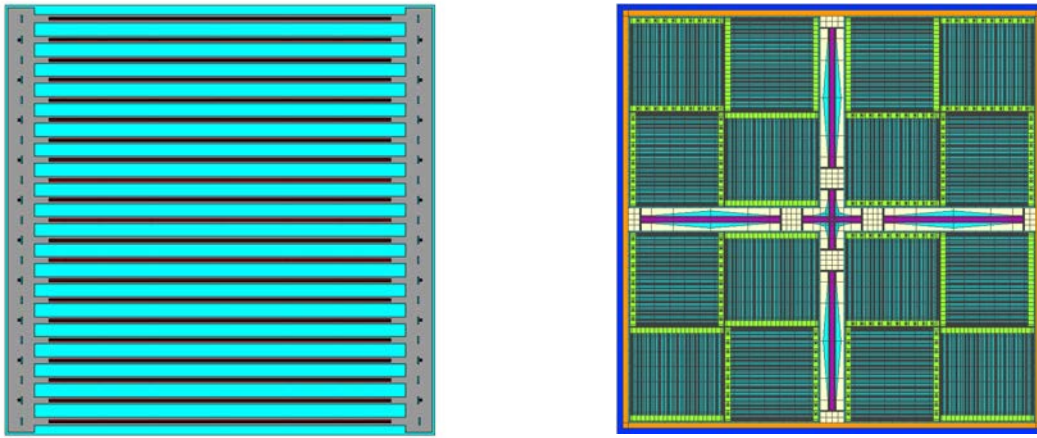


FIG. I-8. 2-D SILENE model of OPAL fuel assembly and core. (courtesy of TechnicAtome, France)

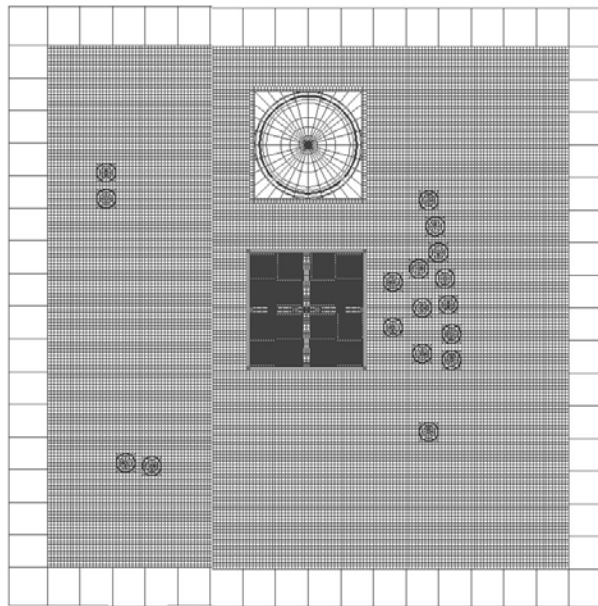


FIG. I-9. 2-D SILENE model of the OPAL reactor. (courtesy of TechnicAtome, France)

When running depletion calculations, the computed APOLLO2 model uses 5×8 meshes in the fuel meat, per fuel plate and 4×5 meshes per cadmium wire (see Fig. I-10).

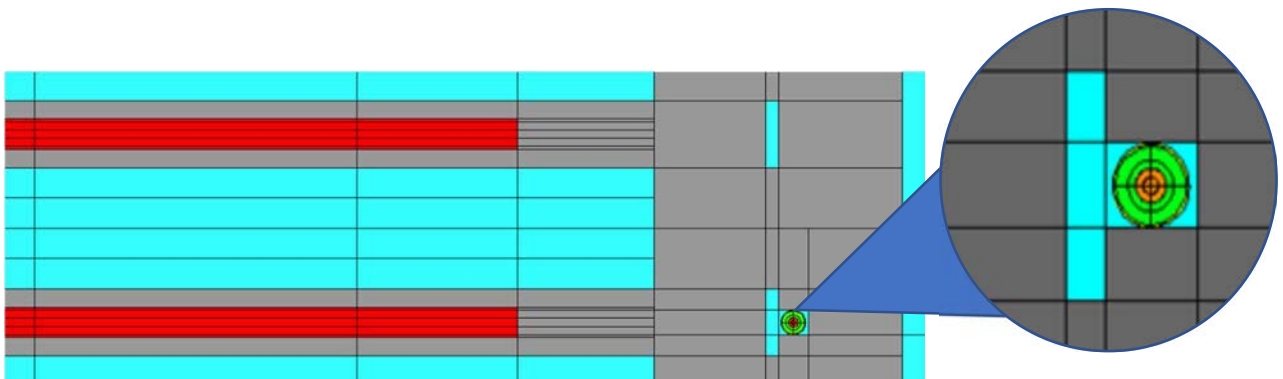


FIG. I-10. 2-D SILENE model of the OPAL fuel plates with Cd wires. (courtesy of TechnicAtome, France)

In its 3-D version, the structure of CRONOS2 imposes a Cartesian mesh. Thus, several approximations were introduced, namely:

- (a) The control rod guide boxes are rectangular (as in Fig. I-11);
- (b) The outer part of the reflector is not modelled. The reflector tank is square (260 cm) with 30 cm of light water around it (Fig. I-12);
- (c) The purity of heavy water is constant (97.5%, as for cycle 7). A correction for changes in heavy water purity is implemented using the TRIPOLI calculation.

When running depletion calculations, the CRONOS2 model computed uses 29 axial meshes in the fuel meat and 15 axial meshes in the cadmium wires.

As a first approach, CRONOS2 was used in its homogeneous version. Each FA was fully homogenized with fuel, aluminium, water and cadmium wires as in Fig. I-11 (left) and Fig. I-13 (left). In addition, an intermediate version with a semi-heterogeneous FA was also modelled (later referred to as “heterogeneous” for these results). Mixing cadmium wires in a fully homogeneous fuel assembly is expected to increase the efficiency of this poison as it is no longer self-shielded. The adopted model for the fuel assembly has a fuel zone that is homogenized, but side plates and water in between are separated (Fig. I-11 right and Fig. I-13 right). This modelling enables the cadmium wires to be fully described.

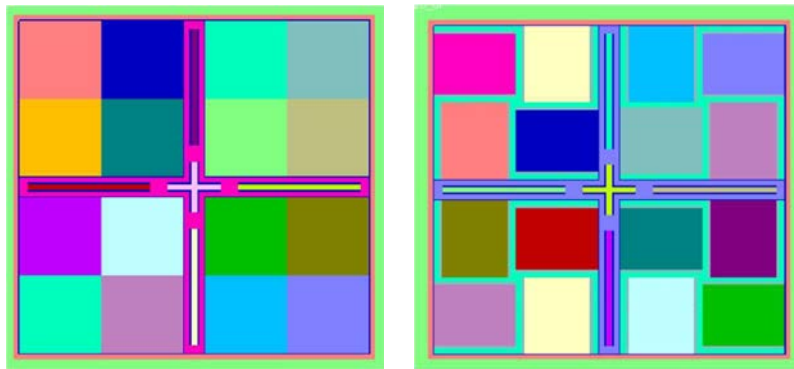


FIG. I-11. Views of the 3-D CRONOS2 model of the OPAL core, homogeneous (left) and semi-heterogeneous (right). (courtesy of TechnicAtome, France)

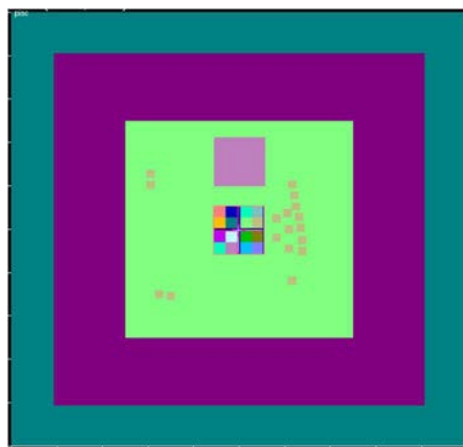


FIG. I-12. 3-D CRONOS2 model of the OPAL reactor. (courtesy of TechnicAtome, France)

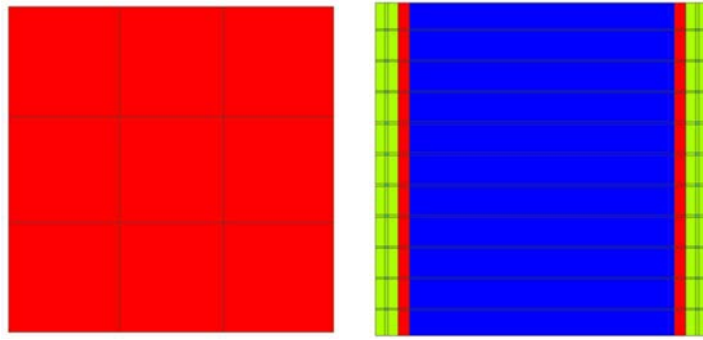


FIG. I-13. Two different CRONOS2 models of the FA: homogeneous (left) and semi-heterogeneous (right) in which the side plates are fully described with Cd wires (green), water on the side is red and the fuel part (blue, centre) is homogenized with its water and cladding. (courtesy of TechnicAtome, France)

I-2.3.3.2. TRIPOLI-4.10

TRIPOLI-4.10 models were built with ROOT [I-9]. The full 3-D capabilities of TRIPOLI-4.10 and the ROOT toolkit make it simple to include all details in the model including the reflector purity and temperature and choice of experimental devices in the reflector. All experimental facilities were easily created and verified using the TRIPOLI-4 viewer, which is also compatible with the ROOT geometry.

Figures I-14 and I-15 illustrate the ROOT generated TRIPOLI-4 model used in this study.

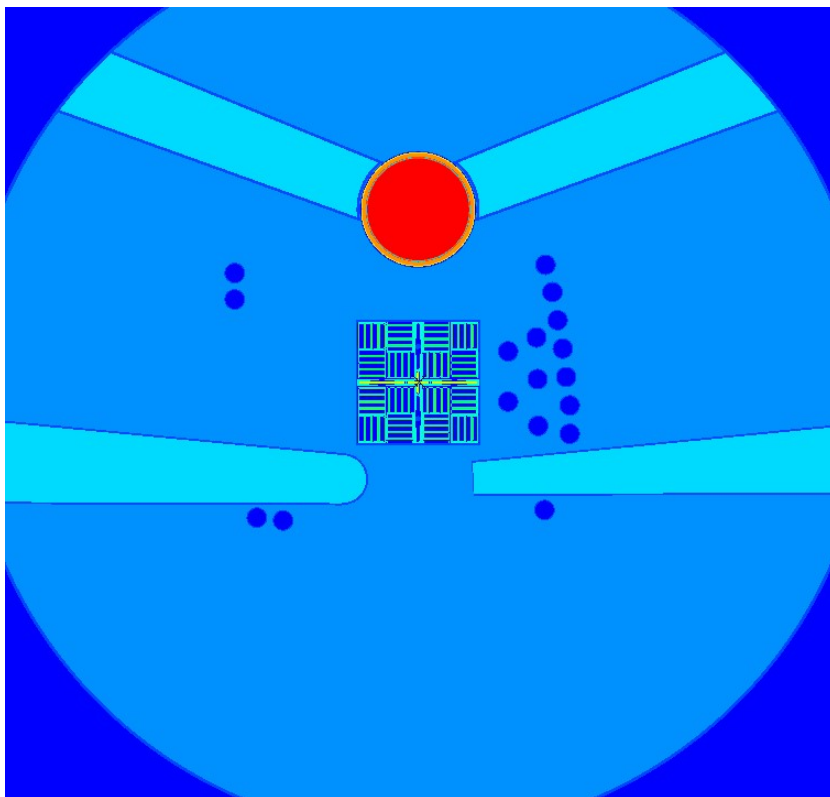


FIG. I-14. ROOT geometry of the TRIPOLI-4 OPAL reactor model. (courtesy of TechnicAtome, France)

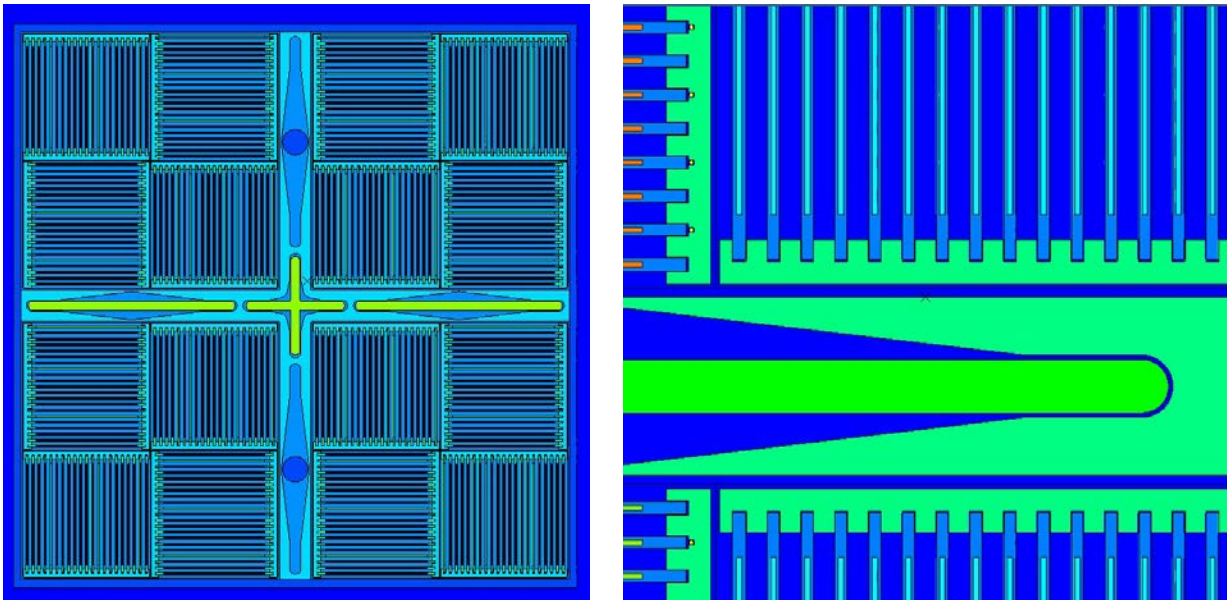


FIG. I-15. ROOT radial geometry of the TRIPOLI-4 OPAL core model. (courtesy of TechnicAtome, France)

As part of this work in its depletion mode, TRIPOLI-4 is run with the two following features: (i) a simple model with one depleted material per cadmium wire (i.e. 20 per FA) and one depleted material per fuel plate (i.e. 21 per FA); and (ii) a more detailed model with 3 axial depleted materials per cadmium wire (i.e. 60 per FA) and 6 axial depleted materials per fuel plate (i.e. 126 per FA).

These simple features have deliberately been computed as a first step in the benchmark. However, due to very satisfactory results (see Section I-3.1.3.2), there is no need for finer meshing in the depleting materials since this would be very time consuming with little gain expected. Any further effort would be dedicated to adding radial meshes in cadmium wires or fuel plates to capture changes in this spatial plane.

TRIPOLI-4 depletion was performed using the simple Euler method, assuming, for each burnup step, the flux is constant and equal to that at the beginning of the step.

I-2.3.4. South Africa (SFA) models

The OSCAR-5 system allows the creation of unified models, which can be exported to different target codes. This ensures consistency between the models for different codes. The system was used to prepare a detailed model for the ANSTO-1 benchmark problem (see Fig. I-16).

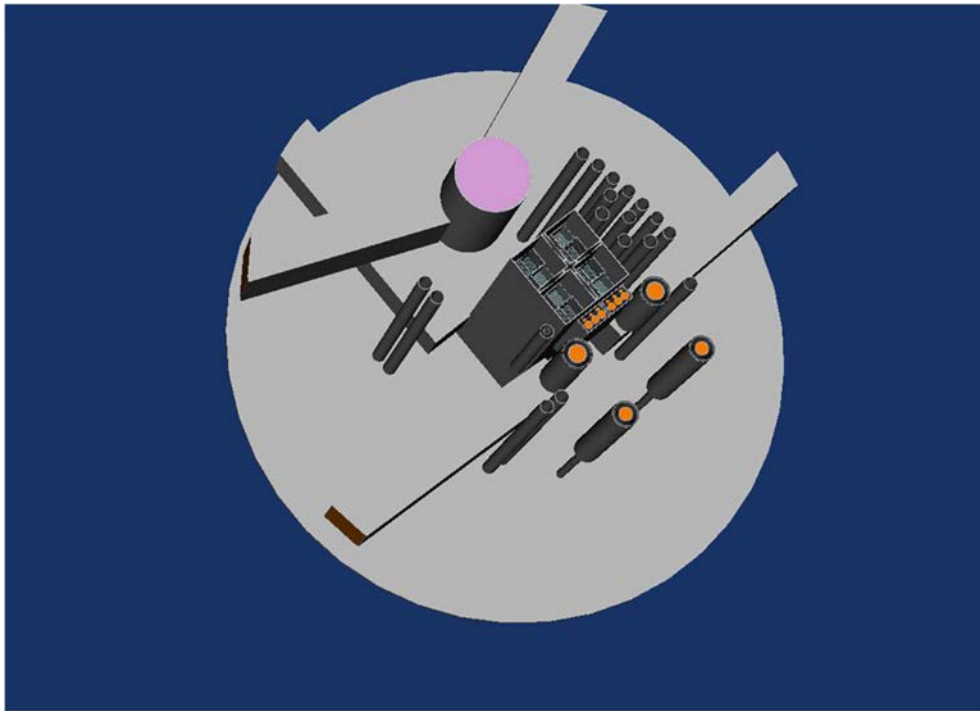


FIG. I-16. View of the OSCAR-5 OPAL reactor model. (courtesy of Necsca, South Africa)

This model was exported to Serpent to perform criticality and burnup analysis. The model was also used to generate a set of homogenized cross-sections and the associated nodal model for the deterministic nodal solver MGRAC, to perform the same set of calculations. The process is depicted in Fig. I-17.

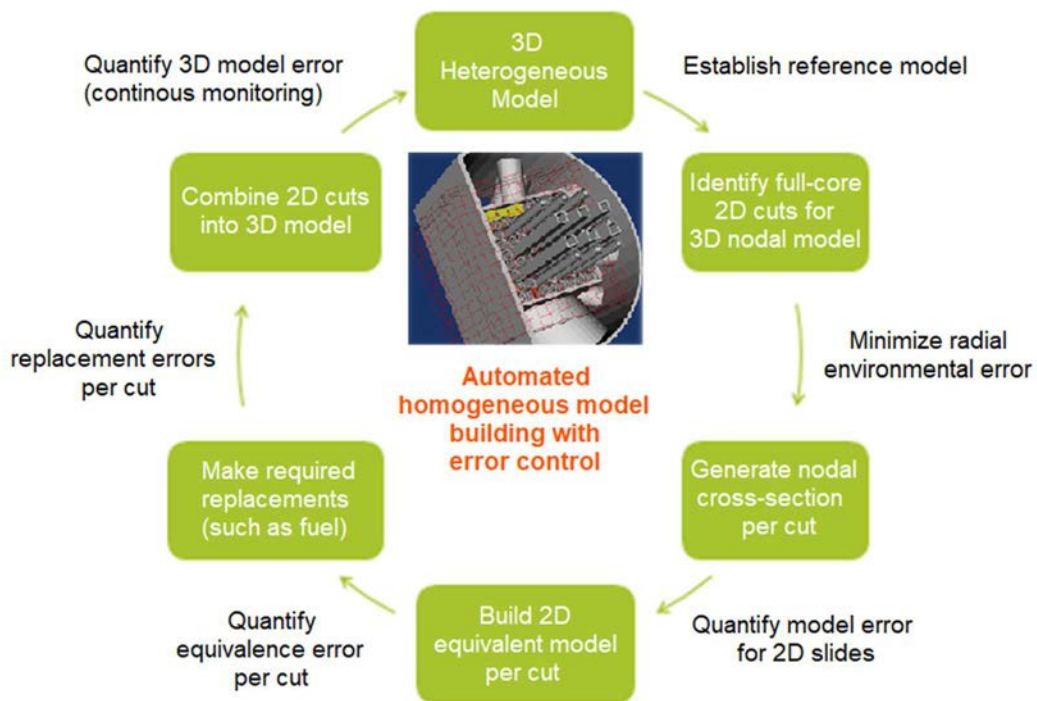


FIG. I-17. Nodal model generation process. (courtesy of Necsca, South Africa)

As shown in Fig. I-17, the nodal model was developed in a staged process, allowing control of the model error as compared to the reference heterogeneous Serpent model. In particular, all non-fuel homogenized multigroup cross-sections were generated from a set of 2-D full core heterogeneous calculations, while fuel models were generated from an infinite lattice environment. The OPAL core, however, represents a challenging problem for a nodal model, as the assumption of a typical fuel environment is not straight forward. To address this, the model building was performed in the following fashion.

1. Analysis of the full problem and determination of the set of cuts required. A set of six cuts through the core was devised which would yield cross-sections at all relevant layers to use in the construction of a nodal core model.
2. Considering the active core, there are three specific full core cuts which capture the various levels of complexity present in the problem very well. Each will be considered in detail, applying the standard approach in model generation, but showing how additional code features have to be applied in order to deal with the complexities of the OPAL core. These cuts are:
 - (a) Unrodded, unwired cut (ARO-UNW);
 - (b) Unrodded, wired cut (ARO-W);
 - (c) Rodded, wired cut (ARI-W).
3. For these cuts, 2-D errors associated with the cross-section generation process and the infinite lattice replacement step were assessed. A series of correction schemes to improve the model were evaluated. These were:
 - (a) Use of a special homogenization scheme for the burnable poisons, namely the usage of assembly side-flux based averaged cross-sections, as opposed to node-averaged flux (termed BA treatment);
 - (b) Use of the nodal rehomogenization scheme to correct the node-average cross-sections for the actual core environment;
 - (c) Use of colourset cross-sections for fuel representation as opposed to the more standard infinite lattice approach, specifically for core positions where this was deemed necessary (termed coloursets);
 - (d) Replacement of the standard nodal core representation with a subdivided representation of 3×3 subzones for each fuel assembly. This was done for two reasons: (i) to improve subzone burnup; and (ii) to improve separation of control rods per nodal mesh for more accurate movement of rods.

Table I-3 shows the staged results of the model building process and the errors introduced at each step the effective multiplication factor k_{eff} and the power of the fuel assembly.

TABLE I-3. ERROR CONTROL DURING MODEL BUILDING PROCESS

Model description	k_{eff}	k_{eff} error (pcm)	Power error Average (Max.) (%)	Subdivided k_{eff}
Serpent 2-D ARO – UNW	1.23959			
MGRAC 2-D ARO – UNW	1.23991	32	0.07 (0.17)	1.23979
Infinite lattice fuel	1.24739	780	0.68 (1.41)	1.24818
Serpent 2-D ARO-W	1.17014			
MGRAC 2-D ARO-W	1.17027	13	0.06 (0.15)	1.17025
Infinite lattice fuel	1.19462	2448	1.29 (2.7)	1.18765
BA treatment	1.16232	-782	1.16 (2.7)	
Serpent 2-D ARI-W	0.94345			
MGRAC 2-D ARI-W	0.94370	15	0.07 (0.15)	
Infinite lattice fuel	0.95964	1619	2.9 (4.8)	
BA treatment	0.94160	-185	2.0 (4.8)	
Serpent 3-D rods mid core	1.00802			
MGRAC 3-D rods mid-core	1.00499	-303	1.98 (4.1)	

The use of this approximate environment in generating fuel cross-sections introduces an environmental error in the nodal equivalence parameters. This error can be seen when going from a “MGRAC 2-D calculation” to a “MGRAC 2-D calculation with infinite fuel replacement”. This error is larger for cases that contain wires when no BA treatment is used, because their effect on the flux shape and spectrum is highly localized. The use of the BA treatment does, however, mitigate this effect to a large degree for reactivity, although less so for assembly power errors.

It is interesting to note that the largest errors in assembly power occur in the all rods in wired case (ARI-W), while the largest errors in k_{eff} occur in the all rods in out wired case (ARO-W). The use of coloursets to reduce the environmental error was explored, but deemed to be infeasible.

The nodalized model, as discussed earlier, applies a subdivided meshing scheme in the fuel assemblies. Fuel assemblies are subdivided into a 3×3 representation as shown in Fig. I-18. One can observe from Table I-3 that the effect of this subdivision was to reduce the k_{eff} error from 2448 pcm to 1751 pcm by better accounting for the local flux distribution through the assembly. In combination with the BA treatment, this approach needs to adequately account for the effect of the cadmium wires in the side plates.

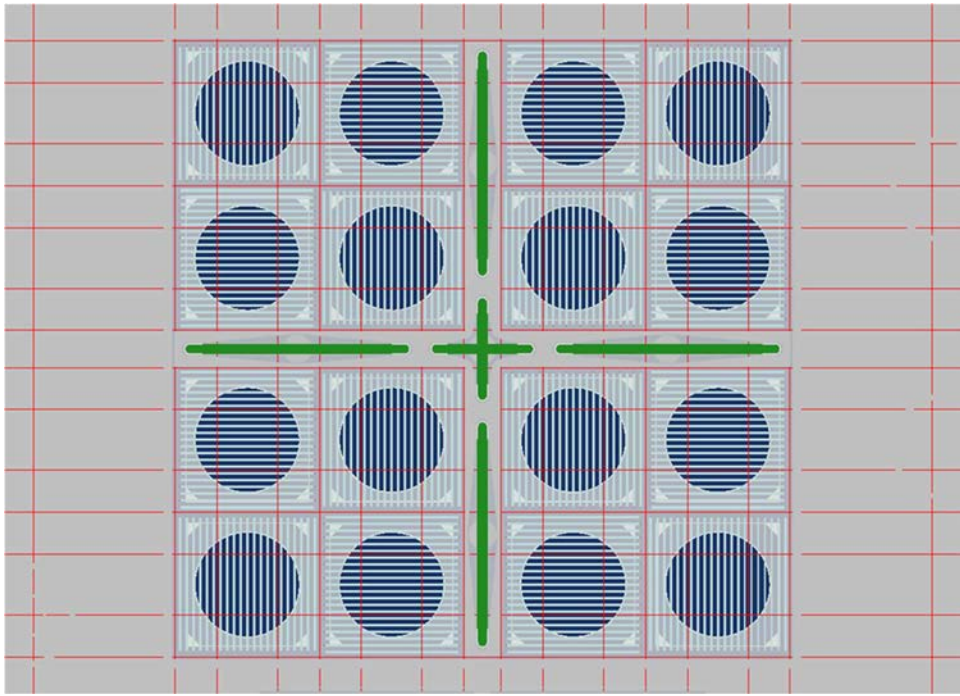


FIG. I-18. Submeshing scheme for fuel region in MGRAC. (courtesy of Necsa, South Africa)

Finally, the step in going from an MGRAC 2-D model to an MGRAC 3-D model also introduces errors in the final homogenized representation of the core. This is because of axial leakage being taken into account in the 3-D model. The stacking of the various 2-D cuts to form a 3-D nodal model is depicted in Fig. I-19.

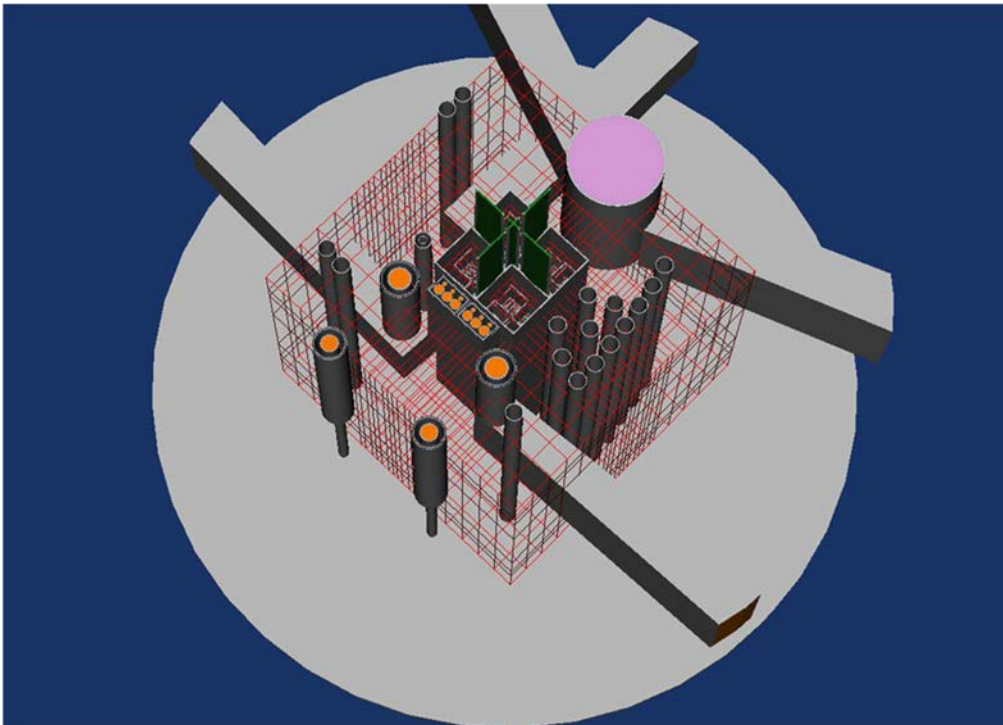


FIG. I-19. Nodalization of the MGRAC model. (courtesy of Necsa, South Africa)

It is important to note that this model building exercise was done with the commissioning core BOC material distribution. As the reactor operates and fuel burns, this will no longer be the case. Given the change over the first few cycles to a standard fuel only core, and the changing heavy water purity, a second set of cross-sections are generated at the start of cycle 10 to improve the non-fuel material representation.

In concluding the model building phase, it is noted that the reactor will typically operate with control rods somewhere between mid-core and all rods out (ARO), so the MGRAC model can be expected to be within roughly 500 pcm from reference and with an error of 3–4% in assembly averaged power. This offset may not remain constant as the model is used to simulate fuel and burnable poison depletion.

The final 3-D MGRAC model used nodal rehomogenization, the effect of which is not quantified here, but which does improve the k_{eff} offset from Serpent. It also used the subdivided fuel shown in Fig. I-18, from an infinite lattice environment, in combination with the BA treatment. All of these combine to the 303 pcm difference from Serpent (see Table I-3) with rods at mid-core.

I-3. RESULTS

The results from the multicycle burnup calculations by the various participants will be presented and then compared and discussed.

I-3.1. Results of the individual participant contributions

This section presents the results of the individual participants who participated in this benchmark.

I-3.1.1. Argentina (ARG) results

Argentina submitted more than one set of results, with each set using a different code or system of codes.

I-3.1.1.1. CONDOR-CITVAP results

Results assuming constant power

For calculations assuming constant power, two schemes are presented:

1. Core burnup performed with ARO at constant power followed by a critical calculation;
2. Core burnup performed at critical configurations.

The results for both approaches are presented in Fig. I-20 with burnup represented by full power days, power at nominal 20 MW for one day.

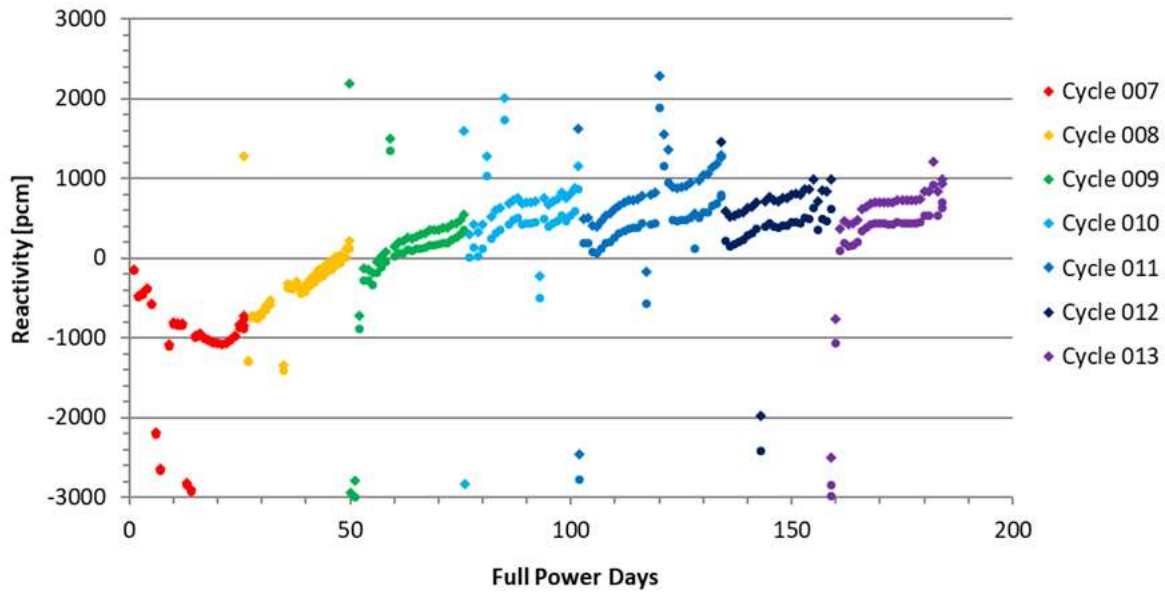


FIG. I-20. CONDOR-CITVAP calculated critical positions for cycles 7 to 13. Diamonds indicate burn with ARO and circles indicate burn at critical configuration. (courtesy of INVAP, Argentina)

It can be gathered from Table I-4 and Fig. I-20 that good agreement with experimental data is obtained for the critical configurations. The average reactivity values over each of the cycles are in the range ± 1000 pcm and the outliers in Fig. I-20 represent configurations with xenon transients. Such transients cannot be modelled with this approach, i.e. which assumes equilibrium xenon at full power.

Furthermore, average differences between ARO and critical burn calculations are less than 400 pcm, which verifies the appropriateness of the approximation usually performed during preliminary engineering stages. This is further supported by the results in Table I-4, where the average by cycle is presented (ignoring configurations with non-equilibrium xenon).

TABLE I-4. CONDOR-CITVAP AVERAGE REACTIVITY FOR CRITICAL POSITIONS

Cycle	ARO burn [pcm]	Critical burn [pcm]	Difference [pcm]
7	-824	-843	19
8	-290	-439	149
9	241	77	164
10	660	386	274
11	779	405	374
12	766	385	382
13	647	366	281
7-13	283	48	235

Results considering power variations

For the third approach, the evolution is calculated considering the reactor power variations and real days reported in Ref. [I-1]. In this approach the xenon transients are considered, thus a significant increase in the total number of calculations is necessary. The results for calculated reactivity at equivalent full power days for burnup at full power and actual reactor power are presented in Fig. I-21, where it can be seen there is good agreement with the experimental data

(i.e. zero reactivity). In Fig. I-21, both types of calculations, real days with power variations and full power days are compared and it can be seen the differences are minor, except for those points in which there is non-equilibrium xenon that are not accounted by the full power calculation. As a general burnup scheme, the full power calculation provides acceptable results for fuel management studies and assessments.

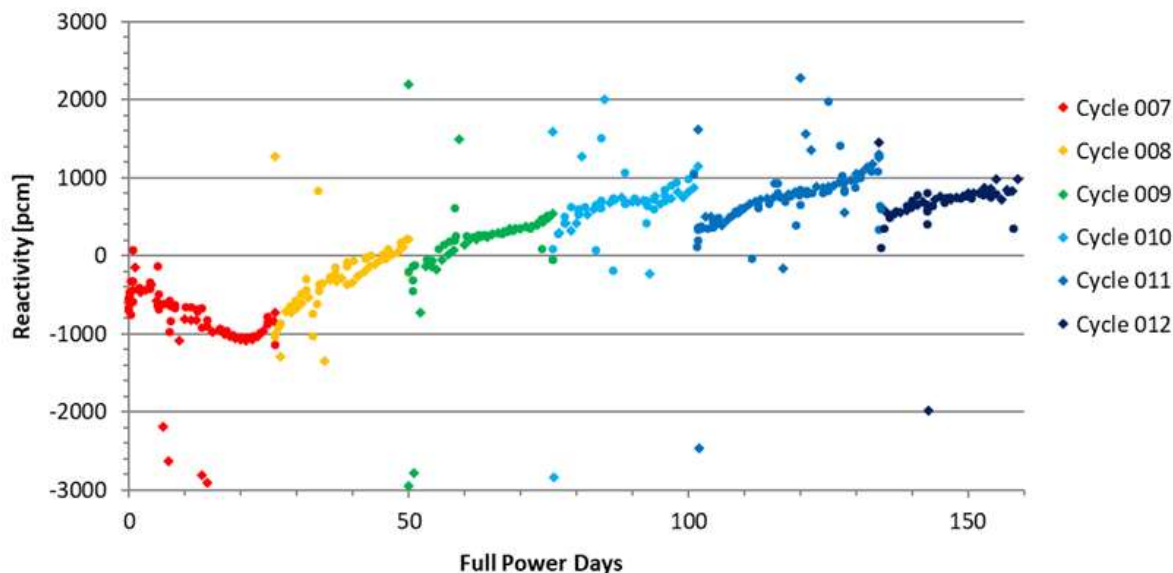


FIG. I-21. CONDOR-CITVAP calculated critical configurations for cycles 7 to 12 burning at full power (diamonds) and actual power (circles). (courtesy of INVAP, Argentina)

I-3.1.1.2. Serpent results

The results of calculations using Serpent for burnup are presented in Fig. I-22. In this case, the burnup was performed with the ARO configuration. The 3σ statistical uncertainty in the results is about 36 pcm which is negligible in the figure. The results obtained from Serpent are generally 200 pcm higher than the CONDOR-CITVAP ARO results, except for cycle 13 which are lower. As a sensitivity study of the effect of cross-section library, results using ENDF/B-VI.8 nuclear data library are provided as cycle averages compared to the current results using ENDF/B-VII.0 in Table I-4. For the average values, the non-equilibrium xenon results were not included so as not to bias the values obtained.

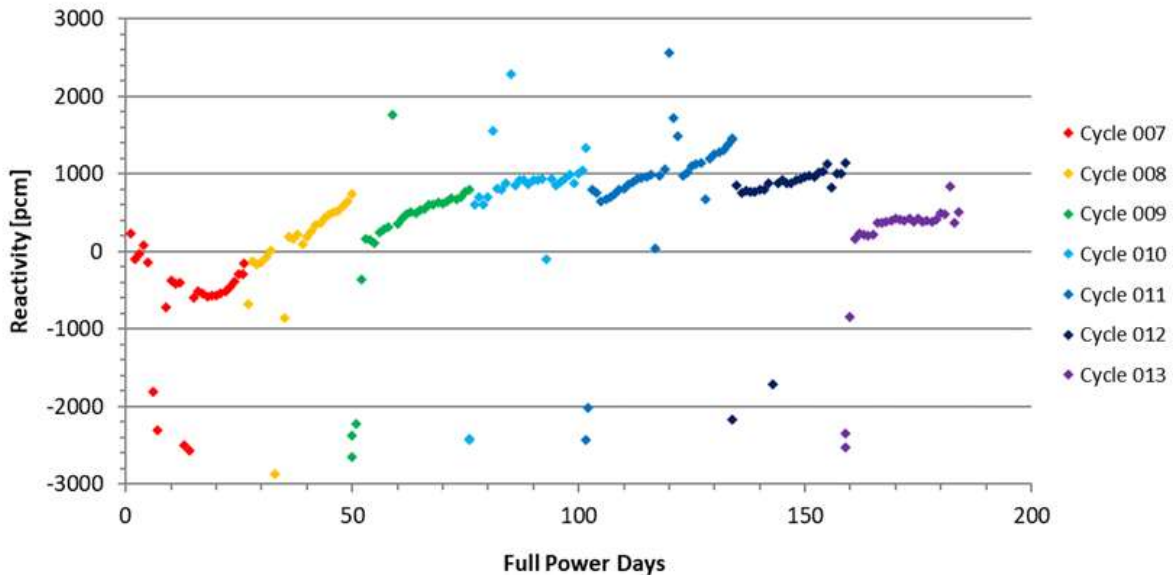


FIG. I-22. Serpent critical positions results for cycles 7 to 13. (courtesy of INVAP, Argentina)

It can be seen from both Table I-5 and Fig. I-22 that reasonable agreement with experimental data is obtained. The differences are in the range ± 1500 pcm, where the outlier values represent measurements without equilibrium xenon, which cannot be modelled correctly with this approach. In addition, the difference between ENDF/B-VI.8 and ENDF/B-VII.0 libraries were determined and the results presented in Table I-5. The results obtained with the latter library yield higher reactivities.

TABLE I-5. SERPENT 2 CYCLE AVERAGE REACTIVITY FOR CRITICAL POSITIONS

Average over cycle	Serpent 2 – ENDF/B-VI.8 [pcm] ¹	Serpent 2 – ENDF/B-VII.0 [pcm]	Difference
7	-698	-355	343
8	-359	171	529
9	-82	458	540
10	300	845	546
11	348	969	621
12	261	928	667
13	-131	339	470
7-13	-52	480	530

¹ See Ref. [I-10].

I-3.1.2. Australia (AUL) results

I-3.1.2.1. CONDOR-CITVAP results

The CITVAP model assumes the power of the reactor is fixed at 20 MW and so the burnup is performed in equivalent full power days (reactor operating at 20 MW). This means the data provided was converted in terms of full power days and the burnup performed accordingly. It also means the model does not account for transients (evolution of xenon) and power changes.

The results are presented in Fig. I-23. There are several outlier points that are clearly due to evolution of xenon (at the start of cycles) and power changes (mid-cycle trips and recoveries). Ignoring these outliers there is a trend from cycle to cycle, in particular cycles 7 to 10 that shows an increase in core reactivity with a more stable behaviour for cycles 11 to 13. In addition, there is behaviour within each cycle that is characterized by an increase in reactivity, then a flat region in the middle and then an increase again at the end of the cycle. This is clear in cycles 9, 10, 11 and 13 but less so for cycle 12.

The results from cycle 11 onwards show very good agreement with operation and hence the model and code are appropriate for burnup of the fuel and the cadmium wires in the fuel assembly. This code and model are used for OPAL operational planning.

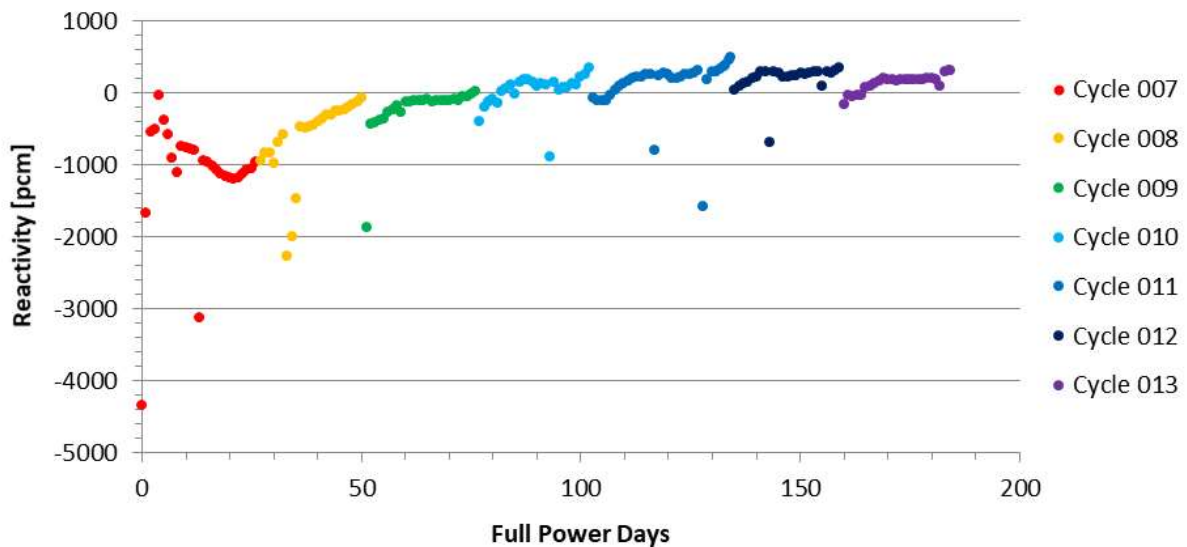


FIG. I-23. Core reactivity calculation using CITVAP model. (courtesy of ANSTO, Australia)

I-3.1.2.2. Serpent results

The Serpent calculation tracks the operation of the reactor as specified in the data provided. This means the burnup calculation is at the specified power for the specified time. The results are presented in Fig. I-24 where the time is real days. The results share some characteristics with those from CITVAP. In particular there is the same trend from cycle-to-cycle with the gradual increase in reactivity and reaching a more or less steady value for the later cycles. Also within a cycle there is the same behaviour that is characterized by an increase in reactivity, then a flat region in the middle and then an increase again. There are also outliers in the Serpent results, although in this case the calculations are expected to follow the xenon and power transients. Perhaps there is not sufficient detail in the operational data to enable this or perhaps this is an issue with some of the data points.

The results from Serpent also show some differences in the detail. Specifically, there is a deviation from the CITVAP trend at cycle 10 where the Serpent results continue to increase in reactivity including a further increase for cycle 11. This ultimately results in slightly, about 200 pcm, higher reactivity values for cycles 12 and 13 compared to CITVAP. These differences are small though and generally the results are in good agreement with CITVAP results. Like the CITVAP results, the Serpent results are overall in good agreement with the operational data and, hence, the model and code are appropriate for burnup of the fuel and the cadmium wires in the fuel assembly. In addition, the capability to model all reflector and beam facilities in

detail means that the Serpent model can be used to calculate results (such as neutron flux and reactivity) for any operational state of the reactor.

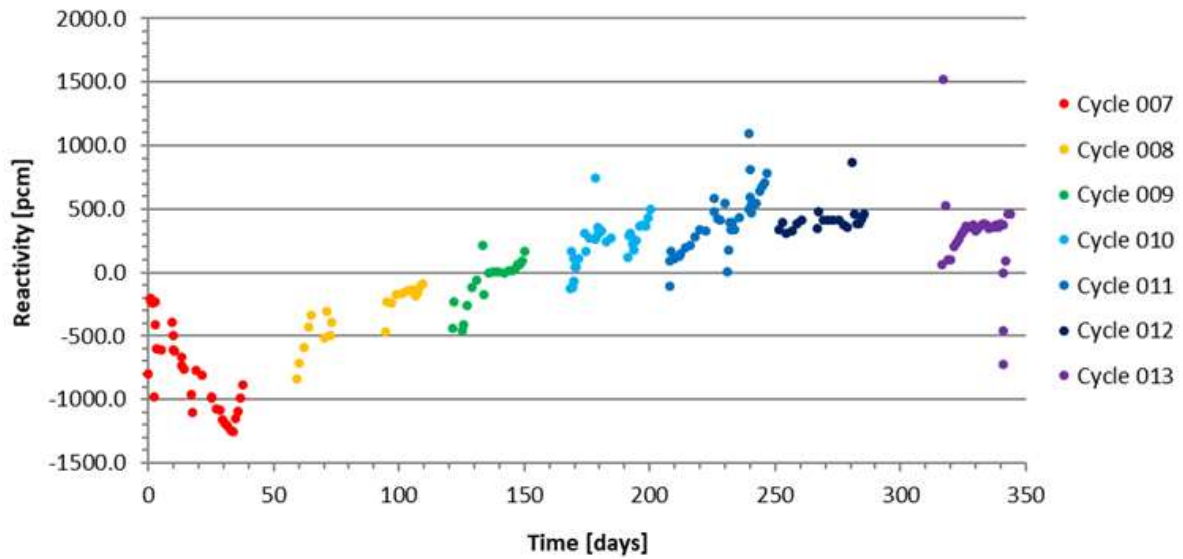


FIG. I-24. Core reactivity calculation using Serpent model. (courtesy of ANSTO, Australia)

I-3.1.3. France (FRA) results

I-3.1.3.1. COCONEUT2.0 results

Homogeneous model

Initially, a full 3-D evolution of the core using the homogeneous representation of the COCONEUT2.0 model was performed. Cross-section tables for the reflector material cannot be modified during the calculation in version 2.0 of COCONEUT (this benchmark highlighted this missing feature, which will be integrated in a future version of this scheme). As a result, the heavy water purity of the reflector (Table I-6) was assumed to be constant and was fixed at the cycle 7 value of 97.5%.

A TRIPOLI-4 calculation of the first step of cycle 7 at 97.5% and another calculation at 99.55% heavy water purity shows a reactivity effect of +1164 pcm due to heavy water purity. For each cycle, a reactivity adjustment was performed, assuming a linear dependence with heavy water purity using the TRIPOLI-4 results and the purity for each cycle.

TABLE I-6. REACTIVITY ADJUSTMENT APPLIED TO ALL COCONEUT CYCLES TO ACCOUNT FOR CONSTANT HEAVY WATER PURITY IN MODEL

Cycle	Heavy water purity [wt%]	Reactivity adjustment [pcm]
7	97.5	0
8	97.1	-227
9	96.9	-341
10	99.55	1164
11	99.24	988

In addition, TRIPOLI-4 calculations performed on COCONEUT-like geometries revealed a reactivity worth of -1686 pcm for the neutron beams not modelled in the reflector tank. Therefore, COCONEUT calculations were corrected by -1686 pcm, to account for the lack of neutron beams in the model. Figure I-25 shows the final results with both beam tube and heavy water purity effects corrected.

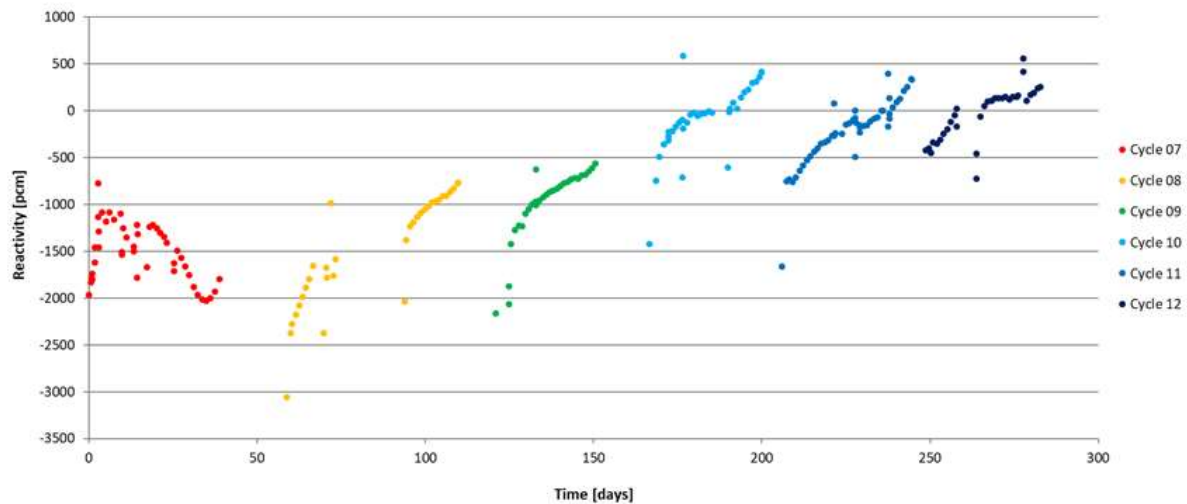


FIG. I-25. COCONEUT (homogeneous) 3-D core calculation, beam tube and heavy water purity corrections taken into account. (courtesy of TechnicAtome, France)

The results show a global shift in reactivity values that increases from approximately -1500 pcm for cycle 7 to 0 pcm for cycle 12. These results appear plausible although the source of this shift in reactivity over the cycles is not clear. Abrupt power changes naturally lead to strong xenon poisoning changes which are difficult to account for from a kinetic point of view. Thus, points occurring just at these steps were discarded as to not bias the results. Figure I-26 shows this filtered data, with power transient points discarded.

The effect of homogenizing all the materials within each fuel assembly is to also mix the cadmium, which is normally concentrated in very small wires, into the whole FA volume. This feature is expected to significantly increase cadmium capture and thus increase the reactivity calculated in the homogeneous model. This may be a source of the increasing reactivity observed over the cycles. In addition, there is also a trend within each cycle with the reactivity values increasing during the cycle. This can also be due to an overestimation of the cadmium burnup because of the homogenization of the materials.

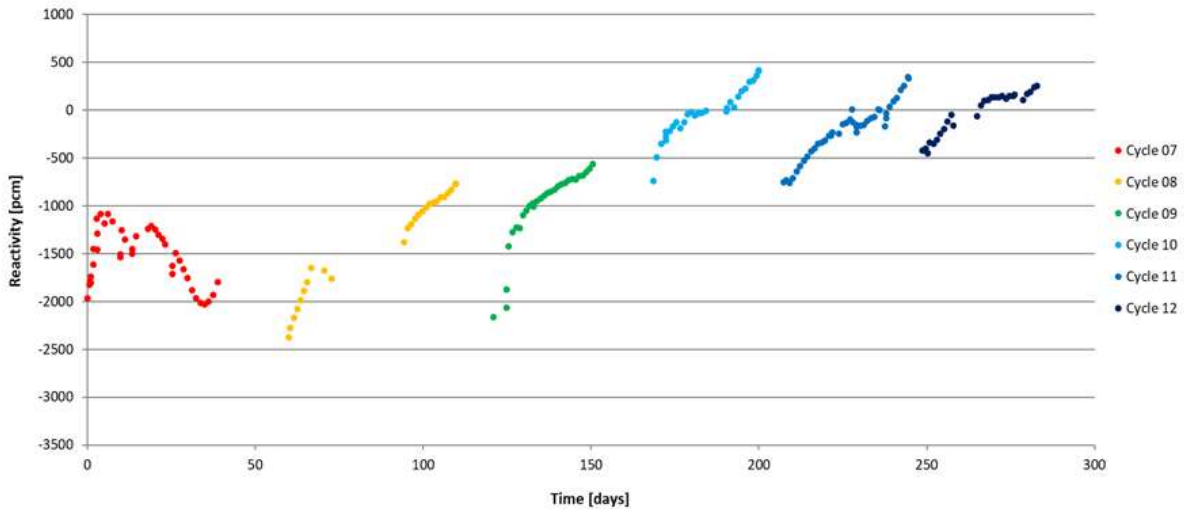


FIG. I-26. COCONEUT (homogeneous) 3-D core calculation, beam tube and heavy water purity corrections taken into account, with xenon transient points discarded. (courtesy of TechnicAtome, France)

Heterogeneous model

As in the previous case (homogeneous), heavy water purity was also assumed constant. Reactivity values were then corrected with respect to values in Table I-6. Figure I-27 shows the results with the beam and heavy water purity corrections applied. In this model the fuel area is still homogenized, but the side plates (containing cadmium wires) and water surrounding them are fully described (see Fig. I-11). As expected the reactivity values are much higher. This time there is a global increase in reactivity from cycle 8 to cycle 12 with values ranging from -300 pcm and +900 pcm. There is a notable exception with cycle 7, which starts with a considerable bias of approximately +1500 pcm and rapidly decreases to 0 pcm at the end of the cycle. This feature still needs to be explained.

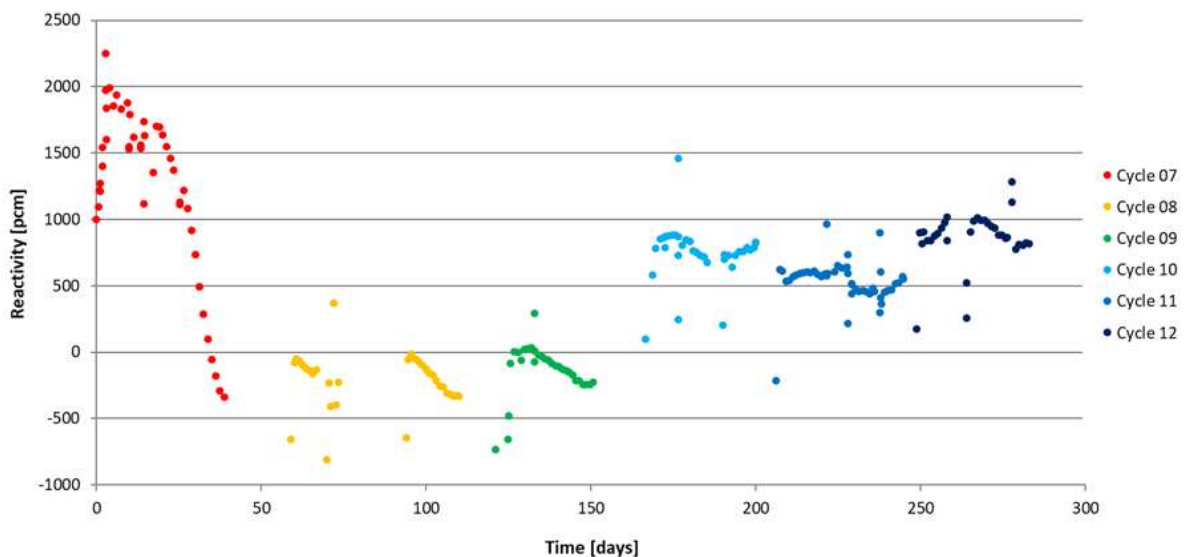


FIG. I-27. COCONEUT (heterogeneous) 3-D core calculation beam tube and heavy water purity corrections taken into account. (courtesy of TechnicAtome, France)

Again, abrupt power changes naturally lead to strong xenon poisoning changes which are difficult to account for from a kinetic point of view. Thus, points occurring just at these steps were discarded as to not bias the results. Figure I-28 shows this filtered data, with power transient points discarded.

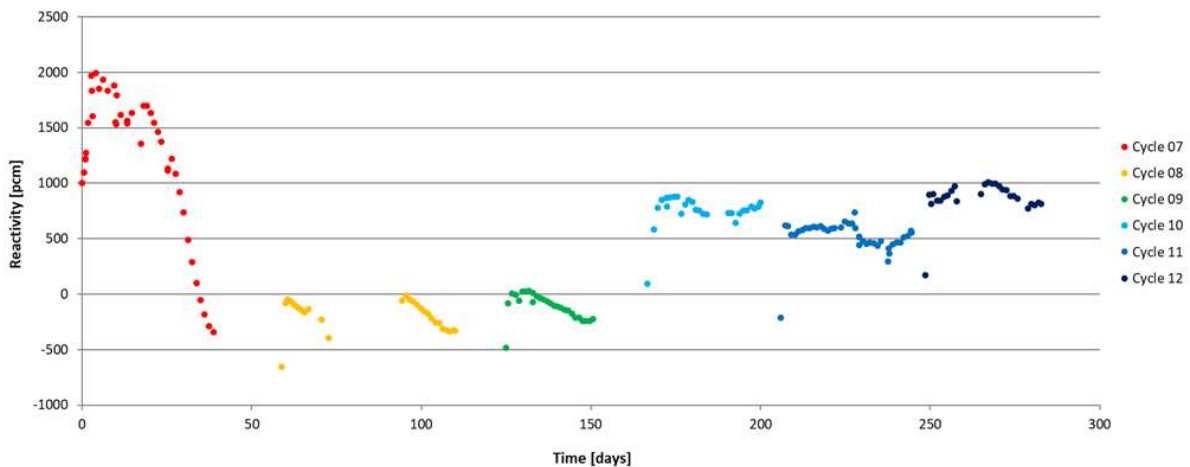


FIG. I-28. COCONEUT (heterogeneous) 3-D core calculation beam tube and heavy water purity corrections taken into account, with xenon transient points discarded. (courtesy of TechnicAtome, France)

These results show good agreement with the operational data, with the exception of cycle 7. There is some uncertainty regarding the heavy water purity correction applied, since a change in reactivity bias is visible after cycle 10. This needs to be investigated further. Unlike in the homogeneous case, there is no visible trend within each cycle for cycles 10 to 12, but the trend seems to be opposite for cycles 8 and 9. This could mean that fully describing the cadmium wires has a significant impact on the calculated depletion rate.

I-3.1.3.2. TRIPOLI-4.10 results

In the TRIPOLI-4 calculations, heavy water purity is modelled for each cycle as specified in Ref. [I-1] and there is no adjustment due to neutron beams since they are properly modelled. Figure I-29 shows the core reactivity evolution during depletion of the OPAL core during cycles 7 to 13, as calculated by TRIPOLI-4 in its depletion mode. The depletion models were first simplified (as detailed in Section I-2.3.3.2) with a single material per cadmium wire and a single material per fuel plate.

As for both COCONEUT 2.0 cases, there is a globally increasing trend in reactivity. The calculated reactivity is about -100 pcm for cycle 7 and increases up to +1500 pcm at cycle 12. Abrupt power changes naturally lead to strong xenon poisoning changes which are difficult to account for from a kinetic point of view. Thus, points occurring just at these steps were discarded and the filtered results are presented in Fig. I-30 for the single axial mesh.

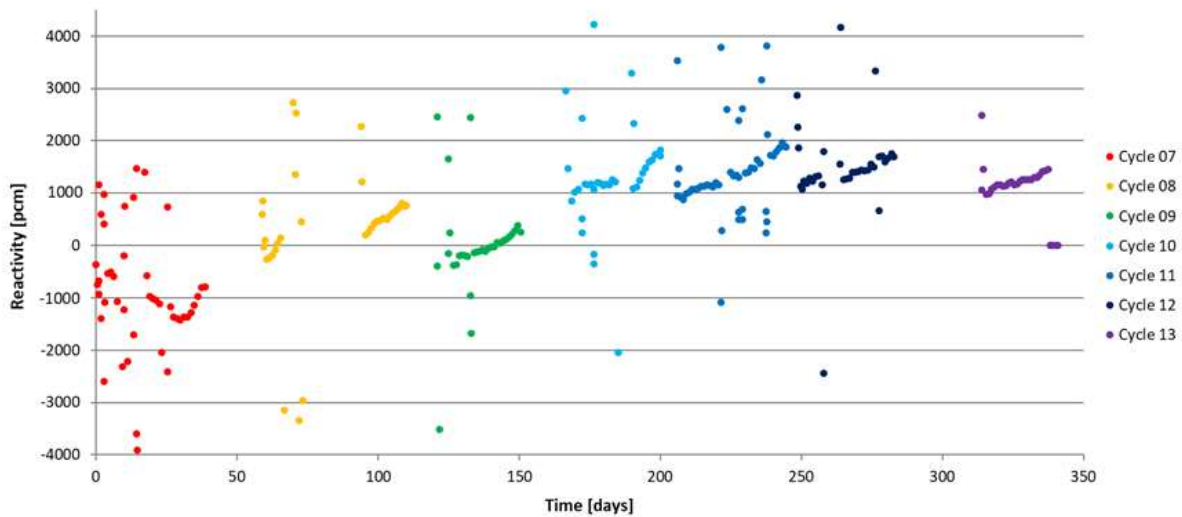


FIG. I-29. TRIPOLI-4 3-D core calculation. (courtesy of TechnicAtome, France)

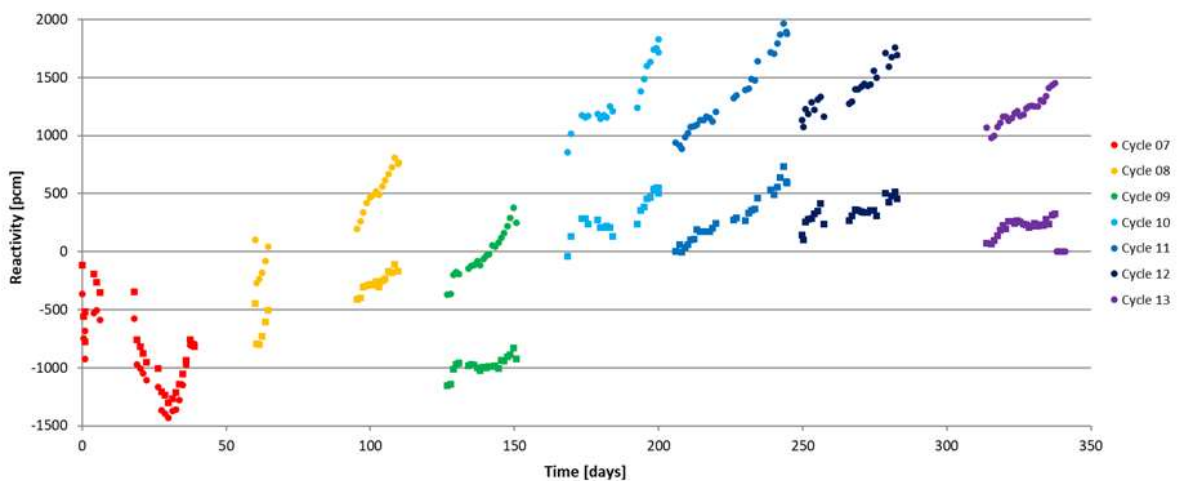


FIG. I-30. TRIPOLI-4 3-D core calculations for two different models: single ● or multiple ■ axial mesh for cadmium wires and fuel plates. (courtesy of TechnicAtome, France)

As in the homogeneous version of COCONEUT, a trend is clearly visible within each cycle with the reactivity increasing during the cycle. This could again be due to an overestimation of the cadmium depletion. Indeed, there is only one material per cadmium wire, which increases its burnup by not taking into account the self-shielding, which implies that the outer layers of cadmium in the wire deplete first and then the inner.

A second calculation was performed with three axial meshes per cadmium wire and six axial meshes per fuel plate. The aim is to assess the sensitivity of the results to the degree of refinement of meshing depleting materials. The three axial meshes in cadmium wires and six in fuel plates is assumed to be a first-step refinement which is supposed to enhance the quality of the calculation and provide some quantitative indication of the impact of axial refinement. This is indicated in Fig. I-30, where both depletion results for the axial meshes adopted are presented. It is evident that a small refinement in the meshes has a considerable impact on the results. The trend in reactivity in each cycle (in pcm/day) is reduced by a factor of approximately 2, and so is the global trend on the multicycle calculation. The mean bias (pcm) is also significantly reduced, dropping from +692 pcm to -124 pcm. In the last cycles (10 to

13), the bias drops by approximately 1000 pcm. Finally, the standard deviation is also reduced by a factor of 2 for each individual cycle, and drops from 887 pcm to 562 pcm over the global depletion calculation.

I-3.1.4. South Africa (SFA) results

Figure I-31 shows the value of reactivity at various points in the seven operating cycles for which data were provided as calculated by Serpent and for five of the cycles as calculated by MGRAC. Both Serpent and MGRAC results show a step change in reactivity at the beginning of cycle 10, though in the case of MGRAC this step is much larger than the one exhibited by Serpent. The heavy water composition was updated at the beginning of cycle 10, in accordance with the benchmark specification.

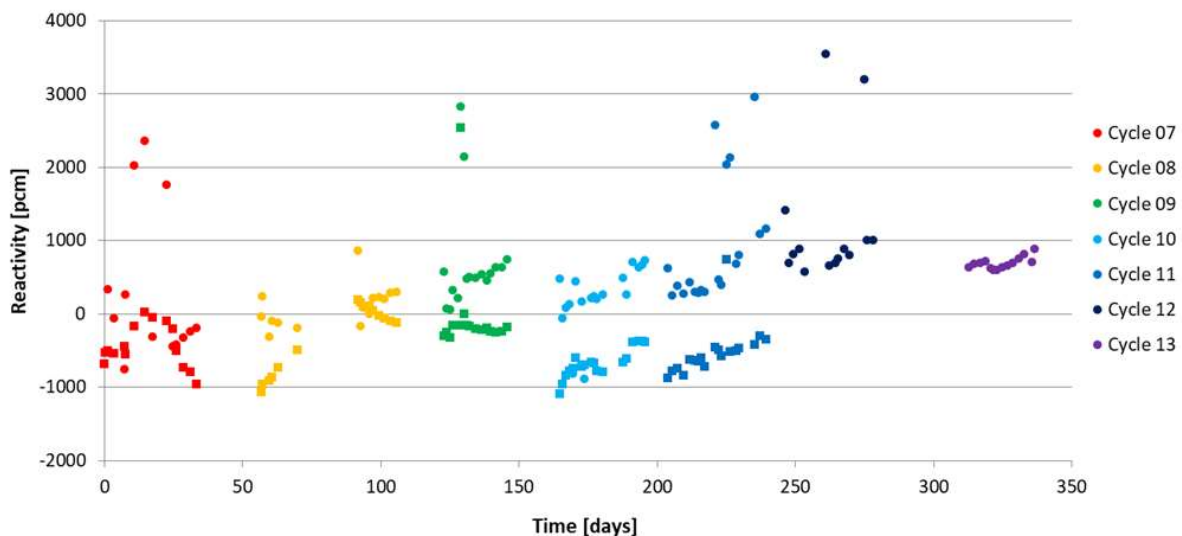


FIG. I-31. Core calculations for two different codes: ●Serpent and ■ MGRAC. (courtesy of Necsa, South Africa)

The difference between Serpent and MGRAC during cycles 7 and 8 is somewhat erratic and generally less than 1000 pcm, however, this difference grows over the course of the following cycles with further depletion. One possibility in this regard is that HEADE may not be depleting the burnable absorber wires correctly, because of the difficulty the collision probability solution has with such localized, highly absorbing regions and therefore depleting the cadmium too slowly.

To address this issue, past work on cadmium wire depletion has resulted in an additional option in HEADE to use an analytic diffusion solution through the wire itself to better estimate the flux shape in the wire. Although somewhat ad hoc, this approach has shown to improve the depletion rate of the cadmium wire. Therefore, a Bessel function fit of the flux through the wire was applied to perform the depletion of the wire.

In addition, to improve the fuel cross-section data, Serpent was used as a lattice code for generating fuel cross-sections for MGRAC in place of HEADE.

In generating the nodal cross-sections, it is not possible to take into account the full reflector effect, since the nodal diffusion solution is not stable with too much reflector in the model. As such, the model used to this point utilized 45 cm of reflector. Given the large amount water

displacing facilities in the pool of the OPAL design, this cut-off is restrictive and further has an impact on the power shape in the core, which might have a knock-on effect on fuel burnup. To improve the limitations of this assumption, the calculation was performed with reflective boundary conditions at the outside of the heavy water tank, with an albedo on this boundary in the thermal group of 0.77.

The cycle depletion calculations were repeated with all of the above enhancements, and the final results are shown in Fig. I-32. This combination, and in particular the use of the ‘extended reflector’, shows an improvement in the alignment between the MGRAC and Serpent results. There is still a clear occurrence at the start of cycle 10 with both Serpent and MGRAC shifting downwards, but MGRAC more so. Ignoring the outliers, which are most likely due to power transients that result in xenon evolution that is unlikely to be captured with sufficient detail by the operational data, the results from both Serpent and MGRAC lie within ± 1000 pcm of critical. This is good agreement with the data and acceptable for operational purposes.

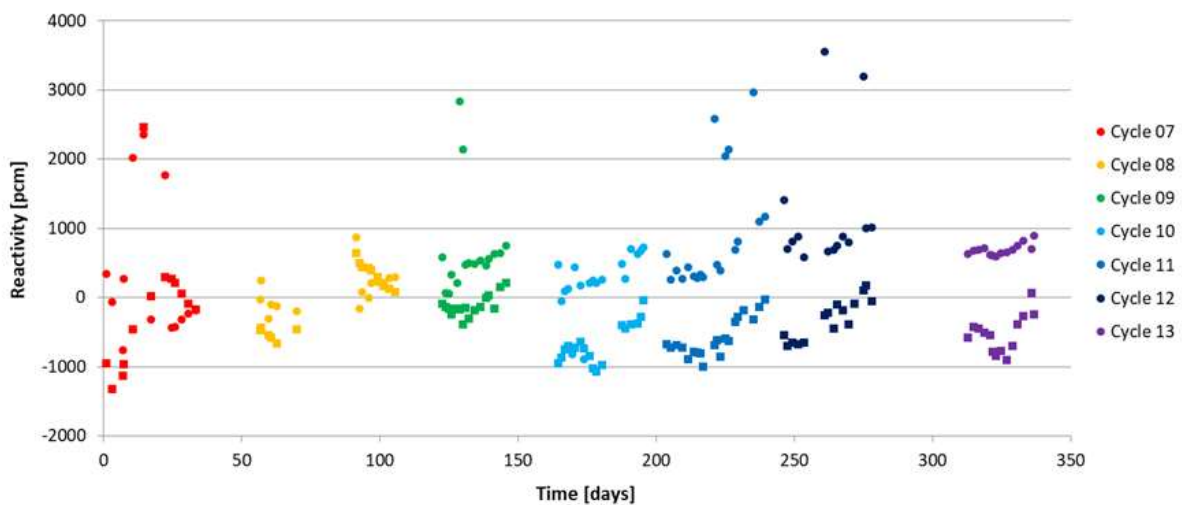


FIG. I-32. Core calculations for two different codes with enhancement in the MGRAC model: ● Serpent and ■ MGRAC. (courtesy of Necsa, South Africa)

I-3.2. Comparison of results

Both deterministic and stochastic codes were used by all participants to perform the burnup calculations for the OPAL core. Each of these methods requires the analyst to make a series of choices regarding construction of the model, such as, approximations adopted to represent the actual geometry, discretisation of the burnup regions, time steps in burnup, number of neutron groups, homogenization of material regions, flux solution method and cross-section libraries. The various choices made by the analysts has produced results that differ when compared in detail but looking at general characteristics and trends the following observations can be made:

1. All participants were able to develop models that provided agreement to within ± 1000 pcm (excluding data points that may have been influenced by xenon transients).
2. Almost all results show an upward trend in reactivity from cycle 7 to cycle 12 (this is not evident in the SFA results).
3. Almost all results show an increase in reactivity (a kick up) at the end of each cycle.
4. Two of the participants had an offset at cycle 10 which coincides with the step change in heavy water purity.

The first observation means that all participants were able to develop models that from an operations perspective provided sufficient accuracy and precision to reliably predict reactor operation. Observations 2 and 3 were thought by some participants to be linked and due to the burnup of the cadmium wires in the fuel assemblies. To investigate this further, all participants performed sensitivity studies on the modelling details of the cadmium wires (increasing the number of axial and radial burnup zones or flux solution within the wires). However, despite the improvement in some results, it did not significantly change the observed trends and it was concluded that those strategies would not address the effects observed. This means there is no plausible explanation for observations 2 and 3. Observation 4 is specific to the deterministic results of FRA and SFA and the stochastic results of FRA and to a lesser degree the stochastic results of SFA. The deterministic results of FRA (COCONUT) require an adjustment in reactivity due to changes in heavy water purity as the COCONUT model does not explicitly account for the change in purity. The method used to account for this may introduce a bias that results in this offset. The deterministic results for SFA (MGRAC) are based on a model that does not represent the complete heavy water reflector and so again an approximation is adopted to represent the actual reflector. This approximation may introduce a bias when there is a step change in the heavy water purity that is seen as a step change in the core reactivity. It is not clear what is causing the significant step change observed in the stochastic FRA (TRIPOLI-4) results and the smaller (perhaps not significant) change in the stochastic SFA (Serpent) results.

I-3.3. Conclusions

A variety of both deterministic and stochastic neutron transport codes were used by four participating organizations to perform the OPAL multicycle burnup benchmark. Overall, the participants were all able to develop models using both deterministic and stochastic codes to obtain results that agreed with the benchmark data to within ± 1000 pcm. It was clear that some of the data provided was not of sufficient detail or accuracy or both to capture the power and the resulting xenon transients that lead to some outlier values. In addition, there were some common trends observed in the results for all or most of the participants, the cause of which is yet to be understood. Despite these unexplained observations, the codes and models have demonstrated the ability to calculate multicycle burnup of both the fuel and burnable cadmium wires within the fuel assemblies to an accuracy sufficient for operational purposes. The increase in speed and memory available of modern computer systems means that stochastic methods with their explicit detailed geometric representation continue to yield reference results as demonstrated by the results of this benchmark. In addition, the results demonstrate the applicability of the benchmark data as a practical and complete set of operational data for performing multicycle benchmark calculations for operational planning of research reactors.

REFERENCES TO ANNEX I

- [I-1] INTERNATIONAL ATOMIC ENERGY AGENCY, Research Reactor Benchmarking Database: Facility Specification and Experimental Data, Technical Reports Series No. 480 (Rev. 1), IAEA, Vienna (in preparation).
- [I-2] VILLARINO, E., MOCHI, I., SARTORIO, P., INVAP Neutronic Calculation Line, *Mecánica Computacional XXXIII* (2014) 3217–3226.
- [I-3] PRINSLOO, R., et al., Recent developments of the OSCAR calculational system, as applied to selected examples from IAEA research reactor benchmarks, Proc. 18th IGORR Conference, Sydney, Australia, 3–7 December (2017).

- [I-4] LACOMBE, J.G., BOURET, C., KOUBBI J., MANIFACIER, L., COCONEUT: Enhancing Neutronic Design for Research Reactors, Proc. RRFM-IGORR Conference 2016, Berlin, Germany, 13–17 March (2016).
- [I-5] TRIPOLI-4 PROJECT TEAM, TRIPOLI-4 Version 10 User Guide, Commissariat à l'énergie atomique et aux énergies alternatives Technical Report, CEA/DEN/DANS/DM2S/SERMA/LTSD/RT/15-5928/A.
- [I-6] LEPPÄNEN, J., PUSA, M., VIITANEN, T., VALTAVIRTA, V., KALTIAISENAHO, T., The Serpent Monte Carlo Code: Status, development and applications in 2013, Ann. Nucl. Energy **82** (2015) 142–150.
- [I-7] VILLARINO, E., HERGENREDER, D., BRAOUDAKIS, G., ERSEZ, T., Calculation of the core parameters measured during the commissioning of the OPAL reactor, Proc. PHYSOR 2010 – Advances in Reactor Physics to Power the Nuclear Renaissance – Pittsburgh, Pennsylvania, USA, 9–14 May (2010).
- [I-8] INTERNATIONAL ATOMIC ENERGY AGENCY, WIMS-D Library Update, IAEA, Vienna (2007).
- [I-9] RADEMAKERS, F., BRUN, R., ROOT: An Object-Oriented Data Analysis Framework, Linux Journal **51** (1998) 6.
- [I-10] FERRARO, D., VILLARINO, E., Full 3-D core calculations with refuelling for the OPAL Research Reactor using Monte Carlo Code Serpent 2, Ann. Nucl. Energy **92** (2016) 369–377.

ANNEX II

BENCHMARK CONSOLIDATED RESULTS AGAINST EXPERIMENTAL DATA FROM ANSTO-2

II-1. INTRODUCTION

The ANSTO-2 benchmark analysis, including the reactor specification and experimental data, is documented in Ref. [II-1]. This benchmark provides valuable data for the analyst to benchmark their codes and methods for estimating dose rates due to activation of reactor materials and components during the removal and installation of in-pile guide and primary shutter assemblies. Estimation of dose rates during maintenance and installation activities is vital for the protection of workers.

This Annex presents the codes and methods used and the results obtained by the various participants as part of the CRP to estimate dose rates during the installation of the new OPAL CG2 neutron guide system including in-pile, shutter and front cover. The scope is to calculate the dose rates due to gamma rays that originate from the activation of the internal components of the OPAL reactor when the fuel assemblies and the targets in the irradiation facilities are all removed. To minimize the number of models and the overall work effort, the bounding case scenario is presented in the benchmark for the necessary tasks. The results are therefore bounding from the dose rate perspective.

II-2. SUMMARY OF THE BENCHMARK SPECIFICATION AND CODES AND MODELS USED

II-2.1. Summary of the benchmark specification

The goal of the benchmark is to calculate dose rates at ten positions, five locations for two different configurations, around the activated internal reactor components when the in-pile guides and primary shutter are removed from their respective cavities. The dose rates were measured at various points while the in-pile was placed in a shielded transport container. Figure II-1 shows one of the configurations, the in-pile 2 metres from the reactor face, with five of the positions numbered for which dose rates are provided in the benchmark. The experiment specification and experiment data [II-1] provide details of the dose rate locations.

To enable the analyst to perform these calculations the following details were provided as part of the benchmark:

- Detailed reactor specification to allow modelling of the relevant components of the reactor. This includes dimensions and material composition of the core, fuel assemblies, control rods, irradiation facilities, beam tubes, cold neutron source and reflector vessel;
- Further details of the outer neutron beam, in-pile and shutter cavity including dimensions and material compositions;
- A simplified operational history to perform the activation calculation;
- Time between last reactor operation and dose rate measurements to allow for decay;
- Dose rate measurements at various locations. This is the goal of the benchmark.

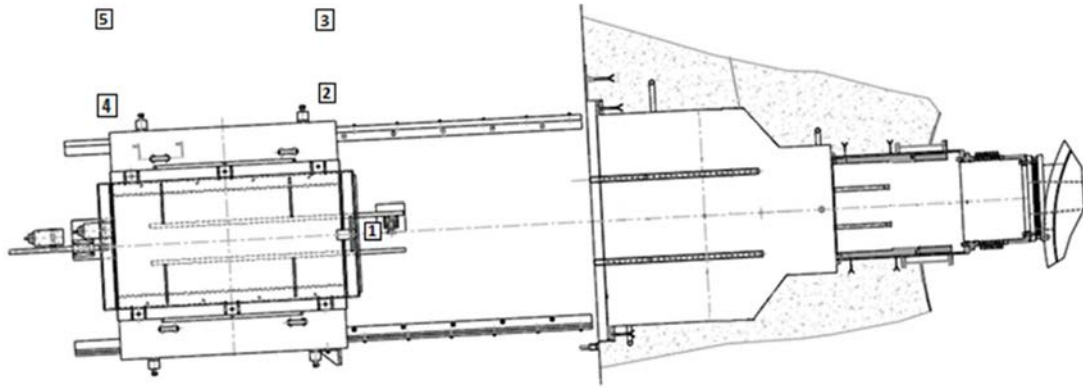


FIG. II-1. Plan view with the in-pile transport shielding 2 metres from reactor face. Radiation point locations 1, 2 and 4 at contact of in-pile shield and locations 3 and 5 at 1 m from in-pile shield. (courtesy of ANSTO, Australia)

II-2.2. Summary of the codes and libraries used

The codes and associated cross-section libraries used to perform the neutron flux, activation, decay and final dose rate calculations are presented in Table II-1, together with information on the calculation made by each code. MCNP [II-2], ORIGEN [II-3], SCALE [II-4], TRIPOLI-4 [II-5] with ROOT [II-6], DARWIN2 [II-7] and MERCURE6 [II-8] were used by the different participants.

TABLE II-1. CODES AND LIBRARIES USED BY THE PARTICIPANTS

Participant	Code (library)	Calculation
Argentina	MCNP5 1.60 (ENDF/B-VI.8)	Neutron flux and dose rate
	SCALE 6.1-ORIGEN (ENDF/B-VI.8)	Activity and gamma spectrum
Australia	MCNP5 1.40 (ENDF/B-VI.8)	Flux and dose rate
	ORIGEN2.0 (built-in libraries)	Activity and gamma spectrum
France	MCNP6.1 (JEFF-3.1.1)	Neutron flux and dose rate
	TRIPOLI-4.10 (JEFF-3.1.1)	Dose rate
	DARWIN2.3 (JEFF-3.1.1)	Activity and gamma spectrum
	MERCURE6.3 (JEF-2.2)	Dose rate

II-2.3. Summary of the models used

The models constructed and the assumptions adopted for the various calculations are presented for each of the participants.

II-2.3.1. Argentina (ARG) models

The benchmark calculations performed, the codes used and the results obtained are described in the following steps:

1. Neutron flux calculations using MCNP5, for a complete 3-D model of the reactor core, cold neutron source (CNS) and cold neutron beam (labelled as inner beam and outer beam in Fig. II-2).
2. Material activation using SCALE-ORIGEN based on an irradiation time of 1192 full power days, followed by 10 days of decay using the material compositions provided and the neutron fluxes calculated in Step 1.

3. Gamma dose rate calculations using MCNP5, using a simplified 3-D model of the CNS, inner beam and outer beam and the gamma ray sources from the activation calculated in Step 2.

It was assumed that the gamma dose rate was only due to the activation of the CNS, inner beam and outer beam and so only these sources were considered in the full dose rate calculations.

II-2.3.1.1. MCNP model for neutron flux

A complete 3-D model of the reactor core, the cold neutron source and the inner beam and outer beam was developed as shown in Fig. II-2. The neutron flux was calculated in the CNS, the inner beam and the outer beam. The main components of the CNS are the moderator vessel, the vessel jacket and the containment vessel. The neutron flux was calculated for each of these components. The inner beam was divided into four zones and the neutron flux calculated for each zone. The outer beam was also divided into four zones and the neutron flux calculated for each zone. The absolute neutron flux normalization was made using a thermal power of 20 MW.

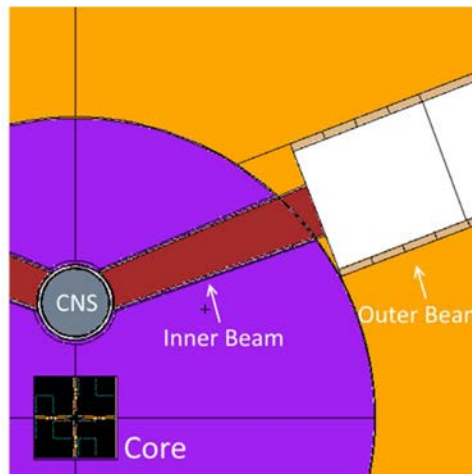


FIG. II-2. MCNP model for neutron flux calculations. (courtesy of INVAP, Argentina)

II-2.3.1.2. Material activation and gamma ray source

The next step was the material activation calculation using SCALE-ORIGEN. The material activation was made assuming 1192 full power days, followed by 10 decay days using the neutron flux (spectrum shape and magnitude) calculated in Step 1. The relevant radioisotopes and half-lives considered for this calculation are indicated in Table II-2.

TABLE II-2. MAIN PHOTON EMITTERS BY MATERIAL

Material	Isotope	Half-life [days]
Zr-Nb	Zr-95	64.03
	Nb-95	34.99
Zircaloy-4	Zr-95	64.03
	Nb-95	34.99
304L SS ^(a)	Cr-51	27.70
	Co-60	1925

^(a) 304L SS is the low carbon version of the austenitic stainless steel 304 SS. While their average alloy composition is basically identical, the maximum carbon content of 304L SS is 0.03%, compared to 0.08% for 304 SS.

II-2.3.1.3. Gamma dose rate model

Finally, the gamma dose rate calculation was performed using a simplified 3-D model developed of the cold neutron beam, including the CNS, the inner beam, the outer beam and the tally locations of the dose points. The MCNP5 model used is shown in Fig. II-3. The gamma ray source terms calculated for each zone from the material activation in Step 2 was used as input.

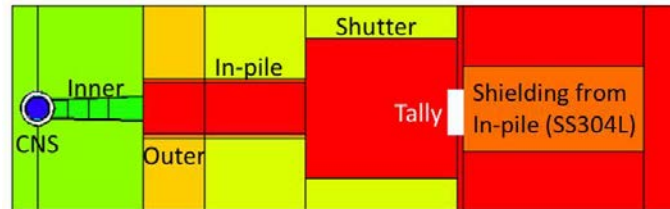


FIG. II-3. MCNP model for photon dose rate calculations. Location 6 is indicated by the Tally region. (courtesy of INVAP, Argentina)

II-2.3.2. Australia (AUL) models

The models constructed and the assumptions adopted for the various calculations are presented in turn for each step of the calculation.

II-2.3.2.1. MCNP model for neutron flux

A detailed 3-D MCNP5 model of the OPAL reactor was constructed using the reactor specification in Ref. [II-1]. In addition, further details of the outer irradiation facilities were used to provide a full description of the reflector facilities. These details, however, do not impact the results. The MCNP model and detail can be seen in Fig. II-4.

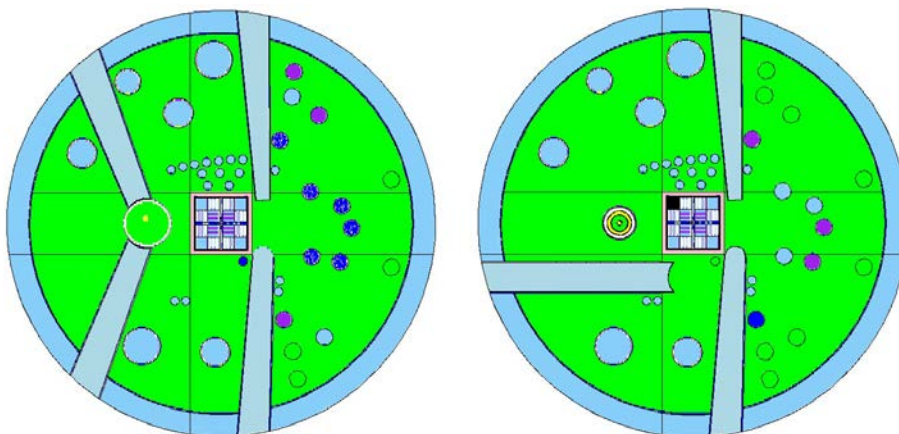


FIG. II-4. Two views at different heights showing the core and reflector vessel internal components with the cold (left) and hot (right) neutron beam tubes. (courtesy of ANSTO, Australia)

The neutron flux was evaluated for major internal components of the OPAL reactor. These selections were made because it was considered that their activation would potentially contribute to the dose rate on the outside of the shutter box during the various stages of the installation process. These components will be in the line of sight or have direct view from outside the shutter box when the manoeuvre is being performed. This includes the removal and

installation of the following: the front cover, the shutter and compensating shielding, and the in-pile.

The source type used in the MCNP5 model was a “KCODE” normalized to 1.5×10^{18} neutrons per second in the core at 20 MW of reactor power. The volume tallies were calculated in 10 cm long segments along the cold neutron beam tube. Also, the maximum flux along the CNS thimble was estimated using a volume tally.

The neutron flux along the in-pile bushing was estimated from the maximum neutron flux inside the neutron guide.

II-2.3.2.2. Material activation and gamma ray source

Using the neutron fluxes from calculation Step 1, the gamma ray source for each different component and material was evaluated using ORIGEN2. There are three different materials for the internal components:

- Zry-4 for the neutron beam tubes;
- Zr-2.5%Nb for the CNS thimble;
- SAE1020 for the in-pile cavity.

The compositions adopted are shown in Tables II-3, II-4 and II-5.

TABLE II-3. Zry-4 CHEMICAL COMPOSITION

Element	Weight [ppm]	Element	Weight [ppm]
Sn	13 000	Mn	<25
Fe	2 300	Si	<25
Cr	1 100	Co	<10
O	1 200	Mg	<10
C	136	Mo	<10
Hf	74	H	4
Ni	51	B	<0.2
Al	41	Cd	<0.2
Cu	32	Zr	balance
N	30		

TABLE II-4. Zr-2.5%Nb CHEMICAL COMPOSITION

Element	Weight [%]
Zr	97.5
Nb	2.5

TABLE II-5. SAE1020 CHEMICAL COMPOSITION

Element	Weight [%]
Fe	balance
Mn	0.45
C	0.2
S	0.05
P	0.04

To simplify the ORIGEN calculations, the activation calculations were performed for the Zry-4 and Zr-2.5%Nb materials using a neutron flux of $1.0 \times 10^{14} \text{ n}\cdot\text{cm}^{-2}\cdot\text{s}^{-1}$ and then normalized to the calculated neutron flux, respectively, using the calculated value at the respective segment. For the SAE1020 of the in-pile cavity, a neutron flux of $1.0 \times 10^{10} \text{ n}\cdot\text{cm}^{-2}\cdot\text{s}^{-1}$ was used. In all the cases, the irradiation time was considered as 10 years, and the decay time after the irradiation corresponds to 7 days which is less than the specified time of 10 days. These assumptions were adopted as a conservative assessment of the dose rates for the planning of the manoeuvre. These assumptions introduce an error of about 5% for the calculated dose rates.

II-2.3.2.3. Gamma dose rate model

Using the information provided in Ref. [II-1], a simple MCNP5 model of the CNS, beam tube and in-pile and shutter cavities was constructed. This is presented in Fig. II-5. The gamma ray sources obtained from the activation calculations for the various components, the CNS thimble, the beam tube and the in-pile bushing were assigned and transport to the dose locations was performed. Gamma flux-to-dose conversion factors were used to provide the required dose rate estimates.

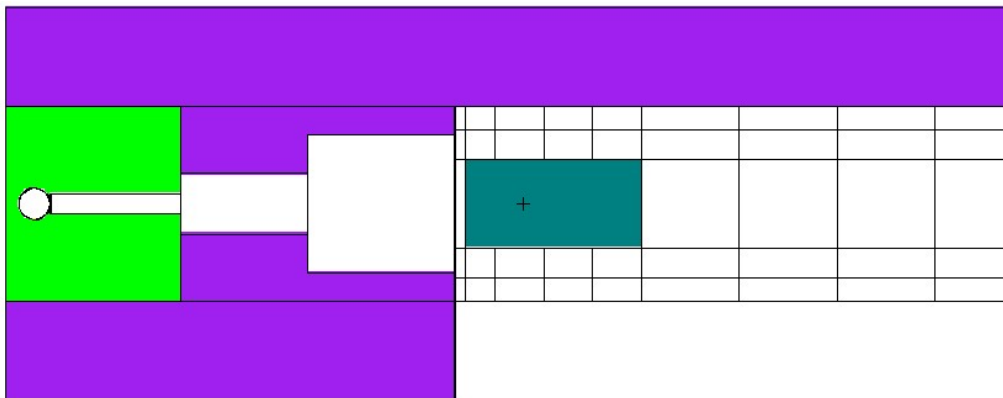


FIG. II-5. CG2 model with the in-pile extracted. (courtesy of ANSTO, Australia)

II-2.3.3. France (FRA) models

The models constructed and the assumptions adopted for the various calculations are presented in turn for each of the calculation steps.

II-2.3.3.1. MCNP model for neutron flux

Neutron fluxes in the various components were calculated with MCNP6. The model developed includes a detailed model of the core with a simplified model of the reflector tank and its internal components (i.e. without irradiation devices in the tank). Neutron fluxes were calculated in all the CNS components and along the beam tube and in-pile cavity. Figure II-6 illustrates the model used for these calculations.

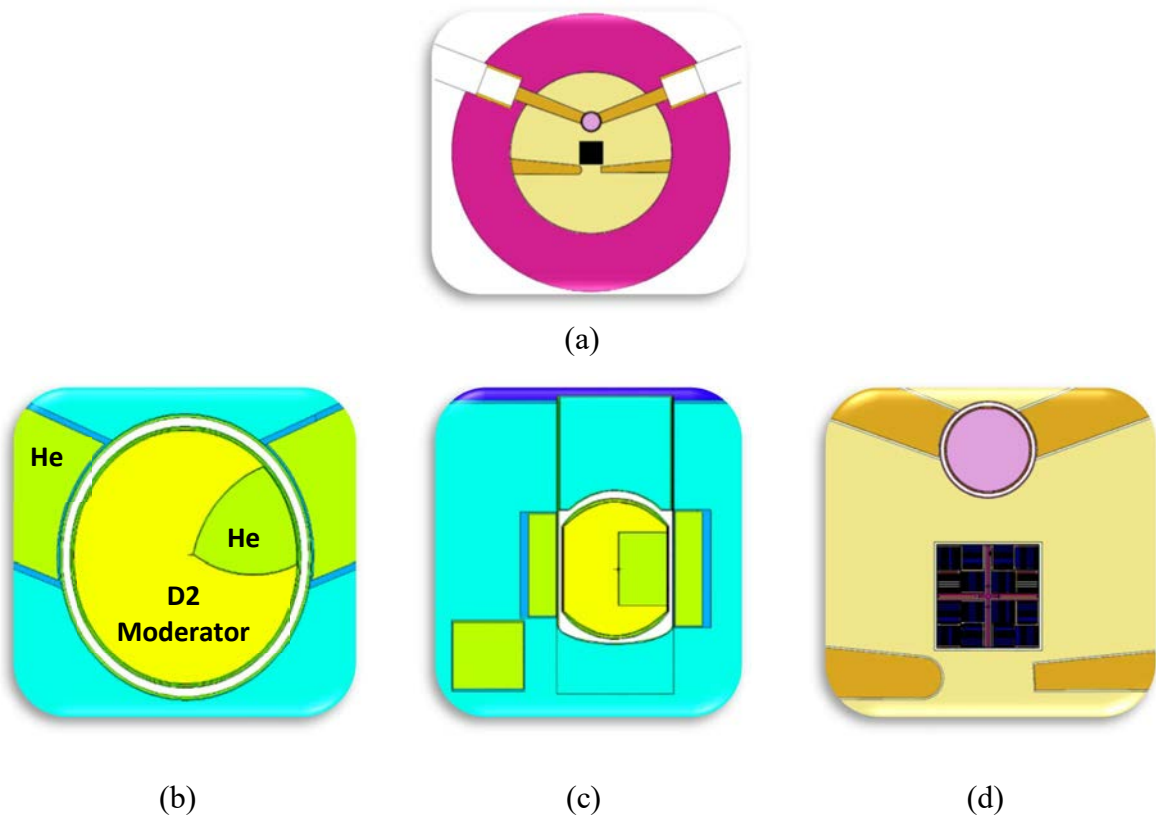


FIG. II–6. Various details of the MCNP model used for flux calculation. (a) indicates the whole reactor model with only the core, beam tubes and CNS, no irradiation facilities. (b), (c), (d) details of the CNS. (courtesy of TechnicAtome, France)

II–2.3.3.2. Material activation and gamma ray source

The total activity in the relevant components was calculated using the DARWIN2 code. DARWIN2 is composed of two modules: INTERPEP and PEPIN. It is highlighted with the bold red line in Fig. II–7. The calculation line used the neutron flux spectra from MCNP6 calculations (determined according to a given geometry, material balance and reactor power) as input. The calculated neutron spectra were input to the INTERPEP module in addition to material compositions and irradiation history (including decay time). The results obtained from the INTERPEP module were the integrated reaction rates over all energy groups. These reaction rates were then used in the PEPIN module to determine photon spectra and activity inventory of materials per radionuclide.

The radionuclides considered were ^{95}Zr and ^{95}Nb for the CNS thimble (Zr–2.5%Nb) and cold neutron beam tube (Zry-4), and ^{59}Fe and ^{60}Co for the in-pile cavity (SAE1020).

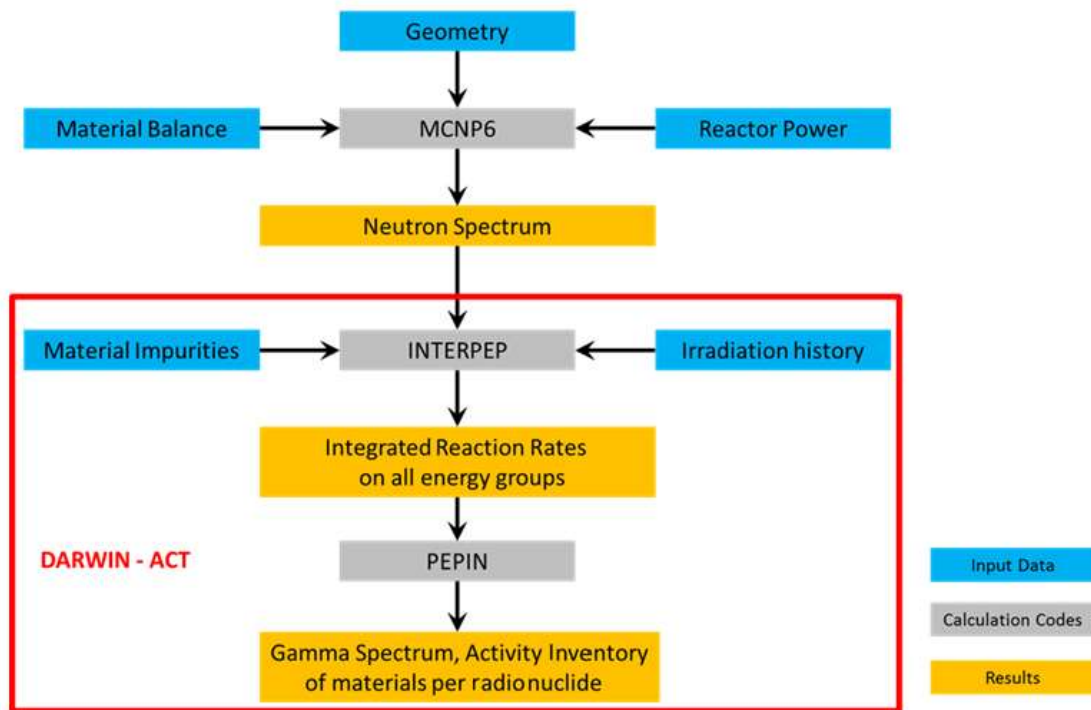


FIG. II-7. Material activation and gamma spectrum calculation line. (courtesy of TechnicAtome, France)

II-2.3.3.3. Gamma dose rate models

Three different models using three different codes were developed to calculate the gamma dose rates using the determined gamma ray source terms. Simple illustrations of the various models are presented in Fig. II-8. Each code and model will be considered in turn.

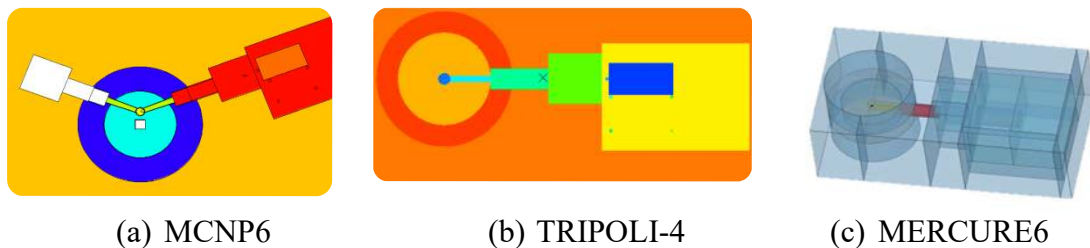


FIG. II-8. The models used to calculate the dose rates for the various codes. (courtesy of TechnicAtome, France)

MCNP6 model

A detailed 3-D model of the CNS, beam tube and in-pile was used to transport the gamma ray source. To improve the statistical accuracy of the results, variance reduction methods were used (the DXTRAN technique of the MCNP code). To provide more information around the points of interest, a mesh tally was also calculated to assess the sensitivity of dose rate with position.

TRIPOLI-4

A simplified 3-D model of the CNS, beam tube and in-pile was used to transport the gamma ray source. To improve the statistical accuracy of the results, spatial weighting was used as a

variance reduction technique. To provide more information around the points of interest, an extended mesh tally was used.

MERCURE6

A simplified 3-D model of the CNS, beam tube and in-pile was used to transport the gamma ray source. The calculation was based on the actual location of the measured dose point. MERCURE6 can only be used for straight line attenuation calculations. For this reason, only points 1, 2, 6 and 7 were calculated using this code.

II-3. RESULTS

The results from the neutron flux, activation, gamma ray source and dose rate calculations, as relevant, by the various participants are presented and then compared and discussed. As the required result was only the dose rate, not all intermediate results have been reported by all participants.

II-3.1. Results of the individual participant contributions

In this section, the results obtained by the individual participants are presented.

II-3.1.1. Argentina (ARG) results

II-3.1.1.1. Neutron flux results

The thermal neutron flux results for the various components of the CNS and the segments of the inner and outer beam tube are presented in Table II-6. These are values averaged over the volume of the components or segments (see Fig. II-2 for the zone locations).

TABLE II-6. THERMAL NEUTRON FLUX IN CNS AND COLD BEAM TUBE

Component	Neutron flux [$n \cdot \text{cm}^{-2} \cdot \text{s}^{-1}$]
Moderator vessel	1.55E+14
Vessel jacket	1.55E+14
Containment vessel	1.55E+14
Inner beam – zone 1	7.95E+13
Inner beam – zone 2	5.34E+13
Inner beam – zone 3	3.41E+13
Inner beam – zone 4	1.97E+13
Outer beam – zone 1	4.05E+11
Outer beam – zone 2	4.06E+11
Outer beam – zone 3	3.11E+11
Outer beam – zone 4	2.22E+11

II-3.1.1.2. Gamma dose rate results

The calculated photon dose rates for some of the positions are presented in Table II-7. For some of the positions, the calculation did not converge sufficiently and the statistical error was too high to yield reliable values and so these were not provided. The result for position 6 shows good agreement with the measurement. The results for positions 7 and 8 are significantly

different even accounting for the statistical uncertainties in the calculations. Calculated dose rates for positions 1 to 5 were not available as the associated statistical error was too high.

TABLE II-7. MEASURED AND CALCULATED GAMMA DOSE RATES

Position	Measurement [mSv/h]	Calculation [mSv/h]
6	500	575 ⁽¹⁾
7	300	180 ⁽²⁾
8	400	70 ⁽²⁾
9	7	n/a ⁽³⁾
10	30	n/a ⁽³⁾

⁽¹⁾ statistical error of the MCNP calculation <<10%

⁽²⁾ statistical error of the MCNP calculation ~10%

⁽³⁾ statistical error of the MCNP calculation >50%

As a further sensitivity study and confirmation of the assumptions adopted regarding the main source regions, the contribution to the dose rate at position 6 was analysed in detail with respect to the various components. The results of this study are presented in Table II-8.

TABLE II-8. DOSE RATE CONTRIBUTIONS FOR POSITION 6

Component	Contribution to dose rate at position 6	
	[mSv/h]	[%]
Moderator vessel	0.61	0.1
Vessel jacket	0.56	0.1
Containment	87.8	15.3
Tip of the beam	60.1	10.4
Inner beam - zone 1	96.6	16.8
Inner beam - zone 2	64.9	11.3
Inner beam - zone 3	52.2	9.1
Inner beam - zone 4	39.7	6.9
Inner beam - zone 5	36.4	6.3
Outer beam - zone 1	34.6	6.0
Outer beam - zone 2	38.9	6.8
Outer beam - zone 3	34.0	5.9
Outer beam - zone 4	28.7	5.0
Total	575.1	100.0

II-3.1.2. Australia (AUL) results

II-3.1.2.1. Neutron flux in the activated components

The neutron fluxes along the cold beam tube obtained from the MCNP simulation are depicted in Table II-9.

The distances in the table above are relative to the inner face of the beam tube. The neutron flux for the CNS thimble in its central region, 20 cm above and below the beam tube centre line was calculated to be $1.0 \times 10^{14} \text{ n}\cdot\text{cm}^{-2}\cdot\text{s}^{-1}$.

Neutron fluxes in the in-pile and shutter cavity are greatly reduced due to the internal components and shielding. As such any activation of these components and resulting gamma ray flux will be minor compared to the beam tube and CNS thimble. Therefore, no further analysis was performed on these components.

TABLE II-9. NEUTRON FLUXES ALONG THE COLD NEUTRON BEAM TUBE

Distance from inner face [cm]	Neutron flux [n·cm ⁻² ·s ⁻¹]	Distance from inner face [cm]	Neutron flux [n·cm ⁻² ·s ⁻¹]
0	8.51E+13	70	1.04E+13
10	5.68E+13	80	8.33E+12
20	4.59E+13	90	6.68E+12
30	3.29E+13	100	5.35E+12
40	2.62E+13	110	4.29E+12
50	1.94E+13	120	3.44E+12
60	1.30E+13		

II-3.1.2.2. Activation of internal components

The isotopic specific activities of the various materials are shown in Tables II-10, II-11 and II-12. The isotopes presented are those relevant from a dose rate perspective. Other isotopes were ignored to simplify the calculation with no impact on the final result.

TABLE II-10. Zry-4 ACTIVATION

Isotope	Specific activity [Bq/g]
Zr-95	6.0E+9
Nb-95	6.3E+9

TABLE II-11. Zr-2.5%Nb ACTIVATION

Isotope	Specific activity [Bq/g]
Zr-95	5.7E+9
Nb-95	1.2E+10

TABLE II-12. SAE1020 ACTIVATION

Isotope	Specific activity [Bq/g]
Fe-59	2.3E+6
Co-60	1.2E+2

II-3.1.2.3. Gamma dose rates

The results for the dose rates obtained using the simplified MCNP model are presented in Table II-13 for the various positions along with the measured data. For some of the positions, the dose rate was very sensitive to the exact position. For these positions, a range of the dose rates has been included for the calculated values.

Agreement is good for most of the positions, with the exception of position 8 and possibly 3. Both positions are similar, with the main difference being the location of the transport shield either at the reactor face or 2 m away. At these positions, the dose rate is very sensitive to the actual position and the measured dose is on the upper range of the calculation for position 3. This sensitivity with actual position may explain the difference for this position. However, there

is a significant discrepancy for position 8 that is outside the range of the calculated dose rates. This raises some doubt concerning the measured value for this position.

TABLE II-13. CALCULATED GAMMA DOSE RATES

Tally location Position – Description	Dose rates [mSv/h]	
	Calculated	Measured
1 – Front face of shield	180 – 300	200
2 – Left side of in-pile shield (front)	40	30
3 – Left side of in-pile shield (front)	2 – 40	40
4 – Left side of in-pile shield (rear)	3	2
5 – Left side of in-pile shield (rear)	9	10
6 – Front face of shield	460 – 500	500
7 – Left side of in-pile shield (front)	250 – 300	300
8 – Left side of in-pile shield (front)	2 – 10	400
9 – Left side of in-pile shield (rear)	5 – 14	7
10 – Left side of in-pile shield (rear)	30 – 40	30

II-3.1.3. France (FRA) results

II-3.1.3.1. Neutron flux in the activated components

Neutron fluxes in all parts of the CNS were calculated. In addition, results are provided for the area of interest 20 cm above and below the centre line of the CNS. The results obtained are presented in Table II-14.

TABLE II-14. THERMAL NEUTRON FLUXES IN CNS

CNS component	Neutron flux [n·cm ⁻² ·s ⁻¹]	Statistical uncertainty [%]
1: Moderator D ₂	1.714E+14	0.30
2: Displacer He	1.008E+14	0.44
3: Containment vessel (all)	7.556E+13	0.22
4: Containment vessel (cylindrical part)	8.121E+13	0.23
5: Containment vessel (cylindrical part – interest area)	1.004E+14	0.23
6: Containment vessel (plug part)	4.772E+13	0.37
7: Containment vessel (spherical part)	5.501E+13	0.36

Figure II-9 presents the calculation components of the CNS. The two red dotted lines mark out the area of interest considered for the calculation.

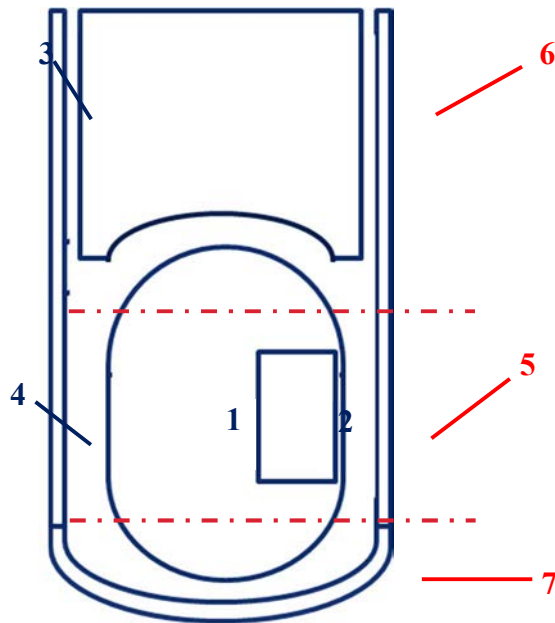


FIG. II-9. Components of the cold neutron source. (courtesy of TechnicAtome, France)

The second step of the neutron flux calculations was related to the determination of the neutron flux along the cold beam tube. Table II-15 presents the results obtained and associated uncertainties.

TABLE II-15. NEUTRON FLUXES IN THE COLD BEAM TUBE AND IN-PILE

Location	Distance from the inner face of beam tube [cm]	Calculated thermal neutron flux [$n \cdot \text{cm}^{-2} \cdot \text{s}^{-1}$]	Statistical uncertainty [%]
Cold beam tube	0	7.78E+13	0.48
	10	6.50E+13	0.62
	20	5.10E+13	0.68
	30	3.97E+13	0.75
	40	3.14E+13	0.83
	50	2.41E+13	0.92
	60	1.90E+13	1.02
	70	1.43E+13	1.16
	80	1.09E+13	1.30
	90	7.89E+12	1.52
	100	5.38E+12	1.80
Outer beam tube	110	3.30E+12	2.13
	120	1.91E+12	2.93
In-pile cavity	170	4.39E+11	5.48
	220	1.70E+11	10.56
	270	9.33E+10	12.27

II-3.1.3.2. Activation of internal components

The specific activities of the various radionuclides in the components, as calculated by DARWIN2, are presented in Table II-16.

TABLE II–16. SPECIFIC ACTIVITIES FOR THE VARIOUS COMPONENTS

Component	Isotope	Calculated specific activity [Bq·g ⁻¹]
CNS thimble (Zr–2.5%Nb)	Zr-95	5.42E+9
	Nb-95	1.22E+10
Beam tube (Zry-4)	Zr-95	6.46E+9
	Nb-95	6.91E+9
In-pile cavity (SAE1020)	Fe-59	3.33E+5
	Co-60	2.00E+1

II–3.1.3.3. Gamma dose rates

The gamma dose rates obtained from MCNP6 and TRIPOLI-4 are presented in Table II–17. The results between the two codes agree very well for all positions. For half of the positions, the results obtained are in good agreement with the measured values, while for the other half (shaded) the results do not agree within the statistical uncertainties. These statistical uncertainties are those given directly by the codes for the dose rate calculation, and do not include the uncertainties from other steps of the calculation. In this sense, they are merely a convergence check. The statistical uncertainties for the TRIPOLI-4 results are higher than for the MCNP6 results. The MCNP6 FMESH dose rates are shown schematically in Fig. II–10. The results indicate that there is significant sensitivity for some of the positions and that an accurate definition of the location and the extent of the measurement volume are required for meaningful comparison.

TABLE II–17. CALCULATED GAMMA DOSE RATES

Position	MCNP6		TRIPOLI-4		Measured Dose rate [mSv/h]
	Dose rate [mSv/h]	Statistical uncertainty [%]	Dose rate [mSv/h]	Statistical uncertainty [%]	
1	255 – 267	1	202 – 211	2	200
2	200 – 205	1	142 – 164	2	30
3	5 – 6	5	1 – 4	15	40
4	2 – 40	5	9 – 90	8	2
5	8 – 14	3	3 – 6	14	10
6	650	0.3	454 – 481	2	500
7	85 – 380	0.5	168 – 363	2	300
8	0.65	6	<1	41	400
9	1 – 8	8	1 – 4	20	7
10	4 – 6	3	2 – 3	25	30

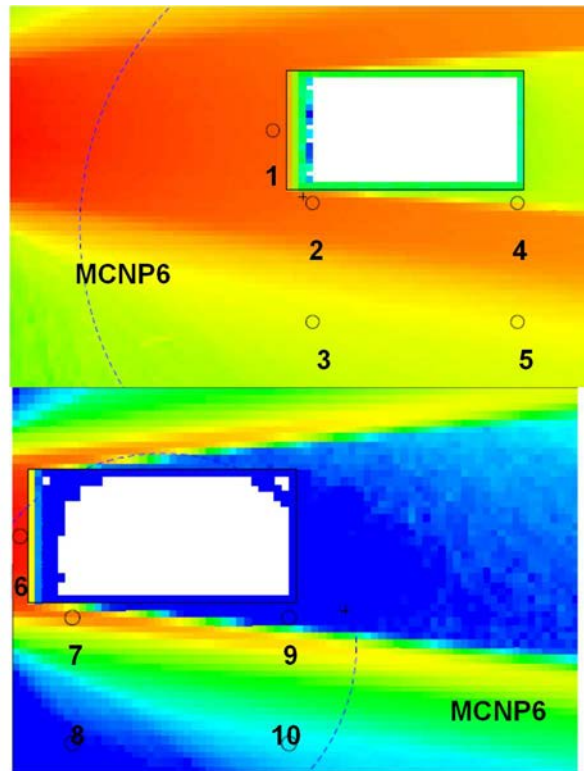


FIG. II-10. MCNP6 FMESH dose rates. (courtesy of TechnicAtome, France)

The results from MERCURE6 are presented in Table II-18. This is only for the positions with straight line attenuation calculations as this is a limitation of the method. These results are in good agreement with the previous results from MCNP6 and TRIPOLI-4 in Table II-16. Positions 1, 6 and 7 are also in good agreement with the measured values but position 2 is not.

TABLE II-18. MERCURE6 DOSE RATES

Position	MERCURE6		Measured
	Dose rate [mSv/h]	Statistical uncertainty [%]	Dose rate [mSv/h]
6	512	4.5	500
7	251	4.5	300
1	229	4.5	200
2	210	4.5	30

II-3.2. Comparison of results

All participants essentially used the same three step method of a detailed 3-D stochastic model to calculate the thermal neutron flux within the relevant activated components, to perform an activation and gamma ray source calculation, and then finally to create a simplified or detailed 3-D model to calculate the dose rate estimates from the gamma ray source. They also all performed some kind of sensitivity analysis for either the source and/or the spatial variation of the dose rate to better understand the problem.

All provided estimates of the thermal neutron flux results, although not all results are directly comparable, as it was left to the analyst to choose suitable regions and components. It appears

that the ARG flux values are higher by some 50% compared to the AUL and FRA values for the containment vessel and for the beam tube. The reason for this is not clear.

Given the good agreement in thermal neutron flux values between AUL and FRA for the containment vessel and beam tube, the resulting specific activities for the corresponding radionuclides were also in good agreement. There was a significant discrepancy for the activities associated with the in-pile cavity of a factor of about 6 but it is not clear why this is the case. At any rate, the contribution from this component has little impact on the final dose rate results.

Finally, the dose rates for all participants are compared in Table II–19. Agreement is very good amongst the participants and the measured values for positions 1 and 6 that, from calculation and specification considerations, are the simplest (see the facility specifications in Ref. [II–1] for details on the positions). This shows that the benchmark specification and data provided are consistent and sufficient to perform the calculations necessary for these positions. For the other positions, the results were not so good, with significant differences for some positions and a range of values provided for others, given the variation in dose rate identified by the participants at those positions. In particular, all participants identified a possible anomalous value for position 8. All participants obtained significantly lower dose rates for this position, and even from a physical perspective it is difficult to understand this value relative to the other positions. Apart from this position, the only participant able to obtain good agreement with measurements was the AUL group.

TABLE II–19. DOSE RATES IN mSv/h FOR ALL CALCULATIONS

Position	FRA MCNP6	FRA TRIPOLI-4	FRA MERCURE6	AUL MCNP5	ARG MCNP5	Measured
1	255 – 267	202 – 211	229	180 – 300		200
2	200 – 205	142 – 164	210	40		30
3	5 – 6	1 – 4		2 – 40		40
4	2 – 40	9 – 90		3		2
5	8 – 14	3 – 6		9		10
6	650	454 – 481	512	460 – 500	575	500
7	85 – 380	168 – 363	251	250 – 300	180	300
8	0.65	<1		2 – 10	70	400
9	1 – 8	1 – 4		5 – 14		7
10	4 – 6	2 – 3		30 – 40		30

II–3.3. Conclusions

Calculation of dose rates due to activation of reactor structures is an important and necessary capability to support maintenance and installation tasks at reactors. The calculation involves several steps and assumptions to enable the calculation to be achieved in a simple and practical manner. The results obtained by the participants indicate that the adopted methods and computational models were able to predict the maximum dose rates associated with the benchmark activity. In addition, most of the other results were indicative of the measured dose rates and, from a radiological perspective, sufficient to support the installation activities.

The benchmark specification and data are sufficient for any analyst to perform the benchmark and serve as a useful and realistic exercise to benchmark any proposed methodology for

activation of reactor structures and subsequent dose rate calculation. The attention of users of the benchmark is drawn to the fact that the measured dose rate at position 8 may not be correct and, thus, may lead to discrepancies with calculated results.

REFERENCES TO ANNEX II

- [II-1] INTERNATIONAL ATOMIC ENERGY AGENCY, Research Reactor Benchmarking Database: Facility Specification and Experimental Data, Technical Reports Series No. 480 (Rev. 1), IAEA, Vienna (in preparation).
- [II-2] PELOWITZ, D.B., MCNP6 User's Manual, Version 1.0, Rev. 0, Los Alamos National Laboratory Report LA-CP-13-00634, Los Alamos, NM (2013).
- [II-3] OAK RIDGE NATIONAL LABORATORY, ORIGEN 2.0: Isotope generation and depletion code – Matrix exponential method, Oak Ridge National Laboratory Report ORNL-RSIC-CCC 371, Oak Ridge, TN (1980).
- [II-4] OAK RIDGE NATIONAL LABORATORY, SCALE: A Comprehensive Modeling and Simulation Suite for Nuclear Safety Analysis and Design, Oak Ridge National Laboratory Report ORNL/TM-2005/39, Version 6.1, Oak Ridge, TN (2011).
- [II-5] TRIPOLI-4 PROJECT TEAM, TRIPOLI-4 Version 10 User Guide, Commissariat à l'énergie atomique et aux énergies alternatives Technical Report, CEA/DEN/DANS/DM2S/SERMA/LTSD/RT/15-5928/A.
- [II-6] RADEMAKERS, F., BRUN, R., ROOT: An Object-Oriented Data Analysis Framework, Linux Journal **51** (1998) 6.
- [II-7] SAN-FELICE, L., ESCHBACH, R., BOURDOT, P., Experimental Validation of the DARWIN2.3 Package for Fuel Cycle Applications, Nucl. Technol. **184** (2013) 217–232.
- [II-8] MERCURE PROJECT TEAM, MERCURE 6.3: User Guide, Commissariat à l'énergie atomique et aux énergies alternatives Technical Report, CEA/DEN/DANS/DM2S/SERMA/LPEC/RT/07-4125/A.

ANNEX III

BENCHMARK CONSOLIDATED RESULTS AGAINST EXPERIMENTAL DATA FROM ANSTO-3

III-1. INTRODUCTION

The ANSTO-3 benchmark analysis, including the reactor specification and experimental data, is documented in Ref. [III-1]. Medical radioisotopes are used commonly throughout the world to diagnose and treat a range of medical conditions. Successful utilization of these radioisotopes involves precisely irradiated targets to meet the tight tolerances on the post-irradiation specific activity of the targets. This can only be achieved by careful and accurate modelling of the irradiation process. This benchmark provides valuable data for the nuclear analyst to validate their calculation codes and methods in this area.

This Annex presents the codes and methods used and the results obtained by the various participants to estimate the activities of gold grains post-irradiation in the OPAL reactor. The scope is to calculate the final activity of the gold grains following irradiation and then decay up to the calibration time.

III-2. SUMMARY OF THE BENCHMARK SPECIFICATION AND CODES AND MODELS USED

III-2.1. Summary of the benchmark specification

The goal of the benchmark is to calculate the activity of Au-198 in the irradiated gold grains following irradiation and decay. To enable the analyst to perform these calculations, the following details were provided as part of the benchmark:

- A detailed reactor specification to allow modelling of the relevant components of the reactor. This includes dimensions and material composition of the core, fuel assemblies, control rods, irradiation facilities, beam tubes, cold neutron source and reflector vessel;
- Further details of the irradiation facility, the target can and gold grains, including dimensions and material compositions;
- A simplified burnup specification of the core during the irradiation cycle;
- Duration of the irradiation and decay time following irradiation up to activity measurements;
- A neutron spectrum in the region of the irradiation can for an alternate simplified calculation;
- Activity measurements for the two irradiations.

III-2.2. Summary of the codes used

The codes and associated cross-section libraries used to perform the flux and reaction rate calculations by the benchmark participants are presented in Table III-1.

TABLE III–1. CODES AND LIBRARIES USED BY THE PARTICIPANTS

Participant	Code (library)
Argentina	MCNP5 1.60 (ENDF/B-VI.8) CONDOR 2.7.01 – CITVAP 3.9.04 (ENDF/B-VII.0)
Australia	MCNP5 1.40 (ENDF/B-VI.8)
Slovenia	MCNP6.1 (ENDF/B-VII.1 and IRDFF-v1.05)

III–2.3. Summary of the models used

The models constructed and the assumptions adopted for the various calculations are presented for each of the participants.

III–2.3.1. Argentina (ARG) models

Two different calculation methods were used to predict the activation of the gold grains in the irradiation facilities. The first calculation method was based on a cell-core scheme with two calculation steps:

- A detailed 2-D calculation, using the CONDOR code, to calculate the activation factor given by the Au-197(n, γ) reaction rate divided by the average flux in the irradiation facility;
- A 3-D core calculation, using the CITVAP code, to calculate the average flux in the irradiation facility.

The second calculation method was based on a complete 3-D model of the core developed using MCNP5, where the irradiation facility and the target were explicitly modelled and the activity during irradiation was calculated directly.

III–2.3.1.1. CONDOR-CITVAP models

The simplified CONDOR 2-D model of a quarter of the core with the facility in the reflector is shown in Fig. III–1. Although the core and reflector are greatly simplified the complete detail of the facility, can and target material is included in the 2-D model, also shown in Fig. III–1.

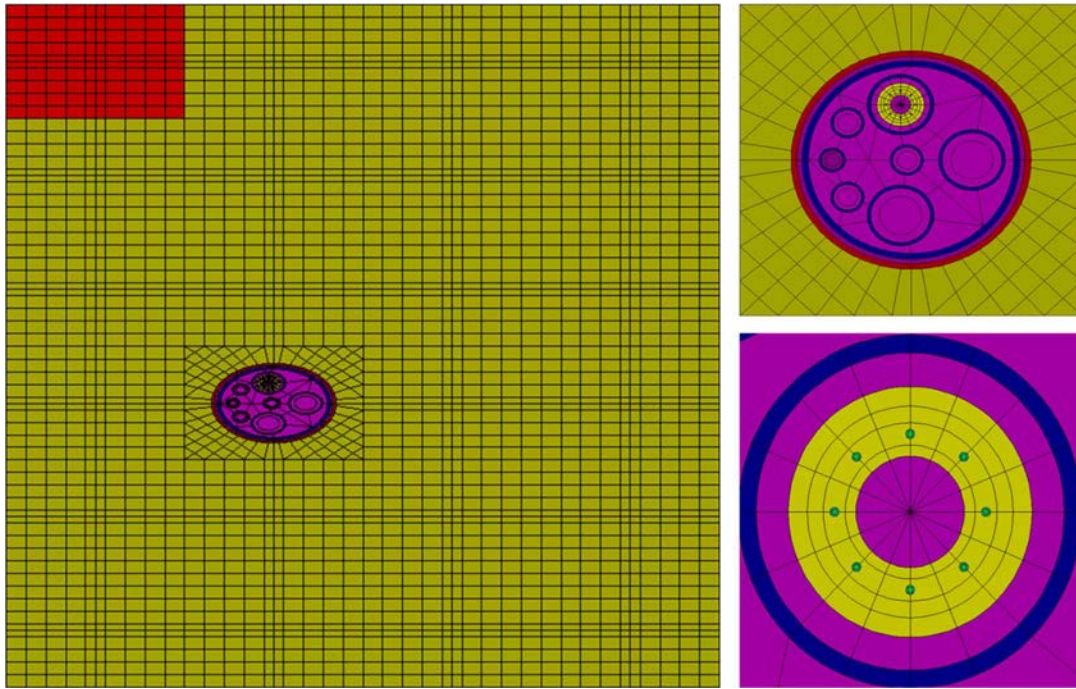


FIG. III-1. CONDOR model of the facility, can and gold grains. (courtesy of INVAP, Argentina)

The WLUP 69 group nuclear data library [III-2] based on ENDF/B-VII.0 was used for the cell calculation. Furthermore, the homogenization and condensation procedure considered three energy groups for the core calculation, with the energy limits presented in Table III-2. The provided fuel assembly burnup distributions (for BOC and EOC) were used to calculate an axial burnup distribution per fuel assembly and the fluence for each fuel assembly frame to determine the depletion of the cadmium wires.

TABLE III-2. ENERGY LIMITS FOR CITVAP CALCULATION

Group	Lower limit [MeV]	Upper limit [MeV]
1	0.821	10 (from library)
2	0.625E-6	0.821
3	0	0.625E-6

Figure III-2 shows the CITVAP core model used for the calculation of the 3-group flux at the pneumatic target tube A of irradiation facility LE6-2 (indicated by the red box). In the following, this will be called the LE6-2A facility.

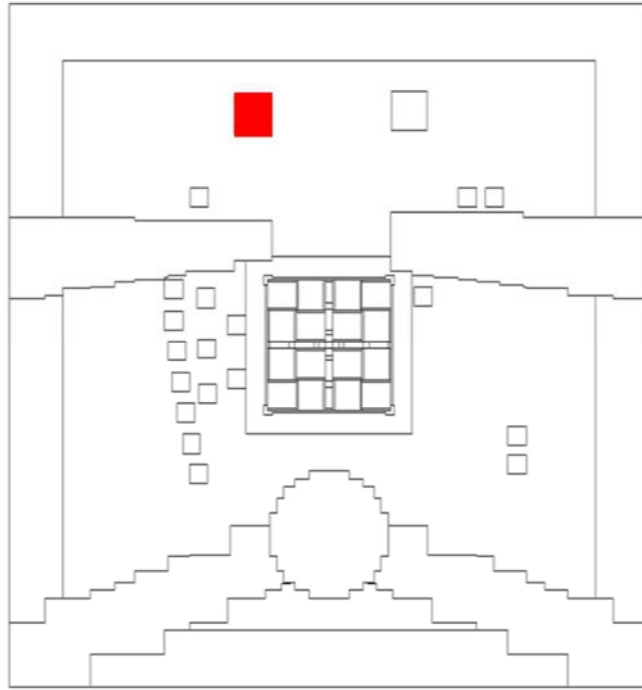


FIG. III-2. CITVAP reactor model with the LE6-2 facility highlighted in red. (courtesy of INVAP, Argentina)

III-2.3.1.2. MCNP model

The MCNP model of the reactor is shown in Fig. III-3. It includes components present in the reactor pool, in addition to those specified in Ref. [III-1] that were known to the analyst. A detailed representation of the LE6-2A facility, the can and target as specified in Ref. [III-1] was also included. This detail is shown in Fig. III-4. The fuel assemblies of the core were modelled considering ten axial divisions for the representation of the burnup distribution and the depletion of cadmium wires. The control rod configuration and the heavy water purity were adjusted according to the benchmark specifications.

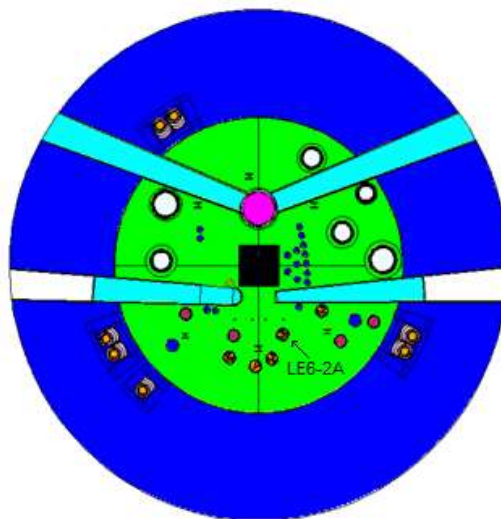


FIG. III-3. MCNP model of the reactor showing all the reflector facilities. (courtesy of INVAP, Argentina)

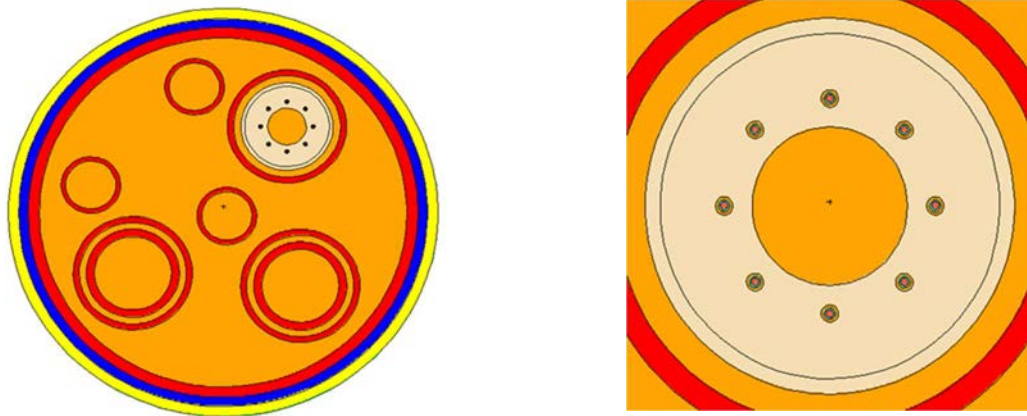


FIG. III-4. MCNP model of LE6-2A facility and can. (courtesy of INVAP, Argentina)

The burnup and fluence profile considered for the MCNP calculations were the same as in CONDOR-CITVAP calculations. The compositions for the different axial divisions of the fuel assemblies and the fuel assembly frames were extracted from the cell calculations performed with the CONDOR code, and then included in the MCNP model.

III-2.3.2. Australia (AUL) models

The models constructed and the assumptions adopted for the various calculations are presented in turn for each of the calculation steps.

III-2.3.2.1. Surface source

A detailed 3-D MCNP model of the OPAL reactor was constructed using the reactor specification, and details of the relevant irradiation facility and the targets were used to provide a full description during the irradiation [III-1]. The MCNP model details are depicted in Figs III-5, III-6 and III-7.

The target can insert and can were modelled as a solid annulus of aluminium with inner diameter of 10 mm and outer diameter of 22.5 mm. The insert cap, aluminium foil and lid were not modelled. The platinum coated gold grains were modelled explicitly, embedded within the aluminium annulus (see Fig. III-7). The can was modelled to be within the LE6-2A facility (see Fig. III-6).

Due to the small volume of the gold grains and the significant self-shielding of Au-197, two MCNP computations were needed to produce statistically meaningful results for flux and reaction rate. The first MCNP computation compiled a surface source file for the outer wall surrounding the LE6-2A facility. The reactor was modelled with the 16 fuel assemblies arranged as for the cycle 21 core, and the control rod positions were 85%, 35%, 35%, 85% and 20% extracted. This was the relevant core state at the time of the initial irradiation request. The heavy water purity was assumed to be 99.56 wt% heavy water which was also the value at the request. The impact of this deviation from the benchmark specification is minor and within the expected cycle-to-cycle variation that will be experienced for different irradiations. As such, it was accepted as a reasonable core and reflector configuration to perform the calculations.

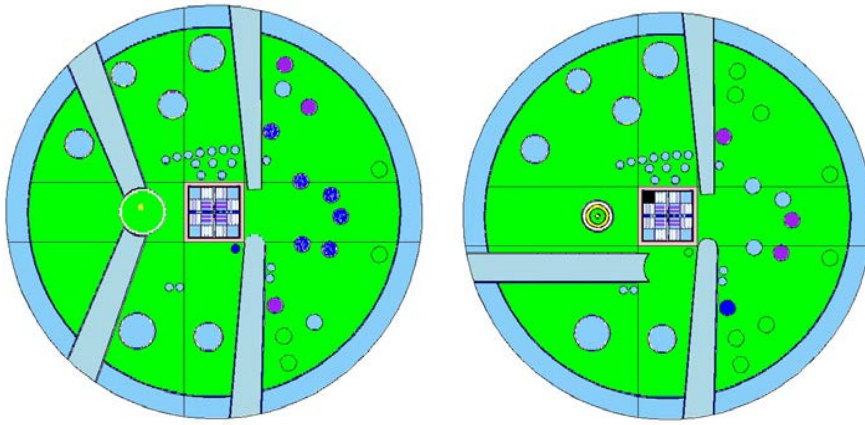


FIG. III-5. Two views at different heights of the MCNP model, showing the core and reflector vessel internal components. (courtesy of ANSTO, Australia)

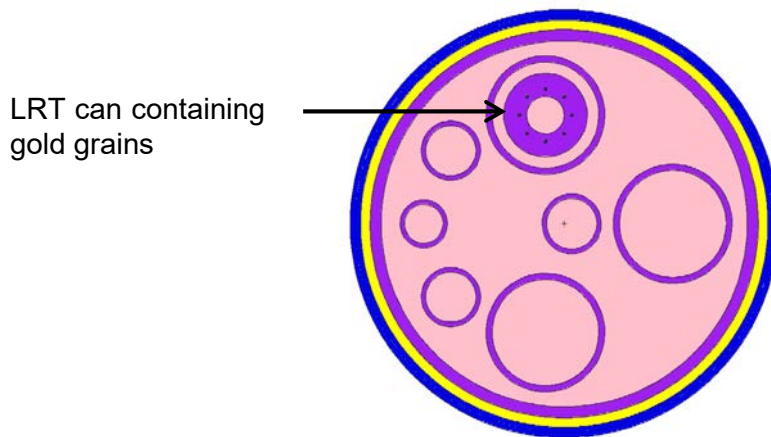


FIG. III-6. MCNP model of the can loaded with gold grains in LE6-2A. (courtesy of ANSTO, Australia)

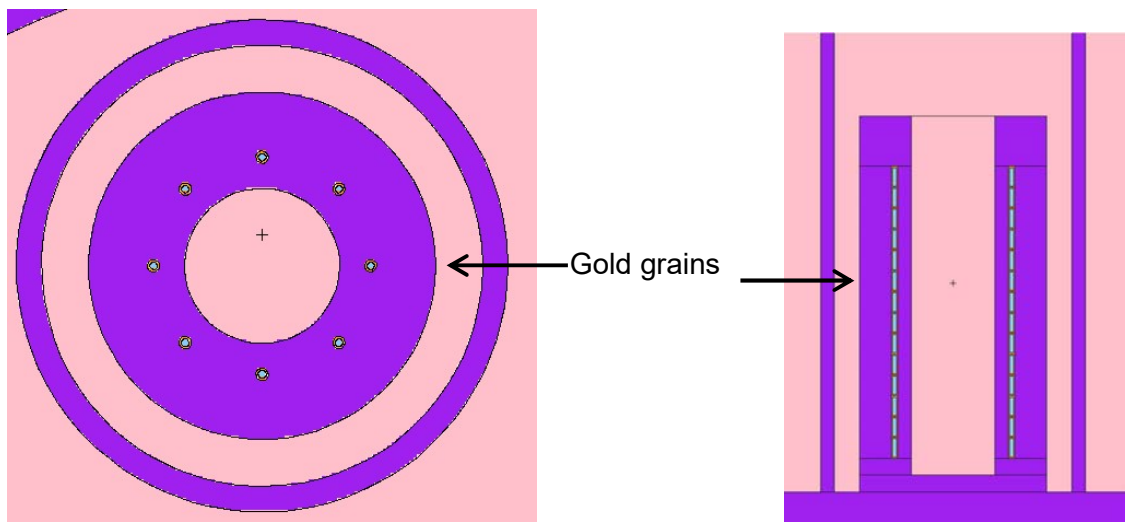


FIG. III-7. MCNP model of the target, showing plan and elevated view of the gold grains, can and insert. (courtesy of ANSTO, Australia)

III-2.3.2.2. Neutron fluxes and reaction rates

The second step used a model which was limited to the contents of the LE6-2A facility within the outer wall. The can containing gold grains was placed in this facility as shown in Fig. III-6. The surface source file written in the previous computation step was run in this computation step for 10 times the number of original particle histories. This resulted in typical statistical errors in the thermal flux and Au-197(n, γ)Au-198 reaction rates tallied over individual grains of 4% (1σ) and significantly less averaged over all the grains in the can.

III-2.3.3. Slovenia (SLO) models

Neutron fluxes and reaction rates were calculated with MCNP6.1. The model developed included only the irradiation can, insert and target. A top and side view of the model are presented in Fig. III-8. The source used was that provided as a 69-group WIMS spectrum in Ref. [III-2] for a cylindrical surface surrounding the target can. Reaction rates for Au-197(n, γ)Au-198 were calculated using cross-sections from the ENDF/B-VII.1 and IRDFF-v1.05 libraries. The reaction rates were normalized using the ratio of the calculated flux at the source surface and the absolute flux at 20 MW.

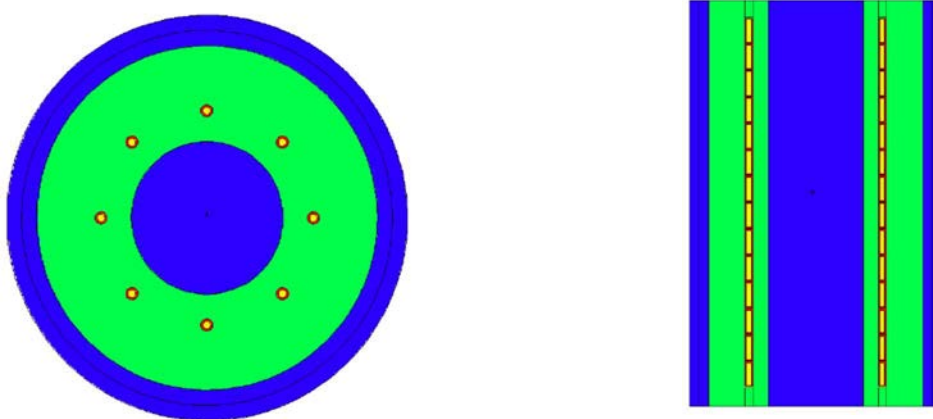


FIG. III-8. Top and side views of the MCNP model. (courtesy of JSI, Slovenia)

III-3. RESULTS

The results from the activation and decay calculations by the various participants is presented and then compared and discussed.

III-3.1. Results of the individual participant contributions

In this section, the results obtained by the individual participants are presented.

III-3.1.1. Argentina (ARG) results

III-3.1.1.1. CONDOR-CITVAP results

The CONDOR result for the ratio of Au-197(n, γ) reaction rate to thermal flux over the facility was multiplied by the thermal flux over the facility from the CITVAP results to obtain the Au-197(n, γ) reaction rate for each of the irradiation conditions. This was used to calculate the buildup during irradiation and then decay until the measurement time. The results are provided in Table III-3.

TABLE III-3. ACTIVITY RESULTS FOR ARG FROM CONDOR-CITVAP

	Irradiation 1	Irradiation 2
Au-197(n, γ) grain reaction rate [s^{-1}]	1.5252E+11	1.5260E+11
Calculated activity [MBq]	195.7	195.0

III-3.1.1.2. MCNP results

The MCNP models were used to directly obtain the Au-197(n, γ) reaction rates for each of the irradiation conditions. These were used to calculate the buildup during irradiation and then decayed until the measurement time. The results are provided in Table III-4.

TABLE III-4. ACTIVITY RESULTS FOR ARG FROM MCNP

	Irradiation 1	Irradiation 2
Au-197(n, γ) grain reaction rate [s^{-1}]	1.5629E+11	1.5474E+11
Calculated activity [MBq]	201	198

III-3.1.2. Australia (AUL) results

The AUL models did not explicitly model each of the core burnup states. This means there is only one value for the Au-197(n, γ) reaction rate. This was used to calculate the buildup during irradiation and then decay until the measurement time. The results are provided in Table III-5.

TABLE III-5. ACTIVITY RESULTS FOR AUL

	Irradiation 1	Irradiation 2
Au-197(n, γ) grain reaction rate [s^{-1}]	1.409E+11	1.409E+11
Calculated activity [MBq]	181	180

III-3.1.3. Slovenia (SLO) results

The SLO model used two different sets of cross-sections and so two sets of Au-197(n, γ) reaction rates were provided. These were used to calculate the buildup during irradiation and then decay until the measurement time. The results are provided in Table III-6. The final activity values have been adjusted for the reactor power during the irradiation from the original results at 20 MW.

TABLE III-6. ACTIVITY RESULTS FOR SLO

	Irradiation 1	Irradiation 2
IRDF library		
Au-197(n, γ) grain reaction rate [s^{-1}]	1.30E+11	1.30E+11
Calculated activity [MBq]	167	166
ENDF/B-VII.1 library		
Au-197(n, γ) grain reaction rate [s^{-1}]	1.25E+11	1.25E+11
Calculated activity [MBq]	160	160

III-3.2. Comparison of results

All participants used a different methodology to calculate the Au-197(n, γ) reaction rate. Even though all participants used the MCNP code to model and calculate the reaction rate, the models and methods were different. In the case of ARG, only one complete model of the reactor, irradiation rig, can and target was used. In the case of AUL, a two-step calculation was performed with an initial surface source calculation and then a calculation of the reaction rate with a detailed model of the irradiation rig, can and target only. Finally, for SLO, a detailed model of the irradiation rig, can and target was used to obtain the reaction rate directly using a provided surface source. Only one of the participants, ARG, explicitly accounted for the core burnup states. SLO performed the calculation using two different cross-section libraries to provide an assessment of the impact of different libraries. In addition, ARG used a deterministic method (CONDOR-CITVAP) to perform the calculations. The final activity results for all participants and the measured activities are provided in Table III-7 for comparison.

TABLE III-7. CALCULATED ACTIVITIES FOR ALL PARTICIPANTS AND MEASURED VALUES

	Irradiation 1	Irradiation 2
Argentina		
CONDOR-CITVAP	195.7 MBq	195.0 MBq
MCNP	201 MBq	198 MBq
Australia	181 MBq	180 MBq
Slovenia		
IRDF	167 MBq	166 MBq
ENDF/B-VII.1	160 MBq	160 MBq
Measurement	182 MBq	181 MBq

The results from ARG are within 10% of the measured activities and this is an acceptable result for radioisotope production planning. In particular, the deterministic models that are generally faster to evaluate were also sufficiently accurate. The AUL results compare very well with the measured values but this calculation does not explicitly account for the core burnup state. The SLO results provide acceptable agreement for the IRDF library but not the ENDF/B-VII.1 library. This result indicates the impact of different libraries. In addition, further analysis and discussion with the provider of the SLO results showed that these were biased by the interpretation of the extent of the surface source and this is evident in the systematically lower values.

III-3.3. Conclusions

Calculation of activities of irradiated materials, in particular for medical radioisotopes, is an important and necessary capability to support utilization of research reactors. The calculation requires accurate data of the target materials, reactor state and irradiation conditions. The ANSTO-3 benchmark provides this data to enable the analyst to verify their calculation tools and methods for such a calculation. The results obtained by the participants indicate that the adopted methodologies and computational models were able to predict the measured activities within the expected tolerance when using the detailed benchmark data. On the other hand, when using the simplified surface source data the axial variation of the flux was not taken into account and this can lead to a bias and inaccurate results.

The benchmark specification and data are sufficient for any analyst to perform the benchmark and serve as a useful and realistic exercise to benchmark any proposed methodology for irradiation and activation of materials.

REFERENCES TO ANNEX III

- [III-1] INTERNATIONAL ATOMIC ENERGY AGENCY, Research Reactor Benchmarking Database: Facility Specification and Experimental Data, Technical Reports Series No. 480 (Rev. 1), IAEA, Vienna (in preparation).
- [III-2] INTERNATIONAL ATOMIC ENERGY AGENCY, WIMS-D Library Update, IAEA, Vienna (2007).

ANNEX IV

BENCHMARK CONSOLIDATED RESULTS AGAINST EXPERIMENTAL DATA FROM ATI-1

IV-1. INTRODUCTION

The ATI-1 benchmark analysis, including the reactor specification and experimental data, is documented in Ref. [IV-1]. It consists of a fuelled experiment [IV-2] conducted at the TRIGA (Training, Research, Isotopes, General Atomics) MARK II reactor of the Atominstitut (ATI) at Technische Universität (TU) Wien. Experimental data were obtained through the analysis by axial gamma ray spectrometry of several irradiated fuel elements (FEs) of known operating history. The measurement purpose was to provide information about fuel composition (e.g. production and depletion of major and minor actinides and fission products) under different irradiation conditions.

Additional input data [IV-3], such as ATI TRIGA reactor core geometry and configuration, in-core neutron flux spectra and distributions, reactor operating history are also provided in Ref. [IV-1].

Two participants (from Austria and Thailand) contributed at the ATI-1 benchmark using Monte Carlo computer codes to model the experiment and calculate data to be compared against experimental values for each scanned fuel element.

IV-1.1. The TRIGA Mark II reactor at ATI

The TRIGA MARK II [IV-4] reactor is a pool-type research reactor moderated and cooled by light water, licensed for 250 kW steady state and up to 250 MW pulse operation. In 2012, the reactor was converted from a highly heterogeneous core which included HEU fuel elements to a full LEU core. As a result, the core load at the time of the performed experiment consisted of 76 stainless steel clad zirconium hydride fuel elements (8.5 wt% enriched 19.95 wt% in ^{235}U) in a cylindrical geometry.

The TRIGA reactor at ATI is equipped with various irradiation facilities inside and outside the reactor core (Fig. IV-1). It incorporates facilities for neutron and gamma irradiation studies as well as for radioisotope production, sample activation and students' training.

The reactor itself was built with heavy and normal concrete. The depth of the reactor pool is 6.40 m with a diameter of 1.98 m. The radiation shielding consists of graphite, water and concrete. There are at least 2.06 m concrete on each radial angle as shielding, whereas on the vertical axis 5.40 m water above the reactor core provides the shielding.

The reactor power is controlled and regulated by three control rods. The shim rod (SHIM) and the safety rod (REG), which are withdrawn from the reactor by a solenoid and the impulse rod (TRANS), which can be withdrawn pneumatically.

The reactor core is surrounded by a graphite reflector in an aluminium cladding. It is 30.5 cm thick radially, with an inside diameter of 45.7 cm and height of 55.9 cm. In the upper part of the reflector, there is an annular groove called rotary groove or 'Lazy Susan'.

A graphite thermal column and radiographic collimator are on opposite sides of the core and extend from the outer face of the reflector assembly into the concrete shield structure. Horizontal access and shielding for the thermal column are provided by a track-mounted heavy concrete door. A dry irradiation facility (2.74 meters long, 2.44 meters wide and 3.66 meters deep) provides the working face of the radiographic collimator. Four horizontal beam ports supply neutrons for irradiation experiments.

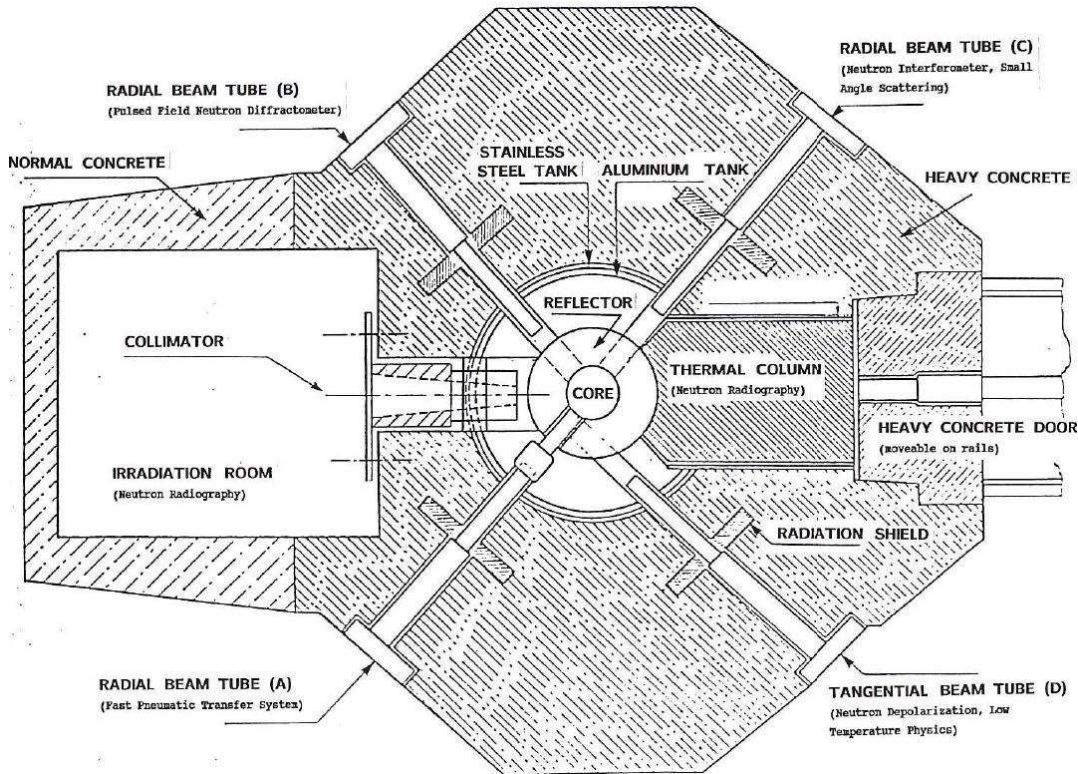


FIG. IV-1. Horizontal section of TRIGA reactor at ATI. (courtesy of ATI, Austria)

IV-1.1.1. Core overview

The reactor core (Fig. IV-2), which is located in the reactor pool and surrounded by an aluminium-graphite reflector, can host 86 fuel elements. The drill holes which provide footholds for the fuel rods are in a circular shape around the core for a total of 90 available positions. The five rings are numbered with A to F, with the A1 position corresponding to the central irradiation core channel and the external ring hosting 30 positions (F1, F2, ... F30).

At the time of experiment, the reactor core (Fig. IV-2) was composed of 76 stainless steel clad fuel elements, 3 control rods, 1 neutron source element, and 8 dummy graphite elements in the F-ring. In addition, three positions were dedicated to in-core irradiation facilities: the central irradiation channel and two pneumatic transfer systems (positions F8 and F11).

The 76 stainless steel clad zirconium hydride fuel elements (8.5 wt% enriched 19.95 wt% in ^{235}U) were all of the same TRIGA fuel type 104.

Typical temperatures inside the fuel elements during operation at 250 kW are measured by means of two thermo-coupled fuel elements in the C and E rings, respectively. The fuel temperature is about 200°C in position C6 and 135°C in position E13, respectively.

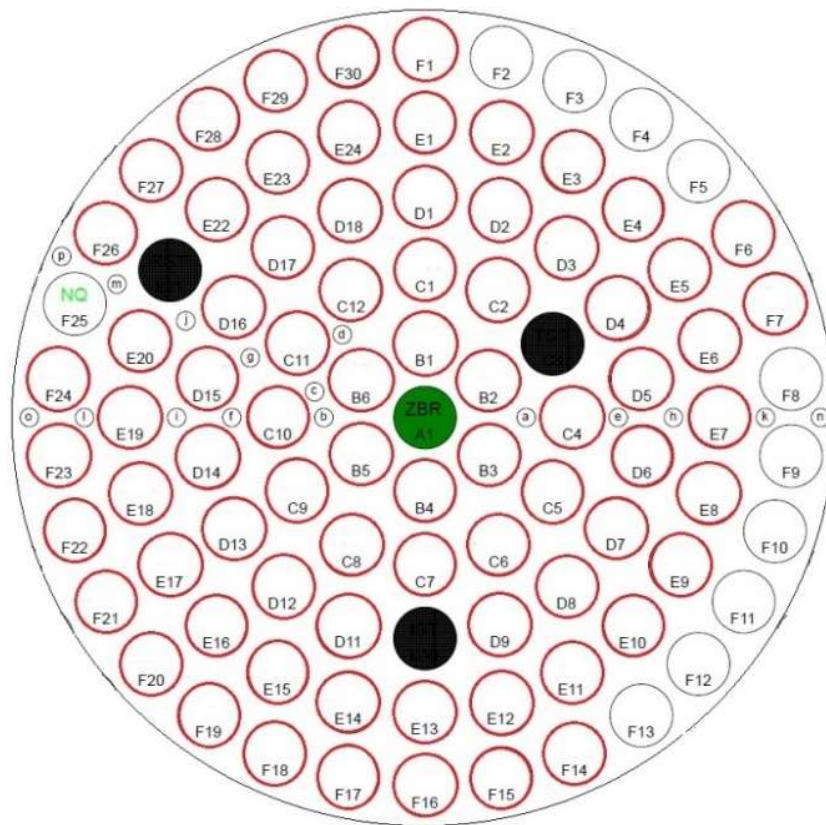


FIG. IV–2. Core configuration of the ATI TRIGA reactor at time of experiment. It includes 76 fuel elements; ZBR indicates the central irradiation channel and NQ the neutron source; the 3 control rods are represented in black colour. (courtesy of ATI, Austria)

Beside the fuel elements, other core components are:

- The three control rods, which contain boron carbide (B_4C) as a neutron absorber material. Three control rods (i.e. safety-transient (IST), shim (TST) and regulating (RST)) are operated in perforated aluminium guide tubes. The positions of all three control rods can be seen in Fig. IV–2. Each control rod is sealed in an aluminium tube containing powdered B_4C . The length of all three rods is the same (i.e. 40 cm) while the diameter of each rod is different as described in Table IV–1.
- A cylindrical Sb–Be photo-neutron source element, which has two cylinders inside (inner Sb cylinder and outer Be cylinder). The inner cylinder has a diameter of 1 cm while the outer Be cylinder has a thickness of 0.5 cm. This source element has a total length of 40.4 cm. The Sb emits gamma radiation which induces (γ, n) reactions in the outer Be cylinder. During normal operation, this source emits 6×10^6 neutrons per second.
- Graphite element(s) (dummy), which are filled with nuclear grade graphite and occupy those grid positions which are not filled by fuel elements. They have the same dimensions as the fuel elements.
- The central irradiation channel, a tube with a length of 38.4 mm which is centred in the reactor core and provides radiation of samples at the maximum available neutron flux density.
- A pneumatic transfer system (F8): The sample can be removed from the irradiation position within 3 seconds.
- A fast pneumatic transfer system (F11): The sample passes the reactor core within 20 milliseconds.

TABLE IV-1. DIMENSIONS AND MATERIAL COMPOSITION OF CONTROL RODS AT ATI TRIGA REACTOR

Component	Dimension (cm)	Material	Density (g/cm ³)
<u>Shim Rod</u>			
Outer diameter	3.2	B ₄ C	2.48
Length	40		
Cladding thickness	0.071		
<u>Regulating Rod</u>			
Outer diameter	2.2	B ₄ C	2.48
Length	40		
Cladding thickness	0.071		
<u>Safety-Transient Rod</u>			
Outer diameter	2.5	B ₄ C	2.48
Length	40		
Cladding thickness	0.071		

IV-2. SUMMARY OF THE BENCHMARK SPECIFICATION AND CODES AND MODELS USED

IV-2.1. Summary of the benchmark specification

In this section, a brief description of the benchmark specification is given. More details can be found in Ref. [IV-1].

IV-2.1.1. Irradiated samples

In this experiment, irradiated samples are the fuel elements themselves. In the present section, their geometry and initial composition is described.

Geometry

The typical TRIGA fuel element presents a cylindrical geometry. The components of a TRIGA fuel element are an enriched U-ZrH fuel meat, two axial graphite reflectors, and a burnable poison (molybdenum disks). The overall dimensions of the fuel elements are 3.76 cm in diameter and 72.06 cm in length. The detailed dimensional information of 104-type TRIGA fuel elements currently used is provided in Table IV-2 and Fig. IV-3.

Composition

The stainless steel clad 104-type fuel element is a homogeneous mixture of about 8.5 wt% of LEU and about 91.5 wt% ZrH; the uranium enrichment is 19.8%. This type of fuel has a central zirconium rod with one lower molybdenum disk as burnable poison. The average weight of the fuel meat alloy per fuel element is 2259.85 g, containing 2067.02 g of ZrH and 191.27 g of uranium. The ²³⁵U isotope content per fuel element is 38.19 g.

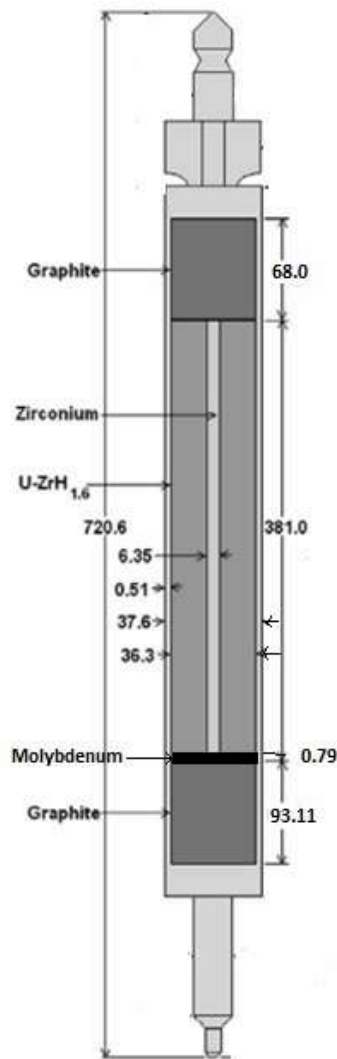


FIG. IV-3. Type 104 TRIGA fuel element (dimensions in mm). (courtesy of ATI, Austria)

TABLE IV-2. GEOMETRICAL AND MATERIAL SPECIFICATIONS OF THE TRIGA FUEL ELEMENT (TYPE 104)

Fuel element type	Type 104
Fuel moderator material	U-Zr-H1.65
Uranium content (wt%)	8.5
Enrichment (%)	19.8
Erbium content (%)	0
Diameter × length of fuel meat (cm)	3.63 × 38.1
Graphite reflector length (cm)	8.81
Cladding material	304 SS
Cladding thickness (mm)	0.51

IV-2.1.2. Experiment description

This experiment consisted in the irradiation of TRIGA fuel elements in the reactor during normal operation and subsequent examination of selected fuel elements along their vertical axis by gamma ray spectrometry to determine the type and amount of individual fission products.

Irradiation history

The measured fuel elements were loaded in the core at the same date, that corresponds to the complete core conversion in November 2012. Before that date, the fuel elements were used for a very short period in the Musashi TRIGA reactor in Japan: that reactor operated from 25 July 1985 till 21 December 1989 with stainless steel clad fuel elements; the average burnup is below 1%.

The fuel elements were irradiated during normal operation at ATI in the periods reported in Table IV–3; their position never changed during these operation cycles.

From the date of core conversion, the core had very slight modification for a total of four configurations as reported in Table IV–4. The first configuration, named Core 1, consisted of 74 fresh fuel elements placed as reported in Fig. IV–2, except the following differences in the F ring: the F6, F7, F14, F15 positions were filled with graphite elements; the F2 and F3 positions were filled with fuel elements.

Normal operation at ATI is performed at the nominal power of 250 kW. Table IV–4 shows the irradiation history during the reference period, including the cumulative produced energy in MWh at the end date of each core configuration.

The fuel elements were cooled down in the reactor tank during a planned shutdown period in 2015 before measurement by gamma ray spectrometry. Measurement date of each fuel element is reported in Table IV–3.

Measurement protocol

The fuel elements were transferred from the core to the fuel scanning machine that allows scanning the elements along the vertical axis and to raise the fuel rods exactly into the desired measurement position. Data were acquired in steps of 10 mm. Details of the experimental determination of fission products in the irradiated fuel elements are given in Ref. [IV–1].

The summary of obtained experimental data is shown in Table IV–5, where the total activity of the detected fission products is provided for each of the analysed fuel elements.

TABLE IV–3. IRRADIATION HISTORY OF THE MEASURED FUEL ELEMENTS AT ATI TRIGA REACTOR AND THEIR IN-CORE LOCATION

FE No.	First irradiation date	Last irradiation date	Date of measurement	In-core position
9213	21/01/2013	25/03/2015	01/12/2015	B2
9214	21/01/2013	25/03/2015	02/12/2015	B4
9905	21/01/2013	25/03/2015	03/12/2015	C1
9915	21/01/2013	25/03/2015	03/12/2015	D1
9932	21/01/2013	25/03/2015	03/12/2015	E1

TABLE IV-4. CORE MODIFICATION AND IRRADIATION HISTORY DURING THE REFERENCE PERIOD (21/01/2013 – 01/04/2015)

Core	Start date	Core modification	End date	Duration (days)	Cumulative MWh	Operation at 250 kW (h)
1	21/01/2013	New core loaded and start of operation	22/07/2013	182	128.86	515.44
2	22/07/2013	Fresh fuel elements in F15 and F14	04/10/2013	74	198.41	278.20
3	04/10/2013	Fuel elements reshuffle: F2 → F6 F3 → F7 Dummy element → F2, F3	14/04/2014	192	324.74	505.33
4	14/04/2014	Fuel elements in F23 removed from the core; Fresh fuel element in F23	01/04/2015	352	547.84	892.40
Total	–	–	–	800	547.84	2191.36 (91.31 days)

TABLE IV-5. TOTAL MEASURED ACTIVITY IN THE DIFFERENT FUEL ELEMENTS FOR EACH FISSION PRODUCT (VALUES REFERRED TO THE DATE OF MEASUREMENT)

Fuel element		Measured activity (Bq)			
Position	ID	Cs-137	Ce-144	Ru-103	Zr-95
B2	9213	(4.62±0.34)E+10	(8.71±0.70)E+11	(9.48±1.14)E+9	(1.22±0.11)E+11
B4	9214	(4.88±0.36)E+10	(8.67±0.69)E+11	(7.95±0.95)E+9	(1.10±0.10)E+11
C1	9905	(5.38±0.39)E+10	(8.79±0.70)E+11	(7.45±0.89)E+9	(8.44±0.80)E+10
D1	9915	(4.92±0.36)E+10	(7.71±0.62)E+11	(6.24±0.75)E+9	(7.95±0.75)E+10
E1	9932	(3.56±0.26)E+10	(6.18±0.49)E+11	(4.61±0.55)E+9	(5.78±0.55)E+10

IV-2.1.3. Input data

The neutron flux and neutron spectrum within the measured fuel elements were also provided as part of the input package for the ATI-1 benchmark [IV-1].

The flux values and neutron spectrum, within each of the measured fuel elements, were obtained by calculation with the MCNP6 code [IV-5]. The flux is provided as flux in a cell (Tally 4). The fuel active part (38.1 cm long) was divided into 9 cylindrical cells (Table IV-6) with exclusion of the central zirconium rod (i.e. each cell resulting in a ‘doughnut cell’).

TABLE IV-6. CELLS COMPOSING FUEL ACTIVE PART USED FOR FLUX AND NEUTRON SPECTRUM EVALUATION WITHIN FUEL ELEMENTS

Cell No.	Top along z axis (cm)	Bottom along z axis (cm)	External cylinder radius (cm)	Internal cylinder radius (cm)
10001	19.05	14.7		
10002	14.7	10.5		
10003	10.5	6.6		
10004	6.6	2.1		
10005	2.1	-2.1	1.815	0.03175
10006	-2.1	-6.6		
10007	-6.6	-10.5		
10008	-10.5	-14.7		
10009	-14.7	-19.05		

The calculation performed with the MCNP6 reactor model produced results in the form of the integral neutron flux over 30 energy groups: the width of the energy groups was chosen to represent constant lethargy intervals.

IV–2.2. Summary of the codes used

To calculate the ATI-1 benchmark two different Monte Carlo codes were selected by the participants. Austria participant used the Serpent 2 code [IV–6]; while Thailand participant used the MCNPX (version 2.6) code [IV–7].

IV–2.3. Summary of the models used

IV–2.3.1. Model used by Austria

The Austria participant, ATI, performed modelling and calculation by means of the Monte Carlo code Serpent 2 [IV–6].

The three-dimensional model of the TRIGA reactor of TU Wien was developed by means of the Serpent 2 code. A top view of the reactor model is shown in Fig. IV–4, a vertical view of the core is shown in Fig. IV–5.

The control rods are not shown because the burnup simulation runs at full power (250 kW) in the all rods out (ARO) configuration. The horizontal beam tubes and the annular groove graphite reflector can also be seen in the top view of the reactor.

The neutron reaction data which Serpent 2 uses for transportation calculation are taken from the OECD/NEA data bank. For the performed calculations, the ENDF/B-VII library was selected.

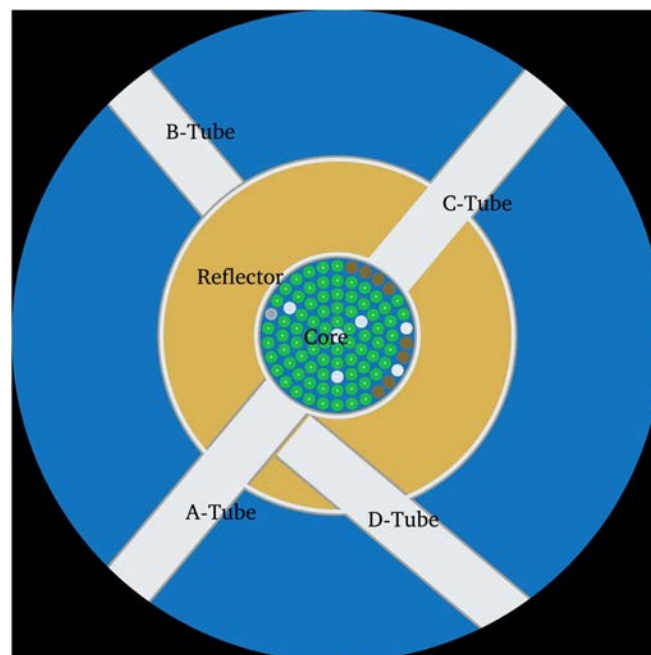


FIG. IV–4. Top view of the reactor obtained by Austria with Serpent 2 ($z = -9.65$ cm). (courtesy of ATI, Austria)

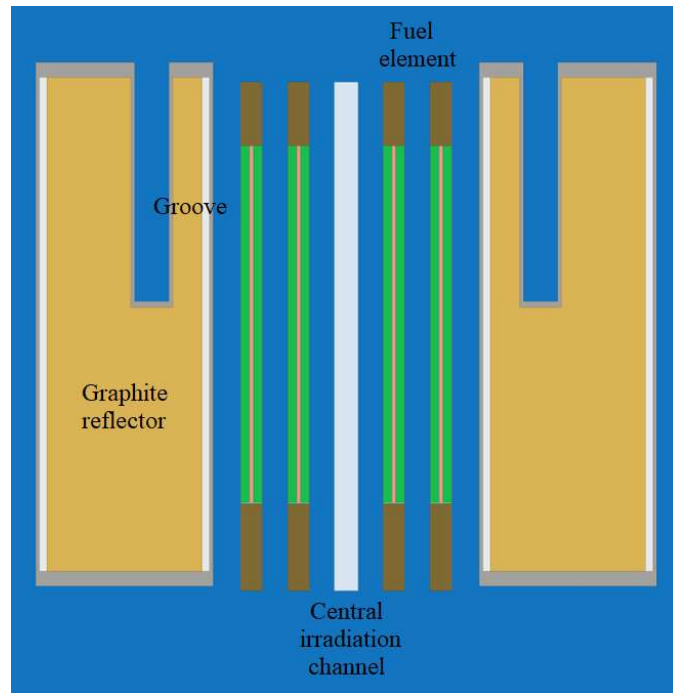


FIG. IV-5. Austria Serpent 2 vertical plots of the core at $y = 0$ cm. (courtesy of ATI, Austria)

The adopted calculation approach [IV-3] included two different simulations and is described as follows.

Serpent Simulation No. 1

The first Serpent burnup simulation was carried out with some simplifications. Due to the fact that the core modifications during the total reference period were minor, the four core configurations were collapsed in a unique one (Core 4) for which the operational time was maximum. It was also assumed that the reactor operated continuously at full power (250 kW) until reaching the total cumulative work: i.e. the simulation run in one step at a power of 250 kW and a duration of 91.31 days. A second step was included for the cooling down time (251 days) till the date of FE(s) measurement. The simulation calculation was set to 1500 cycles (where the first 70 cycles are skipped) with 1 million source neutrons each.

In the case of ^{95}Zr , with this simulation a large discrepancy (up to three times overestimated) was found between the Serpent 2 results and the experimental values. Then, in order to evaluate the activity of this short half-life (<100 days) fission product, the simulation approach was modified as described below.

Serpent Simulation No. 2

A second Serpent simulation was performed considering only the last twelve months of reactor operation before shutdown: the core configuration in this period corresponded to the Core 4 configuration. The production of fission products with half-lives <100 days (e.g. ^{95}Zr) during the previous operation period was assumed to not significantly contribute to the final results.

The simulation was divided into six time intervals, each of two months duration. For each time interval, two calculation steps were selected: one for irradiation (250 kW) and one for decay (0 kW). The number of Serpent calculation steps was then 12.

The duration of the ‘irradiation’ steps was defined by the real operation time in the corresponding two months period, while the duration of the ‘decay’ steps was set in order to cover the remaining part of the two months interval. Only the last decay step was longer, taking into account the cooling down time until the time of measurement.

IV-2.3.2. Model used by Thailand

The method used by Thailand was to adopt the Monte Carlo depletion calculations using MCNPX (version 2.6) [IV-7] as the calculation tool. The modelling data were taken from the reactor and problem specifications as provided by the Austrian participant. However, some data which were not clear or missing were assumed in the modelling process and they are discussed later. There are two calculations methods performed by Thailand for the ATI-1 benchmark.

Method 1: Core depletion using core loading 4 for all burnup cycles

The changes of the core patterns through core loading 1 to core loading 4 are not very significant. The changes occurred only in the outermost ring of the core with few fuel elements added or repositioned. The first modelling by Thailand assumes that the measured fuel elements were not significantly affected by the changes of the core patterns. Therefore, using the latest core loading to perform the burnup calculation is justified. In this modelling, the core loading 4 was adopted as the core pattern for depletion calculation. The MCNPX model of this ATI benchmark case was created as shown in Figs IV-6 and IV-7.

Method 2: Core depletion tracking for each cycle

In this second method, a more explicit core depletion modelling was performed. Essentially, each core loading history was modelled as provided by the specification. Therefore, there are four core loading calculations for this method.

For both Method 1 and Method 2, the following parameters were used for the burnup calculation:

- Three burnup cycles:
 - 21.48 days at 250 kW for cycle 1 (128.859 MWh);
 - 33.07 days at 250 kW for cycle 2 (198.409 MWh);
 - 91.31 days at 250 kW for cycle 3 (547.841 MWh).
- All control rods are half withdrawn.
- All fuel elements are fresh at the beginning of cycle 1.
- Each fuel element is depleted individually – one fuel zone per fuel element.
- Simulation neutron histories: 500 000 histories per cycle with 200 active cycles.
- Use mostly ENDF/B-VII.0 continuous cross-section library (70c).

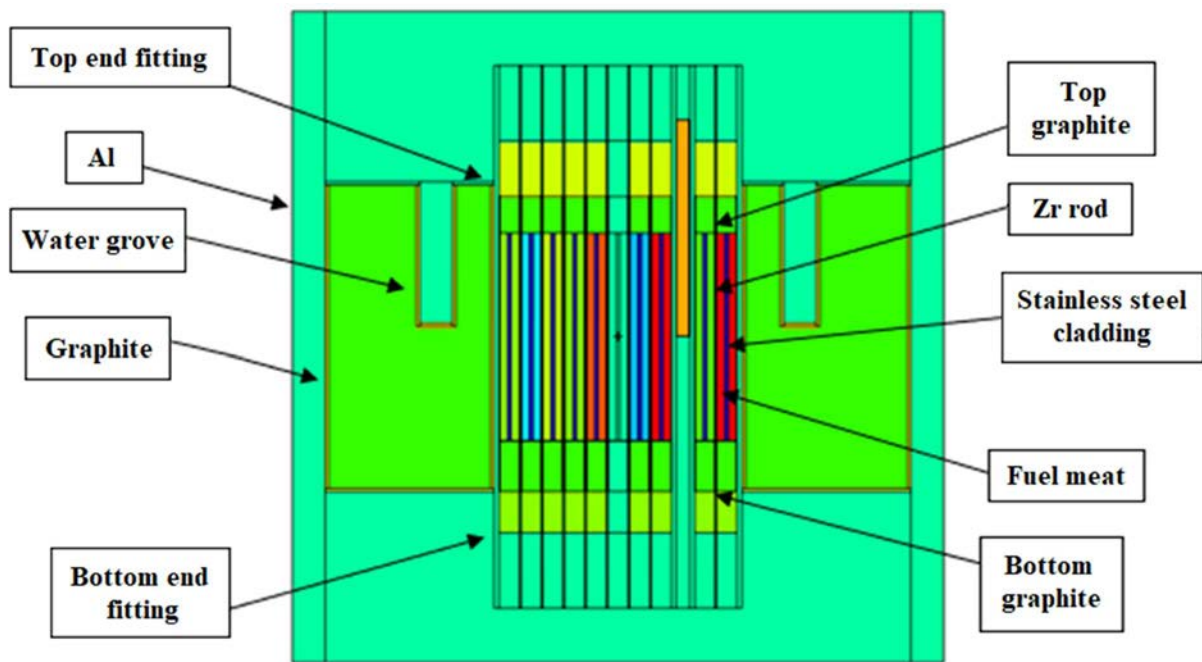


FIG. IV-6. MCNPX model of ATI TRIGA reactor (side view) developed by the Thailand participant. (courtesy of TINT, Thailand)

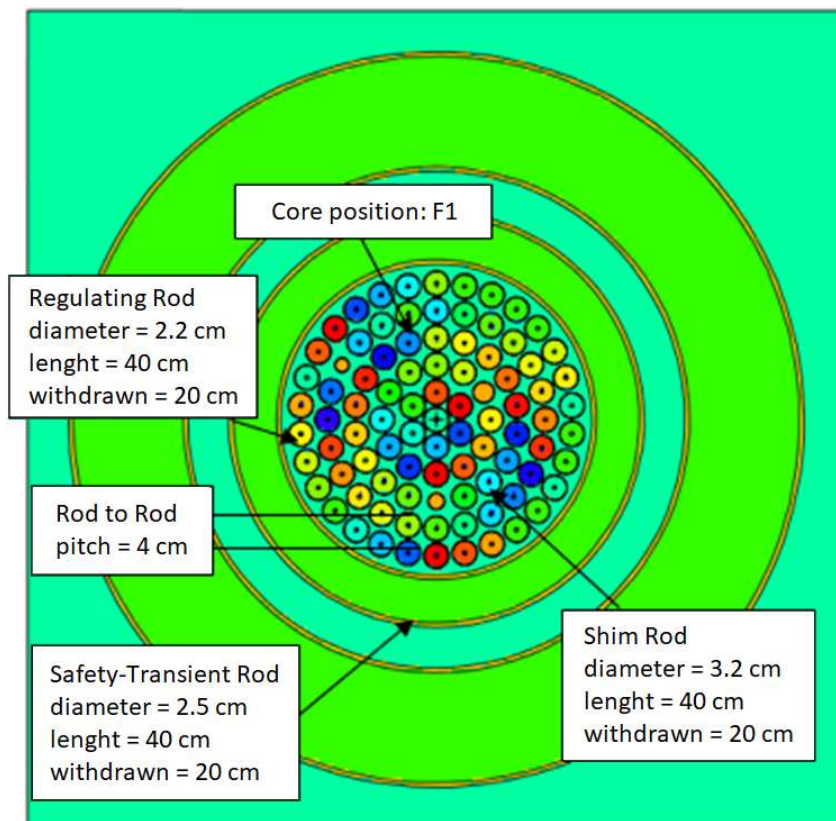


FIG. IV-7. MCNPX model of ATI TRIGA reactor (top view) developed by the Thailand participant. (courtesy of TINT, Thailand)

IV-3. RESULTS

The results of the calculations by the various participants are presented and then compared and discussed.

IV-3.1. Results of the individual participant contributions

In this section, the results obtained by the individual participants are presented.

IV-3.1.1. Austria results

Serpent Simulation No. 1

Results were provided for each burned fuel element (B2, B4, C1, D1, E1): for the main fission products, the total activity in each fuel element at the end of the reference period was calculated. In addition, each fuel element was divided in 38 cylindrical cells (of 1 cm height) along the z-axis to obtain the vertical distribution of the activity.

After each burnup step, Serpent provides an output for all burned materials (in this case the 38 fuel cells), reporting the material composition of all isotopes in atomic density (unit $10^{24}/\text{cm}^3$). Knowing the volume of a burned cell, the activity within the fuel cell was deducted for each isotope. Table IV-7 shows the calculated results obtained by Serpent simulation No. 1 for ^{137}Cs , ^{144}Ce and ^{103}Ru . The results are expressed as $(C-E)/E$ as a percentage, where E is the experimental activity value and C is the calculated value for the respective fission product.

As an example, the Serpent ^{137}Cs activity distribution along the z-axis for the five investigated fuel elements is shown in Fig. IV-8.

The comparison along the vertical axis of experimental and calculated values is shown in Figs IV-9 and IV-10 for one of the investigated fuel elements (FE9905 in position C1).

For the fission product ^{95}Zr , the Serpent simulation No. 1 results were very different to the experimental values. In fact, the simulation sharply overestimates the activity of ^{95}Zr for all fuel elements. Then it has to be considered that the half-life of ^{95}Zr is 64.03 days, comparable with the burnup time (91 days) in the performed one-step calculation. In reality, this operational time was distributed over a period of about three years, i.e. the produced ^{95}Zr also decays during the reference period. This effect was not considered in the simulation and the Serpent activity resulted much higher.

TABLE IV-7. CALCULATED ACTIVITY VALUES EXPRESSED AS $(C-E)/E$ IN PERCENTAGE OBTAINED WITH SERPENT 2 SIMULATION BY AUSTRIA

Fuel element		Serpent Activity $(C-E)/E$ [%]			
Position	ID	Cs-137	Ce-144	Ru-103	Zr-95
B2	9213	18%	11%	13%	-26%
B4	9214	6%	5%	28%	-21%
C1	9905	-18%	-12%	16%	-13%
D1	9915	-24%	-15%	18%	-22%
E1	9932	-17%	-16%	26%	-15%

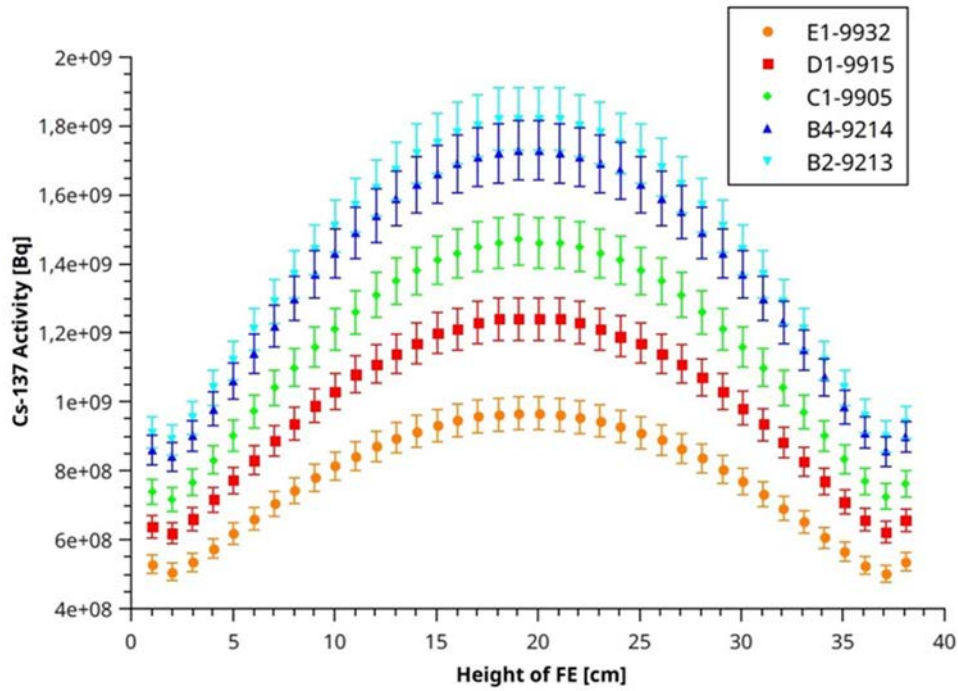


FIG. IV–8. Serpent Cs-137 activity distribution along the z-axis inside the five investigated fuel elements obtained by Austria participant. (courtesy of ATI, Austria)

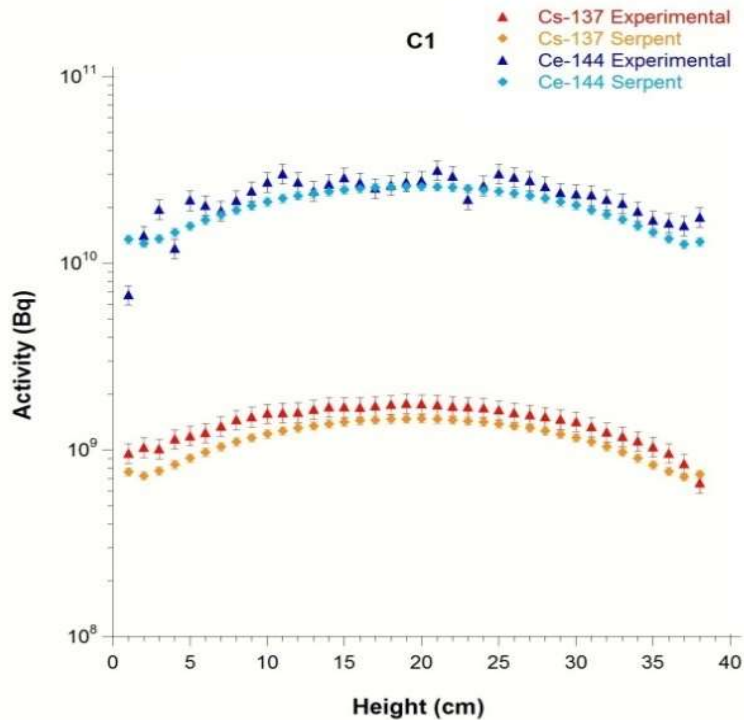


FIG. IV–9. Activity profile (along z axis) of isotopes Cs-137 and Ce-144 in the investigated fuel element 9905 (C1) obtained by Serpent 2 (Austria Simulation No. 1) and compared with experimental values (at time of measurement). (courtesy of ATI, Austria)

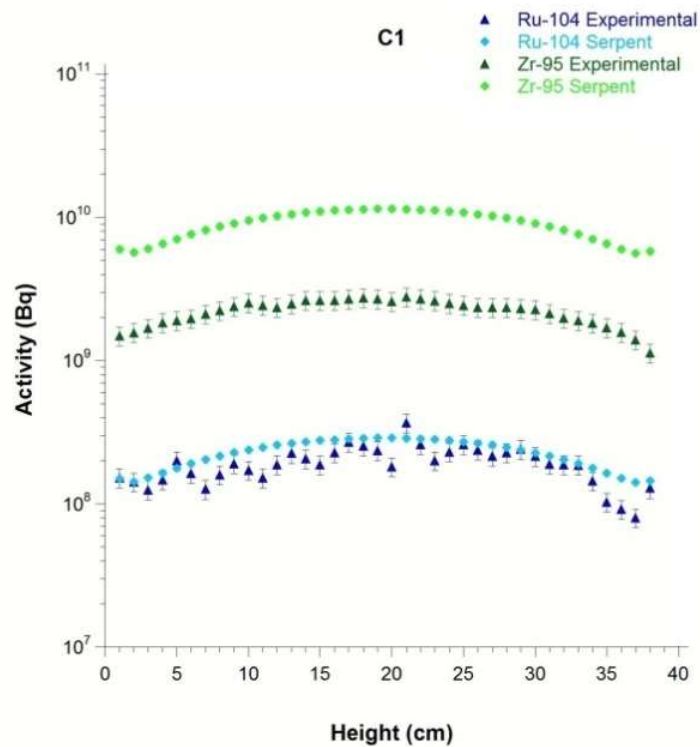


FIG. IV–10. Activity profile (along z axis) of isotopes Ru-104 and Zr-95 in the investigated fuel element 9905 (C1) obtained by Serpent 2 (Austria Simulation No. 1) and by experimental determination (values referred to at time of measurement). (courtesy of ATI, Austria)

Serpent Simulation No. 2

In the Serpent simulation No. 2, ^{95}Zr was produced during the time in which the power was set at 250 kW, followed by a time of decay, that is the buildup and decay behaviour of the total ^{95}Zr activity was reproduced with the simulation.

For isotopes with half-lives like that of ^{95}Zr , ideally a more detailed irradiation history would be needed. This is a common limit of burnup simulation for reactors that are operated and shut down on daily basis.

The calculated ^{95}Zr total activities obtained at the time of the measurement are compared with the experimental values in Table IV–5. Figure IV–11 shows the comparison along the axial profile for one of the analysed fuel elements (FE9905 in C1).

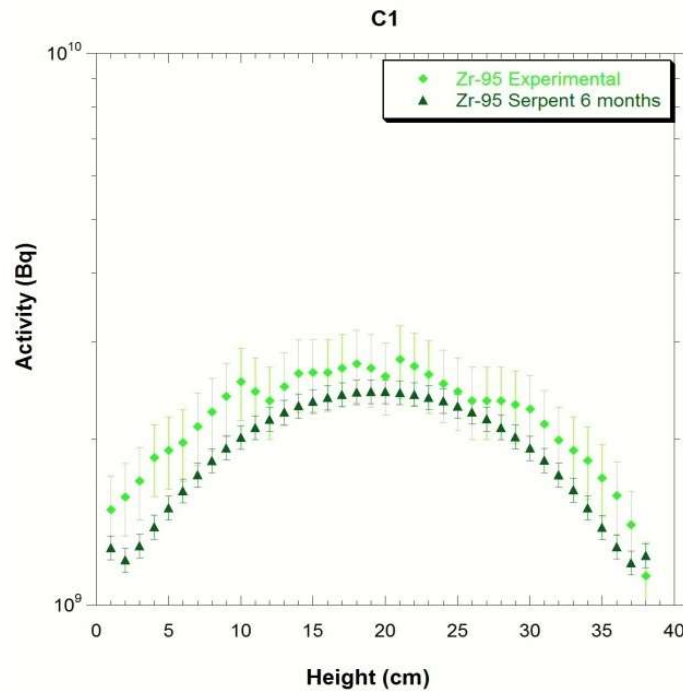


FIG. IV-11. Activity profile (along z axis) of isotopes Zr-95 in the investigated fuel element FE9905 in C1 obtained by Serpent (Austria Simulation No. 2) and by experimental determination. (values referred at time of measurement) (courtesy of ATI, Austria)

IV-3.1.2. Thailand results

As described above, there were two calculation methods performed by Thailand for the ATI-1 benchmark. The two methods provided similar results, with no appreciable differences. The results are given below for Method 1.

The % ^{235}U burned at the beginning of each core loading was calculated using MCNPX and results are presented in Table IV-8.

For comparison with the measurement, the activities of ^{137}Cs and ^{95}Zr were obtained from the MCNPX calculation for each core loading: the results are shown in Tables IV-9 and IV-10, respectively.

TABLE IV-8. % U-235 BURNED AT THE BEGINNING OF CORE LOADING OBTAINED WITH MCNPX BY THAILAND

Core Loading #	B2 9213	B4 9214	C1 9905	D1 9915	E1 9932
1	0.00	0.00	0.00	0.00	0.00
2	0.31	0.35	0.31	0.27	0.23
3	0.78	0.86	0.74	0.66	0.55
4	2.07	2.27	1.96	1.72	1.41

TABLE IV–9. ACTIVITY OF Cs-137 AT THE BEGINNING OF CORE LOADING AND AT THE MEASUREMENT TIME OBTAINED WITH MCNPX BY THAILAND

	Cs-137 MCNPX total activity (Bq)				
	Fuel element				
	B2	B4	C1	D1	E1
Core loading #	9213	9214	9905	9915	9932
1	0.00E+00	0.00E+00	0.00E+00	0.00E+00	0.00E+00
2	1.15E+10	1.26E+10	1.07E+10	9.41E+09	7.54E+09
3	2.92E+10	3.18E+10	2.73E+10	2.39E+10	1.92E+10
4	7.77E+10	8.47E+10	7.27E+10	6.36E+10	5.10E+10
Date of measurement	02/12/2015	02/12/2015	02/12/2015	02/12/2015	02/12/2015
Corrected value (time of meas.)	7.65E+10	8.33E+10	7.16E+10	6.26E+10	5.02E+10
Experiment	4.62E+10	4.88E+10	5.38E+10	4.92E+10	3.56E+10

TABLE IV–10. ACTIVITY OF Zr-95 AT THE BEGINNING OF CORE LOADING AND AT THE MEASUREMENT TIME OBTAINED WITH MCNPX BY THAILAND

	Zr-95 MCNPX total activity (Bq)				
	Fuel element				
	B2	B4	C1	D1	E1
Core loading #	9213	9214	9905	9915	9932
1	0.00E+00	0.00E+00	0.00E+00	0.00E+00	0.00E+00
2	1.96E+12	2.14E+12	1.84E+12	1.61E+12	1.29E+12
3	4.21E+12	4.59E+12	3.96E+12	3.46E+12	2.78E+12
4	7.49E+12	8.16E+12	7.02E+12	6.15E+12	4.92E+12
Date of measurement	02/12/2015	02/12/2015	02/12/2015	02/12/2015	02/12/2015
Corrected value (time of meas.)	4.89E+11	5.33E+11	4.59E+11	4.01E+11	3.22E+11
Experiment	1.22E+11	1.10E+11	8.44E+10	7.95E+10	5.78E+10

IV–3.2. Comparison and discussion of the individual results

The calculation results produced by each participant are discussed and compared in this section.

For ease of comparison, the results that can be compared (i.e. ^{137}Cs and ^{95}Zr activity values at the time of measurement) that were produced by two participants are shown in Table IV–11. The results are expressed as $(C-E)/E$ as a percentage, where E is the experimental activity value and C is the calculated value for the respective fission product.

The activity results produced by Austria (Table IV–7) by Serpent 2 simulation can be considered in fair agreement with the experimental values for all the detected isotopes.

Regarding ^{137}Cs , the activity calculated with Serpent 2 overestimates the measured value for the fuel elements in B2 and B4; while it underestimates the measurement for the other three fuel elements (C1, D1, E1). The explanation for this is that the history of the various fuel elements is different. In fact, the fuel elements B2 and B4 were fresh fuel elements when loaded in the core at the beginning of the reference period. In contrast, the other fuel elements (C1, D1,

E1) were already slightly irradiated in another reactor up until 1989. Some of the ^{137}Cs produced up to that date is still present in those fuel elements; nevertheless their initial burnup was not taken into account in the simulation. This justifies the fact that the measured ^{137}Cs concentration in these fuel elements is higher than the calculated one.

Caesium-137 activity values obtained with the MCNPX model look in general less accurate when compared to the experimental values; nevertheless, the values are of the same order. For all fuel elements, the calculated values overpredict the experimental values. An explanation for this overestimation could be an incorrect interpretation of the input information provided for the operational history. In fact, the assumption adopted in the simulation (see Section IV–2.3.2) seems to overestimate the real total operational time (about 91 days). This assumption would need to be clarified.

In case of ^{144}Ce , results were obtained with the Serpent 2 model by Austria (Table IV–7). Comparing the activities from the measurements with the ones from the simulation, the discrepancies in the total activities are between 5% and 16% for all fuel elements. However, in this case, the different irradiation history of the fuel elements does not affect the results.

The ^{104}Ru , results were also obtained with the Serpent 2 model by Austria (Table IV–7). The activities obtained from the Serpent simulation always exceed the experimental values (with a difference of between 12% and 20%). The experimental and calculated profiles of activity values along the vertical direction are in the same range even if the experimental data show a considerable fluctuation (Fig. IV–10).

For ^{95}Zr , the results obtained with Serpent 2 show discrepancies between 15% and 26% for the total activity in the different fuel elements.

This difference between calculation and measurement can be explained by the irradiation history reproduced with of the simulation. In the simulation, the buildup of ^{95}Zr happens in only few days, while in the remaining time the reactor is turned off. However, this does not correspond to the reality, in which the reactor is operated and switched off daily. Nevertheless, the results show that if there is a need to evaluate the activity of fission products with short half-lives (<100 days), there is no need to run a very long and detailed simulation with Serpent: a time period of about 10 times the isotope half-life is considered sufficient.

TABLE IV–11. COMPARISON OF CALCULATION RESULTS PRODUCED BY AUSTRIA AND THAILAND WITH SERPENT 2 AND MCNPX, RESPECTIVELY

Fuel element		Activity (C–E)/E [%]			
		Cs-137		Zr-95	
Position	ID	Serpent 2 Austria	MCNPX Thailand	Serpent 2 Austria	MCNPX Thailand
B2	9213	18	66	–26	301
B4	9214	6	71	–21	385
C1	9905	–18	33	–13	444
D1	9915	–24	27	–22	404
E1	9932	–17	41	–15	457

Note: C and E stand for the calculated and experimental activity values of the respective fission product.

For clarity of interpretation, both experimental and Serpent ^{95}Zr activity values consider the contribution of the fission reaction only (for the experimental results, the evaluation of ^{95}Zr production due to fission vs. neutron capture is described in Ref. [IV–1]).

The ^{95}Zr results obtained with the MCNPX model show a considerable overestimation of the experimental values for all the evaluated fuel elements. The explanation in this case is quite clear and is due to at least two aspects. First, the simulation did not take into account the buildup and decay scheme during the considered period (as was done in Serpent simulation No. 2). Secondly, as already noted for the ^{137}Cs case, the incorrect interpretation of the input information most likely led to an overestimation of the operational time.

IV–3.3. Conclusions

The irradiation of fuel elements was simulated starting from the new core loading to the date of temporary shutdown of the reactor, then cooling down was calculated to the date of measurement.

For each nuclide, results were provided in the five investigated fuel elements (B2, B4, C1, D1, E1) as total activity (by both Austria and Thailand participants) and as an axial profile along the z -axis (by Austria) for comparison with the experimental data.

Some simulation simplifications were assumed by the two participants in the different calculation models: for example, sometimes the four core configurations during the referenced period were collapsed in a unique one. In all cases, the core configuration at the date of first criticality was set with all fresh fuel elements, even if this does not exactly correspond to reality.

For all the fission product simulations, except for ^{137}Cs , the different irradiation history of the fuel elements (previous irradiation) compared with experimental data does not affect the results. As expected, for the long half-life nuclide ^{137}Cs , the activity calculated by Serpent 2 in C1, D1, E1 fuel elements is lower than the experimental activity.

In conclusion, the comparison showed a fair agreement between the Serpent 2 calculation and measurement results, with differences ranging from 6% to 26%.

The MCNPX model produced results that are in general less accurate when compared against measured values, nevertheless the results can still be considered consistent, taking into consideration the assumptions made in the input to the simulation process.

REFERENCES TO ANNEX IV

- [IV–1] INTERNATIONAL ATOMIC ENERGY AGENCY, Research Reactor Benchmarking Database: Facility Specification and Experimental Data, Technical Reports Series No. 480 (Rev. 1), IAEA, Vienna (in preparation).
- [IV–2] CAGNAZZO, M., et al., Fission products detection in irradiated TRIGA fuel by means of gamma spectroscopy and MCNP calculation, *Appl. Radiat. Isot.* **135** (2018) 123–130.
- [IV–3] CAGNAZZO, M., Neutronic modelling of the new TRIGA core and experimental validation, PhD Thesis, Technische Universität Wien, Fakultät für Physik (2018).
- [IV–4] GENERAL ATOMIC (GA), TRIGA Mark II Reactor General Specifications and Description. General Atomic Company, U.S.A. (1964).

- [IV-5] PELOWITZ, D.B., MCNP6 User's Manual, Version 1.0, Rev. 0, Los Alamos National Laboratory Report LA-CP-13-00634, Los Alamos, NM (2013).
- [IV-6] LEPPÄNEN, J., Serpent – a Continuous-energy Monte Carlo Reactor Physics Burnup Calculation Code User's Manual, VTT Technical Research Centre of Finland, 18 June 2015 (2015).
- [IV-7] PELOWITZ, D.B., MCNPX User's Manual, Version 2.7.0, Los Alamos National Laboratory Report LA-CP-11-00438, Los Alamos, NM (2011).

ANNEX V

BENCHMARK CONSOLIDATED RESULTS AGAINST EXPERIMENTAL DATA FROM ATI-2

V-1. INTRODUCTION

The ATI-2 benchmark analysis, including the reactor specification and experimental data, is documented in Ref. [V-1]. It consists of an activation experiment conducted at the TRIGA (Training, Research, Isotopes, General Atomics) MARK II reactor of the Atominstitut (ATI) at Technische Universität (TU) Wien.

Experimental data were obtained through the irradiation and subsequent analysis by gamma ray spectrometry of fissile and fertile material samples. The purpose of the exercise is to analyse the production and depletion rates of relevant elements in the targets under different irradiation conditions.

Two participants (from Austria and Slovenia) contributed at the ATI-2 benchmark using Monte Carlo computer codes to model the experiment and calculate data to be compared against experimental values.

V-1.1. The TRIGA Mark II reactor at ATI

The TRIGA MARK II [V-2] reactor is a pool-type research reactor moderated and cooled by light water, licensed for 250 kW steady state operation and up to 250 MW pulse operation. A detailed description of the reactor and of the core configuration at the time of the ATI-2 experiment is available in Ref. [V-1]. See also Annex IV.

In the upper part of the graphite reflector, there is an annular groove called ‘Lazy Susan’ (Fig. V-1). This was the irradiation position utilized for the ATI-2 experiment.

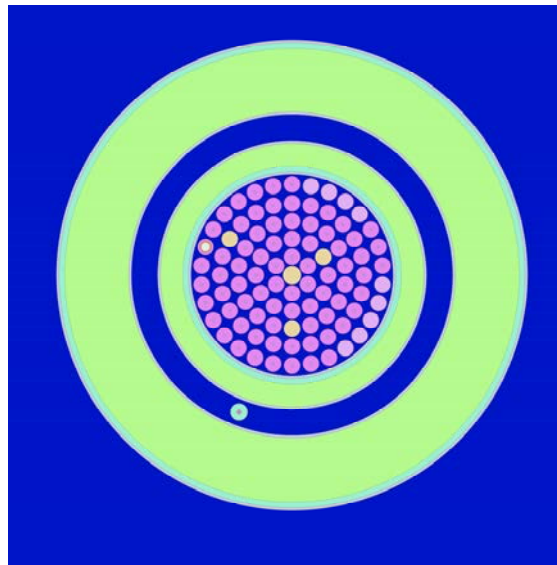


FIG. V-1. Serpent 2 model obtained by Austria participant. The horizontal view of reactor core shows the core, the graphite reflector (green coloured) and the ‘Lazy Susan’ irradiation facility (blue coloured). LSI irradiation position is visible in the Lazy Susan. (courtesy of ATI, Austria).

The ‘Lazy Susan’ (LS) originally hosted a rotary irradiation facility for irradiation of multiple samples. This rotary groove was removed years ago and the corresponding volume is now filled with the reactor tank water. Nevertheless, other irradiation facilities are installed in the annular groove: they consist of five dry vertical aluminium tubes that allow samples to be inserted in the LS facility. The LS1 vertical irradiation tube can be seen in Fig. V–1. The LS facility internal and external radii are 30.5 cm and 36.5 cm, respectively. The LS is separated by the graphite reflector by means of an aluminium cladding of 0.635 cm in thickness. The bottom of the LS facility is elevated to 2.45 cm on the z axis, where the core equatorial position corresponds to $z = 0$.

V–2. SUMMARY OF THE BENCHMARK SPECIFICATION AND CODES AND MODELS USED

V–2.1. Summary of the benchmark specification

In this section a brief description of the benchmark specification is given. More details can be found in Ref. [V–1].

V–2.1.1. Irradiated samples

In this experiment, the irradiated samples are natural uranium foils and natural thorium foils. The samples used were ordered from Goodfellow Cambridge Limited and have the shape of thin plates/foils. The thorium foils have a thickness of 0.125 mm and a diameter of 10.0 mm. The uranium foils, with the same shape, have a thickness of 0.178 mm and a diameter of 10.0 mm.

The masses of the foils are certified in the datasheets. For verification, the samples were weighed at the laboratory by means of a calibrated scale and the values obtained were compared with the data from the certificates (Table V–1). The samples are labelled with U1, U2, U3 and TH1, TH2, TH3. These identification codes were kept unchanged throughout the irradiations and measurements.

TABLE V–1: COMPARISON OF URANIUM AND THORIUM FOIL MASSES

Sample code	Datasheet mass [g]	Measured mass [g]
U1	0.212	0.21212
U2	0.216	0.21605
U3	0.210	0.20843
TH1	0.129	0.12867
TH2	0.124	0.12610
TH3	0.126	0.12647

In addition to the natural isotopic composition of the thorium and uranium samples, both contain impurities such as carbon, metals, calcium, etc. in low concentrations of ppm; however, these impurities have no impact on the analysis.

V–2.1.2. Experiment description

This experiment consisted of the irradiation of the natural U and Th foils in the LS1 irradiation position at the ATI TRIGA reactor and consequent analysis by gamma ray spectrometry to determine the type and amount of fission products.

Irradiation history

The U and Th samples were irradiated in the dry beam tube of the LS1 irradiation channel of the reactor. One irradiation was performed for each foil, with an irradiation thermal power of 5 kW and an irradiation time of 90 minutes.

In each of the six irradiations, a pure copper foil was irradiated in the central irradiation channel and used as flux monitor to verify comparability and consistency between the irradiations.

Measurement protocol

After irradiation, gamma ray spectrometry was performed. Each foil was measured at various times after the end of irradiation to allow a proper sample cooling down and the counting death time to be kept always under 8%. Measurements after a considerably long time (about 100 days) were performed to allow transient equilibrium of certain parent-daughter nuclides to be reached.

The gamma ray spectrometry was performed by means of a coaxial closed-ended HPGe n-type (series C5020, CANBERRA) with 52.8% relative efficiency, 1.81 keV energy resolution at 1.33 MeV and Peak/Compton edge ratio equal to 73.6. The efficiency calibration of the detector was performed by means of a certified solid multigamma calibration source with dimensions and geometry similar to those of the activated foils.

For determination of the fission fragments produced with the highest probability during the natural U foil irradiation, the fission products with a cumulative fission yield, CFY > 2.5% per fission of ^{235}U (Table V-2) were considered.

TABLE V-2: LIST OF THE U-235 FISSION PRODUCTS TAKEN INTO ACCOUNT FOR THE ANALYSIS, THEIR CUMULATIVE FISSION YIELD (CFY) AND HALF-LIVES (Tc-99m WAS EXPECTED AS A PRODUCT OF Mo-99 DECAY)

Element	CFY [% per fission]	Half-life	Element	CFY [% per fission]	Half-life
Zr-95	6.502	64.02 d	Sr-90	5.73	28.81 a
Nb-95	6.498	34.99 d	Ru-103	3.103	39.27 d
Mo-99 (Tc-99m)	6.132 –	2.748 d (6.01 h)	Te-132	4.276	3.20 d
I-133	6.59	20.8 h	I-131	2.878	8.02 d
Xe-133	6.6	5.24 d	I-135	6.39	6.57 h
Xe-135	6.6	5.24 d	Xe-135	6.61	9.14 h
Cs-137	6.221	30.06 a	Ba-140	6.314	12.77 d
La-140	6.315	1.68 d	Pr-144	5.474	17.28 min
Ce-141	5.86	32.50 d	Nd-144	5.475	–
Ce-144	5.474	285 d	Nd-147	2.232	10.98 d

Some of those nuclides (e.g. ^{144}Ce , ^{90}Sr) have a half-life too long for acceptable activity results in short spectrometry measurements; others (e.g. ^{135}I , ^{135}Xe , ^{144}Pr and ^{144}Nd) have a half-life that is too short to still be detectable at the time of measurement. In both cases, those nuclides were not detected.

In addition to fission product determination, the long term gamma measurements (100 days after the end of irradiation) were used for comparison with the pre-irradiation U and Th activity values. The results for the U and Th samples are displayed in Table V-3. As expected, the

activity of ^{238}U as well as ^{235}U inside the uncertainty limits is unchanged before and after irradiation. Similarly, pre- and post-irradiation results do not show differences for the Th foils.

Finally, nearly all fission products predicted were detected by the measurement.

V-2.1.3. Input data

The flux and neutron spectrum at the irradiation position LS1 were also provided as part of the input package for the ATI-2 benchmark.

Flux values and neutron spectra were obtained by calculation [V-3] with both MCNP6 and Serpent 2 codes. The neutron spectrum was given in the form of integral neutron flux over 30 energy groups: the width of the energy groups was chosen to represent constant lethargy intervals. The flux value was provided at irradiation power of 5 kW.

TABLE V-3: COMPARISON OF U AND TH FOILS ACTIVITY VALUES MEASURED BEFORE AND AFTER IRRADIATION. THE UNCERTAINTY OF THE MEASUREMENT IS WITHIN 10%

Sample code	Nuclide	Pre-irradiation activity [Bq]	Post-irradiation activity [Bq]
U1	U-235	125.19	123.44
	U-238	2696.44	2642.35
TH1	Ra-228	527.14	533.31
	Th-232	501.55	477.05

V-2.2. Summary of the codes used

To calculate the ATI-2 benchmark, two different approaches and different Monte Carlo codes were selected by the participants. Austria used the Serpent 2 code, while Slovenia adopted the combination of MCNP and FISPACT codes.

V-2.3. Summary of the models used

V-2.3.1. Model used by Austria

The participant from Austria, ATI, performed the modelling and calculation by means of the Monte Carlo code Serpent 2 [V-4].

The three-dimensional model [V-3] of the TRIGA reactor of TU Wien was developed by means of the Serpent 2 code. The model extends up to the reactor tank, including the graphite reflector, the horizontal beam tubes and the LS. The irradiation of U and Th foils was simulated in the position LS1.

The reactor horizontal and vertical sections of the Serpent-2 model are shown in Figs V-1 and V-2, respectively.

In both figures, it can be seen that the LS penetrates the graphite reflector and is filled with water. The aluminium vertical dry irradiation tube (LS1) used for the experiment was reproduced in Serpent and is visible in detail in Figs V-3 and V-4. The natural U/Th foil in the irradiation position is represented in red.

The simulation options were 1 million source neutrons per cycles, with in total 1500 cycles. To simulate the irradiation, the burnup of the foils material was modelled by Serpent with a burnup time of 90 minutes and a 5 kW reactor power. For the present calculations, the ENDF/B-VII library was selected.

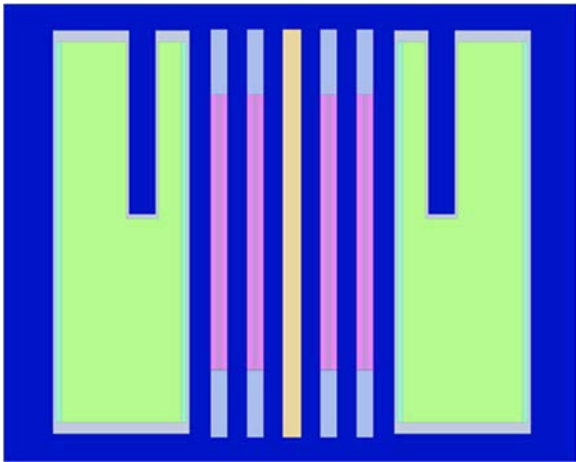


FIG. V-2. The vertical section of the TRIGA core modelled with Serpent-2 by Austria participant. (courtesy of ATI, Austria)

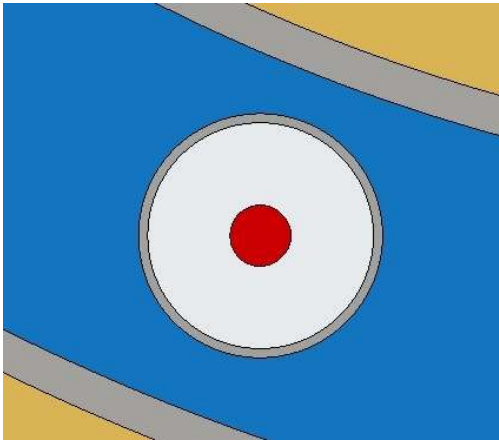


FIG. V-3. Serpent 2 model by Austria participant. Detail of the irradiation facility LSI used for U and Th foils irradiation is shown in the horizontal view. The material foil is represented in red colour. (courtesy of ATI, Austria)

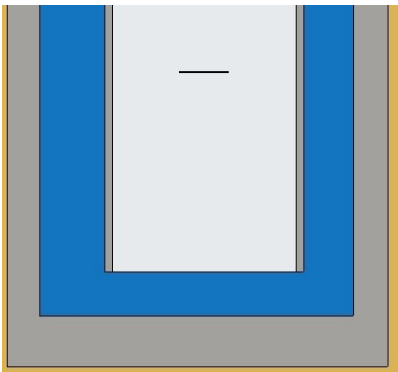


FIG. V-4. Serpent 2 model by Austria participant. Detail of the irradiated foils in the LSI irradiation position is shown in the vertical view. The real position of the foil was reproduced in the simulation. (courtesy of ATI, Austria)

V-2.3.2. Model used by Slovenia

The participant from Slovenia used the supplied data to perform an activation calculation avoiding modelling the entire reactor.

The irradiation position (LS1) was modelled by means of the MCNP6 code, including the U and Th foils. An isotropic neutron source was defined in accordance with the neutron spectrum supplied in the input data package (Fig. V-5). The selected library for this calculation was ENDF/B-VII.1. The neutron spectrum was calculated inside each foil using MCNP.

Knowing the neutron spectrum in the material, the FISPACT code was used to obtain the material composition after application of the irradiation parameters and an appropriate cooling time.

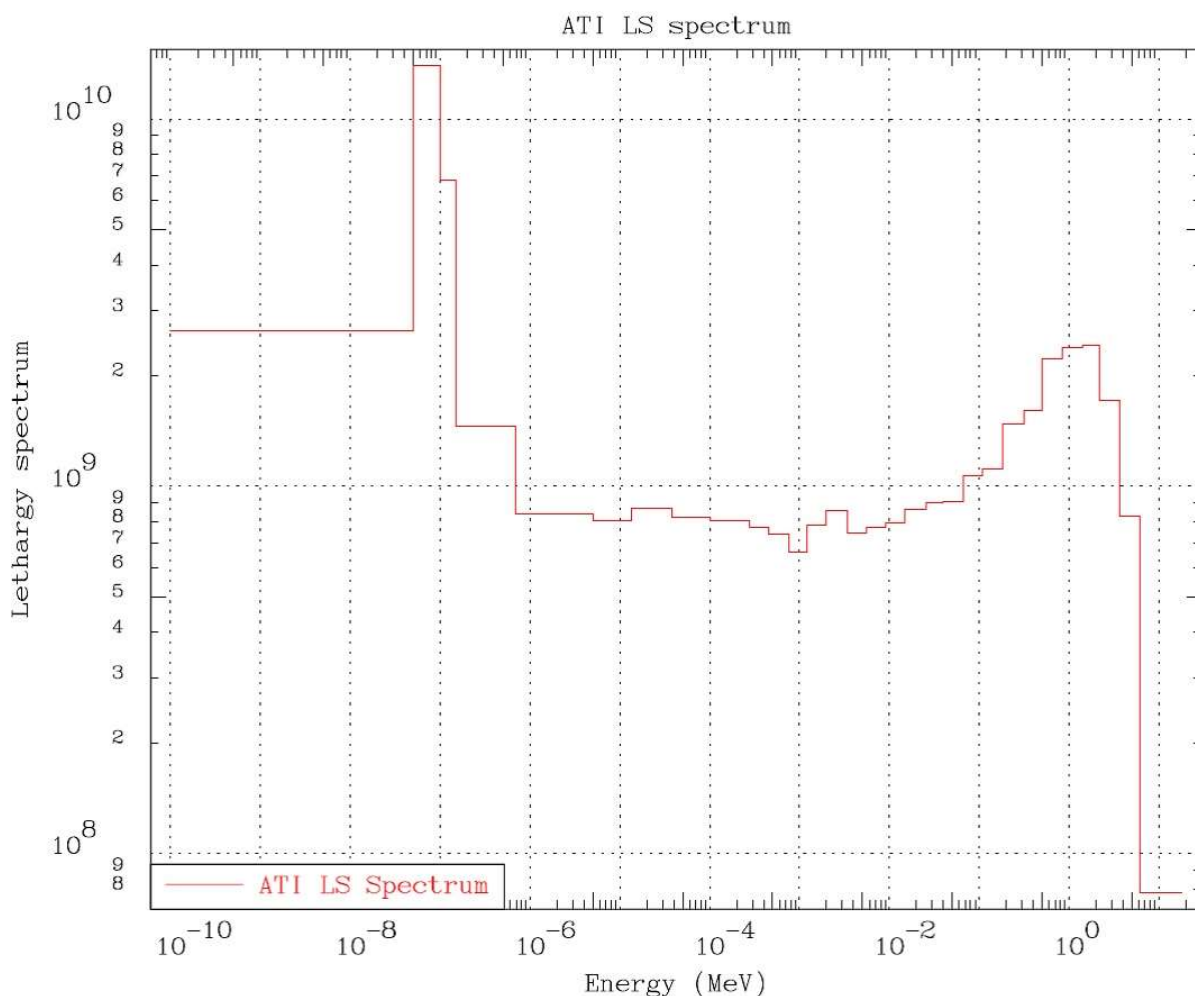


FIG. V-5. Input neutron spectrum used by Slovenia for simulation of the neutron source in the irradiation position (LS1). (courtesy of JSI, Slovenia)

V-3. RESULTS

The results of the calculations by the various participants are presented and then compared and discussed.

V-3.1. Results of the individual participant contributions

V-3.1.1. Austria results

With Serpent it is possible to calculate the activities of every possible generated nuclide. Hence, the output included all the nuclides measured in the experiment. In the present calculation, Serpent was asked to provide the activity values at both the end-of-irradiation time and at the measurement time, for direct comparison.

For the U foil, the comparison of Serpent results against the experimental values is shown in Table V-4 and Fig. V-6. In Table V-4, results are expressed as $(C-E)/E$ as a percentage, where E is the experimental activity value and C is the calculated value for the respective isotope.

The calculated results for the Th foil are presented and compared to experimental values in Table V-4 and Fig. V-7.

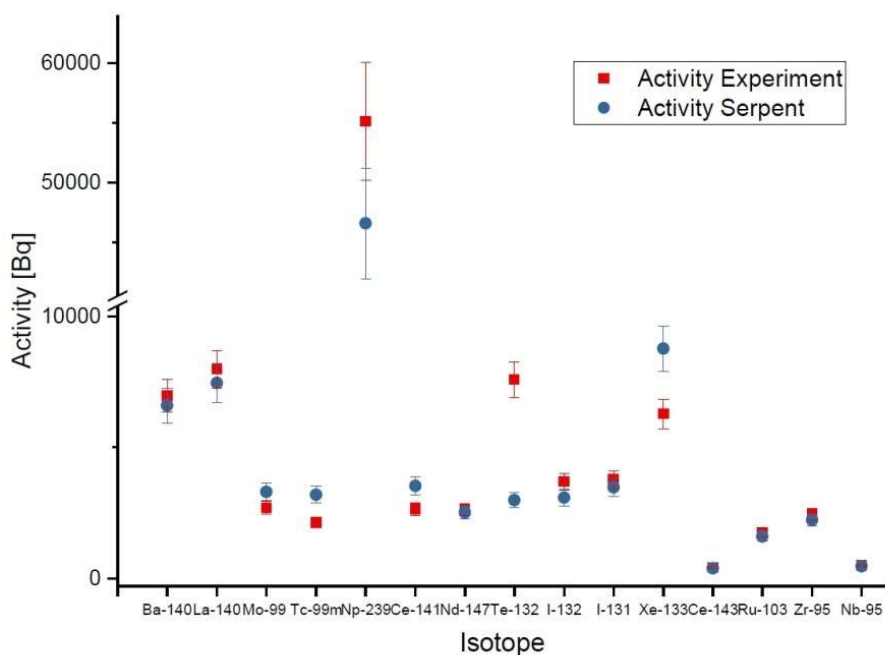


FIG. V-6. Austria calculated (Serpent 2) activity values compared to experimental activity values for the uranium foil. (courtesy of ATI, Austria)

TABLE V-4: COMPARISON OF SERPENT 2 (AUSTRIA) U AND Th ACTIVITY VALUES WITH EXPERIMENTAL VALUES

U foil			Th foil		
Analysed nuclide	Peak [keV]	Serpent 2 Calculated activity (C-E)/E [%]	Analysed nuclide	Peak [keV]	Serpent 2 Calculated activity (C-E)/E [%]
Ba-140	537.303	-5.13%	Th-232	311.904	-19.29%
La-140	487.022	-6.17%	Pa-233	238.632	-2.31%
Mo-99	739.5	-8.08%	Ba-140	537.303	-23.88%
Tc-99m	140.511	21.98%	La-140	487.022	-27.38%
Np-239	277.599	-18.96%			
Ce-141	145.4433	31.39%			
Nd-147	531.06	-9.03%			
Te-132	228.327	-65.75%			
I-132	522.65	-21.36%			
I-131	364.489	-8.42%			
Xe-133	80.9979	37.32%			
Ce-143	293.266	-12.46%			
Ru-103	497.08	-7.92%			
Zr-95	756.729	-8.10%			
Nb-95	765.803	-3.25%			
Cs-137	661.00	0%			

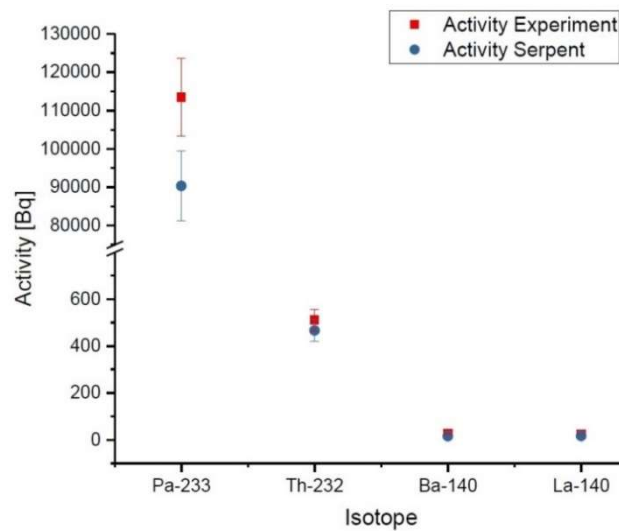


FIG. V-7. Austria calculated (Serpent 2) and experimental activity values for the thorium foil. (courtesy of ATI, Austria)

V-3.1.2. Slovenia results

The results obtained by calculation from Slovenia by combination of the MCNP and FISPACT codes are compared to the experimental activity values in Fig. V-8 for the U foils and in Table V-5 for the Th foils.

In the case of the U foils, the simulation systematically overestimates the experimental values by an average factor of 200. A partial explanation of this can be found in the neutron spectrum assumed as the input spectrum for the MCNP calculation. In fact, from Fig. V–5, it seems there was an incorrect interpretation of the input data: the neutron spectrum used for the calculation is shifted one step forward, which means the first energy interval is provided with a value much lower than expected. This factor could have had an influence on the calculation and it needs to be adjusted in the future.

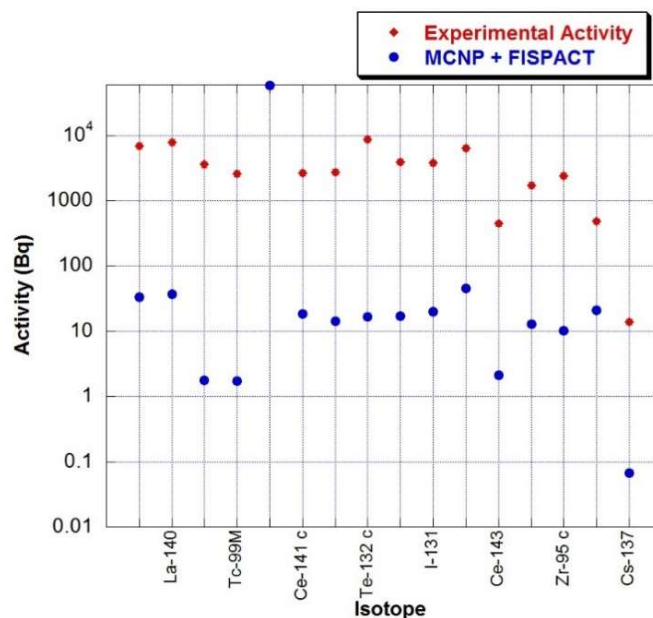


FIG. V–8. Slovenia MCNP-FISPACT calculated results compared against the experimental activity values for the uranium foil. (courtesy of JSI, Slovenia)

TABLE V–5: SLOVENIA CALCULATED ACTIVITY VALUES IN THORIUM FOILS AFTER 27 DAYS AFTER END OF IRRADIATION COMPARED AGAINST EXPERIMENTAL VALUES

Isotope	Measured γ (keV)	Measured activity (Bq)	Calculated activity (Bq)
Pa-133	311.904	1.12E+05	2.19E+04
Th-232	238.632	4.77E+02	5.10E+02
Ba-140	537.303	2.02E+01	7.88E-07
La-140	487.002	2.29E+01	N/A

V–3.2. Discussion of the individual results

For the Austria participant, in case of the U foils, most Serpent determined activities are in good agreement with the experimental values: that is, Serpent results are comparable with the measurement results within the uncertainties (<10%). However, it can be observed that for some isotopes there is a bigger discrepancy between the simulation and the experimental data. The explanation can be that the gamma lines for measurement of those isotopes lay in the low energy region, where the detector uncertainty is larger.

In the case of the Th foils, the Serpent simulation looks less accurate in reproducing the experimental data, and has a bigger discrepancy (20–27%). In this case, most likely the irradiation was sufficient to induce a detectable transmutation of ^{232}Th into ^{233}U : nevertheless, the fission reaction of ^{233}U occurred but produced fission products (such as ^{140}Ba , ^{140}La) in very low amounts, hardly detectable with the instrumentation used.

In general, when comparing the results of the simulation with experimental data, simulation inaccuracies have to be taken into account. In the present simulation, for example, the neutron flux spectrum in the out-of-core region is not exactly the same as in reality. Additionally, the Serpent burnup calculation in thin and small volumes (like the irradiated foils) is not as accurate as in larger volumes (like in the fuel elements).

For the Slovenia participant, the modelling approach was different. In fact, the calculation exercise was performed avoiding modelling of the entire reactor. In this case, the irradiation position (LS1) was modelled by means of the MCNP code, and the neutron spectrum inside the irradiated U and Th foils was calculated. A second step utilized the FISPACT code to obtain the material composition of samples after irradiation.

Simulation results that systematically overestimate the experimental values can be justified considering that the adopted approach relies on the neutron spectrum provided (corresponding to the irradiation position LS1), and on the ability to reproduce the same neutron spectrum in the limited region modelled.

There may have been some discrepancies between the neutron spectrum assumed as an input spectrum (for the MCNP calculation) and the input data provided. This factor could have had an influence on the calculation and it need to be adjusted in the future.

V-3.3. Conclusions

In the ATI-2 benchmark on transmutation rate evaluation, the experiment of natural uranium and thorium sample irradiation was reproduced with different approaches and different codes by the participants.

Austria used Serpent 2 code and modelled the complete reactor, including the irradiation facility utilized for the experiment. The results show that, in the case of the uranium foils, most Serpent 2 determined activities are in good agreement with the experimental values. In the case of the thorium foils, the Serpent 2 simulation is still in fair agreement with the experimental results but with a higher discrepancy. In this case, it has to be noticed that some of the evaluated activities present very low absolute values and this explains the lower precision in the calculated and the experimental data.

Slovenia performed the calculations by means of the combination of MCNP and FISPACT codes. In this case, the input data provided within the benchmark specification package (such as the neutron spectrum at the irradiation position) was used in the first step of the calculation. The calculated results show consistency among themselves even if they systematically overestimate the experimental values.

REFERENCES TO ANNEX V

- [V-1] INTERNATIONAL ATOMIC ENERGY AGENCY, Research Reactor Benchmarking Database: Facility Specification and Experimental Data, Technical Reports Series No. 480 (Rev. 1), IAEA, Vienna (in preparation).
- [V-2] GENERAL ATOMIC (GA), TRIGA Mark II Reactor General Specifications and Description. General Atomic Company, U.S.A. (1964).

- [V-3] CAGNAZZO, M., Neutronic modelling of the new TRIGA core and experimental validation, PhD Thesis, Technische Universität Wien, Fakultät für Physik (2018).
- [V-4] LEPPÄNEN, J., Serpent – a Continuous-energy Monte Carlo Reactor Physics Burnup Calculation Code User’s Manual, VTT Technical Research Centre of Finland, 18 June 2015 (2015).
- [V-5] CAGNAZZO, M., et al., Transmutation rates determination for the study of nuclear fuel composition under irradiation, Proc. European Research Reactor Conference (RRFM) 2018, Munich, Germany, 11–15 March (2018).

system and cobalt irradiation device). Several participants presented in their country reports a summary of this previous validation step, but in this Annex only the burnup measurements and their numerical comparison are provided.

The detailed core layout, and fuel management are given in Egypt's benchmark results for ETRR-2, given in the supplementary files on-line. The main operating data, like the cycle length in full power days and the fuel management performed at the end of each cycle, are summarized in Table VI-1. No critical control rod pattern was provided.

VI-2.2. Summary of the codes and nuclear data libraries used

Four different CPR participants presented the numerical comparison against the measurements. An outline of the codes, and nuclear data libraries used to perform the various calculations will be presented. The detailed information of codes, libraries and models together with the calculation methodology are provided in the individual participants' calculation reports.

VI-2.2.1. Egypt

A deterministic calculation line was used based on the WIMS-D4 [VI-3] and CITVAP [VI-4] codes. The 69 groups WIMS-D4 library was used for the numerical analysis.

Egypt participated in the previous CRP, with a comparison between codes and the measured data, providing a good agreement to perform burnup analysis with a reasonable confidence.

TABLE VI-1. OPERATION INFORMATION FOR ETRR-2

Cycle	Fuel management	Full power days (days)	Measured fuel assembly (FA) (Initial amount of U-235 in g)	Discharge burnup (%)
1	Initial core (Fig. VI-1)	7.3	–	
2	N1 → 6 → 5 → 11 → 16 (out) N2 → 30 → 29 → 28 → 22 (out)	16.0	FA 22 (148.2)	3.26
3	N3 → 25 → 19 → 13 → 14 (out) N4 → 26 → 27 → 20 → 21 (out)	13.75	FA 14 (148.2)	10.07
Cycle	Fuel management	Full power days (days)	Measured fuel assembly (FA) (Initial amount of U-235 in g)	Discharge burnup (%)
4	N5 → 1 → 7 → 8 → 9 (out) N6 → 12 → 18 → 17 → 11 (out)	13.64	–	
5	N7 → 2 → 3 → 4 → 10 (out) N8 → N2 → 24 → 28 → 20 (out)	–	FA 20 (209.0)	20.92

VI-2.2.2. Israel

A Monte Carlo calculation code, MCNP4b [VI-5], coupled with a deterministic calculation code, DRAGON [VI-6], for burnup calculation was used in the benchmark analysis. DRAGON received fluxes in 69 energy groups from the MCNP output for each of the burnup zones in the fuel meat.

The MCNP calculation was carried out with the ENDF/B-VII cross-section library and DRAGON used the WIMS-4D library cross-sections to solve the Bateman equations.

Israel provided, in an individual calculation report, an analysis of the fresh core measurement with the data provided in the former CRP. This validation is not described in this consolidated report, but it provides a good agreement to perform burnup analysis with a reasonable confidence.

VI-2.2.3. South Africa

The OSCAR-5 [VI-7] system was used to perform the numerical analysis. Two different approaches were selected: (i) A deterministic calculation line using HEADE-MGRAC [VI-7]; and (ii) the Serpent 2 [VI-8] Monte Carlo code.

WIMS-E libraries were used for HEADE code, and in the case of the Serpent code ENDF/B-VII.0 based cross-section libraries were used, with decay and fission product data also read from this evaluation.

South Africa provided, in an individual calculation report, an analysis of the fresh core measurement with the data provided in the former CRP. This validation is not described in this consolidated report, but it provides a good agreement to perform burnup analysis with a reasonable confidence.

VI-2.2.4. Argentina

INVAP's calculation line was used for the analysis of the benchmark, and the production deterministic codes CONDOR-CITVAP [VI-9] were selected for the calculations.

As a result, INVAP's proposed scheme for the ETRR-2 benchmark was to develop a comparison between two different approaches: (i) a CONDOR-CITVAP calculation (the INVAP standard approach); and (ii) a CONDOR calculation.

The ESIN2001 69 group nuclear data library was used for cell calculations. This library was selected because it has a wide validation on different research reactors.

Argentina participated in the previous CRP, with a comparison between codes and the measured data, providing a good agreement to perform burnup analysis with a reasonable confidence.

VI-2.3. Summary of the models used

VI-2.3.1. Egypt

Different models were used for the WIMS-D and CITVAP codes. The WIMS-D models for each reactor component are a 1D model preserving the total mass of each material. The WIMSD

69 group nuclear data library was used by the WIMS-D code and the macroscopic cross-sections were condensed to three energies. Energy limits are given in Table VI-2.

TABLE VI-2. CONDENSATION ENERGY LIMITS FOR CITVAP CALCULATION

Group	Lower limit [MeV]	Upper limit [MeV]
1	0.821	20 (from library)
2	0.625E-6	0.821
3	0	0.625E-6

The 1D fuel assembly is a three region model: meat, aluminium (cladding and frame), and coolant. It preserves the total mass of fuel, aluminium and water. The whole fuel assembly is homogenized for the core calculation. Figure VI-2 shows the engineering, core (to be used in CITVAP) and WIMS cell model of the fuel assembly.

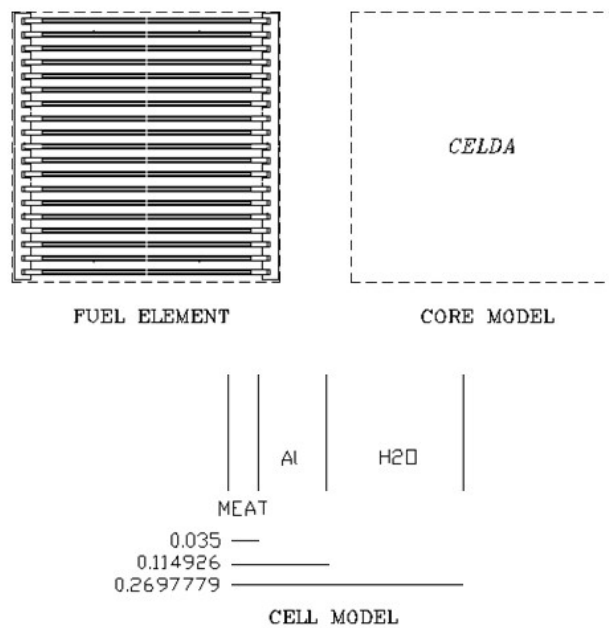


FIG. VI-2. Engineering, core and cell model of the fuel assembly. (courtesy of INVAP, Argentina)

The core was modelled in 3-dimensional XYZ geometry; Figure VI-3 shows a XY cut of the core at the mid-plane of the core. The axial discretization to take into account the axial burnup dependence was 10 axial layers.

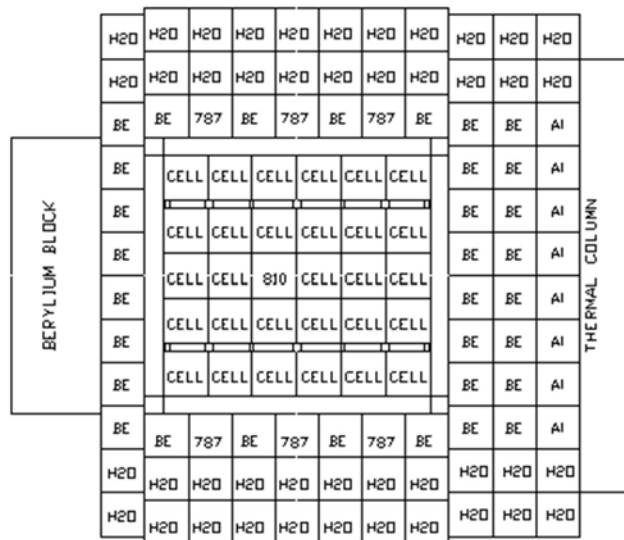


FIG. VI-3. CITVAP core model in XYZ geometry. (courtesy of INVAP, Argentina)

VI-2.3.2. Israel

A summary of the MCNP model is given in Fig. VI-4 (Israel's benchmark results for ETRR-2, are given in the supplementary files on-line). Several detailed areas are provided to illustrate the level of detail taken into account for the analysis. An important modelling criterion was to split the model in 15 axial layers to take account of the axial dependence of the burnup. The fuel plate discretization of the FA, to take account of the burnup effect, was done in three regions: two external fuel plates; and an average internal fuel plate.

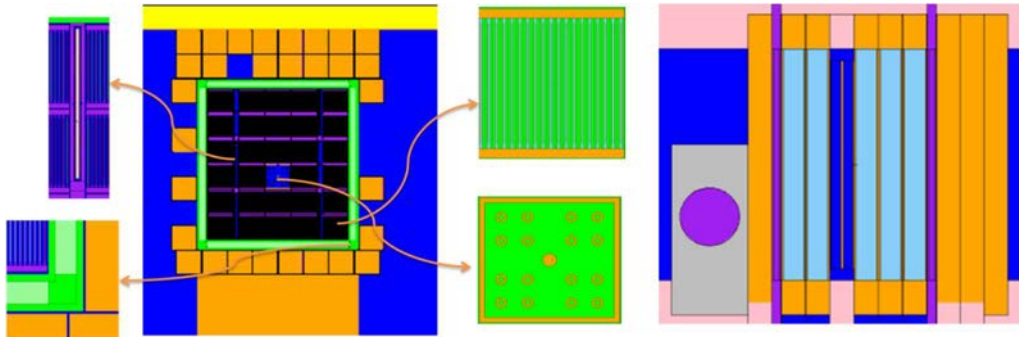


FIG. VI-4. MCNP core model developed by the Israel participant. (courtesy of Soreq, Israel)

VI-2.3.3. South Africa

The OSCAR-5 system allows modelling the reactor using a combination of a set of 3-D models for each reactor component. In Fig. VI-5 (from South Africa's benchmark results for ETRR-2, given in the supplementary files on-line), three dimensional views of all the assembly models are presented. These assemblies were then combined to form the different core configurations.

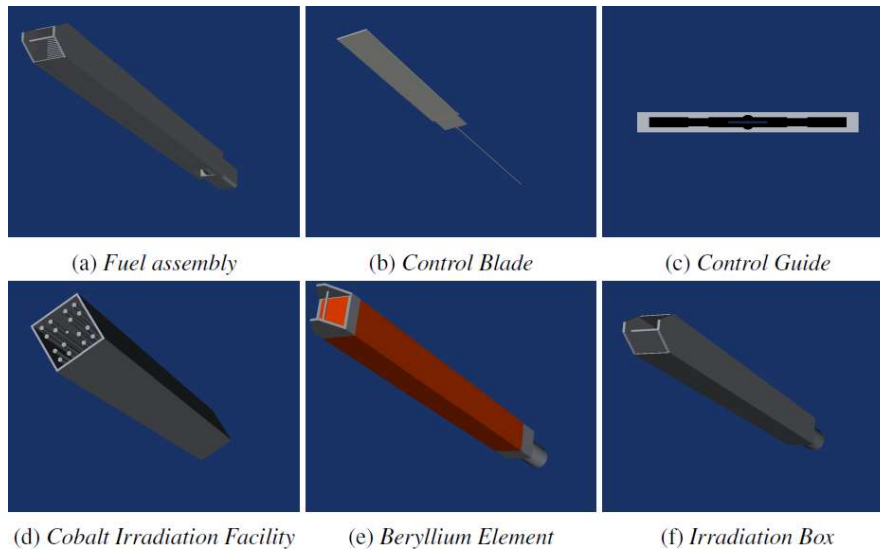


FIG. VI-5. OSCAR-5 3-D view of reactor components. (courtesy of Necsa, South Africa)

Figure VI-6 (from South Africa’s benchmark results for ETRR-2, given in the supplementary files on-line) shows the initial core (cycle 1) used for the burnup analysis.

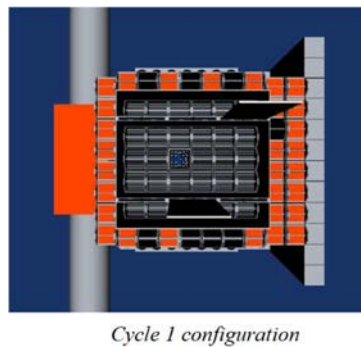


FIG. VI-6. OSCAR-5 3-D view of the initial core. (courtesy of Necsa, South Africa)

No information regarding the number of groups used in the MGRAC calculation and the number of axial layers used to simulate the axial burnup dependence were provided.

VI-2.3.4. Argentina

Different models were used for the CONDOR and CITVAP codes. The modelling criteria used for this benchmark were based on the production standard design methodology. The ESIN2001 69 group nuclear data library was used by the CONDOR code, and the condensation procedure considered three energy groups at core level, with the energy limits presented in Table VI-3.

TABLE VI-3. CONDENSATION ENERGY LIMITS FOR CITVAP CALCULATION

Group	Lower limit [MeV]	Upper limit [MeV]
1	0.821	20 (from library)
2	0.625E-6	0.821
3	0	0.625E-6

Figure VI-7 shows the fuel assembly 2-D model based on an average fuel plate. The whole fuel assembly is homogenized for core calculation.

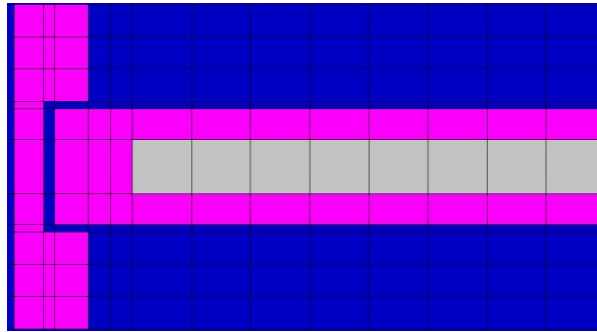


FIG. VI-7. CONDOR 2-D fuel assembly model. (courtesy of INVAP, Argentina)

Figure VI-8 shows the CONDOR model for the cobalt irradiation device. The model is homogenized in two regions: (i) Co pencils (named CO_59); and (ii) the rest of the irradiation facility (named H2O_CO_DEV).

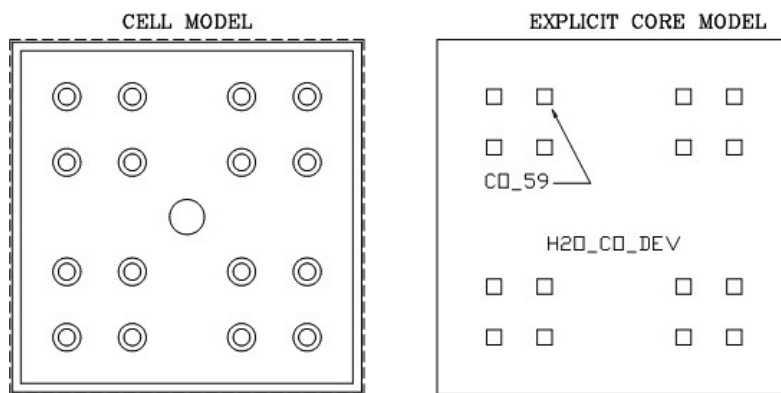


FIG. VI-8. CONDOR model of the Cobalt irradiation facility. (courtesy of INVAP, Argentina)

The core was modelled in 3-dimensional XYZ geometry; Fig. VI-9 shows a XY cut of the core at the mid-plane of the core. The axial discretization to take into account the axial burnup dependence was 20 axial layers.

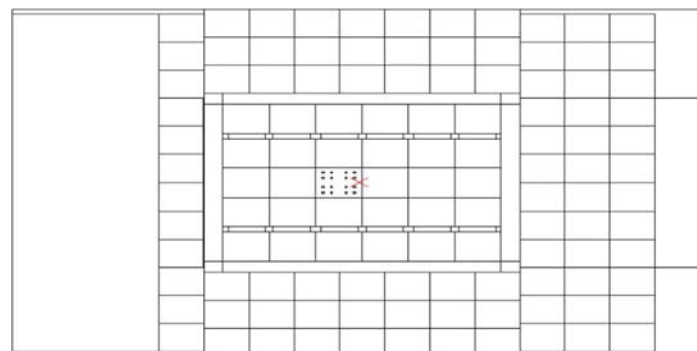


FIG. VI-9. CITVAP core model in XYZ geometry. (courtesy of INVAP, Argentina)

VI-3. RESULTS

The results from the multicycle burnup calculations of fourth participants will be presented and then compared and discussed.

VI-3.1. Results of the individual participant contributions

Two participants (Israel and South Africa) perform a preliminary validation of the calculation codes using the experimental data provided in a previous IAEA CRP. These validations are presented in their individual calculation report and are not described in this consolidated report.

The other two participants (Egypt and Argentina) perform similar analysis in the previous IAEA CRP.

The fourth validations provide a good agreement to perform burnup analysis with a reasonable confidence.

This Annex does not show the participant results individually; instead, the results are shown and compared together with the other participant results.

VI-3.1.1. Egypt (EGY) results

The WIMS-CITVAP codes were used to calculate the burnup of each of the measured fuel assemblies, for comparison with the experimental data. The results are presented in the tables as EGY-CITVAP.

VI-3.1.2. Israel (ISR) results

The MCNP-DRAGON codes were used to calculate the burnup of each measured fuel assemblies, for comparison with the experimental data. The results are presented in the tables as ISR-MCNP.

VI-3.1.3. South Africa (SAF) results

The South Africa results are provided for two different methodologies presented in the OSCAR-5 system. The calculation methodologies are: (i) a deterministic methodology using HEADE-MGRAC and (ii) a stochastic methodology using Serpent. The results are presented in the tables as SAF-MGRAC and SAF-Serpent.

VI-3.1.4. Argentina (ARG) results

The Argentina results show a conceptual calculation with a CONDOR cell code level and a CITVAP 3-D detailed model. The cycle dependent burnup for each of the measured fuel assemblies is provided for both calculation methodologies and the results are compared with the experimental data. The results are presented in the tables as ARG-CONDOR and ARG-CITVAP.

VI-3.2. Comparison of results

Table VI-4 specifies the experimental burnup values $(100 - U-235(t)/U-235(t=0)) \cdot 100$, in % and the calculated data provided by each participant. It also shows the average calculated value for all participants and its standard deviation.

Table VI-5 presents the participants' relative difference $(C-E)/E$ as a percentage, where C is the calculated value, and E is the experimental value.

TABLE VI-4. PARTICIPANTS' CALCULATION AND COMPARISON WITH EXPERIMENTAL RESULTS

Fuel assembly	Measured burnup (%)	EGY CITVAP	ISR MCNP	SFA Serpent	SFA MGRAC	ARG CITVAP	ARG CONDOR	Calc. average	Std. dev. (%)
FE022	3.26	4.23	3.67	3.71	3.82	4.13	3.80	3.89	5.9
FE014	10.07	11.10	11.17	11.77	11.98	11.10	11.50	11.44	3.3
FE020	20.92	22.61	21.01	20.11	20.52	21.69	20.33	21.05	4.5

TABLE VI-5. PARTICIPANTS' DIFFERENCE WITH RESPECT TO THE MEASURED VALUES

Fuel assembly	EGY CITVAP	ISR MCNP	SFA Serpent	SFA MGRAC	ARG CITVAP	ARG CONDOR
FE022	29.8%	12.6%	13.8%	17.2%	26.7%	16.6%
FE014	10.2%	10.9%	16.9%	19.0%	10.2%	14.2%
FE020	8.1%	0.4%	-3.9%	-1.9%	3.7%	-2.8%

VI-3.3. Conclusions

The ETRR-2 benchmark case, which is the multicycle depletion calculation problem, was proposed by Egypt. This benchmark case follows the operation history of ETRR-2, starting from a fresh core during four cycles, and measures the discharge burnup of three fuel assemblies. The burnup measurement was evaluated by measuring the ^{137}Cs activity by gamma ray spectrometry.

Six computer models from four CRP participants were used to compare the fuel assembly discharge burnup. In general, the calculated values agree very well among each other, as it can be seen in the standard deviation of the calculated values.

No significant difference was observed between deterministic and stochastic codes.

The discrepancy in the fuel assembly FE022 is a little higher than the other measurements: this is the FA with a lower burnup and it is observed that the agreement improves for the FAs with a higher burnup.

Additional information, such as the critical control rod position during the reactor operation and the axial burnup profile, would improve this benchmark.

REFERENCES TO ANNEX VI

- [VI-1] INTERNATIONAL ATOMIC ENERGY AGENCY, Research Reactor Benchmarking Database: Facility Specification and Experimental Data, Technical Reports Series No. 480 (Rev. 1), IAEA, Vienna (in preparation).
- [VI-2] INTERNATIONAL ATOMIC ENERGY AGENCY, Benchmarking against Experimental Data of Neutronics and Thermohydraulic Computational Methods and Tools for Operation and Safety Analysis of Research Reactors – Results of a Coordinated Research Project, IAEA-TECDOC-1879, IAEA, Vienna (2019).
- [VI-3] INTERNATIONAL ATOMIC ENERGY AGENCY, WIMS-D Library Update, IAEA, Vienna (2007).

- [VI-4] VILLARINO, E., LECOT, C., Neutronic calculation code CITVAP 3.1., Proc. IX Encontro Nacional de Física de reatores e Termo-hidráulica, Caxambu, Brazil, 25–29 October (1993).
- [VI-5] JOHNSTON, R.R., A General Monte Carlo Neutronics Code, Los Alamos National Laboratory Report LAMS-2856, Los Alamos, NM (1963).
- [VI-6] MARLEAU, G., HÉBERT, A., ROY, R., A user guide for DRAGON version 4, Institut de Génie Nucléaire, Technical Report IGE-294, Montréal, Canada (2011).
- [VI-7] PRINSLOO, R., et al., Recent developments of the OSCAR calculational system, as applied to selected examples from IAEA research reactor benchmarks, Proc. 18th IGORR Conference, Sydney, Australia, 3–7 December (2017).
- [VI-8] LEPPÄNEN, J., Serpent – a Continuous-energy Monte Carlo Reactor Physics Burnup Calculation Code User’s Manual, VTT Technical Research Centre of Finland, 18 June 2015 (2015).
- [VI-9] VILLARINO, E., CONDOR-CITVAP-MCNP calculation line description, Proc. National Meeting of Reactor Physics and Thermal Hydraulics, Rio de Janeiro, Brazil, 11–16 August (2002).

ANNEX VII

BENCHMARK CONSOLIDATED RESULTS AGAINST EXPERIMENTAL DATA FROM EAEA-2

VII-1. INTRODUCTION

The EAEA-2 benchmark analysis for the Egypt second research reactor (ETRR-2), including the reactor specification and experimental data, is documented in Ref. [VII-1].

ETRR-2 is an open pool tank type reactor cooled and moderated with light water and reflected with beryllium and light water. The core configuration is a 6×5 array with 29 fuel elements and a fixed position for irradiating cobalt. The core has been modified to 27 fuel elements to provide two positions for the production of ⁹⁹Mo from LEU as a main product and ¹³¹I as a by-product.

The uranium plates used have a uranium aluminide (UAl_x) as fuel meat and are clad with aluminium. These plates are irradiated in ETRR-2 and then chemically processed in the Radioisotope Production Facility to produce ⁹⁹Mo and ¹³¹I. The characteristics of such plates is given here below:

- ²³⁵U enrichment: 19.75%;
- Plate dimensions: 130 mm × 35 mm × 1.4 mm;
- Meat dimensions: 115 mm × 30 mm × 0.7 mm;
- ²³⁵U mass per plate: 1.4 g;
- Al mass per plate: ~15.7 g.

The fuel burnup is an important parameter to be determined for evaluation of the safety and economy of nuclear fuel management [VII-2]. Burnup can be correlated to many isotope ratios such as ¹³⁴Cs/¹³⁷Cs, ¹⁵⁴Eu/¹⁵⁵Eu, ¹⁵⁴Eu/¹³⁷Cs, ¹⁰⁶Ru/¹³⁷Cs, and ⁹⁵Nb/⁹⁵Zr [VII-3 – VII-5]. This benchmark focuses on relating the burnup of UAl_x plates irradiated in ETRR-2 to the ¹³⁴Cs/¹³⁷Cs activity (or mass) ratio.

VII-2. SUMMARY OF THE BENCHMARK SPECIFICATION AND CODES AND MODELS USED

VII-2.1 Summary of the benchmark specification

The core layout is shown in Fig. VII-1.

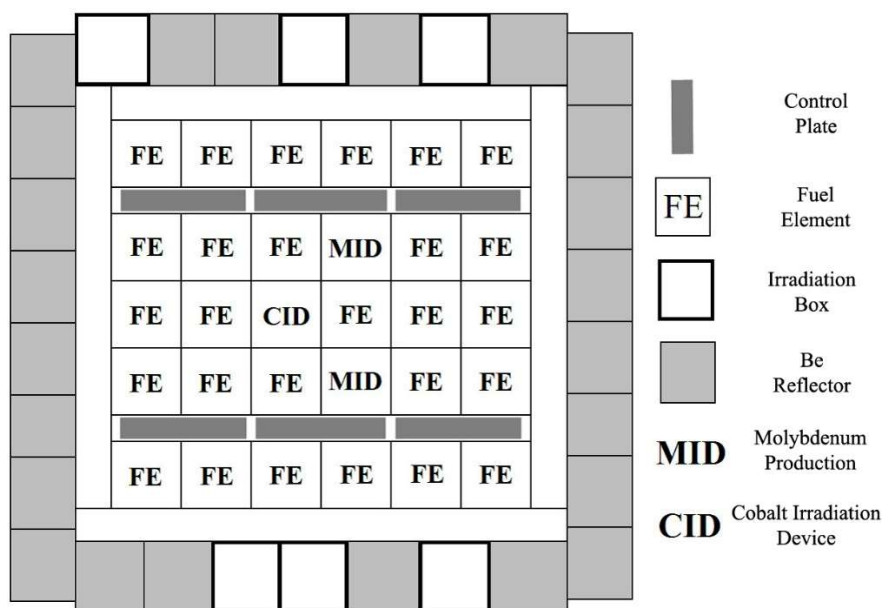


FIG. VII-1. ETRR-2 reactor core layout. (courtesy of Atomic Energy Authority, Egypt)

The target plates were irradiated for 50.33 h at 19 MW. The calculated average thermal neutron flux inside the plates at this power is $1.17 \times 10^{14} \text{ cm}^{-2}\cdot\text{s}^{-1}$. The irradiated UAl_x plates were cooled for 12 h and then transferred to the Radioisotope Production Facility to be digested in NaOH and filtered. Then, the filtrate was passed through an anion-exchange column. A sample was collected from the anion-exchange column loading effluent and suitably diluted. Then, 0.1 ml of the finally diluted sample was withdrawn and placed into a small borosilicate glass vial for gamma ray spectrometry.

It is known that uranium is retained by the filter as sodium diuranate ($\text{Na}_2\text{U}_2\text{O}_7$) along with retention of the majority of lanthanides and partial retention of many other radionuclides such as ^{95}Zr , ^{95}Nb , $^{103, 106}\text{Ru}$, ^{132}Te , etc. The activities of ^{99}Mo , $^{134, 136, 137}\text{Cs}$, $^{131, 132, 133}\text{I}$ are mainly found in the filtrate. After passing through the anion-exchange column, $^{131, 132, 133}\text{I}$ and ^{99}Mo are mainly retained onto the column, while $^{134, 136, 137}\text{Cs}$ radionuclides are mainly passed through the column and collected in the loading effluent.

The sample was measured using a coaxial HPGe N-type detector with relative efficiency of 100% and resolution of 2.1 keV at 1.333 MeV ^{60}Co line. For calibration (energy and efficiency), standard point sources were used, including ^{133}Ba , ^{60}Co , ^{137}Cs and ^{152}Eu . The detector was calibrated at 10 cm from the reactor window.

The sample was counted after a decay time of 56 days (from the end of irradiation to the measurement time). It was found that the gamma ray spectrum included mainly the photopeaks of ^{137}Cs and ^{136}Cs , with a very much lower contribution from ^{134}Cs . In addition, the photopeaks of ^{103}Ru , ^{95}Zr , ^{95}Nb , ^{60}Co and ^{140}La appeared (with a lower contribution than those of ^{136}Cs and ^{137}Cs). Thus, the filtration and anion exchange processes led to a significant decrease in the contribution of many radionuclides and the disappearance of many others, which facilitated the detection and radiometric assay of ^{134}Cs more accurately with no need for longer decay times. Table VII-1 gives the results of the measurements.

The average thermal, epithermal and fast neutron fluxes in the LEU plates have been calculated using the MCNP5 code as given in Table VII-2, while Fig. VII-2 shows the energy dependent flux profile as calculated by the same code.

TABLE VII-1. EAEA-2 BENCHMARK EXPERIMENTAL DATA

Reactor power	Irradiation time	Thermal flux	Cooling time	¹³⁴ Cs/ ¹³⁷ Cs activity ratio	¹³⁴ Cs/ ¹³⁷ Cs mass ratio	σ
19 MW	50.33 hr	$1.15 \times 10^{14} \text{ cm}^{-2} \cdot \text{s}^{-1}$	56 d	9.30×10^{-4}	6.55×10^{-5}	32%

TABLE VII-2. CALCULATED THERMAL, EPITHERMAL AND FAST NEUTRON FLUXES AVERAGED IN THE IRRADIATED TARGETS AS CALCULATED USING THE MCNP5 CODE, 1Σ UNCERTAINTY <1%

Thermal flux ($\text{cm}^{-2} \cdot \text{s}^{-1}$) $E \leq 0.5 \text{ eV}$	Epithermal flux ($\text{cm}^{-2} \cdot \text{s}^{-1}$) $0.5\text{eV} < E \leq 0.5 \text{ MeV}$	Fast flux ($\text{cm}^{-2} \cdot \text{s}^{-1}$) $E > 0.5 \text{ MeV}$
1.17E+14	2.17E+14	1.57E+14

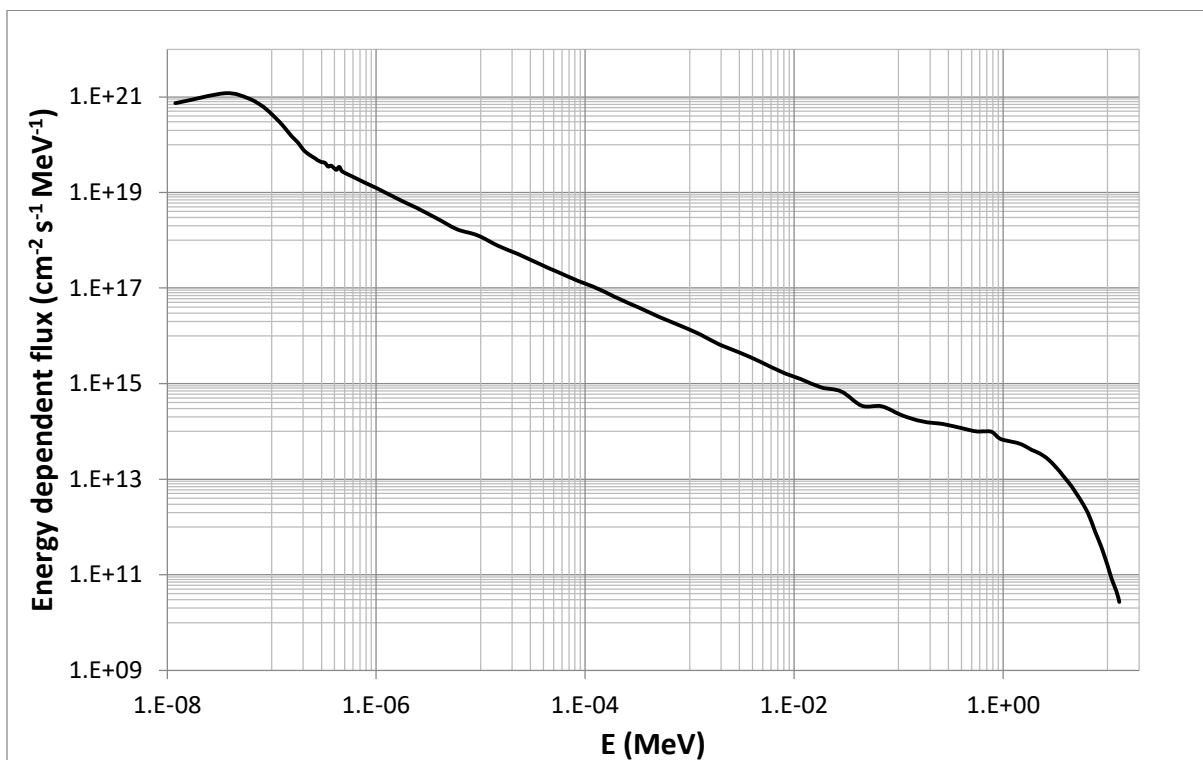


FIG. VII-2. Calculated energy dependent flux averaged in the irradiated targets as calculated using MCNP5. (courtesy of Atomic Energy Authority, Egypt)

VII-2.2 Summary of the models used

VII-2.2.1. MCNPX model (ETRR-2)

The MCNPX [VII-6] software was used to simulate the reactor and to calculate the actinide and non-actinide inventories in LEU. A criticality calculation (KCODE calculations) with the BURN cards was used to calculate the system criticality and the burnup of the fuel and fuel inventory after each time interval (defined in the BURN cards). In the BOPT card, the Tier 3 fission products, which comprise fission products in ENDF/B-VII.0, were specified using cross-section models for nuclides not containing tabular data and then allowing CINDER90 to calculate the 1-group cross-section.

VII-2.2.2. AUS98 code (ANSTO)

The AUS98 [VII-7] neutronic code system is a collection of modular codes developed at ANSTO to solve a range of problems for systems including fission reactors, fusion blankets and other neutron applications. It uses a 200 group neutron and 37 group photon cross-section library based on ENDF/B-VI.1. The system includes modules for reactor lattice calculations, one-dimensional transport calculations, multidimensional diffusion calculations, cell and whole reactor burnup calculations, and flexible editing and auxiliary data processing programs to assist the analyst. The modules are capable of multi-region resonance shielding, coupled neutron and photon transport along with energy deposition and fission product inventory calculations within the one code system. The thermal flux within the fuel meat was normalized to the value provided and the fuel burnt. The resulting radioisotopes were subsequently decayed for the corresponding decay time. The ^{235}U burnup and the masses and activities for ^{134}Cs and ^{137}Cs were calculated for a range of irradiation times and the specified decay time.

VII-2.2.3. Analytical method (ETRR-2)

The ^{235}U burnup and the buildup of ^{134}Cs and ^{137}Cs have been calculated analytically with the neutron flux calculated by MCNP5 [VII-8]. The decrease rate of ^{235}U atoms can be represented by the following differential equation:

$$-\frac{dN^U(t)}{dt} = N^U(t)\sigma_{f+\gamma}\phi \quad (\text{VII-1})$$

Where $\sigma_{f+\gamma}$ indicates the sum of radiative capture and fission neutron cross-section, ϕ indicates the neutron flux, N^U indicates the number of ^{235}U atoms, and t is the irradiation time. Solving the differential equation to get the change of ^{235}U with time:

$$N^U(t) = N_0^U e^{-\sigma_{f+\gamma}\phi t} \quad (\text{VII-2})$$

So, the burnup (% loss of ^{235}U) is:

$$B(t) = 100(1 - e^{-\sigma_{f+\gamma}\phi t}) \quad (\text{VII-3})$$

Weak resonance absorption:

$$\sigma_{f+\gamma}\phi \sim \frac{\sqrt{\pi}}{2}(\sigma_{f+\gamma}\phi)_{th} \quad (\text{VII-4})$$

The rate of ^{137}Cs (denoted by C7) buildup:

$$\frac{dN^{C7}(t)}{dt} = \gamma_{C7}N_0^U e^{-\sigma_{f+\gamma}\phi t} \sigma_f \phi - N^{C7}(t)\sigma_{C7}\phi - N^{C7}(t)\lambda_{C7} \quad (\text{VII-5})$$

Where γ is the fission yield. For short irradiation (\sim days):

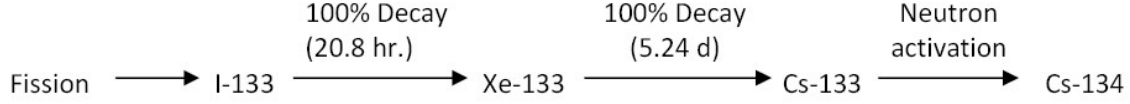
$$N^{C7}(t)\sigma_{C7}\phi + N^{C7}(t)\lambda_{C7} \ll \gamma_{C7}N_0^U e^{-\sigma_{f+\gamma}\phi t} \sigma_f \phi \quad (\text{VII-6})$$

^{137}Cs buildup as function of time:

$$N^{C7}(t) = \frac{\gamma_{C7} N_0^U \sigma_f}{\sigma_{f+\gamma}} N_0^U (1 - e^{-\sigma_{f+\gamma} \phi t}) \quad (\text{VII-7})$$

With $\gamma_{I-133} = 6.59\%$ and $\gamma_{Xe-133} = 6.6\%$.

Therefore, the method for ^{134}Cs production is considered as:



1. ^{133}I buildup (denoted by I3) rate:

$$\frac{dN^{I3}(t)}{dt} = \gamma_{I3} N_0^U e^{-\sigma_{f+\gamma} \phi t} \sigma_f \phi - N^{I3}(t) \sigma_{I3} \phi - N^{I3}(t) \lambda_{I3} \quad (\text{VII-8})$$

$$\sigma_{I3} \phi \ll \lambda_{I3}$$

^{133}I buildup as function of time:

$$N^{I3}(t) = \frac{\gamma_{I3} N_0^U \sigma_f \phi (e^{-\sigma_f \phi t} - e^{-\lambda_{I3} t})}{\lambda_{I3} - \sigma_{f+\gamma} \phi} \quad (\text{VII-9})$$

2. ^{133}Xe buildup (denoted by X3) rate:

$$\frac{dN^{X3}(t)}{dt} = \frac{\gamma_{I3} N_0^U \sigma_f \phi (e^{-\sigma_{f+\gamma} \phi t} - e^{-\lambda_{I3} t})}{\lambda_{I3} - \sigma_{f+\gamma} \phi} \lambda_{I3} - N^{X3}(t) \sigma_{X3} \phi - N^{X3}(t) \lambda_{X3} \quad (\text{VII-10})$$

$$\sigma_{X3} \phi \ll \lambda_{X3}$$

^{133}Xe buildup as function of time:

$$N^{X3}(t) = \frac{a}{b-c} e^{-ct} - \frac{a}{b-d} e^{-dt} + k e^{-b} \quad (\text{VII-11})$$

Where:

$$a = \frac{\gamma_{I3} \lambda_{I3} N_0^U \sigma_f \phi}{\lambda_{I3} - \sigma_{f+\gamma} \phi}; \quad b = \lambda_{X3}; \quad c = \sigma_{f+\gamma} \phi; \quad d = \lambda_{I3}; \quad k = \frac{a}{b-d} - \frac{a}{b-c}$$

3. ^{133}Cs buildup (denoted by C3) rate:

$$\frac{dN^{C3}(t)}{dt} = \left(\frac{a}{b-c} e^{-ct} - \frac{a}{b-d} e^{-dt} + k e^{-bt} \right) \lambda_{X3} - N^{C3}(t) \sigma_{C3} \phi \quad (\text{VII-12})$$

^{133}Cs buildup as function of time:

$$N^{C3}(t) = \frac{ab}{(b-c)(e-c)} e^{-c} - \frac{ab}{(b-d)(e-d)} e^{-dt} + \frac{kb}{e-b} e^{-bt} + F e^{-et} \quad (\text{VII-13})$$

Where:

$$F = \frac{ab}{(b-d)(e-d)} - \frac{ab}{(b-c)(e-c)} - \frac{kb}{e-b}$$

4. ^{134}Cs buildup (denoted by C4) rate:

$$\frac{dN^{C4}(t)}{dt} = \left(\frac{ab}{(b-c)(e-c)} e^{-ct} - \frac{ab}{(b-d)(e-d)} e^{-dt} + \frac{kb}{e-b} e^{-bt} + F e^{-et} \right) \sigma_{C3} \phi - N^{C4}(t) \sigma_{C4} \phi - N^{C4}(t) \lambda_{C4} \quad (\text{VII-14})$$

For short irradiation (\sim days): $N^{C4}(t) \sigma_{C4} \phi + N^{C4}(t) \lambda_{C4} \ll \gamma_{C7} N_0^U e^{-\sigma_f + \gamma \phi t} \sigma_f \phi$

^{133}Cs buildup as function of time:

$$N^{C4}(t) = \frac{-abe}{c(b-c)(e-c)} e^{-ct} + \frac{abe}{d(b-d)(e-d)} e^{-dt} - \frac{kbe}{b(e-b)} e^{-bt} - F e^{-e} + g \quad (\text{VII-15})$$

Where:

$$g = \frac{abe}{c(b-c)(e-c)} - \frac{abe}{d(b-d)(e-d)} + \frac{kbe}{b(e-b)} + F$$

$$\sigma_{C3} \phi = \frac{\sqrt{\pi}}{2} \sigma_{\gamma th} \phi_{th} \left(1 + \frac{Q_0}{f} \right), \text{ assuming } \alpha = 0$$

VII-3. RESULTS

Figure VII-3 gives the burnup of ^{235}U with the irradiation time as calculated using the MCNPX and AUS98 codes and the analytical method. The calculated buildup of ^{137}Cs and ^{134}Cs with the irradiation time is given in Figs VII-4 and VII-5. The $^{134}\text{Cs}/^{137}\text{Cs}$ mass ratio, as a function of the irradiation time, calculated analytically and using MCNPX and AUS98 codes, is shown in Fig. VII-6 with a measured value. The disagreement between the calculations and measurements is due to the large uncertainty in ^{134}Cs activity measurement.

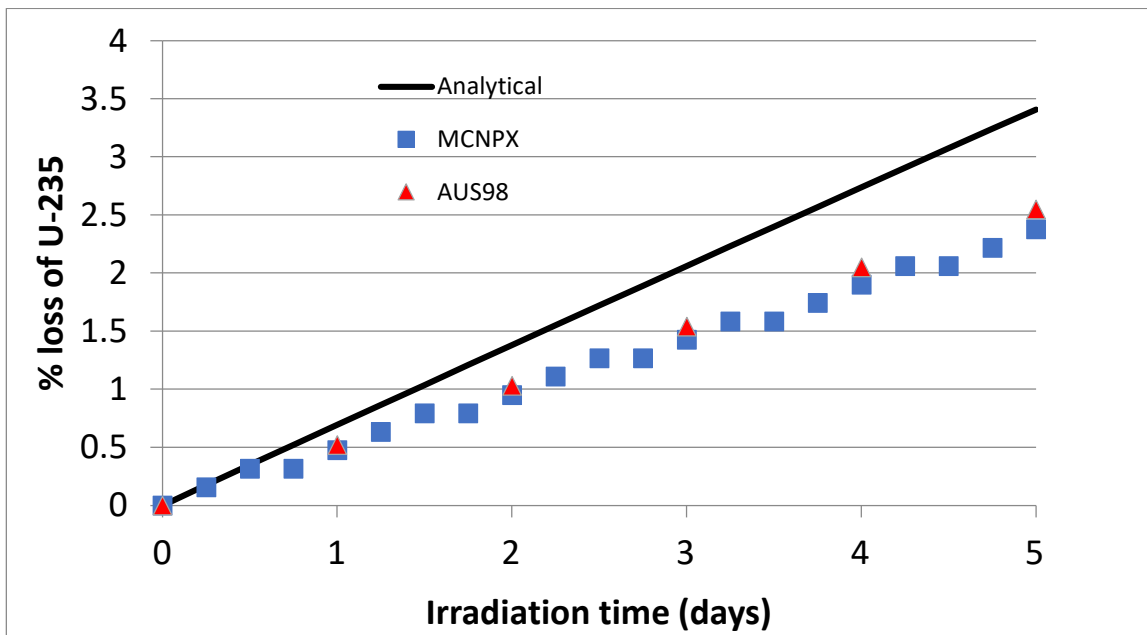


FIG. VII-3. U-235 burnup as calculated using the MCNPX and AUS98 codes and the analytical model. (courtesy of ANSTO, Australia)

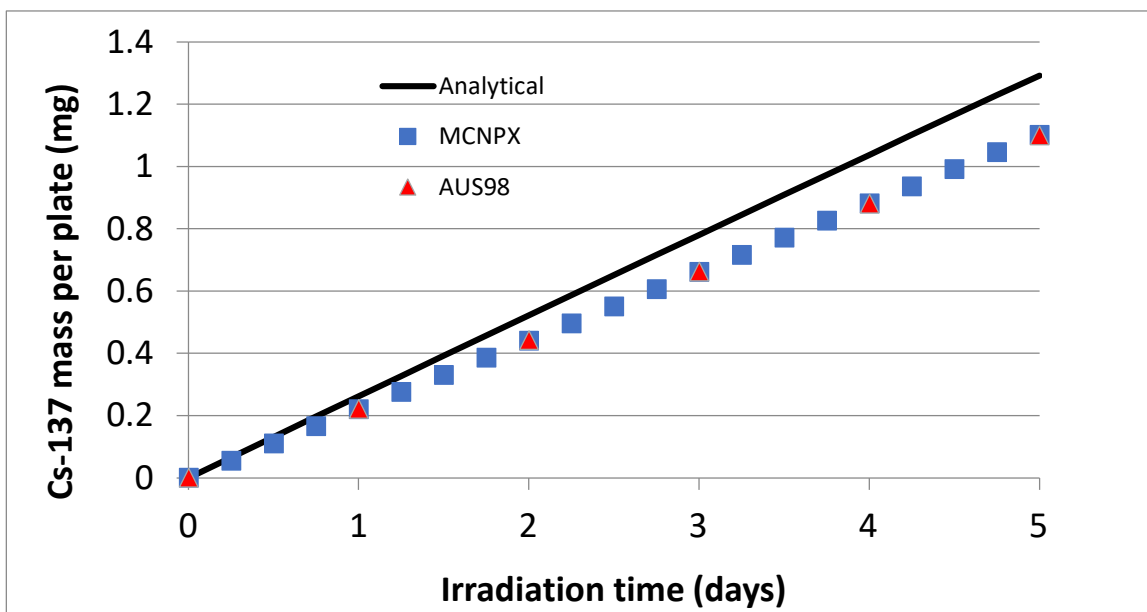


FIG. VII-4. Cs-137 buildup as calculated using the MCNPX and AUS98 codes and the analytical model. (courtesy of ANSTO, Australia)

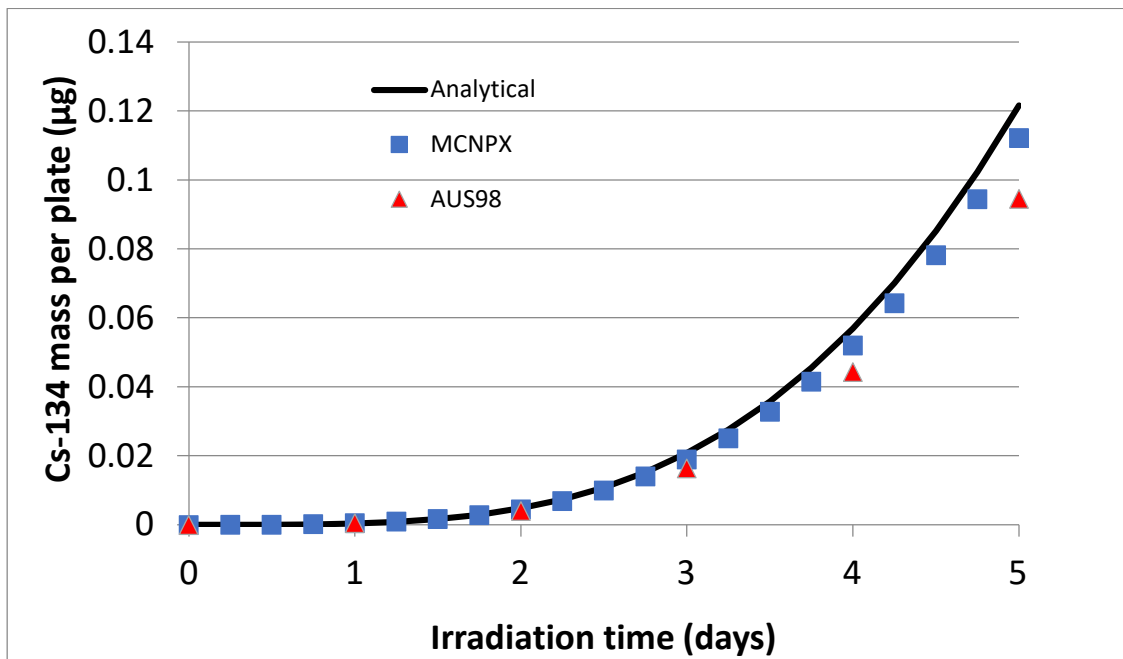


FIG. VII-5. Cs-134 buildups calculated using the MCNPX and AUS98 codes and the analytical model. (courtesy of ANSTO, Australia)

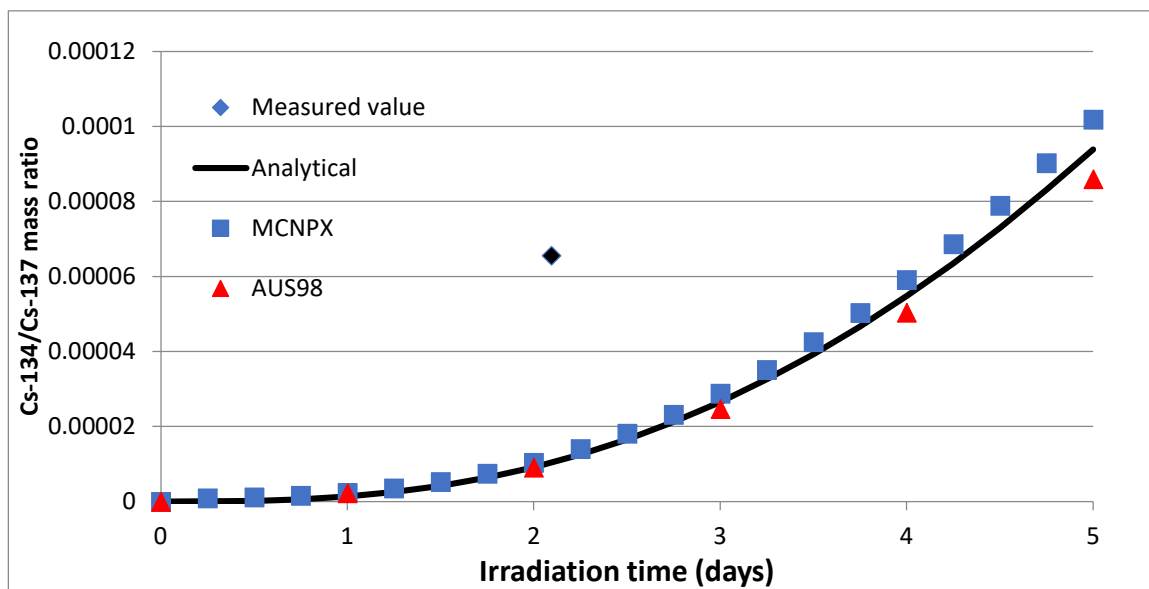


FIG. VII-6. Cs-134/Cs-137 mass ratio as calculated using the MCNPX and AUS98 codes and the analytical model and as measured after an irradiation time of 50.33 hours. (courtesy of ANSTO, Australia)

REFERENCES TO ANNEX VII

- [VII-1] INTERNATIONAL ATOMIC ENERGY AGENCY, Research Reactor Benchmarking Database: Facility Specification and Experimental Data, Technical Reports Series No. 480 (Rev. 1), IAEA, Vienna (in preparation).
- [VII-2] PARK, K.J., et al., Determination of burnup and Pu/U ratio of PWR spent fuels by gamma-ray spectrometry, Nucl. Eng. Technol. **41** (2009) 1307–1314.

- [VII-3] HERMANN, A., BERNDT, R., New possibilities in isotope correlation analysis of spent nuclear fuel, *J. Radioanal. Nucl. Chem.* **80** (1983) 189–198.
- [VII-4] MIN, D.K., et al., “Determination of burnup, cooling time and initial enrichment of PWR spent fuel by use of gamma-ray activity ratios”, in: *Storage of spent fuel from power reactors, Proceedings of a symposium held in Vienna, 9–13 November 1998*, IAEA-TECDOC-1089, IAEA, Vienna (1999) 421–426.
- [VII-5] HADDAD, KH., Burnup effect on $^{95}\text{Nb}/^{95}\text{Zr}$ ratio-cooling time correlation, *J. Nucl. Mater.* **345** (2005) 86–88.
- [VII-6] PELOWITZ, D.B., MCNPX User’s Manual, Version 2.7.0, Los Alamos National Laboratory Report LA-CP-11-00438, Los Alamos, NM (2011).
- [VII-7] ROBINSON, G.S, HARRINGTON, B.V., The 1998 version of the AUS modular neutronics code system, Australian Nuclear Science and Technology Organization ANSTO/E734, Lucas Heights (1998).
- [VII-8] X-5 MONTE CARLO TEAM, MCNP – A General Monte Carlo N-Particle Transport Code, Version 5, Los Alamos National Laboratory Report LA-UR-03-1987, Los Alamos, NM (2008).

ANNEX VIII

BENCHMARK CONSOLIDATED RESULTS AGAINST EXPERIMENTAL DATA FROM INR-1

VIII-1. INTRODUCTION

The INR-1 benchmark analysis for the 14 MW Training, Research, Isotopes, General Atomics (TRIGA) reactor in Pitesti, Romania, including the reactor specification and experimental data, is documented in Ref. [VIII-1].

During its first two decades of operation, the TRIGA 14 MW reactor was mainly used for testing nuclear power plant fuel, typically UO₂ LEU fuel specimens but also natural uranium fuel for Canada deuterium-uranium (CANDU) reactors. Most of these tests were performed in irradiation loops, both in forced and natural circulation. From these activities, a long-run power ramp test on a 2.5% enriched UO₂ fuel was selected. The test was performed inside a natural convection capsule during 1988 and 1989. Thus, the benchmark targets the power plant fuel irradiation and burnup determination by mass spectrometry. The reactor core at that time was composed of 29 HEU fuel bundles at different individual burnups. Reactor design data and operation data for the reactor and capsule were collected and presented as simple as was reasonably possible, while still providing the details needed to calculate the reactivity of the reactor core and the burnup of the test fuel.

VIII-2. SUMMARY OF THE BENCHMARK SPECIFICATION AND CODES AND MODELS USED

An outline of the INR-1 benchmark is presented.

VIII-2.1. Summary of the benchmark specification

The benchmark files provided [VIII-1] give general technical details on the TRIGA 14 MW reactor for the purpose of creating and verifying a computational neutronic model of the facility against critical rods bank position at criticality and excess reactivity of the reference core configuration (RCC) [VIII-2]. The reactor specifications do not include elements that are considered by the data provider as not having a significant influence (grid spacers, radial beam tube, etc.). Also, geometrical details of the bottom and top reflectors for reactor elements are not included. Instead, a simplifying approach was used consisting of providing axial layers of reflectors with defined height and material composition.

The reactor operation data needed in calculating the burnup of the test fuel inside a capsule [VIII-3] are provided in a series of core configurations, with corresponding operation times and reactor power levels. The configuration series describes the irradiation campaign of the test fuel (code A-31) in a simplified manner, collapsing short irradiation periods (created by entries or removal of experiments and reactor scrams) into larger intervals using weighted averages of the power level, when the arrangement of the fuel and other in-core experiments could be reasonably approximated as being the same. No control rods position during cycles is provided: the analysts are expected to calculate the critical rods bank position for the indicated power level for each core configuration at the specified average temperature of the fuel, with xenon accumulated. Burnup of the TRIGA 14 MW core is provided to capture the evolution of the power density in the vicinity of the experiment, since the cumulated energy released by the

reactor during the experiment campaign is about 1300 MWd (out of an estimated initial core lifetime of 8000 MWd). Burnup values of individual TRIGA 14 MW fuel bundles at the start of the experiment are provided, as well as the typical axial burnup profile. Details of the irradiation capsule design and operation data are given and also a homogenized description of the simultaneous in-core experiments. The experimental data provided for the benchmark consist of the isotopic composition of uranium, which was determined by mass spectrometry at the end of irradiation, compared to the initial composition of the test fuel.

VIII–2.2. Summary of the codes used

An outline of the codes and cross-sections libraries used to perform the calculations is presented.

VIII–2.2.1. South Africa

Table VIII–1 shows condensed information about the codes utilized for this benchmark by the Necsa group.

TABLE VIII–1. EXPERIMENTS AND CODES USED BY SOUTH AFRICA

Experiment	Type	Codes used
Reference core configuration	Model building	OSCAR-5
	Criticality	Serpent 2
Irradiation of test fuel element	Material burnup	MGRAC, Serpent 2

All the Serpent 2 [VIII–4] results presented for this benchmark by Necsa were obtained using Serpent 2.1.23 (a slightly modified version to allow rod movements during multistep burnup calculations). The library used was ENDFVII.1.

The homogenized MGRAC cross-section library was produced using the homogenization options in Serpent 2, also based on ENDF/B-VII.1. Some of the lattice calculations performed for fuelled components was done with the HEADE lattice code, which used the WIMSE 172 (XMAS) library based on JEF-2.2.

VIII–2.2.2. Romania

MCNPX [VIII–5] was employed to calculate the benchmark. The code version used by Institute for Nuclear Research (INR) in generating results for this benchmark is v26.0 with ENDF/B-VII.0 libraries.

VIII–2.3. Summary of the models used

This section describes the models produced by the two participants calculating the INR-1 benchmark.

VIII–2.3.1. South Africa

Assembly models for fuel, control rod, reflector and hollow reflector were produced and then combined to form the different core configurations, including the RCC (Fig. VIII–1) using the data given in Ref. [VIII–1] (as described in the South Africa benchmark results for INR-1, given in the supplementary files on-line). These models were exported directly to Serpent 2, but, as

described by the individual contribution report, more work is needed in order to prepare a working MGRAC model. For the test fuel element irradiation modelling, additional models were developed (Fig. VIII-2 and Fig. VIII-3). The fuel element was constructed by stacking 19 fuel pellets on top of each other and surrounding them with Zircaloy cladding. The complicated top and bottom caps of the fuel element were simplified in the model. Temperatures for the fuel in the core (average) were as provided for the four core configurations and the moderator temperature was taken to be 27°C, while the test fuel was modelled with separate conditions (moderator density and temperature and fuel temperature).

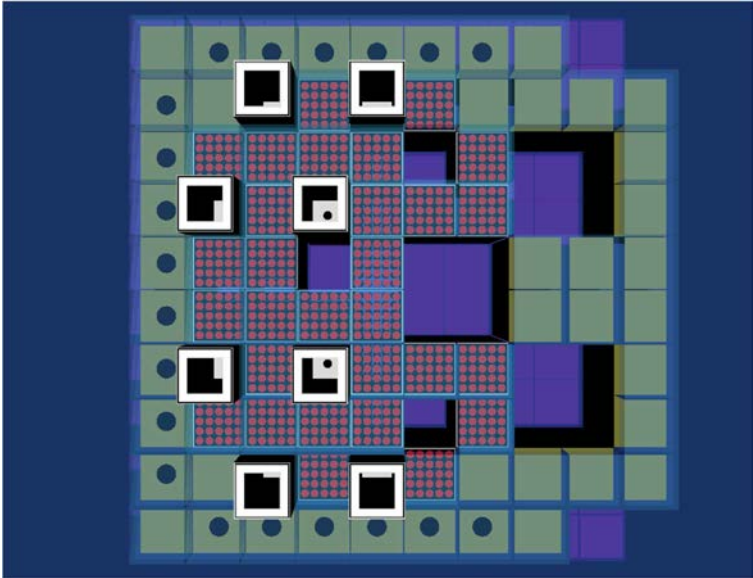


FIG. VIII-1. The reference core configuration (RCC). (courtesy of Necsa, South Africa)

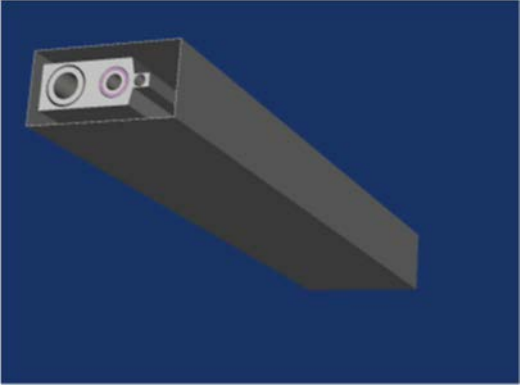


FIG. VIII-2. The capsule. (courtesy of Necsa, South Africa)

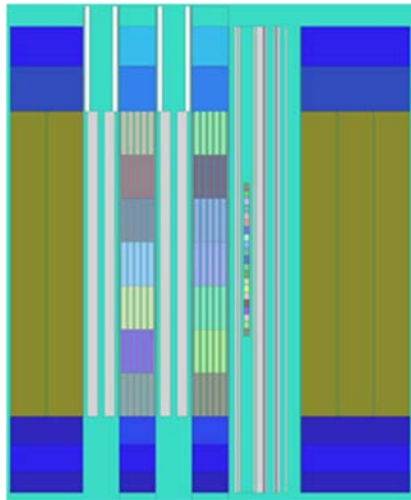


FIG. VIII-3. Test element axial position in core. (courtesy of Necsa, South Africa)

All four core configurations, containing the capsule with the test element inside, were modelled separately, with their corresponding number of fuel bundles and initial burnup for each of these bundles.

The typical axial burnup profile was used to divide the active part of each fuel bundle into 7 equal axial burnup zones. The initial isotopic compositions in each layer were taken from a pre-tabulated set produced by a Serpent 2 burnup calculation, calculated in an ‘infinite’ reactor (only fuel assemblies).

A model for MGRAC was also developed. State dependent nodal parameters for the fuel assemblies were generated using the HEADE lattice code in an infinite environment, that is, with fuel surrounded by fuel only. This approximation for fuel introduces significant errors into the model, and some improvements will have to be considered in future iterations. The biggest concern are the cases where fuel borders control rods. The final three dimensional nodal model was constructed by stacking the two dimensional mixtures on top of one another.

In order to deplete the test fuel element, a lattice model for the test rig was also constructed in HEADE. The fuel element was depleted surrounded by a homogenized fuel mixture, and beryllium reflector on the right (Fig. VIII-4).

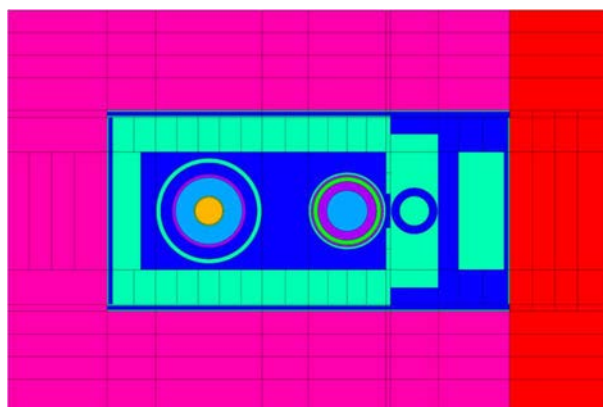


FIG. VIII-4. Lattice model of the test fuel element. (courtesy of Necsa, South Africa)

The final MGRAC model consists of:

- Static position dependent homogenized mixtures for the outer most reflector, and rod nodes, generated by Serpent 2 in the Core 1 configuration;
- Typical coloursets for beryllium reflector and empty core sites, also generated by Serpent 2 from Core 1;
- Fuel assemblies use burnup dependent mixtures generated in an infinite environment by the lattice code HEADE;
- The test fuel element also uses burnup dependent cross-sections generated in an approximate environment by HEADE.

VIII-2.3.2. Romania

The TRIGA 14 MW RCC and the core configurations for the irradiation of the test UO_2 fuel element were modelled with MCNPX (as described in the Romania benchmark results for INR-1, given in the supplementary files on-line). The model for the RCC is presented in Fig. VIII-5.

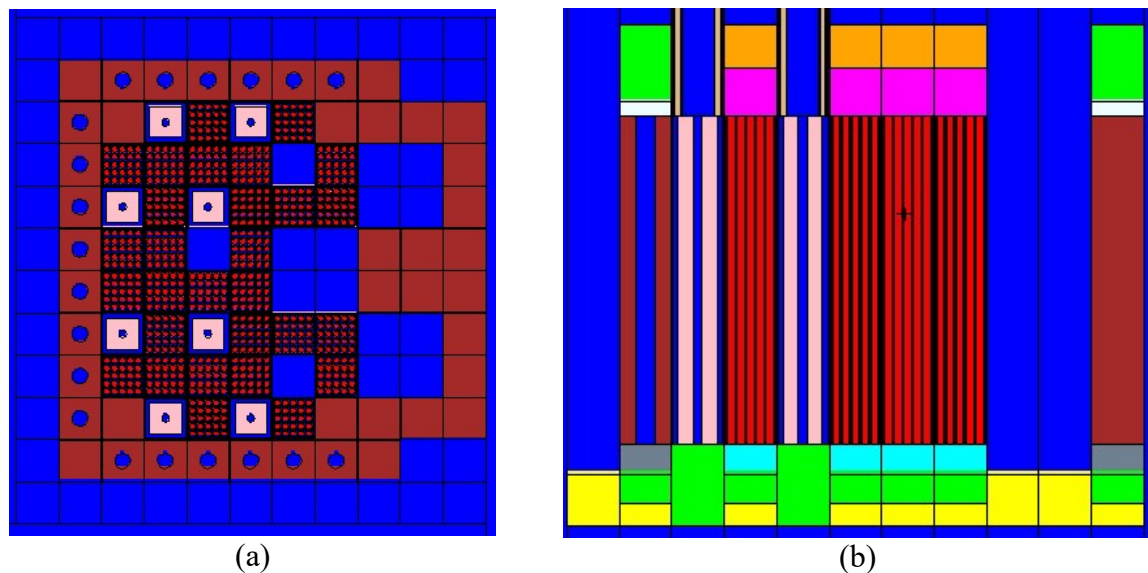


FIG. VIII-5. (a) X-Y cross-section and (b) X-Z cross-section through the TRIGA 14 MW RCC. (courtesy of INR, Romania)

At start of the experimental irradiation of the test fuel element, the TRIGA bundles were modelled at their corresponding burnup, as provided in Ref. [VIII-1]. Also, the capsule C1 which contain the test fuel element, and the rest of the experiments were modelled, as presented in Fig. VIII-6.

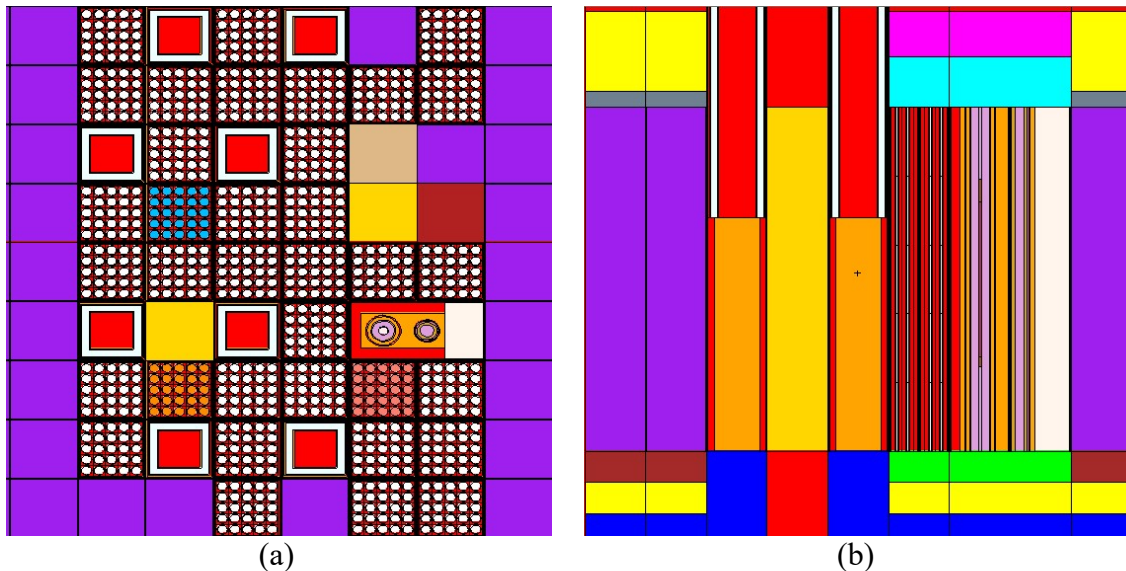


FIG. VIII-6. (a) X-Y modelling and (b) X-Z modelling of TRIGA 14 MW core and experiments. (courtesy of INR, Romania)

Concerning the burnup of the test fuel element, the four core configurations were calculated with the specified power level and operation time for each of these. Control rods were kept in bank at approximately the criticality position with xenon accumulated (63%, 58%, 61% and 68% for each configuration, respectively, with 100% representing the bank out of the core). An iterative process was performed regarding the initial content of ^{236}U and ^{234}U because the original specifications for the uranium used to fabricate the fuel could not be found. Effective temperatures were those given in Ref. [VIII-1], calculated for the UO_2 material cladding and the water in the capsule. TRIGA 14 MW fuel was approximated as being at an average temperature of 500 K for all configurations, although there may be some differences (~ tens of degrees) between configurations (at the end of irradiation the reactor power was about 11 MW compared to 7 MW in the beginning, but there is also an increase in the number of fuel elements, 35 bundles vs. 32).

VIII-3. RESULTS

VIII-3.1. Summary of the individual results

Summaries of the results of each participant calculating the INR-1 benchmark are presented.

VIII-3.1.1. South Africa

The result of the RCC criticality evaluation is shown in Table VIII-2, and the test element average isotopic ratios at the end of the irradiation period are given in Table VIII-3. Other results include: critical bank positions during the irradiation period, the evolution of isotopic ratios R5/8, R6/8 and R4/8 (ratios of the number of ^{235}U , ^{236}U and ^{234}U atoms to ^{238}U atoms) with core configuration, and axial profiles.

Although no experimental measurements of assembly burnup were provided, Fig. VIII-7 shows the difference in TRIGA assembly ^{235}U masses at the end of the irradiation period, as calculated by Serpent 2 and MGRAC. A maximum difference of about 3.7 gram between MGRAC and Serpent 2 is observed, which equates to an 8% difference in fuel burnup.

Finally, the total computational cost to model this experiment is compared between the two codes. Serpent 2 calculations were performed on a single node of an Intel Xeon based cluster with 24 cores, while MGRAC calculations ran on a basic Intel i7 workstation using a single core. The total wall time for depleting the core over all four configurations are 49 hours with Serpent 2 and 1 hour with MGRAC.

TABLE VIII-2. REFERENCE CORE EVALUATION

Code	Critical rods bank position (% withdrawn)	k_{eff}
Serpent 2	54.87	0.99835 (± 0.00025)

TABLE VIII-3. TEST ELEMENT AVERAGE ISOTOPIC RATIOS AT THE END OF THE IRRADIATION PERIOD

Ratio	Experimental	Serpent 2		MGRAC	
		Average	(C-E)/E %	Average	(C-E)/E %
R5/8	0.020902 (± 0.00008)	0.020887	-0.07	0.021453	2.64
R6/8	0.001328 (± 0.000026)	0.001202	-9.49	0.001119	-15.74
R4/8	0.000197 (± 0.000019)	0.000198	0.51	0.000198	0.51

Note: C and E stand for calculated and experimental data, respectively.

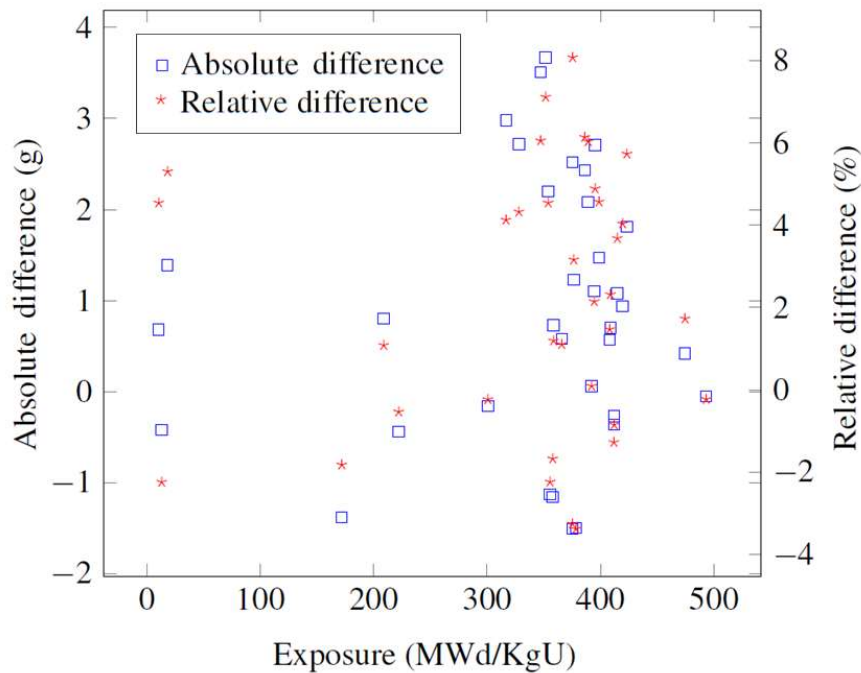


FIG. VIII-7. Difference in burned ^{235}U mass between Serpent 2 and MGRAC. (courtesy of Necs, South Africa)

VIII-3.1.2. Romania

The results of criticality calculations on the RCC are summarized in Table VIII-4. There are three cases calculated at room temperature:

- (a) Final reactor design [VIII-6] ^{235}U mass (41.16 g/pin) and theoretical ^{167}Er derived from HEU fuel density (6.0037 g/cm³);
- (b) Final reactor design [VIII-6] ^{235}U mass (41.16 g/pin) and final reactor design [VIII-6] ^{167}Er mass (2.93 g/pin);
- (c) Control rods in bank at 54.87%, which is the recorded position at criticality.

TABLE VIII-4. SUMMARY OF REACTIVITY CALCULATIONS RESULTS ON RCC

Case	k_{eff}	Standard deviation	Calculated reactivity [\$]	Experimental reactivity [\$]	(C-E)/E [%]
41.16 g/pin U-235 2.835 g/pin Er-167 CRs up	1.06171	0.00053	8.30	7.84	5.87
41.16 g/pin U-235 2.93 g/pin Er-167 CRs up	1.05493	0.00055	7.44	7.84	-5.10
CRs in bank at criticality (54.87%)	0.99912	0.00057	-	-	-

Note: C and E stand for calculated and experimental data, respectively.

The first two cases in Table VIII-4 show the importance of the erbium content in the fuel, the results being expressed in dollars (1\$ = 7 mk) to compare with the reactivity computer determinations. The reactivity computer determines the experimental reactivity by analysing the shape of the time dependent amplitude of a detector signal, proportional to the instantaneous reactor power, during a small positive reactivity transient, e.g. step withdrawal of control rods. The determination of calculated excess reactivity is done by a single k_{eff} calculation, while the experimental excess reactivity is obtained by summation of rods segments worth from calibration when the control rods bank is inserted at criticality (54.87%). This may help to explain the difference between the reactivity calculation and the experimental data.

The MCNPX calculated values and the experimental values for the final isotopic ratios are shown in Table VIII-5. The evolution of each of these ratios with burnup is presented in Figs VIII-8–VIII-10. As stated in the experimental data document, there is no numerical description of the ^{234}U and ^{236}U content before irradiation, so the initial content of these two isotopes is assumed. R5/8 and R4/8 agree well with experimental data, but the estimate for ^{236}U is still too large. However, preserving the trend from Fig. VIII-9 and Fig. VIII-10 for R6/8 and R4/8, respectively, and imposing the experimental final values for the two isotopic ratios, the estimated initial content of ^{234}U in uranium is 0.020 wt%, while the initial content of ^{236}U is 0.047 wt%. This type of calculation allows determining the unknown initial content for these two isotopes, knowing the post-irradiation content of the fuel.

TABLE VIII-5. TEST ELEMENT ISOTOPIC RATIOS AT THE END OF THE IRRADIATION PERIOD BY INR

Ratio	Experimental	MCNPX	(C-E)/E [%]
R5/8	0.020902 (± 0.00008)	0.020891	-0.05
R6/8	0.001328 (± 0.000026)	0.001663	25.23
R4/8	0.000197 (± 0.000019)	0.000196	-0.51

Note: C and E stand for calculated and experimental data, respectively.

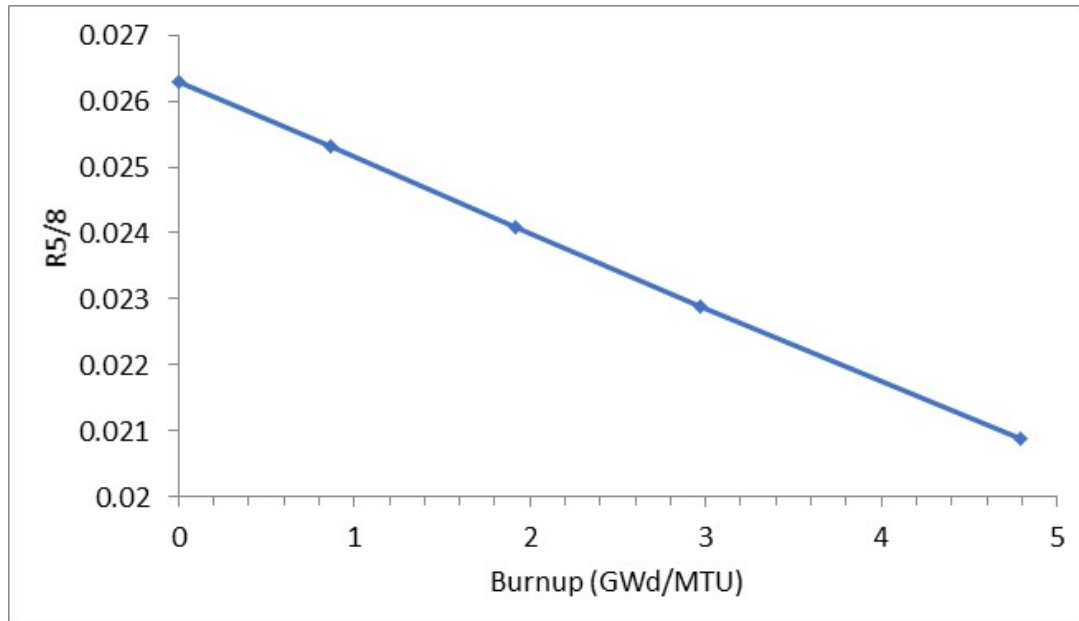


FIG. VIII-8. A-31 calculated R5/8 dependency on MCNPX reported burnup. (courtesy of INR, Romania)

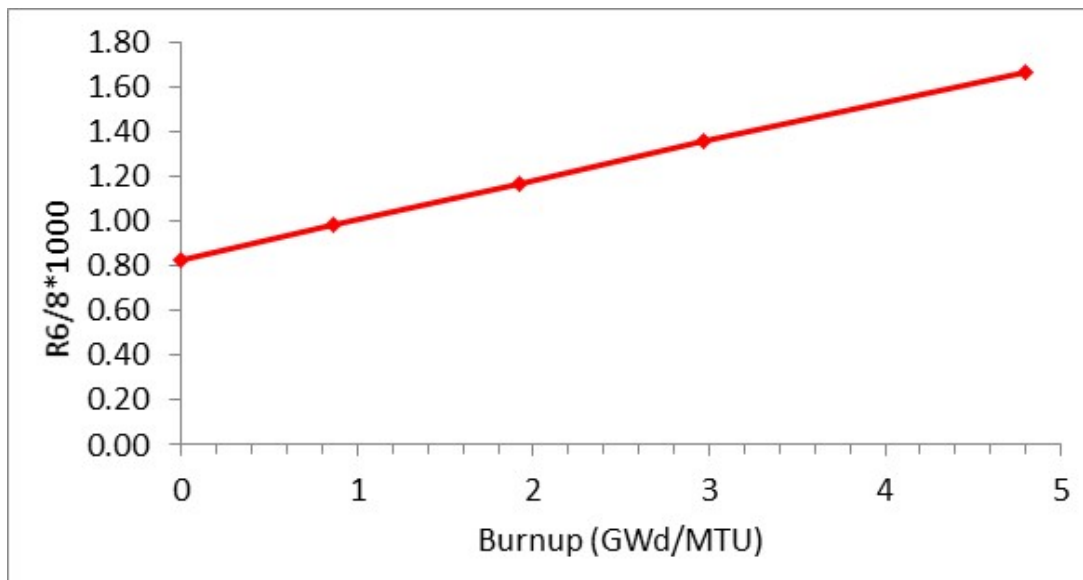


FIG. VIII-9. A-31 calculated R6/8 dependency on MCNPX reported burnup. (courtesy of INR, Romania)

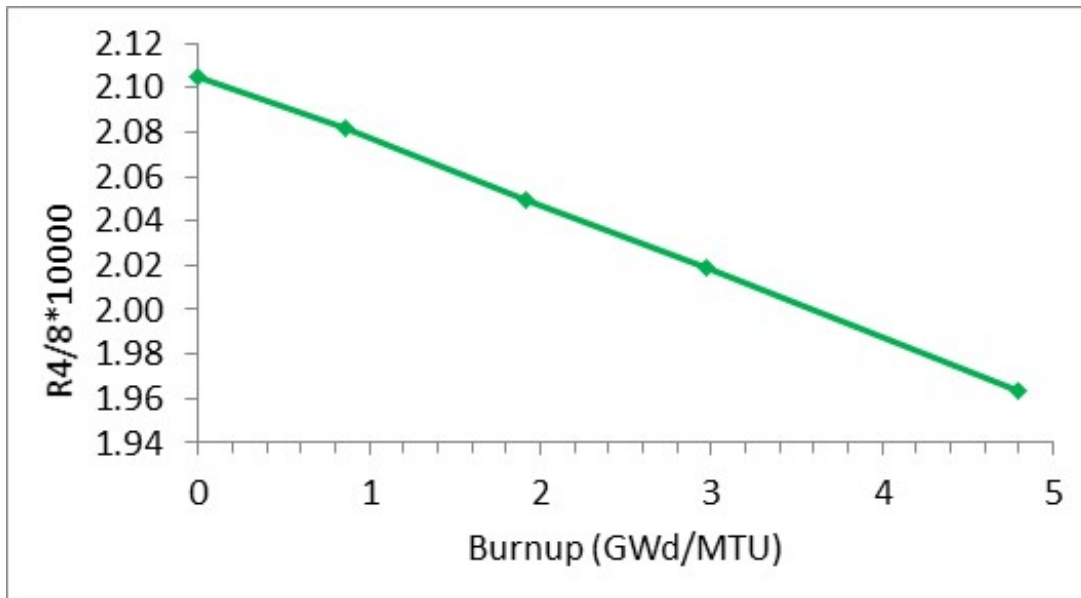


FIG. VIII-10. A-31 calculated R4/8 dependency on MCNPX reported burnup. (courtesy of INR, Romania)

VIII-3.2. Discussion of the consolidated results

The main results of this benchmark concern:

- Reactivity evaluation of the RCC, implying the comparison of control rods position (in bank) at criticality for the cold core;
- Isotopic ratios at the end of irradiation of the test UO₂ fuel element.

The consolidated results on the first of the above bullets are presented in Table VIII-6. The experimental position of control rods at critical yields a k_{eff} reasonably close to 1.00, both by Necsa and INR. This gives confidence in the methods of calculation despite the small differences in modelling: 5 axial zones for INR while Necsa used 7 axial zones, a smaller standard deviation in k_{eff} for Necsa (25 pcm vs. 57 pcm for INR) and, more importantly, the differences in computer codes and libraries used.

TABLE VIII-6. CONSOLIDATED RESULTS ON REACTIVITY CALCULATIONS ON RCC

k_{eff} / standard deviation (for control rods at 54.87% withdrawal)	
Necsa (Serpent 2)	INR (MCNPX)
0.99835/0.00025	0.99912/0.00057

The consolidated results on isotopic ratios at the end of the test fuel irradiation are presented in Table VIII-7. Very good agreement can be seen on R5/8. The initial content of ²³⁴U and ²³⁶U was estimated, and both participants started an iterative study by varying the number densities for the two isotopes. R4/8 changes very little during the irradiation period and agrees well with the experimental value. Since the final value of R6/8 is very sensitive to the initial ²³⁶U content,

the differences are large, and more iterations in varying the initial densities would be needed for each participant to match the experimental value.

TABLE VIII-7. CONSOLIDATED RESULTS ON TEST ELEMENT ISOTOPIC RATIOS

Ratio	Measured	INR		
		MCNPX	Serpent 2	MGRAC
R5/8	0.020902 (± 0.00008)	0.020891	0.020887	0.021453
R6/8	0.001328 (± 0.000026)	0.001663	0.001202	0.001119
R4/8	0.000197 (± 0.000019)	0.000196	0.000198	0.000198

VIII-3.3. Conclusions

The benchmark is focused on the TRIGA 14 MW reactor (for which reactivity results on the cold RCC at reactor startup are provided) and on an isolated low enriched UO₂ test fuel element irradiated in a pressurized capsule. The irradiation campaign was long enough to ensure that calculation of the burnup of the reactor fuel along with that of the test fuel needed to be done, in order to capture the evolution of the power distribution around the capsule. For the test fuel, the isotopic ratios of uranium were determined as a result of destructive examinations.

The benchmark was created with the aim of providing all the data needed, in an unambiguous manner, so as to allow little or no room for interpretation of the data. Of course, this implies making some choices such as: collapsing short-lived core configurations, giving a unique effective TRIGA fuel temperature for all configurations, neglecting the reactivity effects of beam tubes, a unique axial burnup distribution in the core, the homogenization of bottom and top reflector layers, etc. When data are missing, such as for the initial content of ²³⁴U and ²³⁶U, a sensitivity study is suggested.

Two organizations participated in the calculation of the benchmark:

- Necsa from South Africa. Necsa constructed a model using the OSCAR-5 system, and deployed it to the Monte Carlo code Serpent 2 and nodal diffusion code MGRAC for neutronic analysis. The model was used directly in Serpent 2, but an additional homogenization step was performed as part of the deployment to MGRAC.
- INR from Romania: the data provider. INR created a model of the reactor and experiment with MCNPX.

Both participants obtained good results compared to experimental reactivity and burnup measurements.

As expected, the Monte Carlo codes (MCNPX and Serpent 2) are well capable of treating the isolated test fuel in the context of the TRIGA core. When the fuel element was depleted by the lattice code HEADE by Necsa (surrounded by a homogenized fuel mixture, and beryllium reflector on the right), the accuracy of the test pin lattice model was restricted by the capabilities of the code, and a nodal solver is generally not appropriate for such kind of burnup problem.

REFERENCES TO ANNEX VIII

- [VIII-1] INTERNATIONAL ATOMIC ENERGY AGENCY, Research Reactor Benchmarking Database: Facility Specification and Experimental Data, Technical Reports Series No. 480 (Rev. 1), IAEA, Vienna (in preparation).
- [VIII-2] GENERAL ATOMICS, Commissioning Tests of the Steady-State Research/Materials and Testing Reactor for the Institute for Nuclear Technologies, Romania, General Atomics (1979).
- [VIII-3] CIOCANESCU, M., et al., Utilization Report for TRIGA INR Pitesti during 1988 and 1989, Report 2AQ-T-44/03-07-1989 (in Romanian), Institute for Nuclear Research, Pitesti, Romania (1989).
- [VIII-4] LEPPÄNEN, J., Serpent – a Continuous-energy Monte Carlo Reactor Physics Burnup Calculation Code User’s Manual, VTT Technical Research Centre of Finland, 18 June 2015 (2015).
- [VIII-5] X-5 MONTE CARLO TEAM, MCNP – A General Monte Carlo N-Particle Transport Code, Version 5, Los Alamos National Laboratory Report LA-UR-03-1987, Los Alamos, NM (2008).
- [VIII-6] GENERAL ATOMIC COMPANY, Safety Analysis Report of the TRIGA Steady-State Research/Materials and Testing Reactor, GA E-117-323 (1974).

ANNEX IX

BENCHMARK CONSOLIDATED RESULTS AGAINST EXPERIMENTAL DATA FROM IPEN/MB-01

IX-1. INTRODUCTION

The IPEN/MB-01 benchmark analysis, including the reactor specification and experimental data, is documented in Ref. [IX-1]. This benchmark is related to ^{99}Mo production. This isotope is a fission product which is produced by irradiation of a fissile target containing ^{235}U . After irradiation, ^{99}Mo is separated from all irradiated nuclides employing a chemical process. The irradiation of the target is normally performed in the reflector region of the reactor. The reflectors of the new design reactors like OPAL in Australia, HANARO (High-Flux Advanced Neutron Application Reactor) in the Republic of Korea, and the Multipurpose Brazilian Reactor are composed of heavy water in order to optimize the utilization of the neutrons from the core. The reflector region of the west face of the IPEN/MB-01 reactor was adapted to accommodate a heavy water box with an irradiation position (a hole to place the samples) in its centre. Ten miniplates containing $\text{UAl}_x\text{-Al}$ fuel in its centre were produced by the fuel fabrication factory of IPEN. The $\text{UAl}_x\text{-Al}$ is a fuel mixture of the intermetallic compound UAl_x ($x = 1, 2, \text{ or } 3$) and aluminium. The uranium content in each miniplate was 1.9045 g of ^{235}U and 7.82375 g of ^{238}U . These miniplates were accommodated in a special designed irradiation rig. After irradiation, these miniplates were taken to an HPGe detector to infer the ^{99}Mo production. Some preliminary experiments took place, such as the irradiation of gold foils, in order to characterize the neutron field and to make a consistency check for the power normalization.

IX-2. SUMMARY OF THE BENCHMARK SPECIFICATION AND CODES AND MODELS USED

The benchmarks consist of the analysis of the activation experiment of 10 $\text{UAl}_x\text{-Al}$ miniplates placed in the reflector region (west face) of the IPEN/MB-01 reactor. These miniplates were irradiated in a power of 108 W for 60 minutes. After that, the miniplates were removed from the core and taken to the gamma spectrometry equipment to measure the 140 keV photopeak as a function of the decay time and from that to infer the ^{99}Mo activity. The measurements were performed employing a thin HPGe detector for low energy gamma rays. The inference of the experimental ^{99}Mo activity at the end of irradiation takes into account the contributions of ^{99}Mo as well as $^{99\text{m}}\text{Tc}$. Both of these nuclides emit gamma rays of 140.5 keV. The benchmark also reports $^{197}\text{Au}(n,\gamma)$ reaction rates employing diluted gold foils. The reported benchmark quantities are the ^{99}Mo activity at the end of irradiation and the saturated $^{197}\text{Au}(n,\gamma)$ reaction rates. The complete details of the measurement procedure can be found in Ref. [IX-1].

IX-2.1. Summary of the benchmark specification

The benchmark geometric model for the IPEN/MB-01 configuration is shown in Figs IX-1, IX-2 and IX-3 for the radial and axial representations. The geometric model comprises a square array of 28×26 positions immersed in a cylinder of water of 100 cm radius, a heavy water box, and the holder for the $\text{UAl}_x\text{-Al}$ miniplates. The complete description of the benchmark is presented in Ref. [IX-1]. Also, a lot of the material and geometric details related to the IPEN/MB-01 core and surroundings can be found in Ref. [IX-2]. Here, only a few aspects are described.

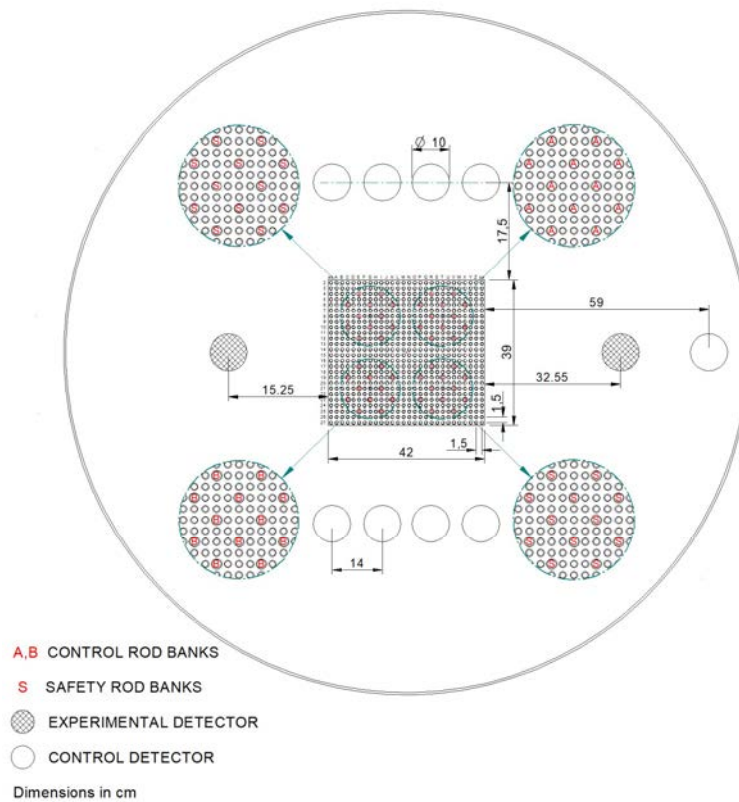


FIG. IX-1. Radial representation of the core and moderator tank (plan view) showing the detectors distribution around the core. Experimental detectors are shown only for illustrative purposes and the heavy water box is not shown here. (courtesy of IPEN, Brazil)

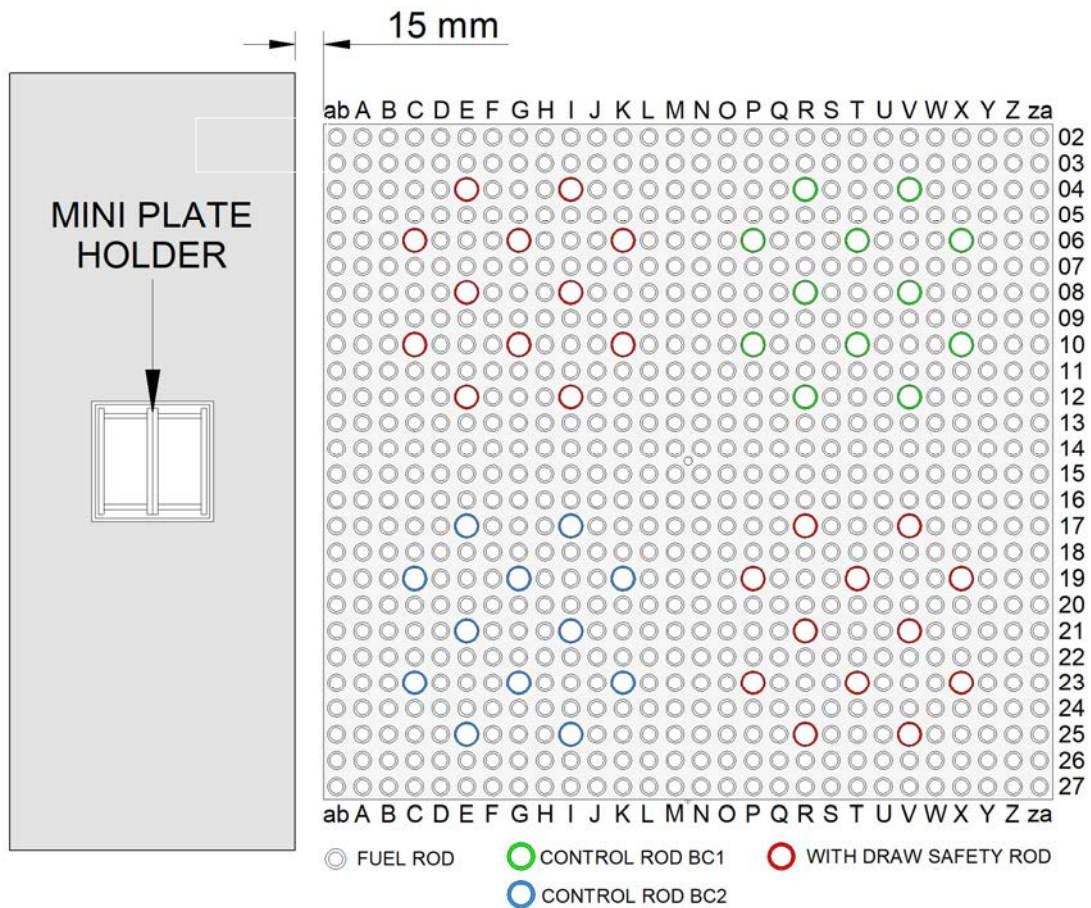


FIG. IX-2. Radial representation showing the heavy water reflector box in the west face of the reactor core. This upper view also shows the square hole in the reflector box where the miniplates holder and the miniplates are inserted. (courtesy of IPEN, Brazil)

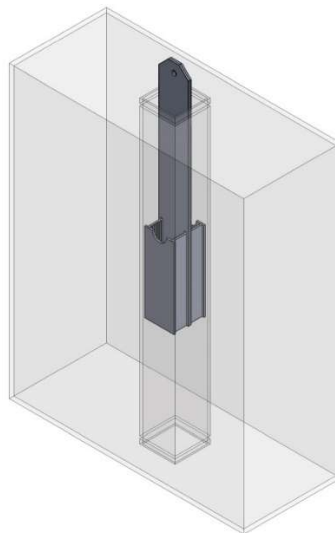


FIG. IX-3. Perspective view of the heavy water box and the UAl_x-Al miniplate holder. (courtesy of IPEN, Brazil)

The experimental benchmark results are presented in Tables IX-1 and IX-2 for the ^{99}Mo activity and the Au reaction rates, respectively, both referred at the end of the irradiation period.

TABLE IX-1. EXPERIMENTAL ⁹⁹Mo ACTIVITY FOR THE EFFECTIVE AREA

Miniplate	Activity (Bq)
1	(8.90 ± 0.50) E+4
2	(8.00 ± 0.40) E+4
3	(7.30 ± 0.40) E+4
4	(6.90 ± 0.40) E+4
5	(7.10 ± 0.40) E+4
6	(6.50 ± 0.30) E+4
7	(6.10 ± 0.30) E+4
8	(6.00 ± 0.30) E+4
9	(5.30 ± 0.30) E+4
10	(6.40 ± 0.30) E+4

TABLE IX-2. EXPERIMENTAL SATURATED ACTIVITY FOR THE DILUTED GOLD FOILS

Gold Foil	Saturated activity (reactions/s)	σ ^(*) (%)
1	127 330	1.1
2	136 091	1.1
3	140 106	1.1
4	141 972	1.1
5	146 306	1.1

(*) σ represents the saturated activity uncertainty.

IX-2.2. Summary of the codes used

The benchmark contributors, number of methodologies, codes and nuclear data libraries used to analyse the IPEN/MB-01 benchmarks are presented in Table IX-3.

TABLE IX-3. METHODOLOGIES EMPLOYED IN THE BENCHMARK ANALYSES

Benchmark contributors	Number of methodologies	Codes (Libraries) used
Argentina	4	<ul style="list-style-type: none"> • Serpent 2 (ENDF/B-VII.0, JEFF-3.2, and ENDF/B-VI.8) • CONDOR CITVAP (ENDF/B-VI.8) • SCALE/KENO-VI (ENDF/B-VII.0) • MCNP5.1 (ENDF/B-VII.0)
Brazil	2	<ul style="list-style-type: none"> • MCNP5 (ENDF/B-VII.0, DCS^(*), ^(**), CCS^(*), ^(***)) • SCALE (ENDF/B-VII.0)
Slovenia	1	<ul style="list-style-type: none"> • MCNP6 (ENDF/B-VII.1, IRDFF-v1.05^(*), IRDF-2002^(*)) • FISPACT-II
South Africa	2	<ul style="list-style-type: none"> • OSCAR-5/MCNP6 (ENDF/B-VII.0) • OSCAR-5/Serpent 2 (ENDF/B-VII.0)

(*) Only for the dilute gold foil activation.

(**) DCS: dosimetry cross-section

(***) CCS: continuous cross-section

IX-2.3. Summary of the models used

All participants employed a complete 3-D configuration of the benchmark model as specified in the calculated input document in Ref. [IX-1]. Assembly models for the fuel rods, control banks, moderator, light and heavy water reflectors, miniplate supports and UAl_x-Al miniplates themselves were produced based on the proposed IPEN/MB-01 model described in the calculated input document in Ref. [IX-1]. There were no distinctions for the IPEN/MB-01 model adopted for all participants. The UAl_x-Al miniplates experiment involves modelling the depletion of a rig containing fissile material, and the diluted gold foil experiment is a material activation study. The analyses of the UAl_x-Al miniplate experiment involve a transmutation analysis capability in the employed code. Here, this capability was not unique. Argentina employed the CONDOR-CITVAP burnup capability. With exception of Slovenia, all other MCNP (5 or 6) and SCALE analyses employed the ORIGEN2 burnup capability available in these codes. Slovenia employed FISPACT-II for the burnup purposes, and Serpent 2 burnup capability adopts the CINDER methodology to cope with this task. All these cases were run requesting a k_{eff} calculation. The neutron flux normalizations were made accordingly to the code employed.

There were two distinct methodologies employed by the participants: stochastic (MCNP, Serpent 2 and SCALE) and deterministic (CONDOR-CITVAP). The stochastic methodology was further divided into the pointwise neutron energy method (MCNP and Serpent 2) and the multigroup method (SCALE). The deterministic methodology (CONDOR-CITVAP) adopted the classical approach of neutron spectral calculations in the reactor cells (fuel, control rods, reflectors, etc.), cell homogenization in a multigroup level and posterior collapsing of the multigroup cross-section into a few-group model. The next task was the solution of the neutron diffusion equation employing the few-group constants generated in the previous step.

The utilization of MCNP code was common to all participants. Brazil and Argentina also reported results employing SCALE. Regarding deterministic codes, Argentina employed CONDOR-CITVAP while South Africa employed the pre-processing capabilities of the OSCAR-5 code to ensure that the models employed in MCNP6 and Serpent 2 were consistent. No other capability of the OSCAR system was employed.

With the exception of Slovenia, all other participants, employed the ENDF/B-VII.0 in all MCNP, SCALE, and Serpent 2 cases. Slovenia employed MCNP6 in conjunction with ENDF/B-VII.1. CONDOR-CITVAP employed ENDF/B-VI.8. In order to obtain a rough estimate of the impact of diverse data on the main results, Argentina also provided results for ENDF/B-VI.8 and JEFF-3.2 ACE nuclear data libraries.

IX-3. RESULTS

IX-3.1. Results of the individual participant contributions

Since the IPEN/MB-01 model was the same for all participants, the difference between calculated and benchmark values reside mostly in the method and code employed to solve the neutron transport equation and the nuclear data library employed.

The criteria for the number of histories employed in MCNP and Serpent 2 for all participants was not unique. Brazil employed 1020 cycles of 1 million histories each. The first 20 cycles were skipped. Argentina chose a total number of histories to obtain a statistical convergence of less than 1% for flux calculations and less than 3% for reaction rates calculations. South Africa

employed 8000 cycles of 128 000 particles per cycle. The first 100 cycles were skipped. Slovenia did not provide the number of histories and the number of cycles skipped.

The comparison of calculated results of the individual benchmarks starts with the k_{eff} eigenvalues, as shown in Table IX–4. Although this parameter is not the main purpose of the benchmark, this comparison was made just for a consistency check of the calculation model.

TABLE IX–4. CRITICALITY ESTIMATE FOR THE MOLYBDENUM EXPERIMENT

Participant	Serpent 2	CONDOR-CITVAP	MCNP5	MCNP6	SCALE/KENOVI
Brazil (IPEN)	–	–	0.99906 (2)	–	1.00496 (9)
Argentina INVAP	0.99905 (6) ^(*)	0.99362	0.99820 (2)	–	0.99830 (3)
South Africa Necsa	0.99959 (2)	–	–	0.99897 (7)	–
Slovenia (JSI)	–	–	–	not available	–

^(*) Uncertainty of the Monte Carlo calculations. It applies to the last significant digit.

The impact of nuclear data libraries on the benchmark k_{eff} results are presented in Table IX–5. The results were provided by Argentina employing Serpent 2 in conjunction with ENDF/B-VII.0, ENDF/B-VI.8 and JEFF-3.2 ACE nuclear data libraries.

TABLE IX–5. SERPENT 2 MODELS MULTIPLICATION FACTOR AND REACTIVITY WITH HEAVY WATER REFLECTOR AND TEN MINIPLATES FOR DIFFERENT NUCLEAR DATA LIBRARIES

Nuclear data library	Multiplication factor	Calculated reactivity (pcm)
ENDF/B-VII.0	0.99905 (6)	–95 (6)
ENDF/B-VI.8	0.99425 (6)	–578 (6)
JEFF-3.2	0.99792 (6)	–208 (6)

Considering the irradiation of ^{99}Mo , the benchmark results for the ^{99}Mo activity at the end of the irradiation period are presented in Tables IX–6–IX–9. These tables present the results employing respectively, MCNP, Serpent 2, SCALE, and CONDOR-CITVAP.

All comparisons are expressed in terms of $(C-E)/E$ as a percentage. C and E are the calculated values and the benchmark values, respectively. The uncertainty in this quantity is given by:

$$\sigma_{(C-E)/E} = \frac{C}{E} \sqrt{\left(\frac{\sigma_C}{C}\right)^2 + \left(\frac{\sigma_E}{E}\right)^2} \quad (\text{IX-1})$$

where σ_C and σ_E are the uncertainties in C and E, respectively.

If the absolute value of $(C-E)/E$ is less than $\sigma_{(C-E)/E}$, the calculated values are inside of the $(1-\sigma)$ range of the total uncertainty. In this case, the agreement between calculated and experimental values can be considered very good.

TABLE IX-6. MCNP ⁹⁹Mo ACTIVITY RESULT COMPARISONS

Miniplate	(C-E)/E (%)	(C-E)/E (%)	(C-E)/E (%)	(C-E)/E (%)
	(MCNP5) INVAP Argentina	(MCNP5) IPEN Brazil	(MCNP6) (Necsa) South Africa	(MCNP6) (JSI) Slovenia
1	8.8 ± 6.1	7.7 ± 6.1	7.3 ± 6.1	7.0 ± 6.0
2	4.9 ± 5.2	3.9 ± 5.2	4.3 ± 5.2	3.0 ± 5.2
3	4.2 ± 5.7	3.3 ± 5.7	3.3 ± 5.7	3.0 ± 7.1
4	4.0 ± 6.0	3.2 ± 6.0	1.7 ± 5.9	2.0 ± 5.9
5	1.3 ± 5.7	-2.0 ± 5.5	-1.9 ± 5.5	-2.7 ± 5.5
6	0.6 ± 4.6	1.2 ± 4.7	-2.4 ± 4.5	-1.4 ± 4.6
7	0.1 ± 4.9	-0.3 ± 4.8	-3.9 ± 4.7	-1.6 ± 6.0
8	0.7 ± 5.0	-1.1 ± 4.9	-1.9 ± 4.9	-2.8 ± 4.9
9	14.5 ± 6.5	12.6 ± 6.4	12.0 ± 6.3	12.0 ± 6.3
10	2.1 ± 4.8	0.7 ± 4.7	2.1 ± 4.8	0.0 ± 4.7

TABLE IX-7. SERPENT ⁹⁹Mo ACTIVITY RESULT COMPARISONS

Miniplate	(C-E)/E (%)	(C-E)/E (%)
	(INVAP) Argentina	(Necsa) South Africa
1	3.6 ± 6.0	9.82 ± 6.2
2	0.5 ± 5.2	6.16 ± 5.3
3	-0.6 ± 5.7	4.45 ± 5.7
4	-1.0 ± 5.9	4.01 ± 6.0
5	-4.3 ± 5.5	-0.95 ± 5.7
6	-3.6 ± 4.5	0.73 ± 4.6
7	-0.2 ± 4.7	-0.30 ± 4.9
8	-5.8 ± 4.9	-0.54 ± 5.0
9	11.1 ± 6.3	15.00 ± 6.5
10	-1.5 ± 4.8	2.12 ± 6.2

TABLE IX-8. SCALE 6.1 ⁹⁹Mo ACTIVITY RESULT COMPARISONS

Miniplate	(C-E)/E (%)	(C-E)/E (%)
	(INVAP) Argentina	(IPEN) Brazil
1	-4.7 ± 5.4	-0.1 ± 5.4
2	-1.7 ± 4.9	-2.8 ± 4.9
3	-1.3 ± 5.4	-3.5 ± 5.4
4	-1.2 ± 5.7	-6.1 ± 5.7
5	4.5 ± 5.9	-11.2 ± 5.9
6	3.2 ± 4.8	-10.2 ± 4.8
7	3.7 ± 5.1	-10.1 ± 5.1
8	4.7 ± 5.2	-9.8 ± 5.2
9	-9.3 ± 5.1	0.8 ± 5.1
10	3.5 ± 4.9	-9.5 ± 4.9

TABLE IX–9. CONDOR-CITVAP ⁹⁹Mo ACTIVITY RESULT COMPARISONS

Miniplate	(C–E)/E (%) (INVAP) Argentina
1	6.3 ± 6.0
2	4.4 ± 5.2
3	5.7 ± 5.8
4	6.7 ± 6.2
5	3.4 ± 5.8
6	1.8 ± 4.7
7	1.6 ± 5.0
8	1.0 ± 5.1
9	15.9 ± 6.6
10	1.5 ± 4.8

The participants' results for the ¹⁹⁷Au(n,γ) reaction rates together with its tally cross-section are given in Table IX–10. Argentina and South Africa did not provide the tally cross-sections for gold. With exception of Slovenia, all other participants employed the ENDF/B-VII.0 in all MCNP and Serpent cases. Slovenia employed ENDF/B-VII.1. The results were provided in two categories: stochastic and deterministic. The stochastic results were provided by MCNP and Serpent 2. Argentina provided results employing the deterministic approach of CONDOR-CITVAP.

TABLE IX–10. COMPARISON OF RESULTS FOR ¹⁹⁷Au(n,γ) REACTION RATE

Country (Institution)	Methodology	Au Foil Position				
		1	2	3	4	5
Argentina (INVAP)	MCNP5	-2.3 ± 3.0	-4.3 ± 3.2	-3.9 ± 3.2	-8.4 ± 3.0	-11.0 ± 2.9
	SCALE	-7.5 ± 5.5	-8.8 ± 5.3	-15.3 ± 4.5	-16.0 ± 4.4	-14.0 ± 4.9
	CONDOR-CITVAP	-4.9 ± 0.7	-6.7 ± 1.4	-7.9 ± 1.3	-7.0 ± 1.3	-8.4 ± 1.3
Brazil (IPEN)	MCNP5 DCS (30y) ^(*)	-1.4 ± 3.2	-8.2 ± 3.2	-10.1 ± 3.1	-8.0 ± 3.4	-9.3 ± 3.2
	MCNP5 CCS (70c) ^(*)	-1.7 ± 2.8	-5.1 ± 2.9	-6.2 ± 2.9	-6.4 ± 2.8	-6.7 ± 2.9
	MCNP6 ENDF/B-VII.1	-2.8 ± 3.0	-7.6 ± 3.2	-7.5 ± 3.2	-8.2 ± 3.0	-7.3 ± 2.9
	MCNP6 IRDF-2002 ^(*)	-2.8 ± 3.0	-8.4 ± 3.0	-7.5 ± 3.3	-8.2 ± 3.0	-7.0 ± 3.1
Slovenia (JSI)	MCNP6 IRDFF-v1.05 ^(*)	-2.8 ± 3.0	-7.6 ± 3.1	-7.4 ± 3.2	-8.2 ± 3.0	-7.3 ± 3.1
	MCNP6 ENDF/B-VII.1 ^(**)	-2.8 ± 3.0	-7.6 ± 3.1	-7.5 ± 3.2	-8.2 ± 3.0	-7.4 ± 3.1
	Serpent	8.3 ± 5.8	14.8 ± 5.2	5.4 ± 6.1	12.3 ± 5.5	7.7 ± 5.3
South Africa (Necsa)	MCNP	2.0 ± 3.3	9.9 ± 3.2	1.0 ± 3.2	2.7 ± 3.5	9.0 ± 3.2

^(*) Only for tally cross-section.

^(**) Tally and overall material cross-sections.

The impact of nuclear data libraries on the benchmark results are presented in Fig. IX–4 for the ^{99}Mo activities. The results were provided by Argentina employing Serpent 2 and the same models as described in the calculated input document in Ref. [IX–1]. The results employed ENDF/B-VII.0, ENDF/B-VI.8 and JEFF-3.2 ACE nuclear data libraries. The maximum absolute differences, calculated as $(C-E)/E$, are presented for each miniplate in Fig. IX–4 to summarize the nuclear data library impact.

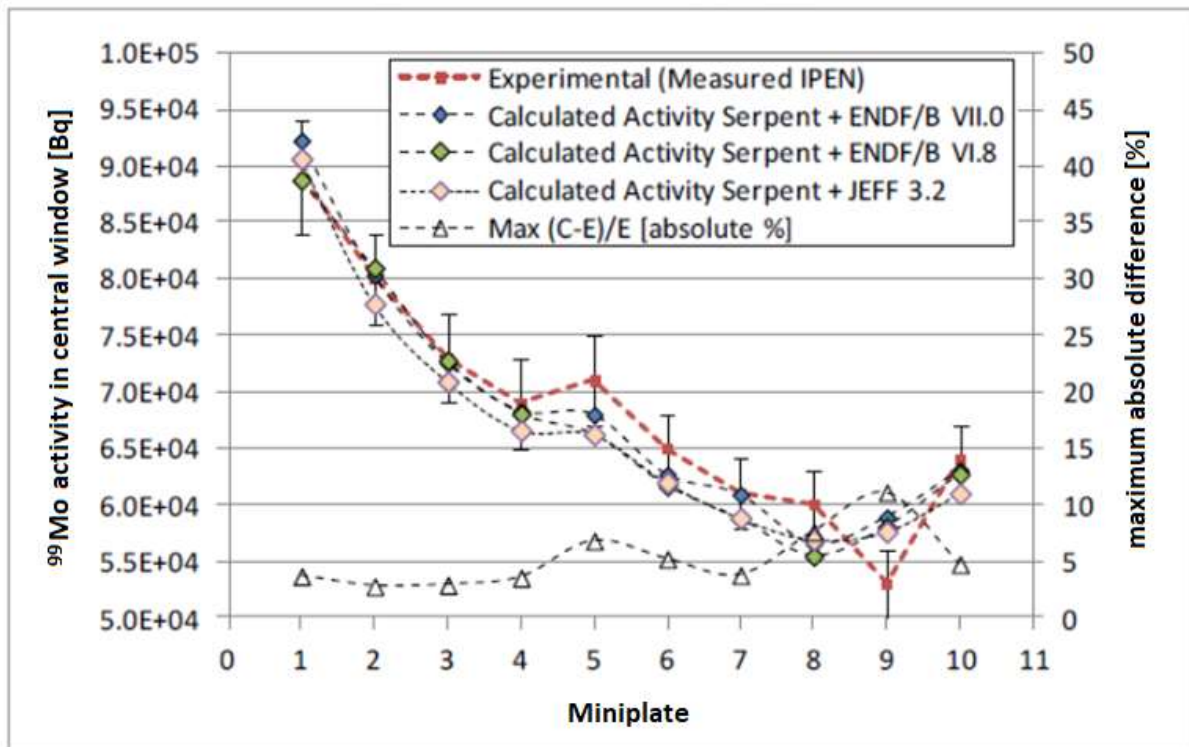


FIG. IX–4. Serpent model ^{99}Mo calculation results comparison for diverse nuclear data libraries and experimental values. (courtesy of INVAP, Argentina)

IX–3.2. Discussion of the consolidated results

The discussion of the consolidated results is presented in this section. Initially the k_{eff} results are presented, followed by the ^{99}Mo activity and the $^{197}\text{Au}(n,\gamma)$ reaction rate results. Finally, the impact of the utilization of different nuclear data libraries in the ^{99}Mo activity results is discussed.

IX–3.2.1. Effective neutron multiplication factor

There was no evaluation of uncertainties for the inferred k_{eff} benchmark values of the configuration under consideration. However, compared to other evaluations of the IPEN/MB-01 reactor and published in the ICSBEP handbook [IX–2], an uncertainty of 80 pcm can be assigned. This will be the uncertainty to be used in this benchmark, and consequently the benchmark value for k_{eff} is 1.00000 ± 00080 .

The k_{eff} results, as shown in Tables IX–4 and IX–5, were very consistent when MCNP, Serpent and SCALE (Argentina) were employed together with the ENDF/B-VII.0 nuclear data library. The results were roughly less than 200 pcm from the critical value and consequently less than

the $(3-\sigma)$ range of the benchmark value. The results of CONDOR-CITVAP and SCALE (Brazil) show discrepancies over 400 pcm. CONDOR-CITVAP employed the ENDF/B-VI.8 nuclear data library and this library underestimates the k_{eff} eigenvalue by around 500 pcm as verified in several other benchmark analyses employing this library [IX-3] and this tendency was also verified for the benchmark under discussion here. The Serpent 2 k_{eff} results, as reported in Table IX-5, employing ENDF/B-VII.0 and JEFF-3.2, are inside of the $(3-\sigma)$ range of the benchmark uncertainty (80 pcm) and can be considered fair. The same cannot be said for ENDF/B-VI.8 result which is underestimated by over 500 pcm. The reason is the same as previously mentioned. Furthermore, it is noted is that, for the same nuclear data library (ENDF/B-VI.8), CONDOR-CITVAP and Serpent 2 produce similar k_{eff} values in spite of the different methodologies. This is an important aspect that reinforces the idea that the reason for the underprediction of k_{eff} is not the methodology employed by these two codes and it is indeed due to the nuclear data library employed. The reason for the SCALE (Brazil) overprediction of k_{eff} is unknown.

IX-3.2.2. ^{99}Mo activity

The comparisons of ^{99}Mo activity results shown in Tables IX-6–IX-8 reveal that the agreements, in a general sense, are very good. Most of the (C-E)/E results are within the $(1-\sigma)$ range of the total uncertainty (Monte Carlo and benchmark) values. Surprisingly, although based on diffusion theory, the deterministic approach adopted by Argentina based on the CONDOR-CITVAP systems provided excellent results. No major trend was noticed from the reported results. Only the results for the miniplate number 9 showed a systematic overprediction in all cases, which might indicate some problems in the experimental value.

IX-3.2.3. $^{197}\text{Au}(n,\gamma)$ reaction rates

The $^{197}\text{Au}(n,\gamma)$ reaction rates are shown in Table IX-9. Here, the modelling of the experiment is significantly more challenging for both MCNP and Serpent 2 codes. The gold foils are thin and the number of neutron histories to get a satisfactory standard deviation in the $^{197}\text{Au}(n,\gamma)$ reaction rates increases significantly. The first aspect to be noted is that the major part of the uncertainty in (C-E)/E is due to the statistical nature of the calculations. In general, the (C-E)/E results are well outside of the $(1-\sigma)$ range of total uncertainty as shown in Table IX-10. This aspect somehow reflects the difficult to obtain a satisfactory standard deviation in the Monte Carlo simulation. The second aspect is the systematic underprediction of the calculated $^{197}\text{Au}(n,\gamma)$ reaction rates. This aspect was found independently of the participant and the computer code employed for the theoretical analysis. Surprisingly, again here, the deterministic approach adopted by Argentina based on the CONDOR-CITVAP systems provided results similar to the Monte Carlo codes.

IX-3.2.4. The impact of the nuclear data libraries

The analyses of the impact of the nuclear data libraries reveal that:

- (a) The impact of the evaluated nuclear data libraries in the Serpent 2 model reactivity calculation is as high as ~ 500 pcm when ENDF/B-VI.8 is employed. Very good results are obtained when ENDF/B-VII.0 and JEFF-3.2 are employed because the (C-E)/E values are inside of the $(1-\sigma)$ range of their total uncertainty, as shown in Table IX-10.
- (b) The impact of the evaluated nuclear data libraries in the Serpent 2 ^{99}Mo activity calculation is generally small. The (C-E)/E value is inside of the $(1-\sigma)$ range of the total uncertainty

and, in the average, as low as ~5% (C/E); if miniplate number 9 is not considered, this difference is reduced to ~3%.

- (c) Regarding $^{197}\text{Au}(n,\gamma)$ reaction rates, there are some nuclear data dependence for the choice of the tally cross-section. The dosimetry cross-section (DCS) data shifted the calculated results farther away from the benchmark values. The utilization of the gold cross-section in the ENDF/B-VII.0 library (70c) provides better results although outside of the $(1-\sigma)$ range of the total uncertainty (benchmark and Monte Carlo uncertainties). Slovenia produced very consistent results employing different libraries.

IX-3.3. Conclusions

The experiments provided by Brazil were very challenging, both in terms of experimental realization and theoretical analyses. They have been successfully accomplished and provided useful information for the reactor physics community. As mentioned in the measurement protocol document, the calibrations both for the reactor power and the HPGe detectors were fundamental. The quality of the benchmark values is intimately related to the calibration process. Furthermore, since the IPEN/MB-01 has been through several and severe revisions from the ICSBEP [IX-2] and IRPhE [IX-4] benchmarks, it is somehow easier to provide the material and geometric data of the facility. The feedback from the participants enhanced to a large extent the quality and usefulness of the proposed benchmark.

The technical analyses of the benchmark results provided by the participants revealed that the state of the art of calculation methods and related nuclear data libraries have reached a very high level of quality and sophistication. In particular, for the ^{99}Mo activity benchmark, the agreement between calculated results and benchmark values was very satisfactory and meets the design goals for the target response. Both stochastic methods and deterministic methods were employed in the theoretical analyses. Only miniplate number 9 showed a systematic overprediction of the calculated results. However, in this case there may be some drawbacks in the experimental data and the reason for the discrepancy remains unknown. The calculated results employing the same code and related nuclear data library but from different participants were very similar, and no clear tendencies were noted. There was no clear tendency when the nuclear data libraries were changed: the calculated results remain nearly the same. This is a very good outcome from the nuclear data community, indicating that the cross-section adjustment related to thermal reactors is now becoming part of the history of the reactor physics area.

The discrepancy in the $^{197}\text{Au}(n,\gamma)$ reaction rates benchmark values was more severe. A systematic and consistent underprediction of the calculated results among all participants has been found. Up to now, the reasons for this underprediction are still unknown.

REFERENCES TO ANNEX IX

- [IX-1] INTERNATIONAL ATOMIC ENERGY AGENCY, Research Reactor Benchmarking Database: Facility Specification and Experimental Data, Technical Reports Series No. 480 (Rev. 1), IAEA, Vienna (in preparation).
- [IX-2] DOS SANTOS, A., et al., "LEU-COMP-THERM-077: Critical Loading Configurations of the IPEN/MB-01 Reactor", in: International Handbook of Evaluated Criticality Safety Benchmark Experiments (BRIGGS, J.B., Ed.), NEA/NSC/DOC (95)03/I, Nuclear Energy Agency, Paris (2004).

- [IX-3] KAHLER, A.C., Monte Carlo Eigenvalue Calculations with ENDF/B-VI.8, JEFF-3.0, and JENDL-3.3 Cross Sections for a Selection of International Criticality Safety Benchmark Evaluation Project Handbook Benchmarks, Nucl. Sci. Eng. **145** (2003) 213–224.
- [IX-4] OECD NUCLEAR ENERGY AGENCY, International Reactor Physics Experiment Evaluation (IRPhE) Project – IRPhE Handbook, NEA 7496, Paris (2019).

ANNEX X

BENCHMARK CONSOLIDATED RESULTS AGAINST EXPERIMENTAL DATA FROM IRR-1

X-1. INTRODUCTION

The IRR-1 benchmark analysis, including the reactor specification and experimental data, is documented in Ref. [X-1]. This benchmark is related to the measurement and evaluation of the remaining ^{235}U content in each fuel assembly (FA) of IRR-1, in order to assess the extension of the reactor lifetime, optimize its operation and improve its safety.

The main characteristics of IRR-1 are given in Table X-1. The contributions of this work to the CRP originally intended to include the following: for reactor operation data, the full irradiation history of the reactor since 1985 (core layouts and irradiation in MWh), and a detailed reactor specification [X-1]; for the experimental part, gamma ray spectrometry results in several FAs.

As the CRP proceeded and peer reviews were given at the research coordination meetings in 2015 and 2016, it became clear that additional experimental data could be provided, which consequently led to a more meaningful benchmark. The experimental data includes also additional information which is substantial to the purpose of this project: a direct non-destructive assay measurement of the ^{235}U depletion in FAs, namely rhenium gamma transmission measurements, in addition to the ^{137}Cs activation data. The experimental methods are explained in detail in the IAEA report that is part of the benchmark [X-1], as well as in other recent publications [X-2, X-3].

Throughout this report, depletion is defined as the fraction of initial ^{235}U nuclei that underwent either fission or radiative capture, and burnup is defined as the fraction of initial ^{235}U nuclei that underwent nuclear fission only.

TABLE X-1. MAIN OPERATING PARAMETERS OF THE IRR-1

Type of reactor	Open pool
Nominal power	5 MW
Maximal thermal neutron flux	
In core	$1 \times 10^{14} \text{ cm}^{-2} \cdot \text{s}^{-1}$
In reflector	$5 \times 10^{13} \text{ cm}^{-2} \cdot \text{s}^{-1}$
Fuel type	MTR, flat parallel plates UAL-Al dispersion fuel
Enrichment	93 wt%
Coolant	light water, downward flow
Moderator	light water
Reflector	graphite + light water
Heat flux	maximum 35.4 W/cm ² , average 11.6 W/cm ²
Nominal total flow rate	650 m ³ /h
Flow rate through FAs	420–520 m ³ /h (24 to 30 FAs)
Experimental facilities	6 radial beam tubes one rabbit system 2 tangential beam tubes
Irradiation positions	typically 1–3

X-2. SUMMARY OF THE BENCHMARK SPECIFICATION AND CODES AND MODELS USED

X-2.1. Summary of the benchmark specification

The benchmark includes detailed information about all 164 MTR fuel cores in the period 1985–2017, as well as the results of the 27 critical height experiments, and the results of the depletion and ^{137}Cs activity distributions in 9 FAs in mid-2017. A typical core arrangement can be seen in Fig. X-1. It includes fuel assemblies, most of them containing 23 fuel plates, but 3 to 5 of them are special fuel assemblies that provide guide boxes for the control absorbers, and contain only 17 fuel plates. The two types of FAs are depicted in Fig. X-2. One of the control rods is made from beryllium instead of the 17 fuel plates. Other types of rods are mentioned in the caption of Fig. X-1.

G	G	G	G	G	G	G	G	G	
G	G	G	S-2	G	D	G	G	G	
G	G	FS	FC	R	FS	FS	G	G	
G	D	FS	FC	FS	FC	FS	G	G	
G	G	FS	F	FS	FS	FS	GS	G	
G	G	FS	FC	FS	BE	FS	G	G	
G	G	FS	FS	FS	FS	FS	G	G	
G	G		FS	FS	FS	G	G	G	
	G	G	G	G	G	G	G		

FS **Standard fuel assembly**

FC **Control fuel assembly**

BE **Beryllium control assembly**

G **Graphite reflector element**

GS, D **Irradiation positions**

R **Regulating assembly**

S-2 **Neutron source**

FIG. X-1. Typical core arrangement. A blank position indicates an empty sealed grid position with no element (just water). (courtesy of Soreq, Israel)

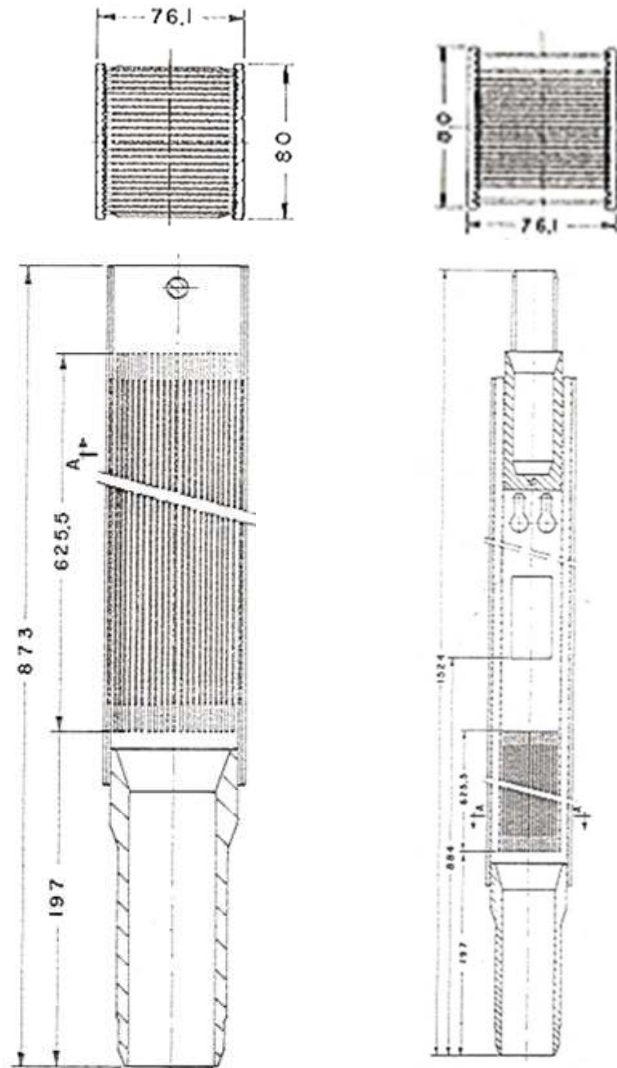


FIG. X-2. Standard fuel assembly (left) and Control (special) fuel assembly (right). (courtesy of Soreq, Israel)

The benchmark is defined by four files, all of them provided in Ref. [X-1]:

- IRR-1 core specifications. It includes detailed description of each of the core elements, the grid and irradiation channel positions;
- Summary of the experiments and their results:
 - Total and axial distribution of ^{235}U depletion in nine FAs. Five of the analysed FAs were used since 1985 and, thus, are part of the benchmark experimental data. The measurements on the remaining four FAs were taken in order to better estimate the uncertainty of the initial burnup in 1985;
 - Total and axial activity distribution of the burnup indicator ^{137}Cs in the nine FAs;
 - 27 critical conditions (core, height of control rods, in the beginning or the end of cycles) throughout the irradiation history 1985–2017.
- An output Excel data file which contains 164 successive core layouts during the years 1985–2017, and the MWh for each core;
- Initial condition of the burnup of the FAs in the starting point of the benchmark (the beginning of the first core in 1985).

X-2.2. Summary of the codes used

The benchmark contributors, number of methodologies, codes and nuclear data libraries used to analyse the IRR-1 benchmarks are presented in Table X-2.

TABLE X-2. CODES USED BY THE TWO GROUPS FOR IRR-1 BENCHMARK

Research group	Codes (library) used
Soreq	MUTZAV: MCNP4b + Dragon 4
Necsa	OSCAR-5: Serpent 2 + MGRAC

X-2.3. Summary of the models used for IRR-1

X-2.3.1. Soreq (Israel) model

An MCNP input file for the IRR-1 first core was created in 1985. 45 burnup zones were included in each FA – 15 axial (z) zones for each of 3 horizontal zones (y), as can be shown in Fig. X-3. The horizontal zones consisted of two burnup zones for the two external fuel plates (first and last plates along the y axis) and one depletion zone for the remaining 21 plates in the middle of the FA. The burnup zones consisted of only the fuel meat.

Using an automated Python script, the 164 burnup cycles of IRR-1 [X-1] were then burnt sequentially with 3.9 million active neutron histories per burnup cycle, assuming constant power, and with the correct MWh for each core (each burnup cycle is defined as one core layout and was burnt using one burnup step). As an example, Fig. X-3 shows the details of one of the core layouts (number 42). The duration of the burnup of each cycle was set to a year's fraction according to the fraction that cycle's irradiation (MWh) represented of the overall irradiation of all the cycles within the same year. Note that some core layouts are split and counted as two burnup cycles within the 164 cycles' count, when their irradiation crossed the beginning of a new year. This was done in order to ensure a resolution of 1 year. In the burnup calculation, the absorber blades were partially inserted at a relative fixed height of 75%, which was their typical position during the last 30 years, however with significant variations in the range 65%–90% [X-1] (thus, this is an approximation). The total burnup during this period was 76.414 GWh.

Compared to the benchmark specifications, some parameters that were used in the simulation need special attention since they are approximations or are ill-defined in the benchmark. The approximations used are listed in the following:

1. The active height of each of the fuel plates was 59.65 cm (60.4 cm nominal in the specifications, with range 58.3–61.0 cm), and their active width was 6.23 cm (6.3 cm nominal in the specifications [X-1], with range 5.9–6.5 cm);
2. Both the upper and lower part of the core (representing the upper and lower passive parts of the fuel plates within the FAs) were replaced by homogenous material of height 15.175 cm and 8.955 cm, respectively, with mixed water and aluminium with a volume ratio of 1:3. (In the specification [X-1], above the active region there are 50.5 mm total of aluminium and water – including the passive part of the plate, the side plates and the aluminium handle. Below the active area and above the grid plate there is about 75 mm of aluminium and water – the passive plate region, the side plate and the hollow leg.) Below the FA, there is 12.195 cm of aluminium, representing the grid plate (the actual dimension of the grid plate in the specifications [X-1] is 15.7 cm),

but the water holes inside the grid were not modelled. All other volumes above, below and surrounding the core were filled with water;

3. Impurities in the fuel meat and cladding and side plates were taken as the maximal detectable tolerance in the benchmark specification [X-1]. No impurities were modelled in the graphite;
4. No radial or tangential irradiation tunnel were modelled;
5. As stated above, for each cycle, the cores were burned by a constant average power (as opposed to the true irradiation history, which had numerous periods of irradiations usually at a full power of 5 MW and breaks within each core), but with the real MWh and the irradiation time corresponding to the cycle duration. Therefore, the resulting power for each burnup cycle in the calculation was usually much lower than 5 MW;
6. 45 burnup zones were used, as described above. Only the fuel meat was considered to be burned;
7. The density of the Ag-In-Cd alloy in the control blades used in the calculation was 9.75 g/cm^3 (in the specification, the total density is assumed to be 10.17 g/cm^3 , according to Ref. [X-4]);
8. The neutron flux in 69 energy groups was used in order to perform the burnup calculation.

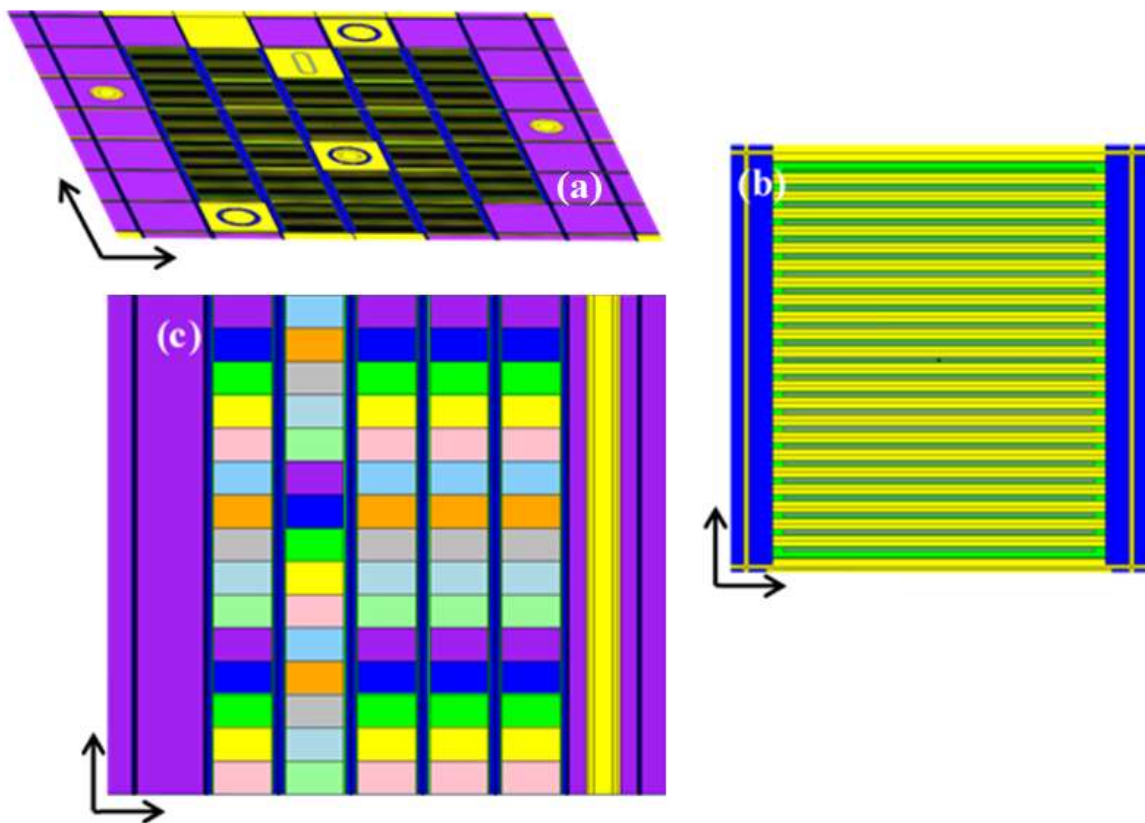


FIG. X-3. (a) 2-D plot cuts of the whole-core discretization of IRR-1 core 42 in the Soreq model in MCNP4b. (a) A tilted x-y plot of plane $z=0$. Colour mark different materials, where purple=graphite, yellow=water, blue=aluminium, and in the dark yellowish area are the fuel plates of the FAs. (b) A zoom-in at the plane $z=0$, shows the details of a single FA with its 23 plates. (c) x-z plot of the plane $y=0$. Note the fuel meat in each FA plate that is split into 15 axial burnup zones, each with its own material definition. (courtesy of Soreq, Israel)

X-2.3.2. Necsa (South Africa) model

Homogenization calculations for all reflector elements were performed using a modified version of core 88 (depicted in Fig. X-4). This was mostly to capture the correct spectrum, as all positions in the core were modelled as loadable, that is, a typical mixture for each component or irradiation device was taken from this calculation, but these components were still allowed to move to any position in the core. The positions at which these mixtures were extracted is shown in Fig. X-4 for the various elements. For example, mixtures for the graphite element were taken from core position 9F (marked G), and empty irradiation sites from position 2D (marked E). Only the reflector region outside the core grid (rows S1, N1, N2 and columns W2, W1, E1, E2 in Fig. X-4) had position dependent cross-sections frozen from this calculation.

State and burnup dependent cross-sections for fuelled components were generated with the Serpent 2 software, in an infinite lattice for the standard fuel assembly, and a colourset surrounded by fuel for the control assemblies. No impurities were taken in the fuel.

For the exposure mesh, the active parts of the assemblies were divided into 10 equal segments. The depletion was performed with the nodal diffusion solver MGRAC.

All 164 core layouts in the irradiation period were modelled explicitly. To account for xenon, a downtime of 5 days was assumed between cores, and the irradiation period for each core layout was divided into a number of sub steps. These steps were chosen to capture the xenon buildup in the core at 5 MW, with a few smaller steps in the beginning, and larger steps once equilibrium xenon was achieved. A constant power of 5 MW was used in every sub step.

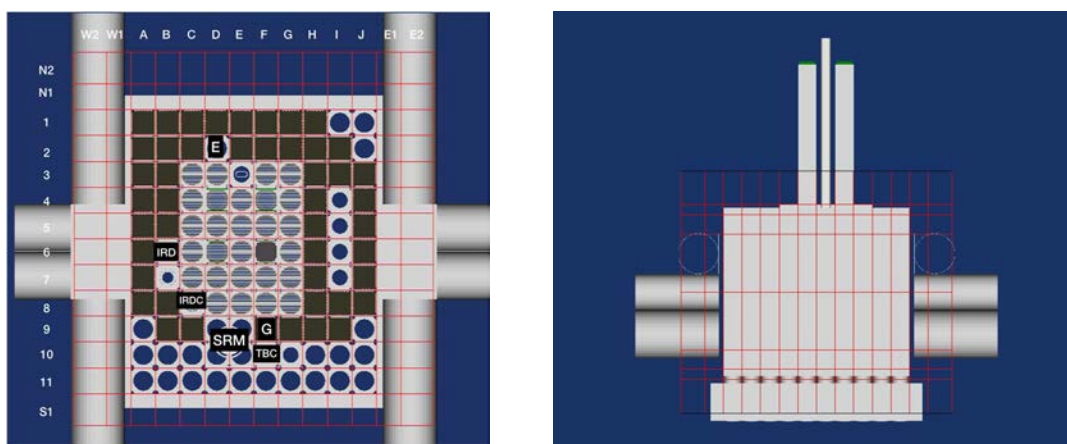


FIG. X-4. Schematic view of IRR-1 core model (OSCAR-5 - COMPOSE) used in the Necsa calculation, including control rods and the irradiation channels in the periphery. (courtesy of Necsa, South Africa)

X-3. RESULTS

X-3.1. Summary of the results of the benchmark

In Fig. X-5, the combined results from Soreq and Necsa are shown for the calculated reactivity at the critical conditions measured during IRR-1 history. All the values are given also in Table X-3. Note that two critical condition calculations from the Necsa group (for cores layouts #130 and #155) that had exceptional values for k_{eff} (not shown here) were checked and found to be due to mistakes in the benchmark itself in its earlier versions (which were corrected in more recent calculation) and therefore are ignored in this report.

In Fig. X-6, the axial distribution of the ^{235}U depletion in FAs F-18 and F-23 are plotted (experimental, from the data in Ref. [X-1], and the calculation of the two participants). One can see that there is a very good agreement between the measured values and the calculated values. The calculated values of depletion distribution of all the five FAs from the calculation of the two groups are presented in Tables X-4 and X-5.

Figure X-7 shows a comparison between the measured remaining mass of ^{235}U in the five FAs that were measured for the benchmark and the calculated values by the two participants. In addition, the comparison (between the measurement and Soreq calculations) for the other four FAs that started burning before 1985 is also shown. Comparison between depletion measurements and calculations on these FAs (columns F-2, F-5, F-6 and F-45 in Fig. X-7) serves as an indication of the precision of the benchmark's initial condition that was taken for Core 1, in 1985. The estimation for the initial condition in 1985 was taken from 2-D diffusion calculations for the burnup until 1980 and 3-D MUTZAV burnup calculations of the cores with mixed fuel during the period 1980–1985, according to logbook data. Sensitivity checks to the details of the 2-D and 3-D burnup indicated that the estimated random error can be up to 5% in the burnup per FA in Core 1. In addition to the total depletion shown in Fig. X-7, the calculation results for these FAs depletion distribution are given in Table X-6. One can check that the calculated distributions of the depletion in these FAs along the z axis also match the measured values very well.

The total amount of ^{235}U per FA was deduced from calculating its average depletion from Tables X-A2–X-A4, and using the initial ^{235}U mass for each FA, that appears in the benchmark specification [X-1].

Finally, Fig. X-8 shows the comparison of the total ^{137}Cs activity per FA between measurement and Soreq calculation, for the 5 FAs that were measured for the benchmark. The calculated values and their deviation from the measured values are presented in Table X-7.

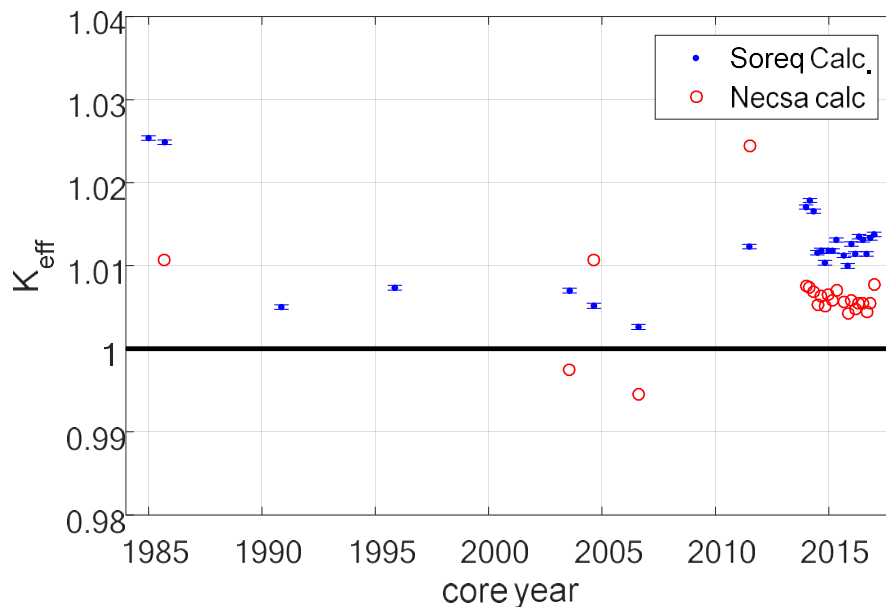


FIG. X-5. Results of the calculation of k_{eff} in critical conditions that was measured during IRR-1 irradiation history. (courtesy of Soreq, Israel)

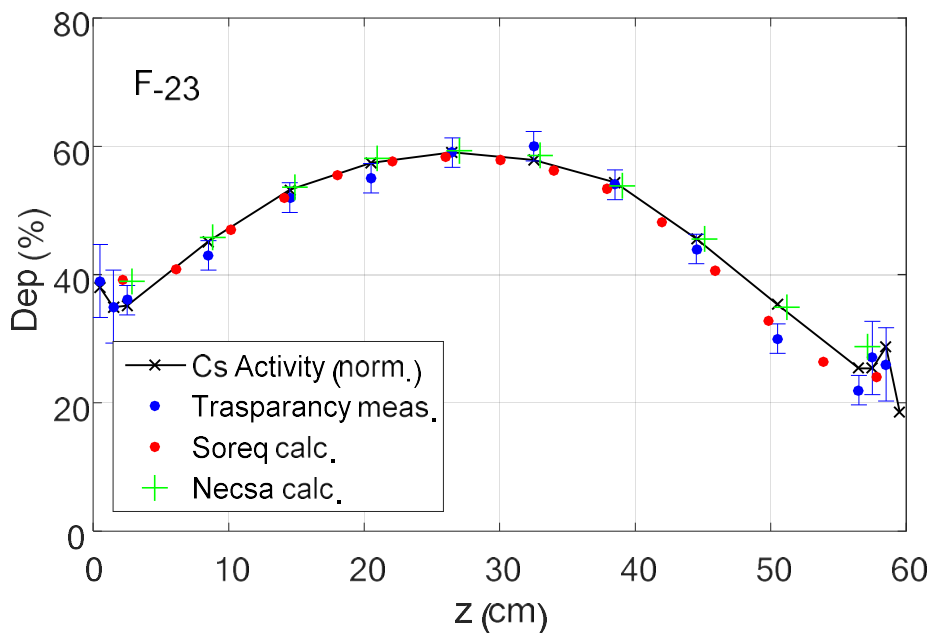
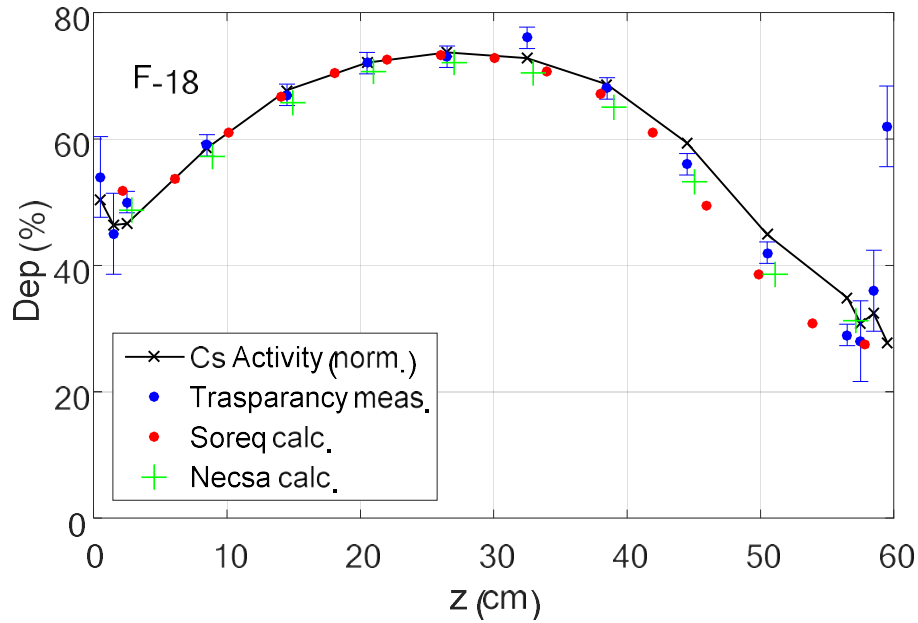


FIG. X-6. ^{235}U depletion distribution in fuel assemblies F-18 (upper) and F-23 (lower) at the EOC of core 164 (2017): Two measurement (transparency to Gamma and ^{137}Cs activity, where the ^{137}Cs activity values are normalized by a factor to match the same average depletion), and Soreq and Necsa calculation results. The relatively higher uncertainties in the transparency data points near the edges originate from statistics (in order to identify the edges, more measured points were taken with shorter measurement duration). (courtesy of Soreq, Israel)

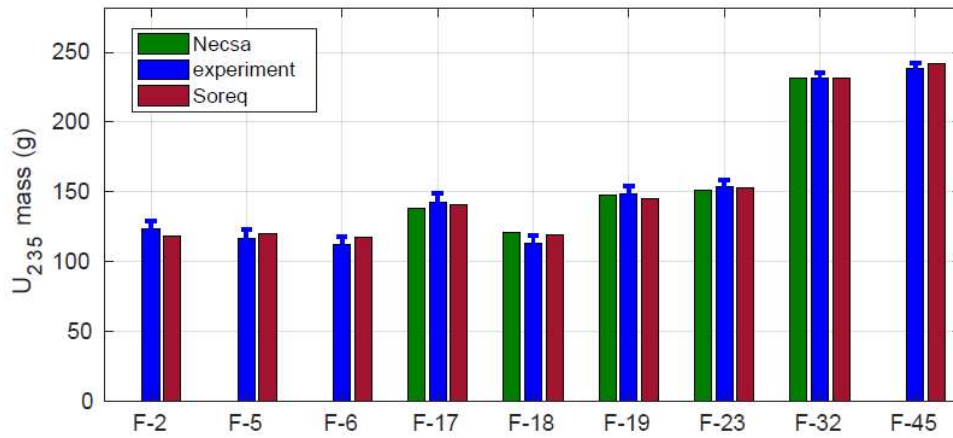


FIG. X-7. Total amount of ^{235}U in the fuel assemblies in EOC of core 164 (in 2017). F-17, F-18, F-19, F-23 and F-32 started burning in 1985 or afterwards, and were measured for the benchmark. (courtesy of Soreq, Israel)

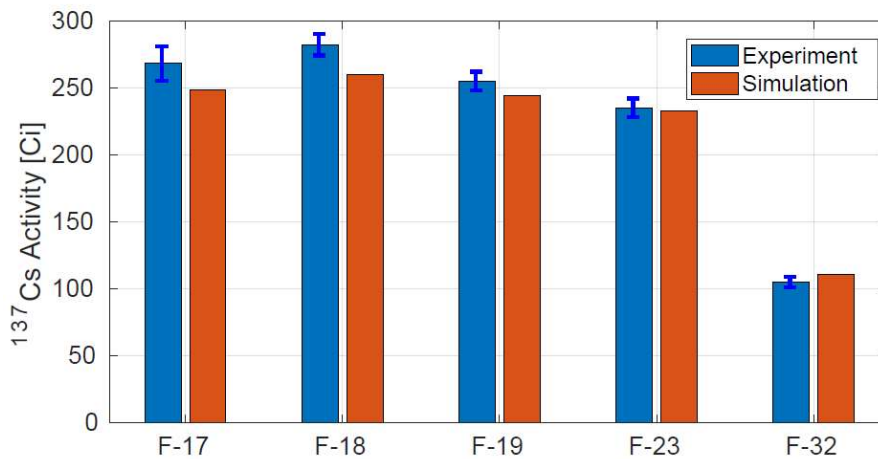


FIG. X-8. ^{137}Cs activity in fuel assemblies, comparison between the values from the Soreq simulation and the measured values. (courtesy of Soreq, Israel)

TABLE X-3. CALCULATED EFFECTIVE NEUTRON MULTIPLICATION FACTOR IN CRITICAL CONFIGURATIONS DURING IRR-1 HISTORY

Core No.	Year	k_{eff} Soreq	k_{eff} NeCSA
1	1986	1.02538	–
2	1987	1.02488	1.01066
13	1992	1.00503	–
42	1996	1.00735	–
86	2002	1.00700	0.99742
92	2003	1.00518	1.01072
103	2006	1.00263	0.99457
130	2011	1.01230	–
146	2013	1.01707	1.00701
147	2014	1.01785	1.00891
148	2014	1.01656	1.01433
149	2014	1.01157	1.0109
150	2014	1.01180	1.00454
151	2015	1.01036	1.00512
152	2015	1.01180	1.00157
153	2015	1.01179	1.00611
154	2015	1.01311	1.00294
156	2015	1.01124	0.99909
157	2015	1.00999	1.00598
158	2015	1.01262	1.00386
159	2016	1.01142	1.00552
160	2016	1.01349	0.99232
161	2016	1.01312	1.00539
162	2017	1.01141	1.00245
163	2017	1.01336	1.0027
164	2017	1.01378	1.010627

TABLE X-4. CALCULATED AXIAL DEPLETION DISTRIBUTION IN THE FIVE BENCHMARK FUEL ASSEMBLIES AT CORE 164 END OF CYCLE (NECSA CALCULATION)

Position* (cm)	F-17 Depletion (%)	F-18 Depletion (%)	F-19 Depletion (%)	F-23 Depletion (%)	F-32 Depletion (%)
3.02	41.6	48.7	39.0	37.0	12.9
9.06	47.9	57.2	45.8	43.9	15.4
15.10	55.6	65.8	53.5	51.5	18.6
21.14	60.3	70.6	58.0	56.0	20.8
27.18	62.1	72.0	59.4	57.6	21.8
33.22	61.2	70.5	58.5	56.7	21.9
39.26	57.5	65.1	53.8	52.3	20.6
45.30	50.4	53.3	45.5	44.4	18.1
51.34	40.5	38.7	35.0	34.2	14.4
57.38	33.7	31.2	28.7	27.5	11.4
Total**	51.1 (+1.4)	57.3 (–2.6)	47.7 (+0.4)	46.1 (+0.8)	17.6 (0)

* The middle of the burnup zones.

** The numbers in brackets are the absolute deviation from the measured values of the total depletion in each FA that appears in Ref. [X-1].

TABLE X-5. CALCULATED AXIAL DEPLETION DISTRIBUTION IN THE FIVE BENCHMARK FUEL ASSEMBLIES AT CORE 164 END OF CYCLE (SOREQ CALCULATION)

Position (cm)	F-17 Depletion (%)	F-18 Depletion (%)	F-19 Depletion (%)	F-23 Depletion (%)	F-32 Depletion (%)
-27.84	29.4	27.5	25.5	24.0	9.6
-23.86	31.6	30.7	28.2	26.5	10.4
-19.88	37.9	38.5	34.7	32.8	12.8
-15.91	45.3	49.5	43.1	40.6	15.9
-11.93	52.3	60.9	51.3	48.2	19.0
-7.95	57.2	67.1	56.3	53.3	21.1
-3.98	60.2	70.7	59.4	56.3	22.4
0.00	61.8	72.7	61.1	57.9	23.1
3.98	62.2	73.3	61.7	58.4	23.3
7.95	61.3	72.5	60.8	57.6	22.8
11.93	59.1	70.4	58.6	55.5	21.8
15.91	55.5	66.6	55.1	52.0	20.1
19.88	50.4	60.9	49.9	46.9	17.9
23.86	44.1	53.7	43.6	40.8	15.2
27.84	42.9	51.7	41.6	39.2	14.6
Total**	50.1 (+0.4)	57.8 (-2.1)	48.7 (+1.4)	46.0 (+0.7)	18.0 (+0.4)

* The middle of the burnup zones.

** The numbers in brackets are the absolute deviation from the measured values of the total depletion in each FA that appears in Ref. [X-1].

TABLE X-6. CALCULATED AXIAL DEPLETION DISTRIBUTION IN THE FOUR FUEL ASSEMBLIES THAT BEGAN BURNING BEFORE 1985, AT CORE 164 END OF CYCLE (SOREQ CALCULATION)

Position* (cm)	F-2 Depletion (%)	F-5 Depletion (%)	F-6 Depletion (%)	F-45 Depletion (%)
-27.84	34.5	31.6	33.7	9.3
-23.86	36.4	34.2	36.3	9.5
-19.88	43.8	42.1	44.0	11.5
-15.91	52.7	51.4	53.0	13.5
-11.93	61.1	60.1	61.2	15.3
-7.95	66.3	65.7	66.5	16.6
-3.98	69.4	69.1	69.9	17.4
0.00	71.1	71.0	71.8	17.8
3.98	71.4	71.6	72.2	17.7
7.95	70.3	70.7	71.4	17.2
11.93	67.9	68.5	69.2	16.3
15.91	63.9	64.7	65.2	14.9
19.88	57.9	59.0	59.7	13.1
23.86	51.0	52.0	52.6	11.1
27.84	49.3	50.2	51.0	10.9
Total**	57.8 (+1.8)	57.5 (-1.2)	58.5 (-1.9)	14.1 (-1.1)

* The middle of the burnup zones.

** The numbers in brackets are the absolute deviation from the measured values of the total depletion in each FA that appears in Ref. [X-1].

TABLE X-7. CALCULATED TOTAL ^{137}Cs ACTIVITY IN THE FIVE BENCHMARK FUEL ASSEMBLIES AT CORE 164 END OF CYCLE (SOREQ CALCULATION)

	F-17	F-18	F-19	F-23	F-32
Cs-137 Activity	9213 GBq (249 Ci)	9620 GBq (260 Ci)	9028 GBq (244 Ci)	8584 GBq (232 Ci)	4070 GBq (110 Ci)
Deviation from measurements	-19 (-7%)	-22 (-8%)	-11 (-4%)	-3 (-1%)	5 (+5%)

X-3.2. Discussion of the consolidated results

Overall, the results show a good agreement between the experimental data and the results of the simulations, as well as among the different codes and users. In the following paragraphs, the comparison of each of the measured quantities is examined in detail.

For the depletion distribution and the total ^{235}U per FA (Figs X-6 and X-7), all the codes predict values consistent within the measurement uncertainty, for all the FAs. This is not trivial, because one can note that the depletion distribution is sensitive to some core parameters which have large variance or uncertainty; in particular, the presence of control rods inside the core during the burnup causes a pronounced up-down asymmetry in the axial distribution near the FA edges (shown in Fig. X-6). Thus, a relative difference of 15–25% in the depletion is observed experimentally between the two opposite edges of the FAs. This measured effect is manifested by the results of the two codes as well. One can even see differences in the asymmetry between Soreq and Necsa calculations (in particular in the distributions in F-23), probably because of the different control rod heights during burnup in the two calculations. However, these differences are not bigger than the measurement uncertainty.

At the very edges of the FAs, there seems to be a rise in the depletion. There can be several reasons for this observation. It might be an artefact due to a finite region edge of the meat in which the ^{235}U decreases continuously. However, it is also possible that it is a real depletion effect, which is due to the existence of the water above and underneath reflecting back the neutrons toward the fuel and overdepleting the edges. It seems that the codes tend to underestimate this effect, or smear it axially. The overdepletion might be underestimated in the simulations due to averaging of the thermal flux over the upper and lower burnup zones which are too large. A comparison of the two experimental results (transparency measurement and ^{137}Cs activity at the edges) shows that sometimes the ^{235}U content decreases while the ^{137}Cs activity increases (e.g. in the edge of F-23 in Fig. X-6), indicating an overdepletion due to the vicinity of the water.

The reactivity predictions (Fig. X-5) show discrepancies between the two codes, with the Soreq code usually overestimating the core reactivity relative to the Necsa simulations, and relative to the measured $k = 1$ value. The spread of the k values calculated by the Soreq group seems to be around $\frac{\Delta k}{k} < 1500$ pcm for most critical cases. The spread of the values calculated by the Necsa group is somewhat smaller – around 1000 pcm.

There is an overestimation of k_{eff} in the first two cores in the history (1986, 1987) that seems to be slightly larger than in the rest of the critical configurations. It may indicate an inaccuracy in the initial condition of the depletion distribution in 1985. In light of the comparative results of the depletion in Fig. X-7, the uncertainties in the benchmark's initial conditions were considered in more detail. Note that the depletion of the four FAs that burned substantially

before 1985 also agreed with the calculation, up to the experimental uncertainty. This may serve as another indication that the estimation of their depletion distribution in 1985 was sufficiently precise.

For the Soreq calculations, the influence of several parameters present in the model on the criticality and on the ^{235}U depletion was investigated. The results are shown in Table X–8. The check numbers in the left column of Table X–8 represent the following:

- Check #1: Changing the number of burnup zones from 15 to 5.
- Check #2: Changing the total power (MWh) by 3% for all cycles. Thereby, checking for a constant bias in all 164 cores, in the power measurement.
- Check #3: Changing the initial condition in Core 1 by +5% burnup (being the maximal possible error, see the above paragraph).
- Check #4: Compare nuclear data and code version. Here, MUTZAV was compared with ENDF/B VII to MCNP6.1 with ENDF/B VIII in a k_{eff} calculation of burnup of a FA in an infinite lattice.
- Check #5: Assess the reactivity variance resulting from the existence of certain impurities (^6Li and ^{10}B) due to manufacturing tolerances.

TABLE X–8. SENSITIVITY CHECKS OF k_{eff} AND OF THE TOTAL DEPLETION PER FUEL ASSEMBLY TO VARIATIONS IN THE CALCULATION MODEL

Check # (see text)	Change in reactivity (pcm)	Change in depletion
1	± 200	<1%
2	± 900	<1%
3	± 200	2%
4	± 400	–
5	+700	–

The comparison between the calculations of ^{137}Cs activity and the experimental results shows that, while agreement is still fairly good, there are relatively larger deviations that can reach up to 8%, e.g. for F-18. This relatively larger deviation may originate from inaccurate conversion of the surface activity to the total activity of ^{137}Cs , which depends strongly on the experimental calibrations, and in particular on the estimation of the exact active area of the plates of each of the FA, which depends in the definition of the meat edges and so involves additional work. Another possible source of error is a gradient in the burnup in the y direction: While the gamma transparency method is insensitive to such a gradient, for the ^{137}Cs activity measurement the gamma rays emitted from the last plates are less likely to reach the detector compared to the gamma rays emitted from the plates that are near the collimator. This is due to absorption by other plates. Therefore, the ^{137}Cs activity measurement is sensitive to the burnup gradient between the plates, and not just to the total burnup.

X–3.3. Conclusions

Overall, there is a good agreement between calculations and experimental results. For the criticality measurements, the agreement is usually up to ~1500 pcm, and for the depletion measurement the agreement is within the measurement uncertainty (~3%). For the ^{137}Cs activity, the deviations between the experimental and calculation results are somewhat bigger

(up to 8%). As discussed above, a possible conclusion is that the measurement of absolute ^{137}Cs activity for MTR spent FAs is harder to calibrate (to translate from net count rate to activity), while the depletion measurement that was via the measurement of transparency to gamma rays from the external source suffered less from this technical issue.

The axial distribution of depletion in the FA was found to be asymmetric. This feature can be explained by the presence of control rods in the upper side, ‘pushing’ the power to the lower side of the core.

Sensitivity checks on the Soreq simulations demonstrated that the depletion distribution is less sensitive to changes in the model (compared with the measurement uncertainty), than criticality calculations. Thus, one cannot use them to validate the very fine details of the model, such as impurities content, or small errors in the measured power. Calculations of k_{eff} at measured critical conditions are more sensitive and can detect those inaccuracies in the models relative to the real core.

REFERENCES TO ANNEX X

- [X-1] INTERNATIONAL ATOMIC ENERGY AGENCY, Research Reactor Benchmarking Database: Facility Specification and Experimental Data, Technical Reports Series No. 480 (Rev. 1), IAEA, Vienna (in preparation).
- [X-2] KRAKOVICH, A., AVIV, O., DANON, L., BEN-MEIR, K., YUNGRAIS, Z., HALFON, S., HAZENSHPRUNG, N., NEDER, I., Depletion measurements using a new gamma transparency method of irradiated MTR-type fuel assemblies, Nucl. Instrum. Methods Phys. Res., Sect. A **903** (2018) 224–233.
- [X-3] KRAKOVICH, A., NEDER, I., STEINITZ, U., HAZENSHPRUNG, N., Whole-Core Monte-Carlo Simulations and Experimental Measurements of IRR1 Fuel Depletion During More Than Thirty Years of Operation, Proc. PHYSOR 2018, 22–26 April 2018, Cancun, Mexico (2018).
- [X-4] INTERNATIONAL ATOMIC ENERGY AGENCY, Thermophysical Properties of Materials for Water Cooled Reactors, IAEA-TECDOC-949, IAEA, Vienna (1997).

ANNEX XI

BENCHMARK CONSOLIDATED RESULTS AGAINST EXPERIMENTAL DATA FROM JSI-1

XI-1. INTRODUCTION

The JSI-1 benchmark analysis, including the reactor specification and experimental data, is documented in Ref. [XI-1]. This benchmark is related to an activation rate case from the Jožef Stefan Institute (JSI) TRIGA Mark II reactor. The experimental activation measurements were performed in the reactor core during several experimental campaigns, aimed at the validation of computational models of the reactor developed at the JSI, to obtain experimental measurements to support neutron spectrum adjustment and perform measurements of nuclear constants relevant for the k_0 standardization of neutron activation analysis. Measurements were performed in different irradiation locations in the core of the JSI TRIGA Mark II reactor. Irradiations of bare samples, as well as cadmium and boron nitride covered samples were performed. The benchmark is based on computational contributions from the JSI (Slovenia) and INVAP (Argentina).

XI-1.1. Description of the JSI TRIGA Mark II reactor

The JSI TRIGA Mark II reactor [XI-2 – XI-4] is a 250 kW light water reactor with an annular graphite reflector cooled by natural convection. The reactor was built in the period from 1962 to 1966, and first criticality was achieved on 31 May 1966. The JSI-1 benchmark analysis, including the reactor description and specification, is documented in Ref. [XI-1]. Figure XI-1 displays the JSI-TRIGA Mark II reactor. Figure XI-2 displays the JSI TRIGA reactor core configuration with the measurement positions (MPs) indicated. Figure XI-3 displays a schematic view of the reactor core and reflector, including the horizontal irradiation channels.

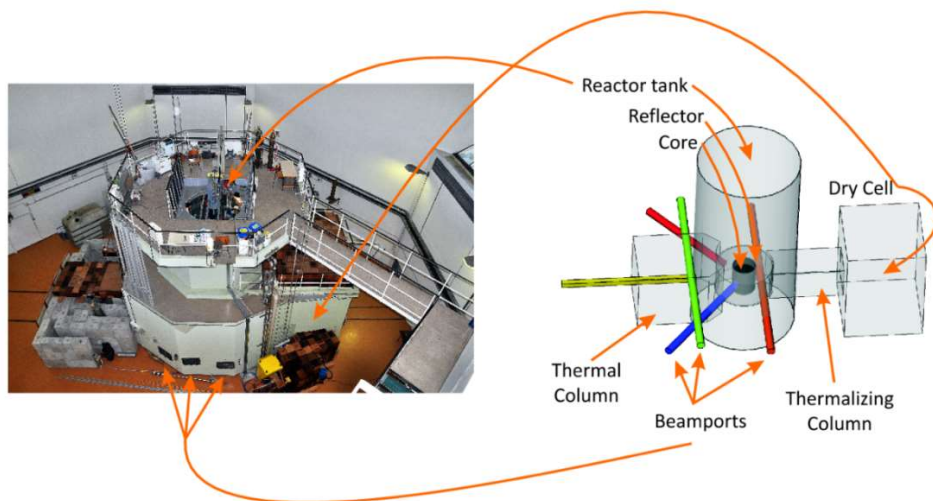


FIG. XI-1. Left: photograph of the reactor, right: schematic view of the main components. (courtesy of JSI, Slovenia)

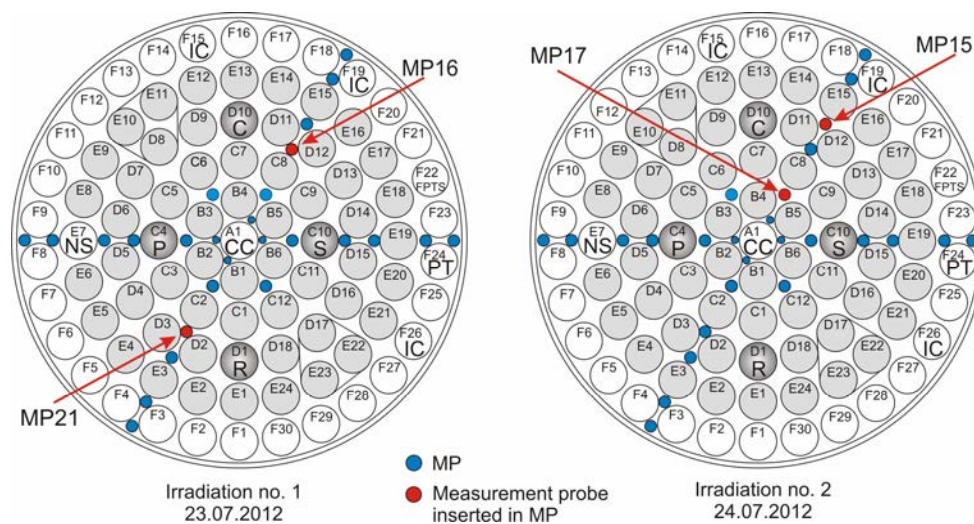


FIG. XI-2. JSI TRIGA Mark II reactor core configuration with the measurement positions (MPs) indicated (blue and red circles). The MPs used in the experiments are indicated as red circles. (courtesy of JSI, Slovenia)

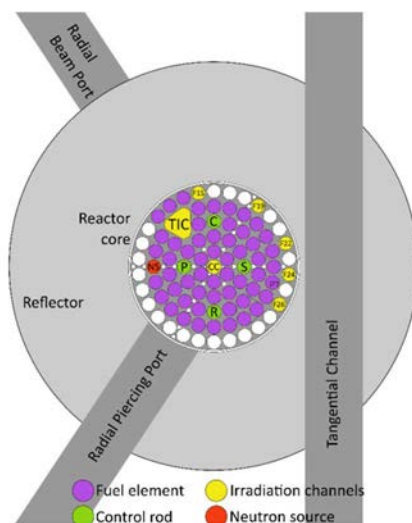


FIG. XI-3. Schematic of the JSI TRIGA reactor core, reflector and horizontal irradiation channels. (courtesy of JSI, Slovenia)

XI-2. SUMMARY OF THE BENCHMARK SPECIFICATION AND CODES AND MODELS USED

Descriptions and objectives of the experimental campaigns, from which the experimental data originate, are given in Ref. [XI-1].

XI-2.1. Experimental data format and sources of uncertainty

The experimental data provided to the CRP were formatted as necessary for processing with the SPCACT code, written by Andrej Trkov. The code calculates the specific saturation activities for the measured nuclear reactions from the following data: the sample masses and mass fractions of the target isotopes; the irradiation, cooling and measurement times; the measured peak areas for specific gamma ray energies; the detection efficiencies at the specific gamma ray energies; and the coincidence correction factors. The SPCACT code computes the uncertainties in the specific saturation activities from the uncertainties in the input data, by sequentially perturbing the values of the input data by their respective uncertainties and taking the square root of the sum of the squares of the differences between the values computed with the perturbed and the unperturbed input data. The uncertainties in the calculated activities are combined from the uncertainties in the following input quantities: the peak areas; the irradiation, cooling and measurement times; the sample masses; and the detection efficiency. The predominant source of uncertainty in the measurements is typically the uncertainty in the detection efficiency. Two data sections correspond to each set of measurements. The first section consists of the raw experimental data, and the second section lists the calculated saturation activities per target atom.

The peak fitting in the recorded gamma-ray spectra was performed using the Hyperlab2005 gamma spectrum analysis program [XI-5]; the detection efficiencies and the coincidence correction factors were obtained using the k_0 -IAEA neutron activation analysis program [XI-6].

Additionally, the experimental data initially provided were compiled into an Excel table, which was also provided to the CRP. A breakdown of the total uncertainty in the experimental data into specific contributions due to the uncertainties in the input quantities data was provided.

XI-2.2. Summary of the codes used

The benchmark contributors, number of methodologies, codes and nuclear data libraries used to analyse the JSI-1 benchmarks are presented in Table XI-1.

TABLE XI-1. METHODOLOGIES EMPLOYED IN THE BENCHMARK ANALYSES

Benchmark contributors	Number of methodologies	Codes (library) used
Argentina	1	MCNP5, FISPACT-II (ENDF/B-VII.2, TENDL-2014)
Slovenia	1	MCNP6 (ENDF/B-VII.1)

XI-2.3. Summary of the models used

XI-2.3.1. JSI – Slovenia

Calculations of the reaction rates were performed with the particle transport code MCNP6 [XI-7] and a computational model of the JSI TRIGA Mark II reactor based on the criticality benchmark model featured in the ICSBEP library [XI-8], existing since the 1990s. Through constant use, the computational model has been significantly upgraded and refined, and validated for the calculation of k_{eff} , reactor kinetic parameters [XI-9] and neutron flux, reaction rate and dose rate distributions [XI-10, XI-11 – XI-14]. The ENDF/B-VII.1 nuclear data library [XI-15] was employed for the particle transport calculations. Reaction rates were calculated using cross-section data from the ENDF/B-VII.1 library.

Calculations were performed in criticality mode. The raw calculated results were normalized with respect to the reactor power level during the irradiations with the following expression [XI-14]:

$$R_{abs} = R_{calc} \frac{P \nu}{w k_{eff}} \quad (XI-1)$$

where R_{abs} is the absolute value of a reaction rate, R_{calc} is the calculation result, P is the reactor power level, ν is the average number of neutrons emitted per fission, w is the average recoverable energy per fission, and k_{eff} is the calculated effective neutron multiplication factor.

Additionally, due to uneven control rod insertion levels, which cause a neutron flux redistribution effect, a correction factor is applied to the measured power level [XI-16]:

$$\frac{S_{corrected}}{S_{nominal}} = \frac{1}{\prod_i [1 - (1 - f_i) g_i(l)]}; \quad f_i = \frac{\phi_i}{\phi_0} \quad (XI-2)$$

Where S denotes the measured neutron flux signal used for the monitoring of the reactor power, f_i is the flux depression factor, defined as the ratio between the neutron flux at the detector location at full insertion of control rod i (ϕ_i) and the flux with all control rods completely withdrawn (ϕ_0), and $g_i(l)$ is the interpolation function between the fully withdrawn ($g_i(l = l_{min}) = 0$) and the fully inserted ($g_i(l = l_{max}) = 1$) control rod position, l being the insertion depth. The depth l is equal to the length of the fuel region in the fuel elements, i.e. 38.1 cm (15 inches).

For the experimental campaigns conducted in the CC, PT and IC40 irradiation channels, samples and filters were modelled explicitly. As the sample dimensions were relatively small (the typical dimensions of the irradiated foils being 5 mm in diameter and 0.1–0.2 mm in thickness), computationally intensive calculations were performed, aimed at achieving acceptable statistical uncertainties in the calculated results. The simulations were run with 1.5×10^9 neutron histories. In general, the statistical uncertainties for the calculated reaction rates are between a few % and 10%; however, in some cases, in particular for threshold reactions and samples under filters, the statistical uncertainties are greater than 15%. Figures XI-4 to XI-6 display plots of the JSI TRIGA Mark II computational model (core and irradiation channels, polyethylene rabbits, neutron filters and samples).

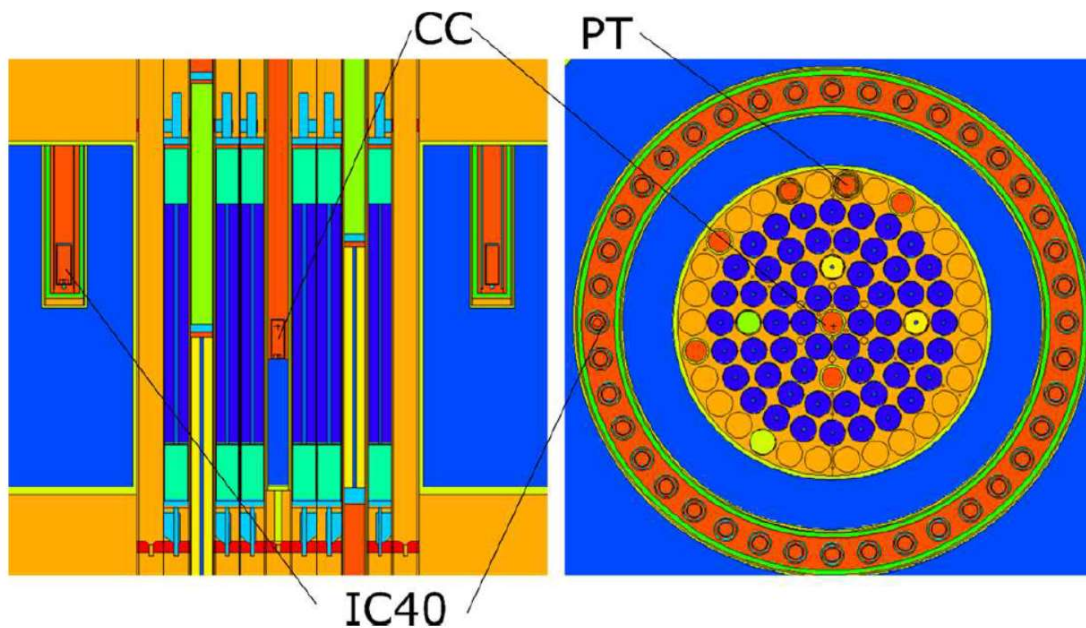


FIG. XI-4. Computational model of the JSI TRIGA Mark II reactor in MCNP. Left: side view, right: top view. (courtesy of JSI, Slovenia)

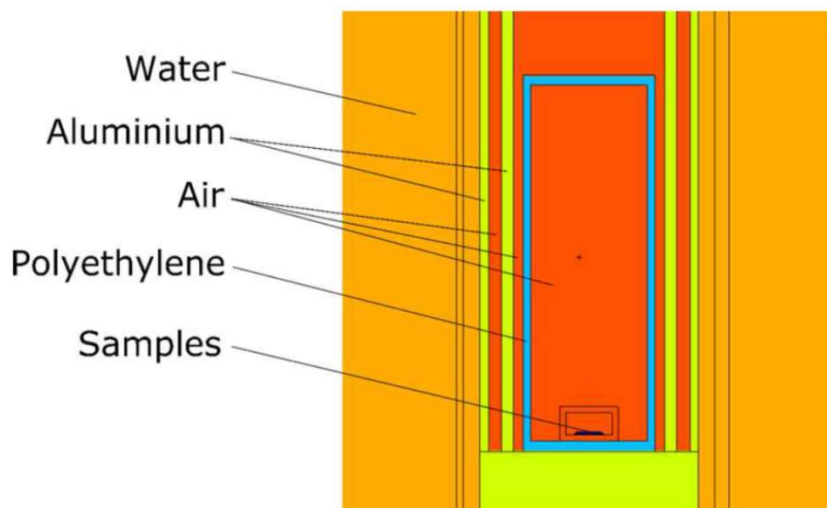


FIG. XI-5. Model of a polyethylene rabbit inserted into an irradiation channel in the reactor core in the MCNP computational model. (courtesy of JSI, Slovenia)

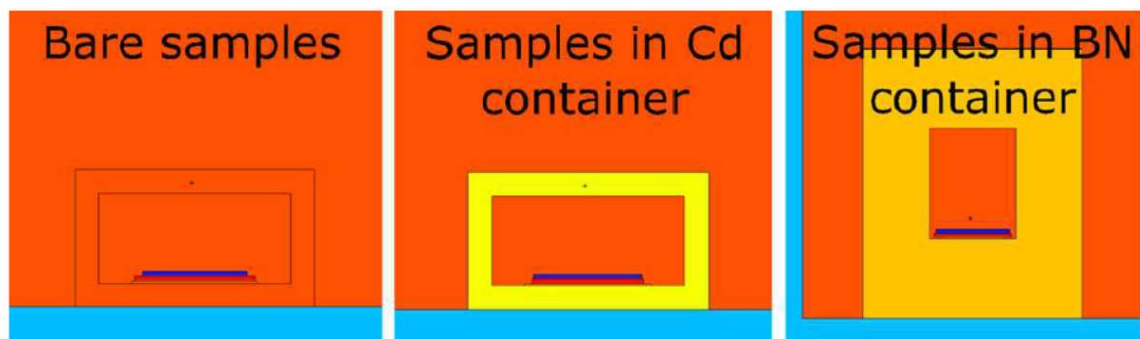


FIG. XI-6. Neutron filters and samples modelled explicitly in the MCNP computational model. The sample diameter is around 5 mm. (courtesy of JSI, Slovenia)

For the experimental campaign conducted in the core positions, in which the axial profiles of the $^{197}\text{Au}(n,\gamma)$ reaction rates were measured, the reaction rates were calculated in sections of the aluminium probes, which were used to introduce the samples in wire form along the depth of the measurement locations.

MCNP computational models of the JSI TRIGA Mark II reactor including the irradiated filters and samples were compiled and made available to the CRP [XI-1]. Additionally, calculated neutron spectra in standard SAND-II 640 energy group structure, corresponding to the irradiations in the CC, PT and IC40 irradiation channels were compiled and made available to the CRP [XI-1].

XI-2.3.2. INVAP – Argentina

The JSI benchmark case received partial coverage in the framework of the CRP by the Argentinian counterpart INVAP [XI-1], who performed calculations of the reaction rates in the CC, PT and IC40 irradiation channels using the FISPACT-II [XI-17] activation code in conjunction with the ENDF/B-VII.1 [XI-15] and TENDL-2014 [XI-18] nuclear data libraries. The reaction rate calculations were performed on the basis of the provided calculated neutron spectra [XI-1].

XI-3. RESULTS

XI-3.1. Results of the individual participant contributions

This section presents the comparison between the experimental results and the results obtained through calculations by JSI and INVAP. In the comparison, in numerous instances, multiple experimental values are presented for one nuclear reaction measured for one particular irradiated sample. The values were derived from multiple measured photopeaks at different gamma ray energies. Table XI-2 lists the gamma ray energies used in the derivation of the reaction rates for the measured nuclear reactions.

TABLE XI-2. PRODUCT AND DECAYING NUCLIDES AND MEASURED GAMMA RAY ENERGIES USED FOR THE DERIVATION OF THE EXPERIMENTAL RESULTS

Nuclear reaction	Product nuclide	Decaying nuclide	Measured gamma ray energies [keV]
Al-27(n, α)	Na-23	Na-23	1368.6
Al-27(n, γ)	Al-28	Al-28	1778.9
Al-27(n,p)	Mg-27	Mg-27	843.8, 1014.4
Au-197(n, γ)	Au-198	Au-198	411.8
Co-59(n, γ)	Co-60	Co-60	1173.2, 1332.5
Fe-58(n, γ)	Fe-59	Fe-59	142.7, 192.3, 334.8, 1099.3, 1291.6
Fe-54(n,p)	Mn-54	Mn-54	834.8
Mn-55(n, γ)	Mn-56	Mn-56	846.8, 1810.7, 2113.1
Sc-45(n, γ)	Sc-46	Sc-46	889.3, 1120.5
Sn-117(n,n')	Sn-117m	Sn-117m	156.0, 158.5
Th-232(n, γ)	Th-233	Pa-233	86.8, 94.7, 98.4, 103.9, 300.1, 311.9, 340.5, 375.4, 398.5, 415.8
U-238(n, γ)	U-239	Np-239	103.7, 106.1, 209.8, 226.4, 228.2, 277.6, 285.8, 315.9, 334.2

The comparison for the different irradiations are given in Tables XI-3–XI-A12. Columns 1, 2 and 3 in the tables state the sample ID numbers, the sample material composition and the

measured reaction rate, respectively. Columns 4 and 5 report the measured reaction rates in units of reactions per second, per target atom and the associated uncertainties ($1-\sigma$) in %. Columns 6, 7 and 8 report the JSI calculated reaction rates nuclear data library (in units of reactions per second, per target atom), the associated uncertainties ($1-\sigma$, statistical) in % and the relative differences between the experimental and calculated values in %, respectively. Columns 9 and 10 and columns 11 and 12 report the INVAP calculated reaction rates (in units of reactions per second, per target atom) and the relative differences between the experimental and calculated values (in %), obtained using the TENDL-2014 and the ENDF/B-VII.1 nuclear data libraries, respectively. Tables XI-9 to XI-A12 include only JSI calculation data.

The uncertainties associated with the JSI calculated values are statistical only. In the comparison between the experimental values and the calculated values, the uncertainty in the reactor power level, affecting the uncertainty in the normalization factor used to derive actual reaction rate values from the raw calculated data (Eq. (XI-1)), needs to be taken into account as an additional source of uncertainty. Based on previous work [XI-10], the uncertainty in the reactor power level is estimated at 5%.

XI-3.2. Comparison and discussion of the individual results

This section provides comments on the comparison of the experimental values and the calculated results for the different experiments. The level of agreement is assessed on the basis of the uncertainties in the experimental and calculated values.

XI-3.2.1. PT irradiation channel

XI-3.2.1.1. Irradiation of Al-0.1%Au, Al-0.2%U and Al-1%Mn samples

- U-238(n, γ): A consistent 20–50% relative difference between the measured and JSI calculated values for bare, Cd and BN filtered samples is observed. The observed discrepancy is in part due to inaccurately known U content in the sample material. The JSI and INVAP calculated results are consistent.
- Au-197(n, γ): Agreement between experimental and calculated values for bare and Cd cases (within 8%), disagreement for BN. Consistency between the JSI and INVAP calculated results, except for the BN case.
- Al-27(n, α): Agreement for bare and BN cases (within 12%), disagreement for Cd. Consistency in approximately half of the calculated values. ENDF/B-VII.1 values by INVAP are consistently lower than the ENDF/B-VII.1 values by JSI.
- Mn-55(n, γ): Agreement between experimental and JSI calculated values for bare case (within 6%), disagreement for the Cd and BN cases. Consistency between JSI and INVAP calculated values for the bare case, inconsistency for the Cd and BN cases. Good agreement between experimental and INVAP calculated values for the Cd and BN cases.

XI-3.2.1.2. Irradiation of Al-0.1%Au, Sn samples

- Sn-117(n, n'): A consistent 50% relative difference is observed between experimental and JSI calculated values, which was attributed to inaccurate cross-sections. Better agreement (relative differences of the order of 10%) is observed between the INVAP calculated values obtained with the TENDL-2014 nuclear data library.

- Au-197(n, γ): Agreement between experimental and JSI calculated values for the bare and BN cases (within 8%), disagreement for the Cd case. Agreement between experimental and INVAP calculated values for all cases (within 6%).
- Al-27(n, α): Agreement between experimental and JSI calculated values for the Cd case (within 1%), disagreement for the bare and BN cases. ENDF/B-VII.1 values by INVAP are consistently lower than the ENDF/B-VII.1 values by JSI. Agreement between experimental and calculated values using TENDL-2014 by INVAP (within 10%).

XI-3.2.1.3. Irradiation of Al-0.1%Au, Fe samples

- Fe-59(n, γ): General disagreement between experimental and calculated data, more pronounced for the Cd and BN cases.
- Au-197(n, γ): General good agreement between experimental and calculated data (within 9%).
- Al-27(n, α): Overall agreement between experimental and JSI calculated data within the uncertainties. ENDF/B-VII.1 values by INVAP are consistently lower than the ENDF/B-VII.1 values by JSI. Better consistency between experimental and calculated values using TENDL-2014 by INVAP.

XI-3.2.1.4. Irradiation of Al-0.1%Au, Al-0.1%Co, Al-2%Sc and Al-1%Th samples

- Co-59(n, γ): Agreement between experimental and JSI calculated values for the bare and Cd cases (within 9%), disagreement for the BN case. TENDL-2014 values by INVAP are consistently low, ENDF/B-VII.1 values by INVAP are consistent with the JSI calculated values, except for the BN case.
- Au-197(n, γ): General good agreement between experimental and calculated data (within 12%).
- Sc-45(n, γ): Agreement between experimental and JSI calculated values for the bare and BN cases (within 2%), disagreement for the Cd case. Agreement between experimental and INVAP calculated values with ENDF/B-VII.1 for the bare and BN cases (within 3%), disagreement for the Cd case. TENDL-2014 values are consistently in disagreement.
- Th-232(n, γ): Overall agreement between experimental and JSI calculated values for the Cd case (within 14%), disagreement for the bare and BN cases. Consistency between all calculated values.

XI-3.2.2. CC irradiation channel, irradiation of Al-0.1%Au samples

- Al-27(n, γ): Consistent disagreement between experimental and calculated values.
- Al-27(n,p): Agreement between experimental and JSI calculated values for the bare case (within 6%), disagreement for the Cd case. Agreement between experimental and INVAP calculated values (within 8%).
- Al-27(n, α): Agreement between experimental and JSI calculated values in all cases (within 11%). Agreement between experimental values and values obtained by INVAP using TENDL-2014 (within 6%). Values obtained using ENDF/B-VII.1 are systematically lower; one value appears to be an error (relative difference of 420%).
- Au-197(n, γ): Agreement between experimental and calculated data in all cases (within 6%).

XI-3.2.3. IC40 irradiation channel

- Al-27(n, γ): Consistent disagreement between experimental and calculated values.
- Al-27(n,p): Consistency between experimental and JSI calculated values; however, the uncertainties in the latter are up to 27%. Agreement between experimental and INVAP calculated values for the bare case (within 6%), relative differences of up to 14% for the Cd case.
- Al-27(n, α): Consistent disagreement between experimental and calculated values; large uncertainties in the JSI calculated values.
- Au-197(n, γ): Consistency between experimental and JSI calculated values; however, the uncertainties in the latter are large. Agreement within 6% between experimental and INVAP calculated values.

XI-3.2.4. Reactor core

- Au-197(n, γ): Overall agreement between experimental and JSI calculated data, within approximately 5% in the centre of the fuel region and mostly within 10% outside the fuel region.

XI-3.3. Conclusions

This Annex presents the JSI TRIGA activation benchmark case JSI-1. The benchmark case collects experimental reaction rate measurements and calculations from several experimental campaigns. Calculations of the reaction rates were performed by the JSI using the particle transport code MCNP6 in conjunction with the ENDF/B-VII.1 nuclear data library. The JSI TRIGA activation benchmark case received partial coverage from the Argentinian counterpart INVAP, who performed activation calculations using the FISPACT-II activation code in conjunction with the ENDF/B-VII.1 and TENDL-2014 nuclear data libraries.

The JSI TRIGA benchmark case is comprised of experimental datasets originating from several experimental campaigns performed at different times, in which different nuclear reaction rates with different energy sensitivities were measured. The comparison between the experimental and calculated reaction rates provides valuable feedback information, both on the representativeness of the computational model and the quality of the nuclear data. However, due to the numerous input physical quantities and possible sources of uncertainty or bias, a precise determination of the cause of observed discrepancies for certain reaction rates is not straightforward. For instance, biases in the material composition of irradiated samples (which are troublesome to identify) will significantly affect the computed reaction rate values and result in incorrect feedback information.

The JSI TRIGA benchmark provides clear indications of the nuclear data quality for certain nuclear reactions. For the Sn-117(n,n') reaction, a consistent 50% relative difference is observed between experimental and JSI calculated values using cross-section data from the ENDF/B-VII.1 nuclear data library, which was attributed to inaccurate cross-sections. Considerably better agreement with the experimental data, i.e. relative differences of the order of 10%, was observed for the INVAP calculated data using the TENDL-2014 nuclear data library. Consistent disagreement between the experimental and calculated values was observed for the Fe-58(n, γ) reaction, which was more pronounced for cadmium and boron nitride covered samples. Overall, good consistency was observed between the experimental and calculated Au-197(n, γ) reaction rates, especially for the experiments performed in the reactor core, this reaction being a standard dosimetry reaction. Systematic differences were observed between

experimental and calculated Al-27(n, γ) reaction rates, the calculated data being consistent, possibly indicating problems with the cross-section data. The experimental measurements of this reaction rate are challenging on account of the short product half-life of around 2.24 minutes. Limited consistency was observed between the experimental and calculated reaction rate values for the threshold reactions on aluminium (Al-27(n,p) and Al-27(n, α)), on which important conclusions are not possible. A systematic difference between the JSI and INVAP calculated Al-27(n, α) reaction rates using the ENDF/B-VII.1 nuclear data library was noted, the JSI data being more consistent with the experimental data. No clear explanation is evident. Limited consistency was observed for the other measured neutron capture reactions, which does not provide any clear indications.

TABLE XI-3. COMPARISON BETWEEN MEASURED AND CALCULATED REACTION RATES PER TARGET ATOM (RR) IN THE PT IRRADIATION CHANNEL

PT channel; Au, Mn, U		JSI Experimental data			JSI Calculated data (E71)			INVAP Calculated data (TENDL-2014)			INVAP Calculated data (E71)		
Sample ID	Sample description	Reaction	Meas. RR [s ⁻¹ / atom]	Unc [%]	Calc. RR [s ⁻¹ / atom]	Unc [%]	Diff [%]	Calc. RR [s ⁻¹ / atom]	Diff [%]	Calc. RR [s ⁻¹ / atom]	Diff [%]		
V023	Al-0.2%-U (bare)	Al-27(n, α)	7.92E-16	6.2	N/C	N/C	N/C	8.55E-16	8.0	5.16E-16	-34.8		
V023	Al-0.2%-U (bare)	U-238(n, γ)	3.38E-11	2.1		37.6			30.5		30.5		
V023	Al-0.2%-U (bare)	U-238(n, γ)	3.07E-11	2.1		51.4			43.7		43.7		
V023	Al-0.2%-U (bare)	U-238(n, γ)	2.92E-11	2.3		58.9			50.8		50.8		
V023	Al-0.2%-U (bare)	U-238(n, γ)	3.43E-11	6.8		35.4			28.5		28.5		
V023	Al-0.2%-U (bare)	U-238(n, γ)	3.42E-11	2.1	4.65E-11	12.1	36.0	4.41E-11	29.1	4.41E-11	29.1		
V023	Al-0.2%-U (bare)	U-238(n, γ)	3.00E-11	2.1		54.9			47.0		47.0		
V023	Al-0.2%-U (bare)	U-238(n, γ)	3.10E-11	3.6		50.0			42.4		42.4		
V023	Al-0.2%-U (bare)	U-238(n, γ)	2.99E-11	2.9		55.5			47.5		47.5		
V023	Al-0.2%-U (bare)	U-238(n, γ)	3.02E-11	2.6		54.1			46.2		46.2		

TABLE XI-3. COMPARISON BETWEEN MEASURED AND CALCULATED REACTION RATES PER TARGET ATOM (RR) IN THE PT IRRADIATION CHANNEL (cont.)

PT channel; Au, Mn, U		JSI Experimental data			JSI Calculated data (E71)			INVAP Calculated data (TENDL-2014)			INVAP Calculated data (E71)		
Sample ID	Sample description	Reaction	Meas. RR [s ⁻¹ / atom]	Unc [%]	Calc. RR [s ⁻¹ / atom]	Unc [%]	Diff [%]	Calc. RR [s ⁻¹ / atom]	Diff [%]	Calc. RR [s ⁻¹ / atom]	Diff [%]		
V024	Al-0.2%-U (Cd)	Al-27(n,α)	8.05E-16	2.1	N/C	N/C	N/C	7.95E-16	-1.2	4.81E-16	-40.2		
V024	Al-0.2%-U (Cd)	U-238(n,γ)	2.80E-11	2.0			26.7		27.4		27.4		
V024	Al-0.2%-U (Cd)	U-238(n,γ)	2.56E-11	2.0			38.8		39.6		39.6		
V024	Al-0.2%-U (Cd)	U-238(n,γ)	2.45E-11	2.1			44.6		45.5		45.5		
V024	Al-0.2%-U (Cd)	U-238(n,γ)	2.86E-11	4.8			24.1		24.9		24.9		
V024	Al-0.2%-U (Cd)	U-238(n,γ)	2.83E-11	2.0	3.55E-11	14.9	25.3	3.57E-11	26.1	3.57E-11	26.1		
V024	Al-0.2%-U (Cd)	U-238(n,γ)	2.51E-11	2.0			41.4		42.3		42.3		
V024	Al-0.2%-U (Cd)	U-238(n,γ)	2.61E-11	2.2			36.1		37.0		37.0		
V024	Al-0.2%-U (Cd)	U-238(n,γ)	2.60E-11	2.1			36.4		37.2		37.2		
V024	Al-0.2%-U (Cd)	U-238(n,γ)	2.53E-11	2.1			40.2		41.1		41.1		
V025	Al-0.2%-U (BN)	Al-27(n,α)	8.26E-16	8.0	N/C	N/C	N/C	7.50E-16	-9.3	4.47E-16	-45.9		
V025	Al-0.2%-U (BN)	U-238(n,γ)	1.31E-11	2.1			23.4		22.6		22.6		
V025	Al-0.2%-U (BN)	U-238(n,γ)	1.19E-11	2.1			35.3		34.3		34.3		
V025	Al-0.2%-U (BN)	U-238(n,γ)	1.13E-11	2.5			42.8		41.8		41.8		
V025	Al-0.2%-U (BN)	U-238(n,γ)	1.75E-11	8.4			-7.7		-8.3		-8.3		
V025	Al-0.2%-U (BN)	U-238(n,γ)	1.29E-11	2.2	1.61E-11	14.8	24.7	1.60E-11	23.9	1.60E-11	23.9		
V025	Al-0.2%-U (BN)	U-238(n,γ)	1.16E-11	2.2			39.5		38.5		38.5		
V025	Al-0.2%-U (BN)	U-238(n,γ)	1.27E-11	4.9			26.6		25.7		25.7		
V025	Al-0.2%-U (BN)	U-238(n,γ)	1.17E-11	3.5			38.1		37.2		37.2		
V025	Al-0.2%-U (BN)	U-238(n,γ)	1.09E-11	3.2			47.2		46.1		46.1		
V029	Al-0.1%-Au (bare)	Al-27(n,α)	7.88E-16	2.1	8.07E-16	10.5	2.5	8.54E-16	8.4	5.16E-16	-34.5		
V029	Al-0.1%-Au (bare)	Au-197(n,γ)	4.70E-10	2.1	4.91E-10	9.1	4.4	4.59E-10	-2.4	4.44E-10	-5.6		

TABLE XI-3. COMPARISON BETWEEN MEASURED AND CALCULATED REACTION RATES PER TARGET ATOM (RR) IN THE PT IRRADIATION CHANNEL (cont.)

PT channel; Au, Mn, U		JSI Experimental data			JSI Calculated data (E71)			INVAP Calculated data (TENDL-2014)			INVAP Calculated data (E71)		
Sample ID	Sample description	Reaction	Meas. RR [s ⁻¹ / atom]	Unc [%]	Calc. RR [s ⁻¹ / atom]	Unc [%]	Diff [%]	Calc. RR [s ⁻¹ / atom]	Diff [%]	Calc. RR [s ⁻¹ / atom]	Diff [%]		
V030	Al-0.1%-Au (Cd)	Al-27(n,α)	8.10E-16	2.2	6.43E-16	9.7	-20.6	7.95E-16	-1.8	4.81E-16	-40.6		
V030	Al-0.1%-Au (Cd)	Au-197(n,γ)	2.04E-10	2.0	1.87E-10	7.7	-8.3	2.03E-10	-0.7	2.03E-10	-0.7		
V035	Al-0.1%-Au (BN)	Al-27(n,α)	7.63E-16	2.3	6.69E-16	13.9	-12.2	9.10E-16	19.3	5.42E-16	-28.9		
V035	Al-0.1%-Au (BN)	Au-197(n,γ)	5.07E-11	2.1	3.94E-11	17.1	-22.3	6.37E-11	25.5	6.37E-11	25.5		
V020	Al-1%-Mn (bare)	Al-27(n,α)	7.73E-16	3.8	N/C	N/C	N/C	8.55E-16	10.6	5.16E-16	-33.2		
V020	Al-1%-Mn (bare)	Mn-55(n,γ)	3.69E-11	2.2			-5.8		-6.1		-6.1		
V020	Al-1%-Mn (bare)	Mn-55(n,γ)	3.53E-11	2.9	3.48E-11	0.7	-1.3	3.47E-11	-1.6	3.47E-11	-1.6		
V020	Al-1%-Mn (bare)	Mn-55(n,γ)	3.48E-11	3.7			0.0		-0.3		-0.3		
V021	Al-1%-Mn (Cd)	Al-27(n,α)	7.95E-16	2.2	N/C	N/C	N/C	7.95E-16	0.0	4.81E-16	-39.5		
V021	Al-1%-Mn (Cd)	Mn-55(n,γ)	1.75E-12	2.3			-15.6		3.1		3.1		
V021	Al-1%-Mn (Cd)	Mn-55(n,γ)	1.70E-12	3.4	1.47E-12	3.2	-13.2	1.80E-12	6.0	1.80E-12	6.0		
V021	Al-1%-Mn (Cd)	Mn-55(n,γ)	1.70E-12	4.7			-13.1		6.1		6.1		
V022	Al-1%-Mn (BN)	Al-27(n,α)	7.93E-16	2.1	N/C	N/C	N/C	7.50E-16	-5.5	4.47E-16	-43.7		
V022	Al-1%-Mn (BN)	Mn-55(n,γ)	1.03E-12	2.7			-21.4		1.3		1.3		
V022	Al-1%-Mn (BN)	Mn-55(n,γ)	9.48E-13	5.5	8.06E-13	6.3	-15.0	1.04E-12	9.7	1.04E-12	9.7		
V022	Al-1%-Mn (BN)	Mn-55(n,γ)	9.85E-13	8.8			-18.2		5.6		5.6		

TABLE XI-4. COMPARISON BETWEEN MEASURED AND CALCULATED REACTION RATES PER TARGET ATOM (RR) IN THE PT IRRADIATION CHANNEL

PT channel; Au, Sn		JSI Experimental data			JSI Calculated data (E71)			INVAP Calculated data (TENDL-2014)			INVAP Calculated data (E71)		
Sample ID	Sample description	Reaction	Meas. RR [s ⁻¹ / atom]	Unc [%]	Calc. RR [s ⁻¹ / atom]	Unc [%]	Diff [%]	Calc. RR [s ⁻¹ / atom]	Diff [%]	Calc. RR [s ⁻¹ / atom]	Diff [%]	Diff [%]	
V041	Enriched Sn (bare)	Sn-117(n,n ⁺)	3.05E-13	3.8	4.52E-13	2.4	48.2	2.67E-13	-12.4	- ¹		N/A	
V041	Enriched Sn (bare)	Sn-117(n,n ⁺)	2.92E-13	2.1			54.6		-8.6				
V042	Enriched Sn (Cd)	Sn-117(n,n ⁺)	3.04E-13	2.3	4.54E-13	2.3	49.2	2.67E-13	-12.2	- ¹		N/A	
V042	Enriched Sn (Cd)	Sn-117(n,n ⁺)	2.94E-13	2.0			54.3		-9.2				
V043	Enriched Sn (BN)	Sn-117(n,n ⁺)	2.93E-13	3.0	4.54E-13	3.9	55.0	2.66E-13	-9.2	- ¹		N/A	
V043	Enriched Sn (BN)	Sn-117(n,n ⁺)	2.90E-13	2.0			56.7		-8.3				
V031	Al-0.1%-Au (bare)	Al-27(n,α)	8.45E-16	9.3	1.03E-15	13.3	21.9	8.64E-16	2.3	5.17E-16		-38.8	
V031	Al-0.1%-Au (bare)	Au-197(n,γ)	4.70E-10	2.2	4.38E-10	4.0	-6.8	4.64E-10	-1.3	4.64E-10		-1.3	
V032	Al-0.1%-Au (Cd)	Al-27(n,α)	7.52E-16	6.9	7.56E-16	10.3	0.6	8.18E-16	8.8	4.85E-16		-35.5	
V032	Al-0.1%-Au (Cd)	Au-197(n,γ)	1.96E-10	2.2	2.32E-10	9.3	18.3	2.08E-10	5.9	2.08E-10		5.9	
V036	Al-0.1%-Au (BN)	Al-27(n,α)	7.19E-16	3.9	9.47E-16	17.3	31.7	7.88E-16	9.6	4.72E-16		-34.3	
V036	Al-0.1%-Au (BN)	Au-197(n,γ)	5.16E-11	2.3	4.72E-11	16.2	-8.4	5.28E-11	2.4	5.28E-11		2.4	

¹ Cross-section not available.

TABLE XI-5. COMPARISON BETWEEN MEASURED AND CALCULATED REACTION RATES PER TARGET ATOM (RR) IN THE PT IRRADIATION CHANNEL

PT channel; Au, Fe		JSI Experimental data			JSI Calculated data (E71)			INVAP Calculated data (TENDL-2014)			INVAP Calculated data (E71)		
Sample ID	Sample description	Reaction	Meas. RR [s ⁻¹ / atom]	Unc [%]	Calc. RR [s ⁻¹ / atom]	Unc [%]	Diff [%]	Calc. RR [s ⁻¹ / atom]	Diff [%]	Calc. RR [s ⁻¹ / atom]	Diff [%]		
V038	Fe (bare)	Fe-58(n, γ)	3.21E-12	2.3			-8.5		4.1		-6.5		
V038	Fe (bare)	Fe-58(n, γ)	3.17E-12	2.1			-7.4		5.5		-5.3		
V038	Fe (bare)	Fe-58(n, γ)	3.19E-12	4.0	2.93E-12	0.8	-8.0	3.34E-12	4.7	3.00E-12	-5.9		
V038	Fe (bare)	Fe-58(n, γ)	3.52E-12	2.0			-16.7		-5.2		-14.8		
V038	Fe (bare)	Fe-58(n, γ)	3.51E-12	2.0			-16.5		-4.9		-14.6		
V038	Fe (bare)	Fe-54(n,p)	7.89E-14	2.1	8.22E-14	1.8	4.2	8.51E-14	7.8	8.49E-14	7.6		
V039	Fe (Cd)	Fe-58(n, γ)	1.52E-13	5.2			25.7		20.5		33.7		
V039	Fe (Cd)	Fe-58(n, γ)	1.39E-13	3.1			37.3		31.6		46.0		
V039	Fe (Cd)	Fe-58(n, γ)	1.28E-13	17.4	1.91E-13	11.0	49.6	1.83E-13	43.5	2.03E-13	59.1		
V039	Fe (Cd)	Fe-58(n, γ)	1.62E-13	2.1			17.9		13.1		25.4		
V039	Fe (Cd)	Fe-58(n, γ)	1.60E-13	2.1			19.4		14.5		27.0		
V039	Fe (Cd)	Fe-54(n,p)	8.11E-14	2.0	8.27E-14	1.8	2.0	8.26E-14	1.9	8.23E-14	1.5		
V040	Fe (BN)	Fe-58(n, γ)	2.90E-13	15.4			-60.3		-63.8		-56.9		
V040	Fe (BN)	Fe-58(n, γ)	8.33E-14	13.5	1.15E-13	21.9	38.5	1.05E-13	26.0	1.25E-13	50.0		
V040	Fe (BN)	Fe-58(n, γ)	9.02E-14	2.8			27.9		16.4		38.5		
V040	Fe (BN)	Fe-58(n, γ)	9.28E-14	3.1			24.4		13.2		34.8		
V040	Fe (BN)	Fe-54(n,p)	7.91E-14	2.1	8.51E-14	4.3	7.5	8.10E-14	2.4	8.09E-14	2.2		
V033	Al-0.1%-Au (bare)	Al-27(n, α)	6.99E-16	8.2	8.51E-16	9.8	21.8	8.60E-16	23.1	5.05E-16	-27.7		
V033	Al-0.1%-Au (bare)	Au-197(n, γ)	4.38E-10	2.2	4.20E-10	4.1	-4.2	4.46E-10	1.8	4.46E-10	1.8		
V034	Al-0.1%-Au (Cd)	Al-27(n, α)	7.27E-16	8.2	7.62E-16	12.9	4.8	8.11E-16	11.5	4.86E-16	-33.2		
V034	Al-0.1%-Au (Cd)	Au-197(n, γ)	1.96E-10	2.2	2.13E-10	10.2	8.8	2.08E-10	6.4	2.08E-10	6.4		
V037	Al-0.1%-Au (BN)	Al-27(n, α)	7.05E-16	4.7	8.36E-16	17.0	18.7	7.58E-16	7.6	4.47E-16	-36.6		
V037	Al-0.1%-Au (BN)	Au-197(n, γ)	5.08E-11	2.3	5.19E-11	15.7	2.3	5.29E-11	4.2	5.29E-11	4.2		

TABLE XI-6. COMPARISON BETWEEN MEASURED AND CALCULATED REACTION RATES PER TARGET ATOM (RR) IN THE PT IRRADIATION CHANNEL

PT channel; Au, Co, Sc, Th		JSI Experimental data			JSI Calculated data (E71)			INVAP Calculated data (TENDL-2014)			INVAP Calculated data (E71)		
Sample ID	Sample description	Reaction	Meas. RR [s ⁻¹ / atom]	Unc [%]	Calc. RR [s ⁻¹ / atom]	Unc [%]	Diff [%]	Calc. RR [s ⁻¹ / atom]	Diff [%]	Calc. RR [s ⁻¹ / atom]	Diff [%]	Diff [%]	
V047	Al-0.1%Co (bare)	Co-59(n,γ)	1.04E-10	2.1	1.01E-10	0.8	-3.1	3.87E-11	-62.9	1.02E-10		-2.3	
V047	Al-0.1%Co (bare)	Co-59(n,γ)	1.03E-10	2.1			-2.1		-62.6			-1.3	
V048	Al-0.1%Co (Cd)	Co-59(n,γ)	8.42E-12	2.2	9.11E-12	5.8	8.3	3.53E-12	-58.1	9.38E-12		11.4	
V048	Al-0.1%Co (Cd)	Co-59(n,γ)	8.34E-12	2.2			9.3		-57.7			12.4	
V049	Al-0.1%Co (BN)	Co-59(n,γ)	4.61E-12	5.7	6.74E-12	11.4	46.2	2.22E-12	-51.8	5.90E-12		28.0	
V049	Al-0.1%Co (BN)	Co-59(n,γ)	4.78E-12	5.7			40.9		-53.6			23.3	
V044	Al-0.1%-Au (bare)	Au-197(n,γ)	4.62E-10	2.1	4.14E-10	3.8	-10.3	4.46E-10	-3.4	4.46E-10		-3.4	
V045	Al-0.1%-Au (Cd)	Au-197(n,γ)	1.95E-10	2.1	2.10E-10	9.0	7.5	2.07E-10	6.1	2.07E-10		6.1	
V046	Al-0.1%-Au (BN)	Au-197(n,γ)	5.01E-11	2.3	4.39E-11	16.5	-12.4	5.34E-11	6.6	4.98E-11		-0.6	
V050	Al-2%-Sc (bare)	Sc-45(n,γ)	6.92E-11	2.0	6.92E-11	0.7	0.0	5.34E-11	-22.8	6.91E-11		-0.1	
V050	Al-2%-Sc (bare)	Sc-45(n,γ)	6.98E-11	2.0			-1.0		-23.5			-1.1	
V051	Al-2%-Sc (Cd)	Sc-45(n,γ)	1.41E-12	2.0	1.55E-12	1.6	9.7	1.20E-12	-14.9	1.59E-12		12.8	
V051	Al-2%-Sc (Cd)	Sc-45(n,γ)	1.42E-12	2.0			8.5		-15.8			11.6	
V052	Al-2%-Sc (BN)	Sc-45(n,γ)	3.62E-13	2.3	3.58E-13	3.3	-1.1	2.77E-13	-23.5	3.72E-13		2.7	
V052	Al-2%-Sc (BN)	Sc-45(n,γ)	3.65E-13	2.3			-2.0		-24.2			1.8	
V026	Al-1%-Th (bare)	Th-232(n,γ)	3.03E-11	2.2			1.8		1.8			0.8	
V026	Al-1%-Th (bare)	Th-232(n,γ)	2.52E-11	2.1			22.3		22.3			21.1	
V026	Al-1%-Th (bare)	Th-232(n,γ)	2.53E-11	2.0			21.7		21.7			20.5	
V026	Al-1%-Th (bare)	Th-232(n,γ)	3.36E-11	2.6			-8.3		-8.3			-9.2	
V026	Al-1%-Th (bare)	Th-232(n,γ)	2.58E-11	2.1			19.4		19.4			18.2	
V026	Al-1%-Th (bare)	Th-232(n,γ)	2.59E-11	2.0			19.1		19.1			18.0	
V026	Al-1%-Th (bare)	Th-232(n,γ)	2.60E-11	2.1			18.7		18.7			17.5	
V026	Al-1%-Th (bare)	Th-232(n,γ)	2.57E-11	2.7			19.8		19.8			18.6	
V026	Al-1%-Th (bare)	Th-232(n,γ)	2.58E-11	2.4			19.2		19.2			18.0	
V026	Al-1%-Th (bare)	Th-232(n,γ)	2.63E-11	2.3			17.1		17.1			16.0	

TABLE XI-6. COMPARISON BETWEEN MEASURED AND CALCULATED REACTION RATES PER TARGET ATOM (RR) IN THE PT IRRADIATION CHANNEL (cont.)

PT channel; Au, Co, Sc, Th		JSI Experimental data			JSI Calculated data (E71)			INVAP Calculated data (TENDL-2014)			INVAP Calculated data (E71)		
Sample ID	Sample description	Reaction	Meas. RR [s ⁻¹ / atom]	Unc [%]	Calc. RR [s ⁻¹ / atom]	Unc [%]	Diff [%]	Calc. RR [s ⁻¹ / atom]	Diff [%]	Calc. RR [s ⁻¹ / atom]	Diff [%]		
V027	Al-1%-Th (Cd)	Th-232(n, γ)	1.08E-11	2.3		-1.0			8.5		7.6		
V027	Al-1%-Th (Cd)	Th-232(n, γ)	9.13E-12	2.1		17.0			28.2		27.1		
V027	Al-1%-Th (Cd)	Th-232(n, γ)	9.33E-12	2.0		14.5			25.4		24.4		
V027	Al-1%-Th (Cd)	Th-232(n, γ)	1.30E-11	2.7		-17.8			-9.9		-10.6		
V027	Al-1%-Th (Cd)	Th-232(n, γ)	9.39E-12	2.1	1.07E-11	13.7		1.17E-11	24.6	1.16E-11	23.5		
V027	Al-1%-Th (Cd)	Th-232(n, γ)	9.41E-12	2.0		13.4			24.3		23.2		
V027	Al-1%-Th (Cd)	Th-232(n, γ)	9.42E-12	2.2		13.4			24.3		23.2		
V027	Al-1%-Th (Cd)	Th-232(n, γ)	9.18E-12	2.9		16.3			27.4		26.3		
V027	Al-1%-Th (Cd)	Th-232(n, γ)	9.43E-12	2.5		13.2			24.1		23.0		
V027	Al-1%-Th (Cd)	Th-232(n, γ)	9.41E-12	2.4		13.5			24.4		23.3		
V028	Al-1%-Th (BN)	Th-232(n, γ)	7.21E-12	2.3		8.8			-0.6		-1.8		
V028	Al-1%-Th (BN)	Th-232(n, γ)	5.95E-12	2.0		31.8			20.5		19.0		
V028	Al-1%-Th (BN)	Th-232(n, γ)	7.88E-12	2.7		-0.4			-9.0		-10.2		
V028	Al-1%-Th (BN)	Th-232(n, γ)	6.04E-12	2.1	7.85E-12	29.9		7.17E-12	18.7	7.08E-12	17.3		
V028	Al-1%-Th (BN)	Th-232(n, γ)	6.05E-12	2.0		29.7			18.6		17.1		
V028	Al-1%-Th (BN)	Th-232(n, γ)	5.99E-12	2.1		31.0			19.7		18.2		
V028	Al-1%-Th (BN)	Th-232(n, γ)	6.08E-12	3.0		29.1			17.9		16.5		
V028	Al-1%-Th (BN)	Th-232(n, γ)	6.24E-12	2.4		25.8			14.9		13.5		
V028	Al-1%-Th (BN)	Th-232(n, γ)	6.14E-12	2.4		27.8			16.8		15.3		

TABLE XI-7. COMPARISON BETWEEN MEASURED AND CALCULATED REACTION RATES PER TARGET ATOM (RR) IN THE CC IRRADIATION CHANNEL

CC channel; Al, Au		JSI Experimental data			JSI Calculated data (E71)			INVAP Calculated data (TENDL-2014)			INVAP Calculated data (E71)		
Sample ID meas. #	Sample description	Reaction	Meas. RR [s ⁻¹ / atom]	Unc [%]	Calc. RR [s ⁻¹ / atom]	Unc [%]	Diff [%]	Calc. RR [s ⁻¹ / atom]	Diff [%]	Calc. RR [s ⁻¹ / atom]	Diff [%]		
V125-3	Al-0.1%-Au (bare)	Al-27(n, γ)	1.55E-12	2.8	9.77E-13	0.6	-37.1	9.83E-13	-36.7	9.85E-13	-36.6		
V125-3	Al-0.1%-Au (bare)	Al-27(n,p)	2.04E-14	2.8	1.92E-14	2.7	-5.8	1.89E-14	-7.3	1.87E-14	-8.3		
V125-3	Al-0.1%-Au (bare)	Al-27(n,p)	2.01E-14	3.0		-4.3	-5.8		-6.8				
V125-4	Al-0.1%-Au (bare)	Al-27(n, α)	3.51E-15	3.4	3.89E-15	7.5	11.1	3.58E-15	2.1	2.16E-15	-38.4		
V125-4	Al-0.1%-Au (bare)	Au-197(n, γ)	1.18E-09	2.8	1.12E-09	3.9	-5.6	1.14E-09	-3.8	1.14E-09	-3.8		
V126-3	Al-0.1%-Au (Cd)	Al-27(n, γ)	8.65E-14	3.9	6.05E-14	1.2	-30.1	6.27E-14	-27.5	6.47E-14	-25.2		
V126-3	Al-0.1%-Au (Cd)	Al-27(n,p)	1.96E-14	2.7	1.77E-14	2.3	-10.1	1.85E-14	-5.8	1.83E-14	-6.9		
V126-3	Al-0.1%-Au (Cd)	Al-27(n,p)	1.95E-14	2.9		-9.4	-5.1		-6.2				
V126-4	Al-0.1%-Au (Cd)	Al-27(n, α)	3.31E-15	3.0	3.53E-15	6.4	6.4	3.50E-15	5.7	1.85E-14	424.8		
V126-4	Al-0.1%-Au (Cd)	Au-197(n, γ)	7.25E-10	2.7	6.78E-10	4.8	-6.5	7.23E-10	-0.3	7.23E-10	-0.3		

TABLE XI-8. COMPARISON BETWEEN MEASURED AND CALCULATED REACTION RATES PER TARGET ATOM (RR) IN THE IC40 IRRADIATION CHANNEL

IC40 channel; Al, Au		JSI Experimental data			JSI Calculated data (E71)			INVAP Calculated data (TENDL-2014)			INVAP Calculated data (E71)		
Sample ID meas. #	Sample description	Reaction	Meas. RR [s ⁻¹ / atom]	Unc [%]	Calc. RR [s ⁻¹ / atom]	Unc [%]	Diff [%]	Calc. RR [s ⁻¹ / atom]	Diff [%]	Calc. RR [s ⁻¹ / atom]	Diff [%]		
V127-3	Al-0.1%-Au (bare)	Al-27(n, γ)	3.32E-13	2.6	2.32E-13	2.2	-30.1	2.44E-13	-26.4	2.44E-13	-26.4		
V127-3	Al-0.1%-Au (bare)	Al-27(n,p)	5.50E-16	4.9	3.84E-16	27.2	-30.2	5.18E-16	-5.9	5.16E-16	-6.2		
V127-3	Al-0.1%-Au (bare)	Al-27(n,p)	5.49E-16	9.6			-30.0		-5.7		-6.0		
V127-5	Al-0.1%-Au (bare)	Al-27(n, α)	9.76E-17	6.0	1.14E-17	77.0	-88.4	7.20E-17	-26.3	4.64E-17	-52.5		
V127-5	Al-0.1%-Au (bare)	Au-197(n, γ)	1.56E-10	2.5	2.01E-10	23.0	29.0	1.58E-10	1.4	1.58E-10	1.4		
V128-1	Al-0.1%-Au (Cd)	Al-27(n, γ)	6.50E-15	2.7	4.78E-15	17.7	-26.5	2.21E-15	-66.0	4.60E-15	-29.2		
V128-3	Al-0.1%-Au (Cd)	Al-27(n,p)	5.46E-16	3.0	5.27E-16	26.5	-3.4	4.95E-16	-9.3	4.82E-16	-11.7		
V128-3	Al-0.1%-Au (Cd)	Al-27(n,p)	5.61E-16	3.7			-6.0		-11.7		-14.0		
V128-4	Al-0.1%-Au (Cd)	Al-27(n, α)	9.62E-17	4.9	1.90E-16	53.7	97.1	9.85E-17	2.4	5.67E-17	-41.1		
V128-4	Al-0.1%-Au (Cd)	Au-197(n, γ)	5.77E-11	2.5	5.92E-11	27.4	2.5	5.45E-11	-5.6	5.45E-11	-5.6		

TABLE XI-9. COMPARISON BETWEEN MEASURED AND CALCULATED REACTION RATES PER TARGET ATOM (RR) IN MP16 POSITION IN THE REACTOR CORE, AS A FUNCTION OF DEPTH FROM TOP OF UPPER REACTOR GRID PLATE

Core, MP 16				JSI Experimental data		JSI Calculated data (E71)		
Sample ID	Depth [cm]	Sample description	Reaction	Meas. RR [s ⁻¹ / atom]	Unc [%]	Calc. RR [s ⁻¹ / atom]	Unc [%]	Diff [%]
V272	1	Al-0.1%-Au	Au-197(n,γ)	5.24E-11	2.5	N/A	N/A	N/A
V273	2	Al-0.1%-Au	Au-197(n,γ)	6.02E-11	2.5	6.29E-11	1.9	4.4
V274	3	Al-0.1%-Au	Au-197(n,γ)	7.34E-11	2.5	7.94E-11	1.6	8.1
V275	4	Al-0.1%-Au	Au-197(n,γ)	9.09E-11	2.5	9.49E-11	1.4	4.4
V276	5	Al-0.1%-Au	Au-197(n,γ)	1.09E-10	2.5	1.13E-10	1.2	4.3
V277	6	Al-0.1%-Au	Au-197(n,γ)	1.29E-10	2.5	1.37E-10	1.2	5.7
V278	7	Al-0.1%-Au	Au-197(n,γ)	1.48E-10	2.5	1.62E-10	1.1	9.9
V279	8	Al-0.1%-Au	Au-197(n,γ)	1.69E-10	2.5	1.82E-10	1.0	8.0
V280	9	Al-0.1%-Au	Au-197(n,γ)	1.89E-10	2.5	2.06E-10	1.0	9.5
V281	10	Al-0.1%-Au	Au-197(n,γ)	2.11E-10	2.5	2.30E-10	0.9	8.9
V282	11	Al-0.1%-Au	Au-197(n,γ)	2.31E-10	2.5	2.51E-10	0.9	9.0
V283	12	Al-0.1%-Au	Au-197(n,γ)	2.47E-10	2.5	2.70E-10	0.9	9.2
V284	13	Al-0.1%-Au	Au-197(n,γ)	2.69E-10	2.5	2.91E-10	0.9	8.2
V285	14	Al-0.1%-Au	Au-197(n,γ)	2.81E-10	2.5	3.06E-10	0.9	8.8
V286	15	Al-0.1%-Au	Au-197(n,γ)	3.10E-10	2.5	3.35E-10	0.9	7.8
V287	16	Al-0.1%-Au	Au-197(n,γ)	3.43E-10	2.5	3.64E-10	0.8	6.2
V288	17	Al-0.1%-Au	Au-197(n,γ)	3.81E-10	2.5	3.97E-10	0.8	4.3
V289	18	Al-0.1%-Au	Au-197(n,γ)	4.16E-10	2.5	4.44E-10	0.8	6.6
V290	19	Al-0.1%-Au	Au-197(n,γ)	4.51E-10	2.5	4.74E-10	0.7	5.0
V291	20	Al-0.1%-Au	Au-197(n,γ)	4.78E-10	2.5	5.09E-10	0.7	6.3
V292	21	Al-0.1%-Au	Au-197(n,γ)	5.11E-10	2.5	5.33E-10	0.7	4.5
V293	22	Al-0.1%-Au	Au-197(n,γ)	5.36E-10	2.5	5.58E-10	0.7	4.1
V294	23	Al-0.1%-Au	Au-197(n,γ)	5.69E-10	2.5	6.02E-10	0.7	5.9
V295	24	Al-0.1%-Au	Au-197(n,γ)	5.93E-10	2.5	6.33E-10	0.6	6.7

TABLE XI-9. COMPARISON BETWEEN MEASURED AND CALCULATED REACTION RATES PER TARGET ATOM (RR) IN MP16 POSITION IN THE REACTOR CORE, AS A FUNCTION OF DEPTH FROM TOP OF UPPER REACTOR GRID PLATE (cont.)

Core, MP 16		JSI Experimental data			JSI Calculated data (E71)			
Sample ID	Depth [cm]	Sample description	Reaction	Meas. RR [s ⁻¹ / atom]	Unc [%]	Calc. RR [s ⁻¹ / atom]	Unc [%]	Diff [%]
V296	25	Al-0.1%-Au	Au-197(n,γ)	6.24E-10	2.5	6.56E-10	0.6	5.1
V297	26	Al-0.1%-Au	Au-197(n,γ)	6.38E-10	2.5	6.82E-10	0.6	6.9
V298	27	Al-0.1%-Au	Au-197(n,γ)	6.65E-10	2.5	7.11E-10	0.6	6.8
V299	28	Al-0.1%-Au	Au-197(n,γ)	6.96E-10	2.5	7.34E-10	0.6	5.3
V300	29	Al-0.1%-Au	Au-197(n,γ)	7.13E-10	2.5	7.60E-10	0.6	6.6
V301	30	Al-0.1%-Au	Au-197(n,γ)	7.37E-10	2.5	7.79E-10	0.6	5.6
V302	31	Al-0.1%-Au	Au-197(n,γ)	7.53E-10	2.5	7.98E-10	0.6	6.0
V303	32	Al-0.1%-Au	Au-197(n,γ)	7.73E-10	2.5	8.12E-10	0.6	5.0
V304	33	Al-0.1%-Au	Au-197(n,γ)	7.81E-10	2.5	8.10E-10	0.6	3.7
V305	34	Al-0.1%-Au	Au-197(n,γ)	7.95E-10	2.5	8.27E-10	0.6	4.0
V306	35	Al-0.1%-Au	Au-197(n,γ)	8.02E-10	2.5	8.36E-10	0.6	4.2
V307	36	Al-0.1%-Au	Au-197(n,γ)	8.09E-10	2.5	8.41E-10	0.6	3.9
V308	37	Al-0.1%-Au	Au-197(n,γ)	8.10E-10	2.5	8.35E-10	0.6	3.1
V309	38	Al-0.1%-Au	Au-197(n,γ)	7.97E-10	2.5	8.20E-10	0.6	2.9
V310	39	Al-0.1%-Au	Au-197(n,γ)	7.80E-10	2.5	8.17E-10	0.6	4.8
V311	40	Al-0.1%-Au	Au-197(n,γ)	7.65E-10	2.5	7.90E-10	0.6	3.3
V312	41	Al-0.1%-Au	Au-197(n,γ)	7.41E-10	2.5	7.70E-10	0.6	3.9
V313	42	Al-0.1%-Au	Au-197(n,γ)	7.18E-10	2.5	7.45E-10	0.6	3.7
V314	43	Al-0.1%-Au	Au-197(n,γ)	6.95E-10	2.5	7.13E-10	0.6	2.5
V315	44	Al-0.1%-Au	Au-197(n,γ)	6.66E-10	2.5	6.83E-10	0.6	2.5
V316	45	Al-0.1%-Au	Au-197(n,γ)	6.38E-10	2.5	6.44E-10	0.6	0.8
V317	46	Al-0.1%-Au	Au-197(n,γ)	6.03E-10	2.5	6.06E-10	0.6	0.5
V318	47	Al-0.1%-Au	Au-197(n,γ)	5.61E-10	2.5	5.66E-10	0.7	0.8
V319	48	Al-0.1%-Au	Au-197(n,γ)	5.25E-10	2.5	5.19E-10	0.7	-1.0

TABLE XI-9. COMPARISON BETWEEN MEASURED AND CALCULATED REACTION RATES PER TARGET ATOM (RR) IN MP16 POSITION IN THE REACTOR CORE, AS A FUNCTION OF DEPTH FROM TOP OF UPPER REACTOR GRID PLATE (cont.)

Core, MP 16									
Sample ID	Depth [cm]	Sample description	Reaction	JSI Experimental data			JSI Calculated data (E71)		
				Meas. RR [s ⁻¹ / atom]	Unc [%]	Calc. RR [s ⁻¹ / atom]	Unc [%]	Diff [%]	
V320	49	Al-0.1%-Au	Au-197(n,γ)	4.84E-10	2.5	4.78E-10	0.7	-1.3	
V321	50	Al-0.1%-Au	Au-197(n,γ)	4.38E-10	2.5	4.37E-10	0.7	0.0	
V322	51	Al-0.1%-Au	Au-197(n,γ)	4.08E-10	2.5	4.13E-10	0.8	1.0	
V323	52	Al-0.1%-Au	Au-197(n,γ)	3.86E-10	2.5	3.95E-10	0.8	2.3	
V324	53	Al-0.1%-Au	Au-197(n,γ)	3.70E-10	2.5	3.74E-10	0.8	1.1	
V325	54	Al-0.1%-Au	Au-197(n,γ)	3.43E-10	2.5	3.52E-10	0.8	2.5	
V326	55	Al-0.1%-Au	Au-197(n,γ)	3.19E-10	2.5	3.25E-10	0.8	1.8	
V327	56	Al-0.1%-Au	Au-197(n,γ)	2.94E-10	2.5	2.96E-10	0.8	0.4	
V328	57	Al-0.1%-Au	Au-197(n,γ)	2.63E-10	2.5	2.60E-10	0.8	-1.2	
V329	58	Al-0.1%-Au	Au-197(n,γ)	2.32E-10	2.5	2.31E-10	0.9	-0.5	
V330	59	Al-0.1%-Au	Au-197(n,γ)	2.02E-10	2.5	1.98E-10	1.0	-1.6	
V331	60	Al-0.1%-Au	Au-197(n,γ)	1.71E-10	2.5	1.67E-10	1.1	-2.4	
V332	61	Al-0.1%-Au	Au-197(n,γ)	1.44E-10	2.5	1.37E-10	1.2	-4.9	
V333	62	Al-0.1%-Au	Au-197(n,γ)	1.23E-10	2.5	1.14E-10	1.3	-7.6	
V334	63	Al-0.1%-Au	Au-197(n,γ)	1.04E-10	2.5	9.23E-11	1.3	-11.6	
V335	64	Al-0.1%-Au	Au-197(n,γ)	8.64E-11	2.5	7.56E-11	1.4	-12.5	
V336	65	Al-0.1%-Au	Au-197(n,γ)	7.14E-11	2.5	6.28E-11	1.6	-12.0	
V337	66	Al-0.1%-Au	Au-197(n,γ)	5.78E-11	2.5	5.11E-11	1.7	-11.5	
V338	67	Al-0.1%-Au	Au-197(n,γ)	4.73E-11	2.5	4.53E-11	2.0	-4.3	
V339	68	Al-0.1%-Au	Au-197(n,γ)	4.33E-11	2.5	4.00E-11	1.8	-7.6	
V340	69	Al-0.1%-Au	Au-197(n,γ)	4.23E-11	2.5	3.90E-11	3.2	-7.7	

TABLE XI-10. COMPARISON BETWEEN MEASURED AND CALCULATED REACTION RATES PER TARGET ATOM (RR) IN MP21 POSITION IN THE REACTOR CORE, AS A FUNCTION OF DEPTH FROM TOP OF UPPER REACTOR GRID PLATE

Core, MP 21				JSI Experimental data			JSI Calculated data (E71)		
Sample ID	Depth [cm]	Sample description	Reaction	Meas. RR [s ⁻¹ / atom]	Unc [%]	Calc. RR [s ⁻¹ / atom]	Unc [%]	Diff [%]	
V203	1	Al-0.1%-Au	Au-197(n, γ)	5.46E-11	2.5	4.77E-11	7.3	-12.6	
V204	2	Al-0.1%-Au	Au-197(n, γ)	6.58E-11	2.5	7.02E-11	7.7	6.7	
V205	3	Al-0.1%-Au	Au-197(n, γ)	8.16E-11	2.5	8.24E-11	6.6	1.0	
V206	4	Al-0.1%-Au	Au-197(n, γ)	1.02E-10	2.5	9.86E-11	5.6	-3.1	
V207	5	Al-0.1%-Au	Au-197(n, γ)	1.22E-10	2.5	1.09E-10	5.0	-10.3	
V208	6	Al-0.1%-Au	Au-197(n, γ)	1.42E-10	2.5	1.42E-10	4.4	-0.2	
V209	7	Al-0.1%-Au	Au-197(n, γ)	1.63E-10	2.5	1.69E-10	4.6	3.5	
V210	8	Al-0.1%-Au	Au-197(n, γ)	1.86E-10	2.5	1.97E-10	4.3	5.8	
V211	9	Al-0.1%-Au	Au-197(n, γ)	2.06E-10	2.5	2.28E-10	3.9	10.7	
V212	10	Al-0.1%-Au	Au-197(n, γ)	2.33E-10	2.5	2.44E-10	3.7	4.9	
V213	11	Al-0.1%-Au	Au-197(n, γ)	2.51E-10	2.5	2.65E-10	3.4	5.5	
V214	12	Al-0.1%-Au	Au-197(n, γ)	2.69E-10	2.5	2.97E-10	3.6	10.2	
V215	13	Al-0.1%-Au	Au-197(n, γ)	2.90E-10	2.5	3.08E-10	3.5	6.2	
V216	14	Al-0.1%-Au	Au-197(n, γ)	3.13E-10	2.5	3.26E-10	3.5	4.3	
V217	15	Al-0.1%-Au	Au-197(n, γ)	3.48E-10	2.5	3.82E-10	3.4	9.6	
V218	16	Al-0.1%-Au	Au-197(n, γ)	3.84E-10	2.5	3.82E-10	3.1	-0.3	
V219	17	Al-0.1%-Au	Au-197(n, γ)	4.25E-10	2.5	4.45E-10	3.2	4.7	
V220	18	Al-0.1%-Au	Au-197(n, γ)	4.72E-10	2.5	5.00E-10	3.0	5.9	
V221	19	Al-0.1%-Au	Au-197(n, γ)	5.07E-10	2.5	5.43E-10	2.9	6.9	
V222	20	Al-0.1%-Au	Au-197(n, γ)	5.49E-10	2.5	5.56E-10	2.7	1.3	
V223	21	Al-0.1%-Au	Au-197(n, γ)	5.85E-10	2.5	6.16E-10	2.6	5.3	
V224	22	Al-0.1%-Au	Au-197(n, γ)	6.18E-10	2.5	6.29E-10	2.5	1.7	
V225	23	Al-0.1%-Au	Au-197(n, γ)	6.61E-10	2.5	6.65E-10	2.4	0.6	
V226	24	Al-0.1%-Au	Au-197(n, γ)	6.96E-10	2.5	7.23E-10	2.5	3.9	

TABLE XI-10. COMPARISON BETWEEN MEASURED AND CALCULATED REACTION RATES PER TARGET ATOM (RR) IN MP21 POSITION IN THE REACTOR CORE, AS A FUNCTION OF DEPTH FROM TOP OF UPPER REACTOR GRID PLATE (cont.)

Core, MP 21				JSI Experimental data			JSI Calculated data (E71)		
Sample ID	Depth [cm]	Sample description	Reaction	Meas. RR [s ⁻¹ / atom]	Unc [%]	Calc. RR [s ⁻¹ / atom]	Unc [%]	Diff [%]	
V227	25	Al-0.1%-Au	Au-197(n, γ)	7.22E-10	2.5	7.42E-10	2.4	2.7	
V228	26	Al-0.1%-Au	Au-197(n, γ)	7.48E-10	2.5	7.74E-10	2.4	3.4	
V229	27	Al-0.1%-Au	Au-197(n, γ)	7.60E-10	2.5	7.90E-10	2.3	4.0	
V230	28	Al-0.1%-Au	Au-197(n, γ)	7.89E-10	2.5	8.14E-10	2.2	3.1	
V231	29	Al-0.1%-Au	Au-197(n, γ)	8.17E-10	2.5	7.89E-10	2.2	-3.4	
V232	30	Al-0.1%-Au	Au-197(n, γ)	8.31E-10	2.5	8.29E-10	2.3	-0.2	
V233	31	Al-0.1%-Au	Au-197(n, γ)	8.40E-10	2.5	8.32E-10	2.2	-0.9	
V234	32	Al-0.1%-Au	Au-197(n, γ)	8.46E-10	2.5	8.46E-10	2.2	-0.1	
V235	33	Al-0.1%-Au	Au-197(n, γ)	8.56E-10	2.5	8.43E-10	2.2	-1.5	
V236	34	Al-0.1%-Au	Au-197(n, γ)	8.54E-10	2.5	8.74E-10	2.3	2.4	
V237	35	Al-0.1%-Au	Au-197(n, γ)	8.51E-10	2.5	8.74E-10	2.3	2.7	
V238	36	Al-0.1%-Au	Au-197(n, γ)	8.51E-10	2.5	8.19E-10	2.2	-3.8	
V239	37	Al-0.1%-Au	Au-197(n, γ)	8.43E-10	2.5	8.47E-10	2.3	0.4	
V240	38	Al-0.1%-Au	Au-197(n, γ)	8.35E-10	2.5	7.97E-10	2.3	-4.6	
V241	39	Al-0.1%-Au	Au-197(n, γ)	8.18E-10	2.5	8.25E-10	2.3	0.9	
V242	40	Al-0.1%-Au	Au-197(n, γ)	7.98E-10	2.5	7.93E-10	2.3	-0.6	
V243	41	Al-0.1%-Au	Au-197(n, γ)	7.72E-10	2.5	7.80E-10	2.4	1.1	
V244	42	Al-0.1%-Au	Au-197(n, γ)	7.51E-10	2.5	7.56E-10	2.4	0.7	
V245	43	Al-0.1%-Au	Au-197(n, γ)	7.21E-10	2.5	7.36E-10	2.5	2.1	
V246	44	Al-0.1%-Au	Au-197(n, γ)	6.89E-10	2.5	6.72E-10	2.5	-2.4	
V247	45	Al-0.1%-Au	Au-197(n, γ)	6.54E-10	2.5	6.52E-10	2.7	-0.3	
V248	46	Al-0.1%-Au	Au-197(n, γ)	6.18E-10	2.5	6.09E-10	2.7	-1.5	
V249	47	Al-0.1%-Au	Au-197(n, γ)	5.74E-10	2.5	5.52E-10	2.7	-3.7	
V250	48	Al-0.1%-Au	Au-197(n, γ)	5.28E-10	2.5	5.25E-10	2.8	-0.6	

TABLE XI-10. COMPARISON BETWEEN MEASURED AND CALCULATED REACTION RATES PER TARGET ATOM (RR) IN MP21 POSITION IN THE REACTOR CORE, AS A FUNCTION OF DEPTH FROM TOP OF UPPER REACTOR GRID PLATE (cont.)

Core, MP 21				JSI Experimental data			JSI Calculated data (E71)		
Sample ID	Depth [cm]	Sample description	Reaction	Meas. RR [s ⁻¹ / atom]	Unc [%]	Calc. RR [s ⁻¹ / atom]	Unc [%]	Diff [%]	
V251	49	Al-0.1%-Au	Au-197(n, γ)	4.84E-10	2.5	4.68E-10	3.0	-3.3	
V252	50	Al-0.1%-Au	Au-197(n, γ)	4.48E-10	2.5	4.34E-10	3.0	-3.1	
V253	51	Al-0.1%-Au	Au-197(n, γ)	4.14E-10	2.5	4.22E-10	3.2	2.0	
V254	52	Al-0.1%-Au	Au-197(n, γ)	3.93E-10	2.5	4.02E-10	3.1	2.2	
V255	53	Al-0.1%-Au	Au-197(n, γ)	3.71E-10	2.5	3.69E-10	3.1	-0.6	
V256	54	Al-0.1%-Au	Au-197(n, γ)	3.46E-10	2.5	3.41E-10	3.1	-1.4	
V257	55	Al-0.1%-Au	Au-197(n, γ)	3.23E-10	2.5	3.34E-10	3.2	3.4	
V258	56	Al-0.1%-Au	Au-197(n, γ)	2.94E-10	2.5	2.94E-10	3.4	0.0	
V259	57	Al-0.1%-Au	Au-197(n, γ)	2.64E-10	2.5	2.51E-10	3.5	-4.8	
V260	58	Al-0.1%-Au	Au-197(n, γ)	2.33E-10	2.5	2.20E-10	3.5	-5.7	
V261	59	Al-0.1%-Au	Au-197(n, γ)	2.01E-10	2.5	1.88E-10	3.9	-6.3	
V262	60	Al-0.1%-Au	Au-197(n, γ)	1.69E-10	2.5	1.63E-10	4.4	-3.2	
V263	61	Al-0.1%-Au	Au-197(n, γ)	1.39E-10	2.5	1.28E-10	4.6	-7.6	
V264	62	Al-0.1%-Au	Au-197(n, γ)	1.19E-10	2.5	1.05E-10	4.7	-12.0	
V265	63	Al-0.1%-Au	Au-197(n, γ)	1.00E-10	2.5	8.25E-11	5.3	-17.5	
V266	64	Al-0.1%-Au	Au-197(n, γ)	8.33E-11	2.5	7.11E-11	5.6	-14.7	
V267	65	Al-0.1%-Au	Au-197(n, γ)	6.78E-11	2.5	5.70E-11	6.6	-15.9	
V268	66	Al-0.1%-Au	Au-197(n, γ)	5.43E-11	2.5	5.19E-11	7.4	-4.4	
V269	67	Al-0.1%-Au	Au-197(n, γ)	4.50E-11	2.5	3.99E-11	6.4	-11.4	
V270	68	Al-0.1%-Au	Au-197(n, γ)	4.18E-11	2.5	3.90E-11	7.3	-6.6	
V271	69	Al-0.1%-Au	Au-197(n, γ)	3.93E-11	2.5	3.85E-11	13.6	-2.1	

TABLE XI-11. COMPARISON BETWEEN MEASURED AND CALCULATED REACTION RATES PER TARGET ATOM (RR) IN MP15 POSITION IN THE REACTOR CORE, AS A FUNCTION OF DEPTH FROM TOP OF UPPER REACTOR GRID PLATE

Core, MP 15				JSI Experimental data		JSI Calculated data (E71)		
Sample ID	Depth [cm]	Sample description	Reaction	Meas. RR [s ⁻¹ / atom]	Unc [%]	Calc. RR [s ⁻¹ / atom]	Unc [%]	Diff [%]
V341	1	Al-0.1%-Au	Au-197(n, γ)	4.86E-11	2.5	5.84E-11	8.9	20.2
V342	2	Al-0.1%-Au	Au-197(n, γ)	5.72E-11	2.5	5.83E-11	6.9	1.9
V343	3	Al-0.1%-Au	Au-197(n, γ)	7.05E-11	2.5	7.09E-11	6.4	0.7
V344	4	Al-0.1%-Au	Au-197(n, γ)	8.65E-11	2.5	8.72E-11	5.8	0.8
V345	5	Al-0.1%-Au	Au-197(n, γ)	1.04E-10	2.5	9.71E-11	5.1	-6.4
V346	6	Al-0.1%-Au	Au-197(n, γ)	1.20E-10	2.5	1.22E-10	5.1	1.4
V347	7	Al-0.1%-Au	Au-197(n, γ)	1.38E-10	2.5	1.37E-10	4.6	-0.5
V348	8	Al-0.1%-Au	Au-197(n, γ)	1.55E-10	2.5	1.58E-10	4.3	1.6
V349	9	Al-0.1%-Au	Au-197(n, γ)	1.73E-10	2.5	1.73E-10	3.9	0.3
V350	10	Al-0.1%-Au	Au-197(n, γ)	1.90E-10	2.5	1.93E-10	3.9	1.5
V351	11	Al-0.1%-Au	Au-197(n, γ)	2.08E-10	2.5	2.01E-10	3.9	-3.4
V352	12	Al-0.1%-Au	Au-197(n, γ)	2.20E-10	2.5	2.36E-10	4.0	7.4
V353	13	Al-0.1%-Au	Au-197(n, γ)	2.34E-10	2.5	2.49E-10	3.8	6.4
V354	14	Al-0.1%-Au	Au-197(n, γ)	2.49E-10	2.5	2.43E-10	3.7	-2.2
V355	15	Al-0.1%-Au	Au-197(n, γ)	2.73E-10	2.5	2.82E-10	3.6	3.5
V356	16	Al-0.1%-Au	Au-197(n, γ)	3.01E-10	2.5	3.37E-10	3.7	12.0
V357	17	Al-0.1%-Au	Au-197(n, γ)	3.28E-10	2.5	3.35E-10	3.6	1.9
V358	18	Al-0.1%-Au	Au-197(n, γ)	3.57E-10	2.5	3.85E-10	3.3	7.8
V359	19	Al-0.1%-Au	Au-197(n, γ)	3.89E-10	2.5	4.15E-10	3.2	6.7
V360	20	Al-0.1%-Au	Au-197(n, γ)	4.15E-10	2.5	4.30E-10	3.2	3.5
V361	21	Al-0.1%-Au	Au-197(n, γ)	4.45E-10	2.5	4.64E-10	3.1	4.3
V362	22	Al-0.1%-Au	Au-197(n, γ)	4.68E-10	2.5	4.85E-10	3.0	3.6
V363	23	Al-0.1%-Au	Au-197(n, γ)	4.90E-10	2.5	5.07E-10	2.9	3.5
V364	24	Al-0.1%-Au	Au-197(n, γ)	5.08E-10	2.5	5.51E-10	2.8	8.5

TABLE XI-11. COMPARISON BETWEEN MEASURED AND CALCULATED REACTION RATES PER TARGET ATOM (RR) IN MP15 POSITION IN THE REACTOR CORE, AS A FUNCTION OF DEPTH FROM TOP OF UPPER REACTOR GRID PLATE (cont.)

Core, MP 15				JSI Experimental data			JSI Calculated data (E71)		
Sample ID	Depth [cm]	Sample description	Reaction	Meas. RR [s ⁻¹ / atom]	Unc [%]	Calc. RR [s ⁻¹ / atom]	Unc [%]	Diff [%]	
V365	25	Al-0.1%-Au	Au-197(n,γ)	5.28E-10	2.5	5.65E-10	2.8	7.0	
V366	26	Al-0.1%-Au	Au-197(n,γ)	5.50E-10	2.5	5.78E-10	2.6	5.1	
V367	27	Al-0.1%-Au	Au-197(n,γ)	5.73E-10	2.5	5.85E-10	2.6	2.2	
V368	28	Al-0.1%-Au	Au-197(n,γ)	5.92E-10	2.5	6.19E-10	2.7	4.6	
V369	29	Al-0.1%-Au	Au-197(n,γ)	6.08E-10	2.5	6.43E-10	2.6	5.8	
V370	30	Al-0.1%-Au	Au-197(n,γ)	6.30E-10	2.5	6.50E-10	2.5	3.3	
V371	31	Al-0.1%-Au	Au-197(n,γ)	6.49E-10	2.5	6.55E-10	2.5	0.8	
V372	32	Al-0.1%-Au	Au-197(n,γ)	6.58E-10	2.5	6.89E-10	2.5	4.7	
V373	33	Al-0.1%-Au	Au-197(n,γ)	6.75E-10	2.5	7.02E-10	2.4	4.0	
V374	34	Al-0.1%-Au	Au-197(n,γ)	6.76E-10	2.5	6.76E-10	2.3	0.0	
V375	35	Al-0.1%-Au	Au-197(n,γ)	6.80E-10	2.5	6.99E-10	2.4	2.8	
V376	36	Al-0.1%-Au	Au-197(n,γ)	6.90E-10	2.5	6.73E-10	2.4	-2.4	
V377	37	Al-0.1%-Au	Au-197(n,γ)	6.86E-10	2.5	6.89E-10	2.5	0.3	
V378	38	Al-0.1%-Au	Au-197(n,γ)	6.81E-10	2.5	7.20E-10	2.5	5.8	
V379	39	Al-0.1%-Au	Au-197(n,γ)	6.74E-10	2.5	6.73E-10	2.4	-0.2	
V380	40	Al-0.1%-Au	Au-197(n,γ)	6.57E-10	2.5	6.30E-10	2.4	-4.2	
V381	41	Al-0.1%-Au	Au-197(n,γ)	6.52E-10	2.5	6.55E-10	2.5	0.5	
V382	42	Al-0.1%-Au	Au-197(n,γ)	6.27E-10	2.5	6.34E-10	2.5	1.1	
V383	43	Al-0.1%-Au	Au-197(n,γ)	6.04E-10	2.5	6.24E-10	2.6	3.3	
V384	44	Al-0.1%-Au	Au-197(n,γ)	5.78E-10	2.5	5.57E-10	2.6	-3.6	
V385	45	Al-0.1%-Au	Au-197(n,γ)	5.50E-10	2.5	5.34E-10	2.9	-3.0	
V386	46	Al-0.1%-Au	Au-197(n,γ)	5.18E-10	2.5	5.16E-10	2.9	-0.4	
V387	47	Al-0.1%-Au	Au-197(n,γ)	4.85E-10	2.5	5.05E-10	2.9	4.2	
V388	48	Al-0.1%-Au	Au-197(n,γ)	4.52E-10	2.5	4.53E-10	3.1	0.3	

TABLE XI-11. COMPARISON BETWEEN MEASURED AND CALCULATED REACTION RATES PER TARGET ATOM (RR) IN MP15 POSITION IN THE REACTOR CORE, AS A FUNCTION OF DEPTH FROM TOP OF UPPER REACTOR GRID PLATE (cont.)

Core, MP 15				JSI Experimental data		JSI Calculated data (E71)		
Sample ID	Depth [cm]	Sample description	Reaction	Meas. RR [s ⁻¹ / atom]	Unc [%]	Calc. RR [s ⁻¹ / atom]	Unc [%]	Diff [%]
V389	49	Al-0.1%-Au	Au-197(n,γ)	4.13E-10	2.5	4.42E-10	3.2	6.9
V390	50	Al-0.1%-Au	Au-197(n,γ)	3.80E-10	2.5	4.01E-10	3.1	5.6
V391	51	Al-0.1%-Au	Au-197(n,γ)	3.56E-10	2.5	3.66E-10	3.2	2.9
V392	52	Al-0.1%-Au	Au-197(n,γ)	3.39E-10	2.5	3.45E-10	3.1	1.7
V393	53	Al-0.1%-Au	Au-197(n,γ)	3.23E-10	2.5	3.17E-10	2.9	-2.0
V394	54	Al-0.1%-Au	Au-197(n,γ)	3.05E-10	2.5	2.90E-10	3.0	-4.9
V395	55	Al-0.1%-Au	Au-197(n,γ)	2.82E-10	2.5	2.84E-10	3.3	1.0
V396	56	Al-0.1%-Au	Au-197(n,γ)	2.55E-10	2.5	2.71E-10	3.4	6.3
V397	57	Al-0.1%-Au	Au-197(n,γ)	2.29E-10	2.5	2.28E-10	3.5	-0.7
V398	58	Al-0.1%-Au	Au-197(n,γ)	2.03E-10	2.5	2.05E-10	3.8	1.0
V399	59	Al-0.1%-Au	Au-197(n,γ)	1.75E-10	2.5	1.61E-10	3.8	-7.8
V400	60	Al-0.1%-Au	Au-197(n,γ)	1.48E-10	2.5	1.48E-10	4.4	-0.4
V401	61	Al-0.1%-Au	Au-197(n,γ)	1.25E-10	2.5	1.15E-10	4.6	-7.7
V402	62	Al-0.1%-Au	Au-197(n,γ)	1.06E-10	2.5	9.84E-11	4.8	-7.2
V403	63	Al-0.1%-Au	Au-197(n,γ)	8.95E-11	2.5	9.13E-11	5.6	2.0
V404	64	Al-0.1%-Au	Au-197(n,γ)	7.45E-11	2.5	7.42E-11	5.7	-0.4
V405	65	Al-0.1%-Au	Au-197(n,γ)	6.12E-11	2.5	6.13E-11	7.1	0.2
V406	66	Al-0.1%-Au	Au-197(n,γ)	4.99E-11	2.5	4.75E-11	7.4	-4.8
V407	67	Al-0.1%-Au	Au-197(n,γ)	4.13E-11	2.5	4.30E-11	8.1	3.9
V408	68	Al-0.1%-Au	Au-197(n,γ)	3.84E-11	2.5	3.41E-11	7.8	-11.2
V409	69	Al-0.1%-Au	Au-197(n,γ)	3.78E-11	2.5	3.45E-11	7.4	-8.9

TABLE XI-12. COMPARISON BETWEEN MEASURED AND CALCULATED REACTION RATES PER TARGET ATOM (RR) IN MP17 POSITION IN THE REACTOR CORE, AS A FUNCTION OF DEPTH FROM TOP OF UPPER REACTOR GRID PLATE

Core, MP 17				JSI Experimental data		JSI Calculated data (E71)		
Sample ID	Depth [cm]	Sample description	Reaction	Meas. RR [s ⁻¹ /atom]	Unc [%]	Calc. RR [s ⁻¹ /atom]	Unc [%]	Diff [%]
V410	2	Al-0.1%-Au	Au-197(n, γ)	8.08E-11	2.5	7.28E-11	6.3	-9.9
V411	3	Al-0.1%-Au	Au-197(n, γ)	1.01E-10	2.5	8.46E-11	6.4	-16.5
V412	4	Al-0.1%-Au	Au-197(n, γ)	1.23E-10	2.5	1.07E-10	5.3	-13.0
V413	5	Al-0.1%-Au	Au-197(n, γ)	1.46E-10	2.5	1.24E-10	4.7	-15.1
V414	6	Al-0.1%-Au	Au-197(n, γ)	1.71E-10	2.5	1.57E-10	4.6	-8.2
V415	7	Al-0.1%-Au	Au-197(n, γ)	1.98E-10	2.5	1.79E-10	4.0	-9.7
V416	8	Al-0.1%-Au	Au-197(n, γ)	2.25E-10	2.5	2.20E-10	3.8	-2.2
V417	9	Al-0.1%-Au	Au-197(n, γ)	2.54E-10	2.5	2.45E-10	3.8	-3.2
V418	10	Al-0.1%-Au	Au-197(n, γ)	2.85E-10	2.5	2.66E-10	3.3	-6.5
V419	11	Al-0.1%-Au	Au-197(n, γ)	3.12E-10	2.5	3.06E-10	3.3	-1.8
V420	12	Al-0.1%-Au	Au-197(n, γ)	3.41E-10	2.5	3.35E-10	3.2	-1.8
V421	13	Al-0.1%-Au	Au-197(n, γ)	3.69E-10	2.5	3.61E-10	3.0	-2.2
V422	14	Al-0.1%-Au	Au-197(n, γ)	4.04E-10	2.5	3.96E-10	2.9	-1.9
V423	15	Al-0.1%-Au	Au-197(n, γ)	4.46E-10	2.5	4.61E-10	3.0	3.4
V424	16	Al-0.1%-Au	Au-197(n, γ)	4.89E-10	2.5	4.84E-10	2.9	-0.9
V425	17	Al-0.1%-Au	Au-197(n, γ)	5.39E-10	2.5	5.38E-10	2.7	-0.3
V426	18	Al-0.1%-Au	Au-197(n, γ)	5.91E-10	2.5	5.77E-10	2.6	-2.4
V427	19	Al-0.1%-Au	Au-197(n, γ)	6.30E-10	2.5	6.21E-10	2.5	-1.4
V428	20	Al-0.1%-Au	Au-197(n, γ)	6.75E-10	2.5	6.62E-10	2.4	-1.9
V429	21	Al-0.1%-Au	Au-197(n, γ)	7.18E-10	2.5	7.03E-10	2.3	-2.2
V430	22	Al-0.1%-Au	Au-197(n, γ)	7.62E-10	2.5	7.52E-10	2.2	-1.4
V431	23	Al-0.1%-Au	Au-197(n, γ)	7.97E-10	2.5	8.10E-10	2.2	1.6
V432	24	Al-0.1%-Au	Au-197(n, γ)	8.45E-10	2.5	8.56E-10	2.1	1.3
V433	25	Al-0.1%-Au	Au-197(n, γ)	8.73E-10	2.5	9.22E-10	2.1	5.6

TABLE XI-12. COMPARISON BETWEEN MEASURED AND CALCULATED REACTION RATES PER TARGET ATOM (RR) IN MP17 POSITION IN THE REACTOR CORE, AS A FUNCTION OF DEPTH FROM TOP OF UPPER REACTOR GRID PLATE (cont.)

Core, MP 17				JSI Experimental data			JSI Calculated data (E71)		
Sample ID	Depth [cm]	Sample description	Reaction	Meas. RR [s ⁻¹ /atom]	Unc [%]	Calc. RR [s ⁻¹ /atom]	Unc [%]	Diff [%]	
V434	26	Al-0.1%-Au	Au-197(n, γ)	9.08E-10	2.5	9.84E-10	2.1	8.4	
V435	27	Al-0.1%-Au	Au-197(n, γ)	9.38E-10	2.5	9.83E-10	2.1	4.8	
V436	28	Al-0.1%-Au	Au-197(n, γ)	9.63E-10	2.5	1.01E-09	2.0	5.0	
V437	29	Al-0.1%-Au	Au-197(n, γ)	9.88E-10	2.5	1.06E-09	2.0	7.1	
V438	30	Al-0.1%-Au	Au-197(n, γ)	1.00E-09	2.5	1.06E-09	1.9	5.5	
V439	31	Al-0.1%-Au	Au-197(n, γ)	1.03E-09	2.5	1.07E-09	1.9	3.7	
V440	32	Al-0.1%-Au	Au-197(n, γ)	1.04E-09	2.5	1.12E-09	1.9	8.1	
V441	33	Al-0.1%-Au	Au-197(n, γ)	1.05E-09	2.5	1.13E-09	1.9	7.9	
V442	34	Al-0.1%-Au	Au-197(n, γ)	1.06E-09	2.5	1.12E-09	1.9	5.2	
V443	35	Al-0.1%-Au	Au-197(n, γ)	1.05E-09	2.5	1.10E-09	1.8	4.7	
V444	36	Al-0.1%-Au	Au-197(n, γ)	1.06E-09	2.5	1.13E-09	1.9	6.6	
V445	37	Al-0.1%-Au	Au-197(n, γ)	1.08E-09	2.5	1.12E-09	1.9	4.2	
V446	38	Al-0.1%-Au	Au-197(n, γ)	1.07E-09	2.5	1.12E-09	1.9	4.1	
V447	39	Al-0.1%-Au	Au-197(n, γ)	1.03E-09	2.5	1.09E-09	1.9	5.4	
V448	40	Al-0.1%-Au	Au-197(n, γ)	1.01E-09	2.5	1.07E-09	1.9	5.7	
V449	41	Al-0.1%-Au	Au-197(n, γ)	9.92E-10	2.5	1.09E-09	1.9	9.5	
V450	42	Al-0.1%-Au	Au-197(n, γ)	9.57E-10	2.5	1.04E-09	2.0	8.6	
V451	43	Al-0.1%-Au	Au-197(n, γ)	9.18E-10	2.5	1.01E-09	2.0	10.0	
V452	44	Al-0.1%-Au	Au-197(n, γ)	8.88E-10	2.5	9.73E-10	2.1	9.6	
V453	45	Al-0.1%-Au	Au-197(n, γ)	8.42E-10	2.5	8.89E-10	2.1	5.5	
V454	46	Al-0.1%-Au	Au-197(n, γ)	7.86E-10	2.5	8.64E-10	2.2	9.9	
V455	47	Al-0.1%-Au	Au-197(n, γ)	7.30E-10	2.5	8.16E-10	2.1	11.9	
V456	48	Al-0.1%-Au	Au-197(n, γ)	6.69E-10	2.5	7.38E-10	2.3	10.3	
V457	49	Al-0.1%-Au	Au-197(n, γ)	6.23E-10	2.5	6.91E-10	2.4	10.8	

TABLE XI-12. COMPARISON BETWEEN MEASURED AND CALCULATED REACTION RATES PER TARGET ATOM (RR) IN MP17 POSITION IN THE REACTOR CORE, AS A FUNCTION OF DEPTH FROM TOP OF UPPER REACTOR GRID PLATE (cont.)

Core, MP 17				JSI Experimental data		JSI Calculated data (E71)	
Sample ID	Depth [cm]	Sample description	Reaction	Meas. RR [s ⁻¹ /atom]	Unc [%]	Calc. RR [s ⁻¹ /atom]	Diff [%]
V458	50	Al-0.1%-Au	Au-197(n, γ)	5.64E-10	2.5	6.45E-10	14.4
V459	51	Al-0.1%-Au	Au-197(n, γ)	5.18E-10	2.5	5.72E-10	10.4
V460	52	Al-0.1%-Au	Au-197(n, γ)	4.81E-10	2.5	5.43E-10	12.9
V461	53	Al-0.1%-Au	Au-197(n, γ)	4.50E-10	2.5	5.07E-10	12.6
V462	54	Al-0.1%-Au	Au-197(n, γ)	4.22E-10	2.5	4.66E-10	10.5
V463	55	Al-0.1%-Au	Au-197(n, γ)	3.87E-10	2.5	4.10E-10	5.9
V464	56	Al-0.1%-Au	Au-197(n, γ)	3.51E-10	2.5	3.96E-10	12.8
V465	57	Al-0.1%-Au	Au-197(n, γ)	3.90E-10	2.5	3.58E-10	-8.2
V466	58	Al-0.1%-Au	Au-197(n, γ)	3.21E-10	2.5	3.02E-10	-5.9
V467	59	Al-0.1%-Au	Au-197(n, γ)	2.41E-10	2.5	2.79E-10	15.7
V468	60	Al-0.1%-Au	Au-197(n, γ)	2.07E-10	2.5	2.45E-10	17.9
V469	61	Al-0.1%-Au	Au-197(n, γ)	1.75E-10	2.5	2.03E-10	16.1
V470	62	Al-0.1%-Au	Au-197(n, γ)	1.48E-10	2.5	1.75E-10	18.2
V471	63	Al-0.1%-Au	Au-197(n, γ)	1.27E-10	2.5	1.45E-10	14.5
V472	64	Al-0.1%-Au	Au-197(n, γ)	1.06E-10	2.5	1.28E-10	20.7
V473	65	Al-0.1%-Au	Au-197(n, γ)	8.55E-11	2.5	1.05E-10	22.8
V474	66	Al-0.1%-Au	Au-197(n, γ)	7.03E-11	2.5	8.45E-11	20.2
V475	67	Al-0.1%-Au	Au-197(n, γ)	5.70E-11	2.5	6.34E-11	11.1
V476	68	Al-0.1%-Au	Au-197(n, γ)	5.22E-11	2.5	5.25E-11	0.8
V477	69	Al-0.1%-Au	Au-197(n, γ)	4.92E-11	2.5	5.31E-11	7.9
V478	70	Al-0.1%-Au	Au-197(n, γ)	4.44E-11	2.5	5.17E-11	16.4

REFERENCES TO ANNEX XI

- [XI-1] INTERNATIONAL ATOMIC ENERGY AGENCY, Research Reactor Benchmarking Database: Facility Specification and Experimental Data, Technical Reports Series No. 480 (Rev. 1), IAEA, Vienna (in preparation).
- [XI-2] Safety report for the TRIGA Mark II reactor in Podgorica, Revision 3, IJS Report No. 5823, June 1992 (in Slovenian).
- [XI-3] MELE, I., RAVNIK, M., TRKOV, A., TRIGA Mark II Benchmark Experiment, Part I: Steady-State Operation, Nucl. Technol. **105** (1994) 37–51.
- [XI-4] MELE, I., RAVNIK, M., TRKOV, A., TRIGA Mark II Benchmark Experiment, Part II: Pulse Operation, Nucl. Technol. **105** (1994) 52–58.
- [XI-5] HyperLab 2005, Quick start guide for main module. HyperLabs Software, Budapest, Hungary (2005).
- [XI-6] ROSSBACH, M., BLAAUW, M., Progress in the k_0 -IAEA program, Nucl. Instrum. Methods Phys. Res., Sect. A **564** (2006) 698–701.
- [XI-7] GOORLEY, J.T., et al., Initial MCNP6 Release Overview – MCNP6 version 1.0, Los Alamos National Laboratory Report LA-UR-13-22934, Los Alamos, NM (2013).
- [XI-8] JERAJ, R., RAVNIK, M., TRIGA Mark II reactor: U[20]-Zirconium Hydride fuel rods in water with graphite reflector, IEU-COMP-THERM-003, International Handbook of Evaluated Criticality Safety Benchmarks Experiments, NEA/NSC/DOC, (95)03, 1999.
- [XI-9] SNOJ, L., et al., Calculation of kinetic parameters for mixed TRIGA cores with Monte Carlo, Ann. Nucl. Energy **37** (2010) 223–229.
- [XI-10] RADULOVIĆ, V., et al., Validation of absolute axial neutron flux distribution calculations with MCNP with $^{197}\text{Au}(n,\gamma)^{198}\text{Au}$ reaction rate distribution measurements at the JSI TRIGA Mark II reactor, Appl. Radiat. Isot. **84** (2014) 57–65.
- [XI-11] SNOJ, L., et al., Analysis of neutron flux distribution for the validation of computational methods for the optimization of research reactor utilization, Appl. Radiat. Isot. **69** (2011) 136–141.
- [XI-12] SNOJ, L., ŽEROVNIK, G., TRKOV, A., Computational analysis of irradiation facilities at the JSI TRIGA reactor, Appl. Radiat. Isot. **70** (2012) 483–488.
- [XI-13] AMBROŽIČ, K., ŽEROVNIK, G., SNOJ, L., Computational analysis of the dose rates at JSI TRIGA reactor irradiation facilities, Appl. Radiat. Isot. **130** (2017) 140–152.
- [XI-14] ŽEROVNIK, G., PODVRATNIK, M., SNOJ, L., On normalization of fluxes and reaction rates in MCNP criticality calculations, Ann. Nucl. Energy **63** (2014) 126–128.
- [XI-15] CHADWICK, M.B., et al., ENDF/B-VII.1 Nuclear Data for Science and Technology: Cross Sections, Covariances, Fission Product Yields and Decay Data, Nuclear Data Sheets **112** (2011) 2887–2996.
- [XI-16] TRKOV, A., et al., Application of the rod-insertion method for control rod worth measurements in research reactors, Kerntechnik **60** (1995) 255–261.
- [XI-17] SUBLET, J.-CH., et al., FISPACT-II: An Advanced Simulation System for Activation, Transmutation and Material Modelling, Nuclear Data Sheets **139** (2017) 77–137.
- [XI-18] TENDL-2014: TALYS-based evaluated nuclear data library, KONING, A.J., et al., www.talys.eu/tendl-2014.html

ANNEX XII

BENCHMARK CONSOLIDATED RESULTS AGAINST EXPERIMENTAL DATA FROM NECSA-1 AND NECSA-2

XII-1. INTRODUCTION

This Annex provides a consolidation and technical comparison between the calculational contributions received from various CRP participants with regard to modelling of the SAFARI-1 benchmark problem. SAFARI-1 is a tank-in-pool type material testing reactor (MTR) operated by Necsa. The full specification of this benchmark, including the reactor specification and experimental data, is documented in Ref. [XII-1].

The SAFARI-1 facility related experiments (NECSA-1 and NECSA-2) described in Ref. [XII-1] include, for numerous cycles, critical conditions, BOC flux wire mapping experiments, spectral measurements and control rod calibration experiments. During the specified timeframe spanned by the experiments, the SAFARI-1 reactor underwent a beryllium reflector element replacement. This activity was accompanied by a series of flux foil measurements, which are additionally included in this benchmark.

The information provided in Ref. [XII-1] reflects, as accurately as attainable, the geometric and material layout of the reactor core for all conditions considered, and thus allows code packages that are able to model high levels of heterogeneity to be fully tested. All experiments make use of the same core component descriptions, although core layout and configuration may differ between cases. Care was taken to avoid the description of commercially sensitive in-core components. Where such components have a significant impact on core parameters, simplified equivalent definitions were provided.

The facility and experimental description in Ref. [XII-1] is structured into three parts (A, B and C), with each part containing a number of scenarios, gradually increasing in complexity. In this way, the benchmark can be used for both code-to-code verification as well as code-to-experiment validation of the codes and associated models.

This consolidated report refers to two experimental contributions from Necsa. NECSA-1 relates to all experiments associated to the multicycle modelling, and contains Experiments 1-3, and NECSA-2 relates to experiments associated with the beryllium poison buildup modelling, and contains Experiment 4. In summary:

- NECSA-1 with three associated experiments. Experiment 1 refers to multicycle criticality, Experiment 2 refers to multicycle Cu wire activation experiments, and Experiment 3 refers to multicycle control rod calibration.
- NECSA-2 with one associated experiment. Experiment 4 refers to the set of measurements (both criticality and foil activation) conducted during the reflector element replacement.

This Annex considers three submissions to this benchmark problem:

- A set of results supplied by Necsa (South Africa) for NECSA-1 and NECSA-2 (all experiments);
- A set of results supplied by INVAP (Argentina) for a subset of NECSA-1;

- A set of results supplied by INR (Romania) for NECSA-2.

XII-2. SUMMARY OF THE BENCHMARK SPECIFICATION AND CODES AND MODELS USED

XII-2.1. Summary of the benchmark specification

SAFARI-1 is a tank-in-pool type reactor using plate type LEU fuel. The core is reflected by beryllium on three sides, with the fourth side directly facing the reactor pool. The reactor is nominally operated at 20 MW, and follows a continuous operational regime with a typical cycle length of 30 days.

In the benchmark specification, core and structural components are described in full geometric detail. However, because of commercial sensitivity, the molybdenum rigs and in-core sample holders are replaced by an equivalent semi-homogeneous representation.

An XY view of the reactor at the axial level $Z=0.0$ cm (core centreline) is shown in Fig. XII-2 where the main components of the reactor core are detailed. Note that, as in the following figures of this Annex, the beam tube corresponding to the large facility nozzle is empty but it can be flooded with water according to the configuration to be calculated.

XII-2.1.1. NECSA-1: Experiment 1 (all multicycle reactivity estimates)

While the benchmark specification itself is divided into a series of scenarios, in this Annex the results are structured as follows: Experiment 1 will refer to the multicycle reactivity estimation of the operational period from C1108-1 to C1211-1 (see Table XII-1). The result considered here is the accuracy of the k_{eff} estimate over and within these cycles. Full plant data for these cycles were provided in both a fine scale (data dump every 4 minutes) and a processed scale (multiday steps).

TABLE XII-1. SET OF CYCLES AND EXPERIMENTS PROVIDED

Cycle number	Experiments
C1108-1	Criticality and wire activation
C1109-1	Criticality, wires, control calibration
C1110-1	Criticality and wires
C1111-1	Criticality and wires
C1201-1	Criticality, wires, control calibration
C1202-1	Criticality and wires
C1203-1	Criticality and wires
C1204-1	Criticality, wires, control calibration
C1205-1	Criticality and wires
C1206-1	Criticality and wires
C1207-1,2,3,4	Criticality and wires
C1208-1	Criticality, wires, control calibration
C1209-1	Criticality and wires
C1210-1	Criticality and wires
C1211-1	Criticality, wires, control calibration

The main aim in Experiment 1 is to calculate the reactivity via core-follow analyses for all cycles with supplied operational data.

XII-2.1.2. NECSA-1: Experiment 2 (all Cu wire experiments)

This experiment contains a multiple set of Cu wire activation experiments performed at BOC of each cycle in the multicycle set. The Cu wire is inserted in every fuel element. Prior to the experimental cases, this scenario has a number of stepwise code-to-code tests defined in Scenarios A.1–A.4.

For each cycle, a Cu wire activation experiment is conducted at BOC at low power to estimate the flux profile in the centre of each fuel element (as well as fuel followers). After irradiation and cooling, the length of the wire is scanned in 2 cm segments and counts are captured. All counts, along with the time of counting for each segment, are provided to allow a comparison between calculated and measured activation rates in the wire.

The main aim in Experiment 2 is to perform the multicycle Cu wire activation experiments and not whether the burnup calculated by the participant in Experiment 1 shows any significant impact on the accuracy of the results over the operational year.

XII-2.1.3. NECSA-1: Experiment 3 (Scenario C in benchmark – all control rod calibration experiments)

In each cycle for which fresh control elements are loaded, control rod calibration experiments are performed at BOC. This occurs only for cycles C1109-1, C1201-1, C1204-1, C1208-1 and C1211-1. The compensation procedure applied is fully described and experimental data for differential and integrated rod worths are supplied in Ref. [XII-1].

The control rod calibration experiment is performed with the period method and the calibration of each rod is controlled with all five remaining rods in a bank.

XII-2.1.4. NECSA-2: Experiment 4 (Beryllium activation experiment)

In October 2011 and as part of the ageing management programme of the SAFARI-1 research reactor, the old beryllium reflector elements were replaced with a new set supplied by Brush Wellman. The operation with the old beryllium reflector spans 45 years of the reactor operation. All beryllium reflector elements were replaced, except A3 and A4. Two experiments were conducted to evaluate the effects associated with poison buildup in beryllium on the neutron flux and reactivity.

Two sets of experimental foil irradiation measurements were performed with 1% cobalt and nickel foils at the end of cycle C1108-1. In the first set of measurements, foils were irradiated in A5 and D2 hollow elements with the old set of reflectors in place; the second measurement set was performed with the new set, except for A3 and A4. The foils were irradiated at 2 MW for 30 minutes. The reactivity effects due to the beryllium reflector replacement were investigated.

The specifications of the old beryllium reflector elements (i.e. as at commissioning of the SAFARI-1 reactor in 1965) and the new set, installed in the reactor in October 2011, are given in Ref. [XII-1], along with the power and fluence history. Note that there were no ⁹⁹Mo rigs during the measurements. The summary of the measurements conducted and submitted as part of the specifications [XII-1] is provided in Table XII-2.

TABLE XII-2. SUMMARY OF THE EXPERIMENTAL MEASUREMENTS FOR BERYLLIUM ACTIVATION

Scenario	Scenario B2.1	Scenario B2.2 (foils case)	Scenario B2.3 (reactivity case)	Scenario B2.4 (reactivity case)	Scenario B2.5 (foils case)
Critical bank (mm)	624.0	Rods 1-4 & 6: 627.0 Rod 5: 628	Rods 1-4 & 6: 624.0 Rod 5: 604.5	Rods 1-4 & 6: 624.0 Rod 5: 516.7	Rods 1-4 & 6: 605.0 Rod 5: 604
Reactivity worth (\$)	-	-	0.15	0.55	-

In addition to the foil activation, reactivity effects accompanying the replacement were measured. The reactivity and foils activation measurements were conducted as follows:

1. Criticality case: the critical bank position was obtained with old beryllium reflectors in place for EOC C1108-1.
2. Foil activation: 1% Co and 100% Ni foil irradiation for 30 minutes at 2 MW with all old beryllium reflectors in place.
3. Criticality case: Replacement of the old two highest worth elements, i.e. D2 and F2 with the new reflector elements while keeping the rest of the old elements in place.
4. Criticality case: replacement of all the old elements with new ones, except for A3 and A4.
5. Foil activation case: 1% Co and 100% Ni foil irradiation for 30 minutes at 2 MW with new beryllium in place, except for A3 and A4.

XII-2.2. Summary of codes

A detailed description of the codes are available in the benchmark publication, and in this section only a mapping of experiments to code names are presented in Table XII-3.

TABLE XII-3. SUMMARY OF CODES USED PER COUNTRY

Country	Code (library)	Experiment / Scenario	Library
South Africa	OSCAR-5/Serpent	NECSA-1: Experiment 1 NECSA-1: Experiment 3	ENDF/B-VII.1
	OSCAR-5/MGRAC	NECSA-1: Experiments 1, 2, 3	WIMSE 172 group Christmas structure library
	OSCAR-5/MCNP6 FISPACT-II	NECSA-2: Experiment 4 NECSA-2: Experiment 4	ENDF/B-VII.1 -
Argentina	CONDOR-CITVAP	NECSA-1: Experiment 2	ESIN2001 library (69 energy groups)
	MCNP5	NECSA-1: Experiment 2	ENDF/B-VI.8
Romania	MCNPX and SCALE6	NECSA-2: Experiment 4	ENDF/B-VII.1

XII-2.3. Summary of models

This section provides a description of the computational models used for this benchmark, by various participants and experiments in the benchmark. Model descriptions are extracted from the individual country reports of participants.

XII-2.3.1. South Africa

The OSCAR-5 system [XII-2] was used to prepare a code independent model for the SAFARI-1 benchmark problem. Calculations were performed using ENDF/B-VII.1 in conjunction with Serpent [II-4] calculations. Fuel lattice cross-sections were in some cases calculated with the in-house HEADE code, which uses JEF-2.2 based cross-sections (WIMSE 172 group Christmas structure library).

This model was exported to Serpent to perform criticality and burnup analysis. The model was also used to generate a set of homogenized cross-sections and the associated nodal model for the deterministic nodal solver MGRAC, to perform criticality and burnup calculations. The homogenized model was developed via the COMPOSE subsystem of OSCAR-5. The grid on which homogenized cross-sections were generated is overlaid in Fig. XII-1.

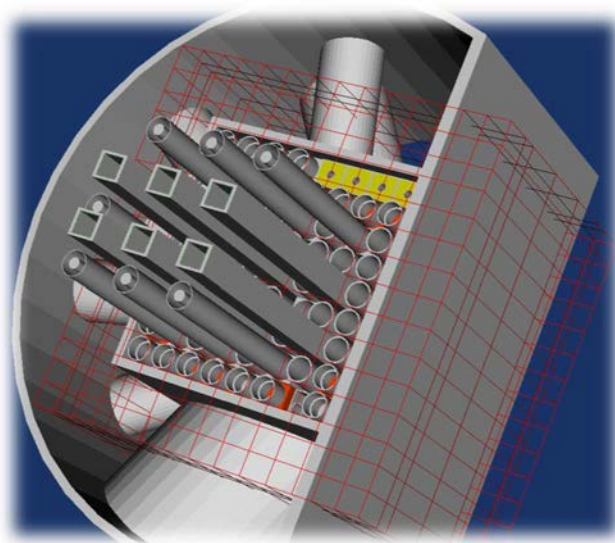


FIG. XII-1. View of the OSCAR-5 SAFARI-1 reactor model, with the nodal homogenization grid overlaid. (courtesy of Necsa, South Africa)

The nodal model is developed in a staged process, allowing control of the model error as compared to the reference heterogeneous Serpent model. In particular, all non-fuel homogenized multigroup cross-sections are generated from a set of 2-D full-core heterogeneous calculations, while fuel models are generated from an infinite lattice environment. Table XII-4 shows the staged results of the model building process and the numerical impact of approximations quantified at each step. From the table, it can be gathered how the impact of numerical approximations evolves as the model is built. This is done by firstly considering the impact of the homogenization approximations in 2-D, then adding infinite lattice cross-sections for fuel components, and finally in moving to 3-D.

TABLE XII-4. STAGED MODEL BUILDING

Model description	k_{eff}
Serpent 3-D rods mid core	1.09924 (± 0.00017)
Serpent 2-D ARO	1.33530
MGRAC 2-D ARO	15 pcm offset
MGRAC 2-D ARO with infinite fuel and follower replacements	300 pcm offset
Serpent 2-D ARI	1.05232
MGRAC 2-D ARI	180 pcm offset
MGRAC 2-D ARI with infinite fuel	690 pcm offset
MGRAC 3-D rods mid-core	380 pcm offset

The use of this approximate environment in generating fuel cross-sections introduces a numerical environmental offset in the nodal equivalence parameters. This bias (offset) can be seen when going from an MGRAC 2-D calculation to an MGRAC 2-D calculation with infinite fuel replacement. This bias is the largest for the all rods in (ARI) case because the fuel next to control rods sees a very different core environment than the fuel next to fuel (infinite fuel environment).

Finally, the step in going from a MGRAC 2-D model to a MGRAC 3-D model also introduces errors in the final homogenized representation of the core. This is because of axial leakage being taken into account in the 3-D model via diffusion theory.

It is important to note that this model building exercise was done with fresh fuel. As the reactor operates and fuel burns, this will no longer be the case. Furthermore, the reactor will typically operate with control rods somewhere between mid-core and all rods out (ARO), so one can expect the MGRAC model to be within roughly 400 pcm from reference and with a difference of 4.25% in assembly averaged power.

XII-2.3.1.1. Models for Experiment 1

The first experiment considered is a multicycle reactivity estimation over the provided cycles.

In order to reproduce the plant reactivity level, the operational data provided in the benchmark is converted to the code specific case data. Data in the benchmark were provided in two scales – fine scale data on the granularity of minutes, and aggregated data processed to steps in the order of days. Both data were considered. Some potential sources of variation in the obtained results are noted here:

- At the moment of the criticality case, the reactor is assumed to be operating in a steady-state condition. If this is not the case, due to recent control rod movement or ongoing xenon transients, the calculated k_{eff} might deviate from the typical critical offset.
- The loaded rig-state of the reactor is not provided as part of the plant data and, thus, the on-line loading of samples and targets will cause additional noise in the calculated reactivity. Furthermore, an approximate homogenized model of the fuelled target plates is provided in the benchmark specification, and this could bias the results somewhat.

Both the MGRAC and Serpent models were utilized to model this experiment.

XII-2.3.1.2. Models for Experiment 2

The experiment is modelled utilizing the MGRAC SAFARI-1 model. The model contains a point copper detector in the centre of each element, but does not include the water displacement effect of the aluminium sword on which the wire is mounted. The nodal solver MGRAC performs flux reconstruction to estimate the intra-nodal flux shape within the fuel assembly, and then integrates the reconstructed flux at the assembly centre with the detector cross-section to determine an activation rate for the wire in the given position. This experiment is not modelled with the Serpent core model.

XII-2.3.1.3. Models for Experiment 3

Control rod calibration simulations are performed each time SAFARI-1 loads a new control rod into the core. During the cycles considered, five such experiments were performed, specifically for cycles 1109-1, 1201-1, 1204-1, 1208-1 and 1211-1.

For every cycle, each rod is calibrated individually, with the remaining rods grouped as a bank in order to compensate for the calibrated rod's movement. An OSCAR-5 calculation is set up to simulate each of the control rod calibration experiments. Thus, a calculation is done for each rod individually, where the bank and rod positions match the measured positions exactly. These calculations are run and the k_{eff} values are obtained at each control rod positions in the experiment. The incremental rod worth (cents) for each step j (with a new control rod position) is calculated as follows:

$$\text{rod worth}_j = 100 \times \frac{1}{\beta_{\text{eff}}} \frac{k_{j+1} - k_j}{k_{j+1} \times k_j} \quad (\text{XII-1})$$

The value for $\beta_{\text{eff}} = 0.0075$ is the same as that used by the reactivity meter in SAFARI-1. The set of rod worths for each control rod is used to calculate the differential and integral rod worths for each rod, and the calculated integral rod worths, or S-curves, are plotted against the measured curves.

Both the MGRAC and Serpent models are utilized to model this experiment.

XII-2.3.1.4. Models for Experiment 4

The model from the previous experiments can be largely re-used for this case, with the exception of foil activation structures. The experimental foil holder as well the holder's detailed model in MCNP [XII-4, XII-5] is shown in Fig. XII-2.

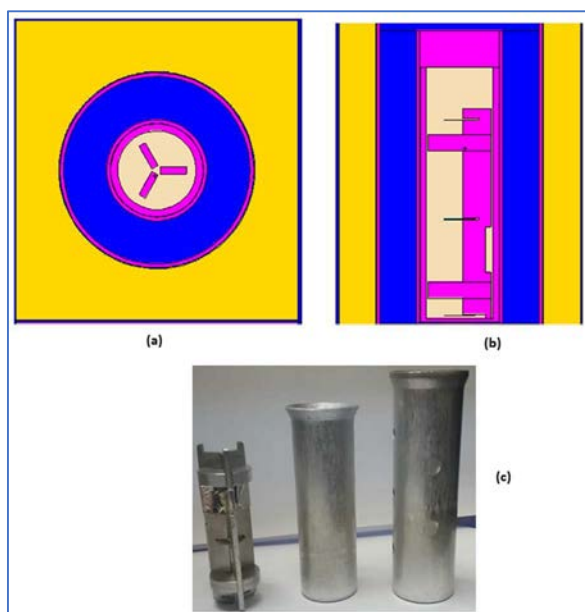


FIG. XII-2. Foil irradiation in hollow beryllium element: (a) radial view and (b) axial view of the foils holder's MCNP model, (c) Aluminium foil holder, rabbit, Aluminium holder. (courtesy of Necsa, South Africa)

All the above-mentioned cases were modelled in the detailed MCNP model with the correct beryllium reflectors and fuel isotopic composition. The fuel isotopic composition was obtained from the OSCAR-4 calculations, and the beryllium reflector isotopic composition for the old beryllium reflectors, after 45 years of reactor operation, was calculated using FISPACT-II. A radial view of the detailed MCNP SAFARI-1 model is shown in Fig. XII-3.

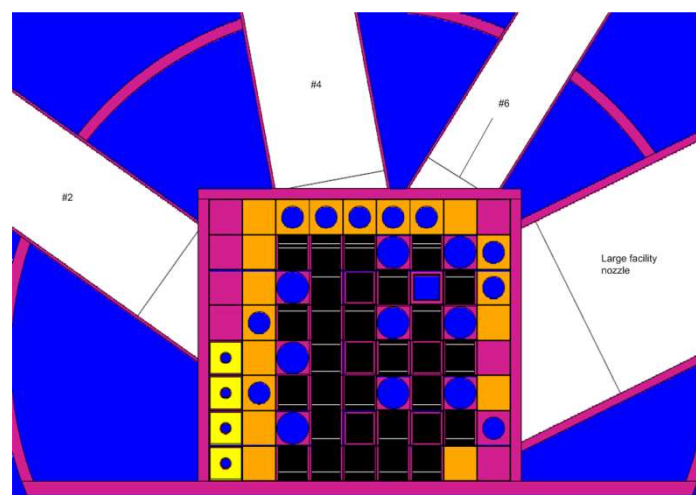


FIG. XII-3. Radial view of the SAFARI-1 MCNP model by Necsa. (courtesy of Necsa, South Africa)

XII-2.3.2. Argentina

This section describes the calculational contribution provided by INVAP (Argentina) to NECSA-1.

The cases calculated are presented in Table XII-5, where the main calculation scope and codes are described, with references to individual scenarios (which are detailed in Ref. [XII-1]).

TABLE XII-5. INVAP PROPOSED NEUTRONIC ANALYSIS ALTERNATIVES FOR SAFARI-1 BENCHMARK

#	Proposed calculation scheme	Calculation results to be presented
1	CONDOR-CITVAP	<ul style="list-style-type: none"> ✓ Scenario A.1: criticality calculations for the fresh core for different control rod configurations (all rods in 0%, 50% and 100%, code-to-code comparison) ✓ Scenario A.2: criticality calculations at BOC for C1211 cycle for different control rod configurations (all rods in 0%, 50% and 100%, code-to-code comparison) ✓ Scenario A.5: control rods calibration at BOC for C1211 cycle (comparison with experimental data)
2	MCNP5-1.60	<ul style="list-style-type: none"> ✓ Scenario A.1: criticality calculations for the fresh core

The following sections present the models developed and the results obtained for each case, where the comparisons with measured data reported by SAFARI-1 were carried out.

XII-2.3.2.1. Models for Experiments 1, 2 and 3 with CONDOR-CITVAP

A full 3-D model of the SAFARI-1 reactor was developed using the deterministic line CONDOR-CITVAP [XII-6], following a cell-core calculation scheme (Figs XII-4 and XII-5). The cross-section library used for all CONDOR-CITVAP calculations was the ESIN2001 library (69 energy groups).

The model for the fuel assemblies consisted of a symmetry segment of one-fourth of the assembly as shown in Fig. XII-6. The macroscopic cross-sections were homogenized in a single zone corresponding to the total volume of the grid position.

Three models were developed for the control assemblies, one for each axial zone of the component (the absorber zone, the follower zone and the coupling zone). The control assembly was surrounded by a homogeneous material representing the adjacent fuel elements.

The cell model for fuel, as an example of the modelling approach, is shown in Fig. XII-4.

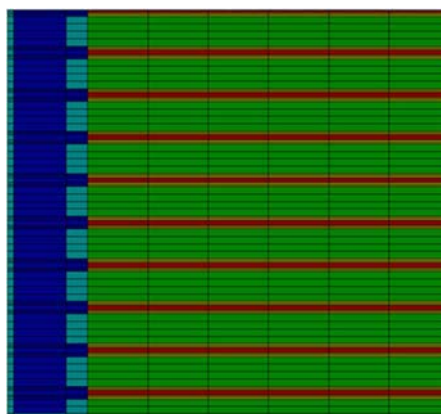


FIG. XII-4. Standard fuel element – Cell level model (CONDOR) by INVAP to indicate the collision probability meshing scheme. (courtesy of INVAP, Argentina)

Individual cell models were developed for the aluminium, graphite and beryllium reflectors as well as the molybdenum irradiation devices, the beam tubes and the core box.

The 3-D core model was developed using CITVAP (Fig. XII-5), representing the different components of the reactor which included the core box and the beam tubes. The following considerations were taken into account in the creation of the model:

- Only the active length of the core was considered in the model for the case of fuel assemblies, reflectors and irradiation devices;
- The total volume associated with the travel distance of the rods was considered in the model for the case of the control assemblies;
- The beam tubes were modelled as cuboids that maintained their total volume.

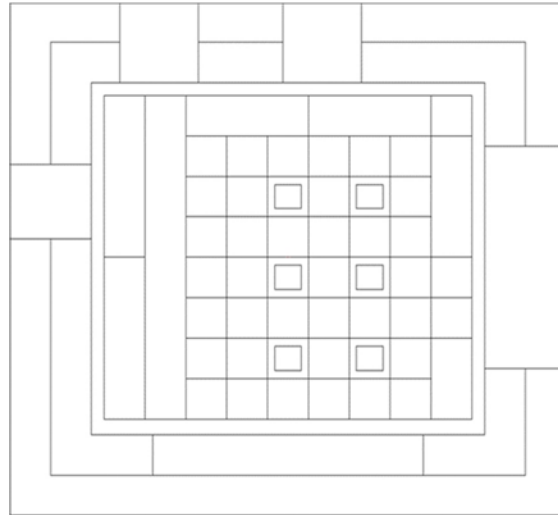


FIG. XII-5. Core model (CITVAP) by INVAP. (courtesy of INVAP, Argentina)

XII-2.3.2.2. Models for Experiment 1 with MCNP5

The calculations proposed in Scenario A.1 were evaluated using a full 3-D MCNP model of the SAFARI-1 reactor (Fig. XII-6). This alternative methodology provided results that were used to verify the ones obtained with the CONDOR-CITVAP model for the same scenario.

A full 3-D model of the fresh core was developed, which considered its different components, including the core box and the beam tubes. Once again, for the majority of the components only the active length of the core was considered in the model, except for the control assemblies, where all the travel distances of the rods were modelled. All calculations were performed using ENDF/B-VI.8 nuclear data libraries.

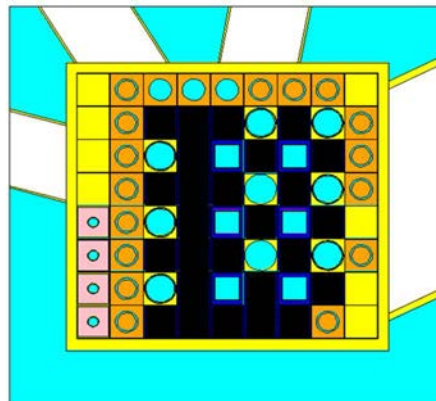


FIG. XII-6. MCNP model for the core. (courtesy of INVAP, Argentina)

XII-2.3.3. Romania

This section describes the contribution from Romania to the NECSA-2, related to the poison concentration buildup in beryllium reflector elements. Calculations were performed for Experiment 4.

XII-2.3.3.1. Models for Experiment 4

The MCNPX model of the SAFARI-1 reactor is shown in Fig. XII-7.

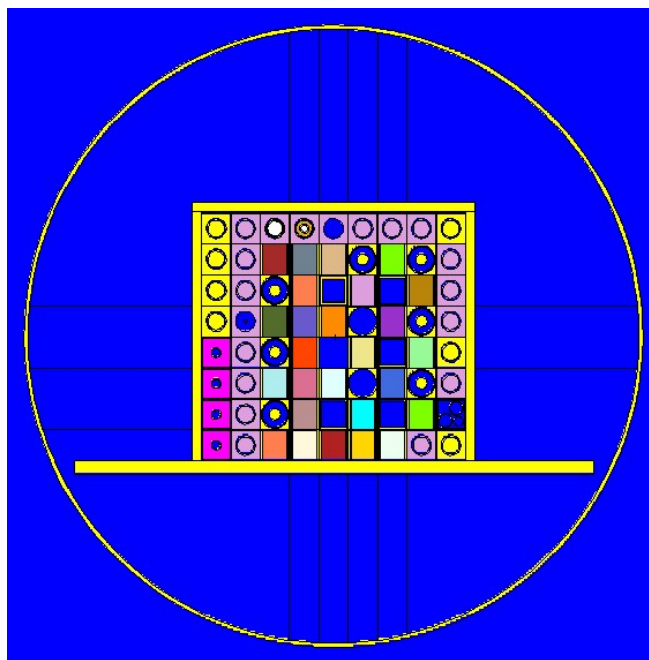


FIG. XII-7. Radial view of the Romanian MCNPX model for the SAFARI-1 reactor. (courtesy of INR, Romania)

The number densities of fuel assemblies provided in Ref. [XII-1] were transferred to the MCNPX [XII-4, XII-8] model. The D2 beryllium reflector was modelled as a solid element for reactivity calculations and the beam tubes were not modelled. The MCNPX model uses 30 inactive cycles and 9970 active cycles with 5000 particles history, resulting in a standard deviation of less than 11 pcm. MCNPX was used for reactivity calculations.

The SCALE 6 [XII-7] module CSAS1X was used to generate 44 group cross-section libraries, which were then used in COUPLE to generate an ORIGEN-S activation cross-section library. Similar to FISPACT, ORIGEN-S was used to compute isotopic evolution in beryllium reflector elements.

XII-3. RESULTS

This section provides an overview of the major results presented by each of the countries involved in calculating the SAFARI-1 benchmark.

XII-3.1. Results of the individual participant contributions

In this section, the results obtained by the individual participants are presented.

XII-3.1.1. South Africa

XII-3.1.1.1. Experiment 1

Prior to performing the experimental modelling, Ref. [XII-1] contains a number of purely numerical cases for code-to-code comparison, as confirmation that the base model is set up correctly between participants. The results from using OSCAR-5/MGRAC are presented in Tables XII-6 and XII-7.

Preliminary code-to-code results for numerical comparison of a fresh core

Table XII-6 presents the reactivity of the core for different configurations of the control assemblies (0%, 50% and 100%) that were obtained using the OSCAR-5 model for the fresh core.

TABLE XII-6. NUMERICAL FRESH CORE RESULTS OBTAINED USING OSCAR-5/MGRAC MODEL

CR position	k_{eff} : no target rig	k_{eff} : target loaded
0%	1.19104	1.20569
50%	1.06273	1.07879
100%	0.94306	0.96793

Preliminary code-to-code results for numerical comparison of a burned core

Table XII-7 presents the results of repeating the calculations of Scenario A.1 at BOC for cycle C1211.

TABLE XII-7. NUMERICAL BURNED CORE RESULTS OBTAINED USING OSCAR-5/MGRAC MODEL

CR position	k_{eff} : no target rig	k_{eff} : target loaded
0%	1.07519	0.87063
50%	0.94289	0.96276
100%	0.84278	1.09362

Multicycle reactivity results

The primary result for this experiment is the final reactivity comparison over the one year operational period, which forms part of Scenario C in the benchmark specification. The OSCAR-4/MGRAC results and the Serpent results are shown in Fig. XII-8.

The initial cycles show some multicycle trends as the effect of the provided initial number densities ‘burn out’, but after four to five cycles the level mostly stabilizes. After filtering out the outliers, the average value and standard deviation of the multicycle k_{eff} yields 1.00508 and 537 pcm, respectively, for OSCAR-5/Serpent, whereas the corresponding values for OSCAR-5/MGRAC are 1.00329 and 417 pcm.

The multicycle analysis above was conducted by processing the detailed plant data. Figure XII-9 reports the same results, but compares the OSCAR-5/MGRAC models between the usage of the aggregated data (provided as an option in the benchmark specification) to the detailed plant data.

The choice of data aggregation method clearly creates a critical offset in the estimated k_{eff} values, but with very similar standard deviation values. The aggregated data set exhibits an average k_{eff} value of 0.99880 with a standard deviation of 560 pcm. The aggregated data were generated via an automated algorithm which aims to detect sharp changes in plant data, while the detailed processing was conducted by creating steps via manual observation of the data.

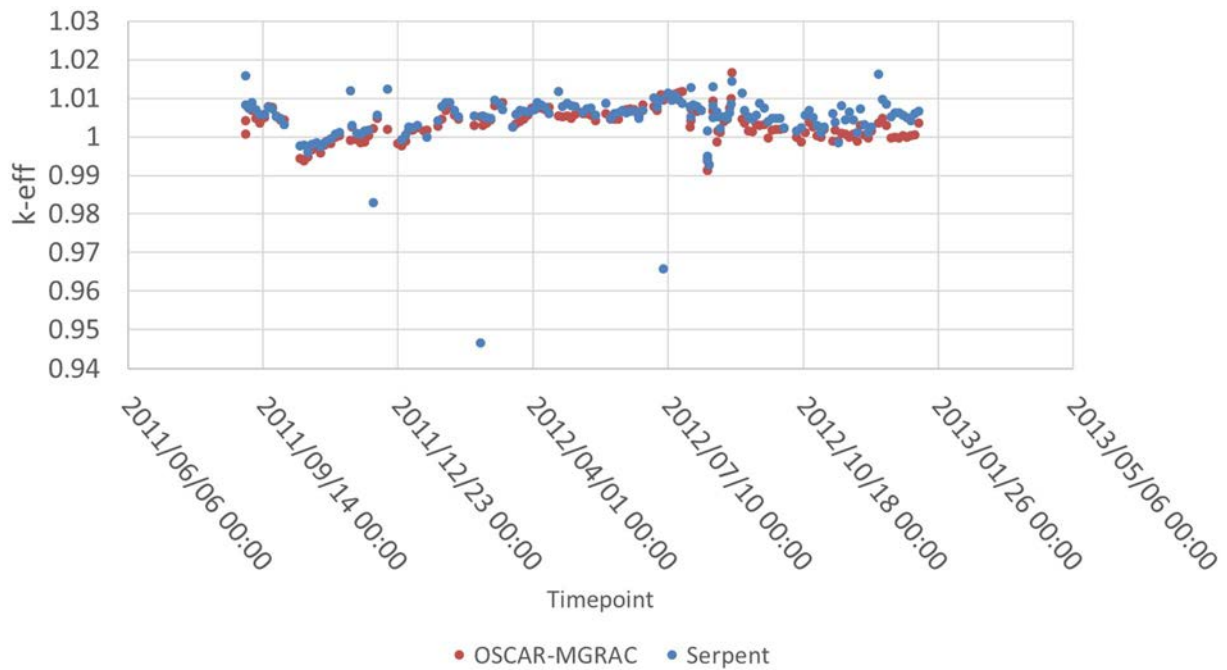


FIG. XII-8. OSCAR-5 Reactivity estimates for cycles C1108-1 to C1211-1 by Necsa. (courtesy of Necsa, South Africa)

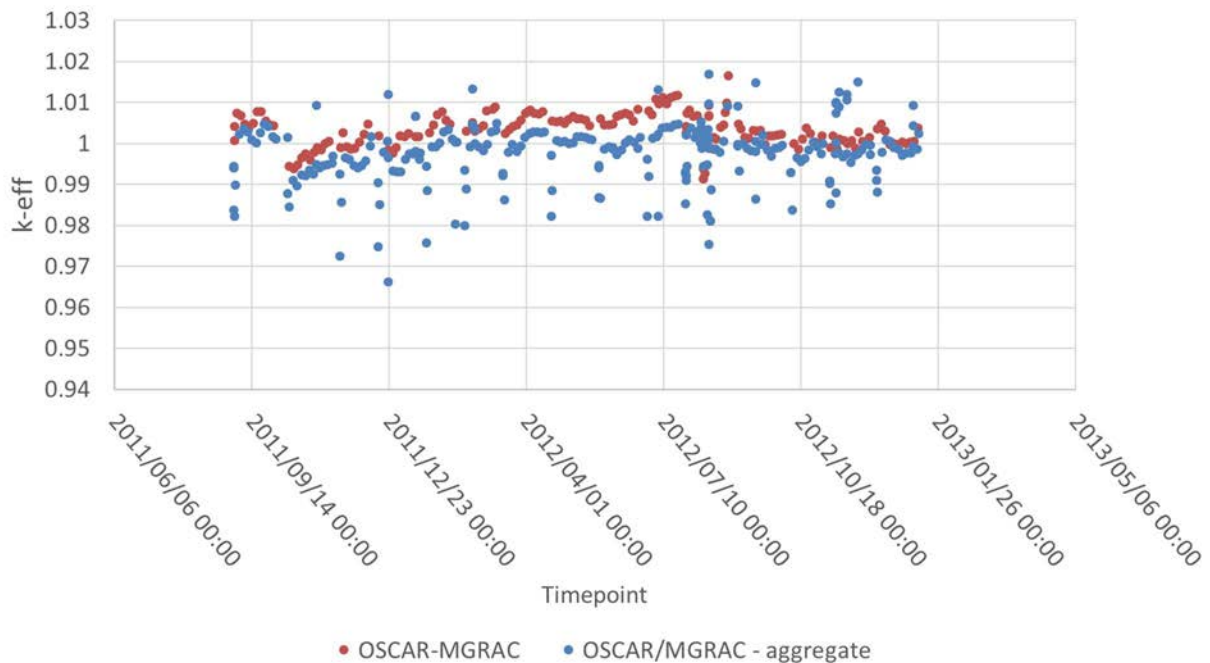


FIG. XII-9: OSCAR-5 Reactivity estimates for cycles C1108-1 to C1211-1 for both the direct plant data processing and the provided aggregated data by Necsa. (courtesy of Necsa, South Africa)

More results are included in the country specific report, such as maps of ^{235}U assembly masses at the end of the multicycle depletion period.

XII-3.1.1.2. Experiment 2

Detailed OSCAR-5/MGRAC Cu wire activation rates are presented as well as the associated results template for each wire, in every cycle. Of interest is the average deviation compared to the experimental value per position, as analysed over the set of provided cycles (Fig. XII-10).

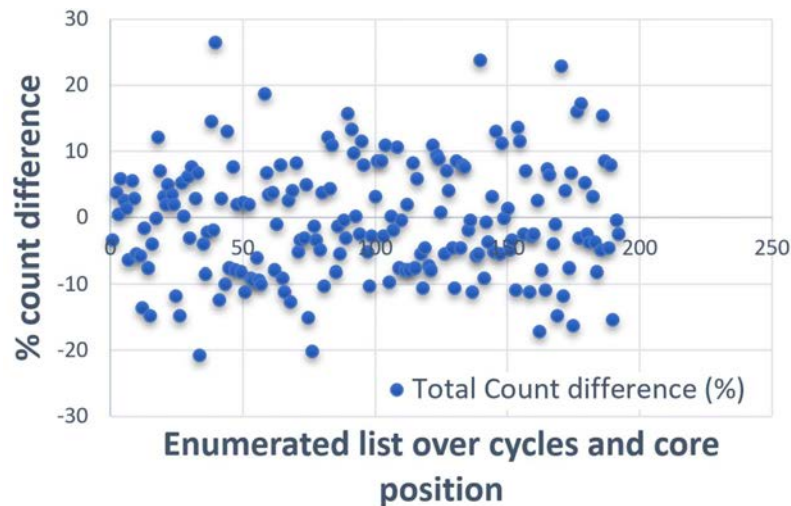


FIG. XII-10. OSCAR-5/MGRAC activation percentage difference per position for cycles C1108-1 to C1211-1 – plot for all core positions over all cycles. (courtesy of Necsa, South Africa)

The average total count per position deviation to experiment is 6.4%, with a standard deviation of 4%. This calculation was only performed with the OSCAR-5/MGRAC model. Given that the experimental uncertainty is expected to be between 5% and 10% for individual count measurements, these values compare well over the multicycle period, and indicate that the burnup calculation (for which this experiment acts as a proxy) is conducted with consistent accuracy.

XII-3.1.1.3. Experiment 3

Detailed control rod calibration curves are presented in the associated results template for each rod and for every cycle that calibration experiments are conducted in. Of interest is the average total worth deviation compared to the experimental value per position, as analysed over the set of provided cycles (Fig. XII-11).

The difference in total worth estimate per rod, as tabulated over all the cycles in which the control rod calibration experiment was conducted, shows good agreement between OSCAR-5/MGRAC and OSCAR-5/Serpent. Statistically, the two models show similar offset trends, with the OSCAR-5/Serpent model exhibiting an average offset of 40 cents and a standard deviation of 29 cents. The OSCAR-5/MGRAC model shows an average offset of 35 cents and a standard deviation of 26 cents.

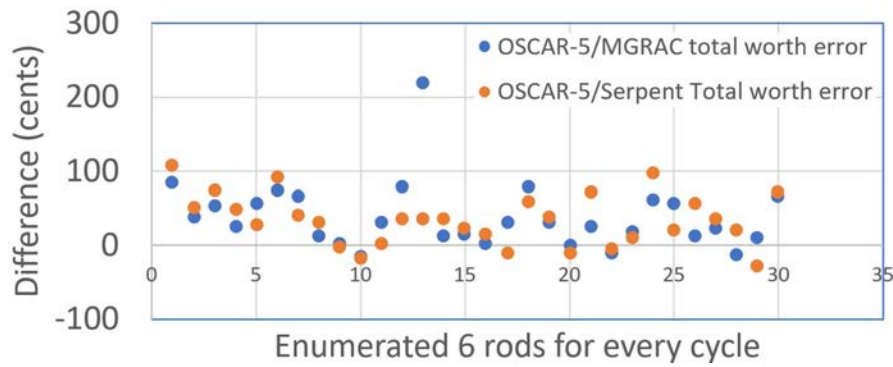


FIG. XII-11. OSCAR-5 control calibration error per position for cycles C1108-1 to C1211-1. (courtesy of NeCSA, South Africa)

XII-3.1.1.4. Experiment 4

The MCNP code criticality calculations were performed with 1×10^5 particle histories, 100 inactive cycles and 500 active cycles resulting in a standard deviation of less than 12 pcm. The comparisons of the measured and calculated activities for both foils are given in Tables XII-8 and XII-9. The reactivity results are found in Table XII-10.

The calculated results of both foils for the old and new beryllium reflectors underestimate the measured results by between 3% and 30%. The results of the old beryllium reflector seem to compare better than those of the new set when compared to measured activities. In general, the nickel foil result appears to be the worst.

TABLE XII-8. MEASURED AND CALCULATED (MCNP AND FISPACT) ACTIVITIES FOR THE OLD BERYLLIUM REFLECTOR BY NECSA

Foil	Beryllium position	Axial position	Measured activity (Bq/g)		Calculated activity (Bq/g)		C/E
			Present	Discharge	Present	Discharge	Discharge
Co-59	A5	D1 (top)	3.550E+05	3.564E+05	4.24E+05	4.257E+05	1.19
Ni-58		Y7 (middle)	4.010E+05	4.603E+05	4.46E+05	5.111E+05	1.11
Co-59		D2 (bottom)	3.600E+05	3.622E+05	4.35E+05	4.371E+05	1.21
Co-59	D2	D3 (top)	3.700E+05	3.718E+05	3.82E+05	3.839E+05	1.03
Ni-58		Y8 (middle)	3.320E+05	3.810E+05	4.23E+05	4.849E+05	1.27
Co-59		D4 (bottom)	3.660E+05	3.675E+05	3.91E+05	3.928E+05	1.07

TABLE XII-9. MEASURE AND CALCULATED (MCNP AND FISPACT) ACTIVITIES FOR THE NEW BERYLLIUM REFLECTOR BY NECSA

Foil	Beryllium position	Axial position	Measured activity (Bq/g)		Calculated activity (Bq/g)		C/E
			Present	Discharge	Present	Discharge	Discharge
Co-59	A5	D7 (top)	3.950E+05	3.971E+05	4.50E+05	4.521E+05	1.14
Ni-58		S1 (middle)	3.650E+05	4.185E+05	5.20E+05	5.969E+05	1.43
Co-59		D8 (bottom)	4.180E+05	4.206E+05	4.85E+05	4.878E+05	1.16
Co-59	D2	D9 (top)	3.660E+05	3.681E+05	4.01E+05	4.032E+05	1.10
Ni-58		S2 (middle)	3.180E+05	3.648E+05	4.15E+05	4.755E+05	1.30
Co-59		E1 (bottom)	3.690E+05	3.713E+05	4.36E+05	4.385E+05	1.18

TABLE XII–10. REACTIVITY WORTH DUE TO BERYLLIUM REFLECTOR REPLACEMENT

Scenario	All old Beryllium reflectors	New D2 and F2 Beryllium reflectors	All new Beryllium reflectors
Critical bank (mm)	All rods: 604.5	Rods 1–4 & 6: 624.0 Rod 5: 604.5	Rods 1–4 & 6: 624.0 Rod 5: 516.7
Measured worth (\$)	–	0.15	0.55
Calculated worth (\$)	–	0.07	0.60

XII–3.1.2. Argentina

Not all the experiments were fully performed by Argentina. The focus of Argentina was to calculate the start-up experiments mostly found in Scenario A.5 of the benchmark specification. This included a few test cases for Experiment 1 (mostly fresh core), a single cycle set of Cu wire experiments as per Experiment 2 (for cycle C1211-1), and a single cycle set of control rod calibration experiments as per Experiment 3 (also for cycle C1211-1).

XII–3.1.2.1. Experiment 1

Scenarios A.1, A.2 and A.5 were evaluated using the CONDOR-CITVAP model. The following tables in this section present the results.

Numerical results for fresh core criticality cases, for code-to-code comparison

Table XII–11 presents the reactivity of the core for different configurations of the control assemblies (0%, 50% and 100%) that were obtained using the CONDOR-CITVAP model for the fresh core.

TABLE XII–11. NUMERICAL FRESH CORE RESULTS OBTAINED USING THE CONDOR-CITVAP MODEL BY INVAP

CR position	Reactivity [pcm]
0%	17 510
50%	8 880
100%	–2 450

Numerical results for burned core criticality cases, for code-to-code comparison

Table XII–12 presents the results of repeating the calculations from the previous section, but for the condition of BOC for cycle C1211 (burned core).

TABLE XII–12. NUMERICAL BURNED CORE RESULTS OBTAINED USING THE CONDOR-CITVAP MODEL BY INVAP

CR position	Reactivity [pcm]
0%	6 690
50%	–4 240
100%	–15 820

XII–3.1.2.2. Experiment 2

A comparison between a copper wire activation experiment and a calculation was performed using the CONDOR-CITVAP model.

In the experiment, the wires were loaded into the core, which was operated at low power for a short period of time, and then unloaded and measured.

Some of the information needed for the comparison between the calculation and the experimental data presented was assumed, namely:

1. Control rod configuration;
2. Position of the wires in the XY plane;
3. Normalization factor of the axial profile.

The reactor was set in a critical state using the six control rods as a single bank. The position of the wires was assumed in the geometrical centre of the fuel assembly and the different curves were normalized using the wire with the maximum number of counts.

The comparison was performed for a reference position (B3 in the reactor grid) as shown in Fig. XII-12. INVAP already superimposed their results on the calculated results supplied by the data provider (Necsa). The differences are discussed in Section XII-3.2.

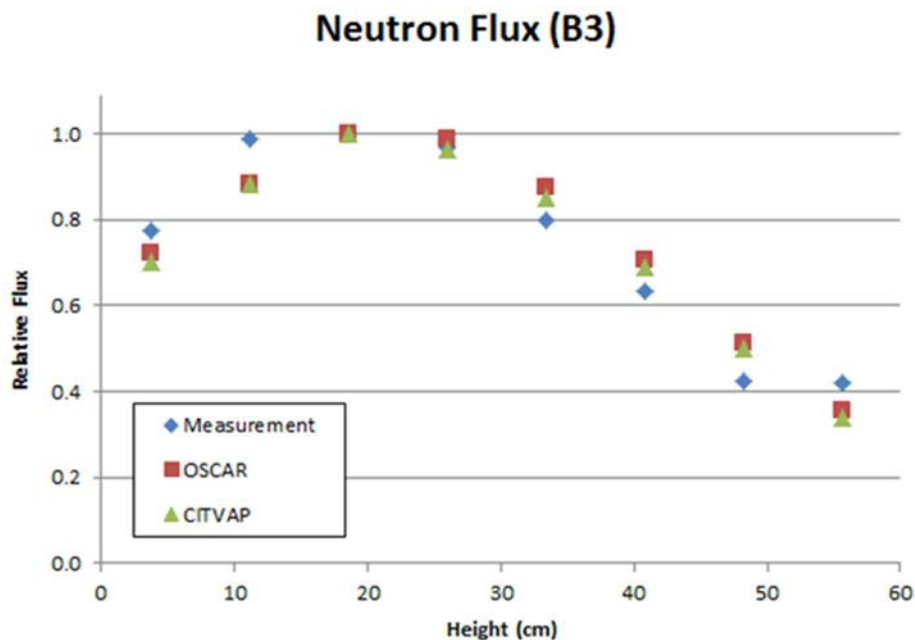


FIG. XII-12. Relative flux profile in position B3 showing both INVAP and Necsa results. (courtesy of INVAP, Argentina)

Results of the comparison show a good agreement between the shape of the flux profile obtained by calculation and in the experiment carried out in the position of the grid analysed. However, in order to compare the difference in the absolute values of the flux, additional information is needed.

XII-3.1.2.3. Experiment 3

Experiment 3 in general refers to control rod calibration experiments for all cycles for which data were provided. INVAP performed these calibrations with CONDOR-CITVAP, and specifically for cycle C1211-1. The total control rod worths are given in Table XII-13.

TABLE XII-13. COMPARISON BETWEEN CALCULATION AND EXPERIMENT OF THE TOTAL REACTIVITY WORTH OF THE CONTROL RODS BY INVAP, CALCULATED WITH CONDOR-CITVAP

CR	Grid position	Calculated total worth [cents]	Measured total worth [cents]	Difference [%]
1	C5	539.1	519.1	3.9
2	C7	336.3	348.4	-3.5
3	E7	385.8	381.9	1.0
4	G7	257.0	287.3	-10.5
5	G5	401.2	386.9	3.7
6	E5	610.2	564.6	8.2

The results showed a good agreement with the experimental data. The absolute value of the differences found in the total worth of the control rods varied between 1.0% and 10.5%.

XII-3.1.3. Romania

XII-3.1.3.1. Experiment 4

The calculational results obtained by Romania are summarized in Table XII-14..

TABLE XII-14. CALCULATIONAL OF BERYLLIUM POISON EFFECT USING MCNPX BY ROMANIA

Scenario	Critical bank prior	k_{eff}	Std. dev. (pcm)	Critical bank for partial replacement ^{1,2}	k_{eff}	Std. dev. (pcm)	Critical bank for full replacement ^{1,2}	$k_{eff}^{1,2}$	Std. dev. (pcm)
Critical bank (mm)	624.0	1.00120	11	Rods 1-4 & 6: 624.0 Rod 5: 604.5	1.00220	11	Rods 1-4 & 6: 624.0 Rod 5: 516.7	1.00591	11
Reactivity worth (\$)	-			0.1329 ± 0.021			0.6236 ± 0.021		

¹ The bank rods position remained the same: 624.0.

² All these results were obtained considering that the D2 beryllium block was solid. MCNPX input used 30 inactive cycles and 9970 active cycles of 5000 particles each.

For the foil measurements, 1% Co/Al foils and Ni foils in the A5 and D2 positions were calculated for cycle C1108-1 in terms of Bq/g foil, to allow comparison with the benchmark data. The rabbit was modelled and placed at axial fuel midheight. For the measurements, the reactor power level was 2 MW for 1% Co/Al foils, and 2.1 MW for Ni. The rates of the (n,p) reaction on ⁵⁸Ni and (n, γ) on ⁵⁹Co were normalized at these power levels. The specific activity was:

$$A = R \cdot (1 - \exp(-\lambda t)) \quad (\text{XII-2})$$

where R is the saturation specific activity and λ is the decay constant; the time t was 20 min in each case.

The calculated data compared with the benchmark data from Table XII–12 and Table XII–13 are presented in Table XII–15.

TABLE XII–15. ACTIVITY OF FOILS, CALCULATED AND EXPERIMENTAL VALUES

Reflector block	Ni		Co	
	Calc. (10^5 Bq/g foil)	Exp. (10^5 Bq/g foil)	Calc. (10^5 Bq/g foil)	Exp. (10^5 Bq/g foil)
A5	2.86	4.60	6.52	3.56
D2	2.46	3.81	6.79	3.72

XII–3.2. Comparison and discussion of the individual results

This section highlights the level of consistency, or lack thereof, between individual participant results performed for the same experiments. In this particular benchmark, which contains a combination of multicycle depletion, snap-shot flux and rod worth experiments for multiple cycles and beryllium activation experiments, only a small subset of experiments shows overlapping results between participants. These areas of overlapping are discussed in this section.

XII–3.2.1. Experiment 1

Although only South Africa perform the multicycle depletion analysis, Argentina did calculate the fresh and burned core verification cases (Tables XII–16 and XII–17).

TABLE XII–16. RESULTS OF SCENARIO A.1 COMPARED BETWEEN SOUTH AFRICA AND ARGENTINA, WITH TARGET RIGS LOADED

CR position	Argentina CONDOR-CITVAP: Reactivity [pcm]	Argentina MCNP: Reactivity [pcm]	South Africa OSCAR-5/MGRAC: Reactivity [pcm]
0%	17 510	17 080	17 060
50%	8 880	7 860	7 306
100%	–2 450	–2 880	–3 300

TABLE XII–17. RESULTS OF SCENARIO A.2 COMPARED BETWEEN SOUTH AFRICA AND ARGENTINA, WITH TARGET RIGS LOADED

CR position	Argentina CONDOR-CITVAP: Reactivity [pcm]	South Africa OSCAR-5/MGRAC: Reactivity [pcm]
0%	6 690	8 560
50%	–4 240	–3 868
100%	–15 820	–14 859

The above tables generally indicate reasonable agreement, with all reactivity states differing by less than 1000 pcm, with the exception of the all-rods out case for the burned core in Table XII–17, which differs by almost 2000 pcm. However, since these are code-to-code comparisons, one would have expected somewhat better agreement. These differences will have to be further investigated, and the further results for the NECSA-1 experiments have to be monitored to see whether these differences translate to the experimental analysis cases.

XII-3.2.2. Experiment 2

Experiment 2 spans the Cu wire experiments over the full set of provided cycles. Overlapping results between participants occur only with regard to cycle C1211-1, and in particular with regard to the wire activation shape in core position B3.

The South Africa result with OSCAR-5/MGRAC and the Argentina result with CONDOR-CITVAP are compared in Fig. XII-14. The comparison shows very good agreement in this specific core position, with both shape and level agreeing well between experiment and both calculational submissions (within a few percent per axial position).

Results by South Africa for the other cycles showed that the general quality of comparisons over multiple cycles and core positions shows a standard deviation of 10% to 15% in terms of assembly averaged wire activation rate. From this perspective, core position B3 in cycle C1211-1 exhibits exceptionally good agreement.

XII-3.2.3. Experiment 3

Experiment 3 spans the control rod calibration experiments over the full set of provided cycles. Overlapping between participants occur only with regard to cycle C1211-1. The results are compared in Table XII-18.

TABLE XII-18. COMPARISON BETWEEN CALCULATION AND EXPERIMENT OF THE TOTAL REACTIVITY WORTH OF THE CONTROL RODS (CR)

CR	Grid position	Argentina:	South Africa:	South Africa:
		Calculated total worth [cents] (rel. % difference to measurement)	OSCAR-5/ MGRAC Calculated total worth [cents] (rel. % difference to measurement)	OSCAR-5/ Serpent Calculated total worth [cents] (rel. % difference to measurement)
1	C5	539.1 (3.9%)	575.1 (10.7%)	538.9 (3.8%)
2	C7	336.3 (-3.5%)	362.2 (3.9%)	406.1 (16.5%)
3	E7	385.8 (1.0%)	406.4 (6.4%)	417.4 (9.3%)
4	G7	257.0 (-10.5%)	275.4 (-4.1%)	307.9 (7.1%)
5	G5	401.2 (3.7%)	398.5 (3%)	359.1 (-7.1%)
6	E5	610.2 (8.2%)	630.6 (11.7%)	636.6 (12.7%)

From the total worth comparisons, it can be concluded that all three sets of results agree well with the measured worths, and all the contributions are, excluding single outliers, within approximately 10%. The calculated worths from South Africa are, for almost all cases, slightly higher than those from Argentina.

If the multicycle accuracy presented by South Africa in Fig. XII-13 is being considered over all the available control rod calibration experiments, it can be seen that the offsets observed in this cycle, by all participants, are typical of the behaviour over all cycles. A possible source of this general overestimation could be the fact that no participant has modelled the depletion of the control absorber (cadmium box) over the six cycles for which a follower control assembly is resident in the core. However, this aspect has not yet been investigated.

XII-3.2.4. Experiment 4

The consolidated results on calculated and measured activities for South African and Romanian submissions are summarized in Tables XII-19 and XII-20. The activation results reflect two measurement points for cobalt and one for nickel in each position in accordance with the experiment.

It can be seen from the activation results that, in general, the calculated results do not compare particularly well to the experimental measurements for both countries. The Romanian result shows a general overestimation in the cobalt results and a slight underestimation of the nickel result. The South African calculation also somewhat overestimated the measured results for both old and new reflector elements. These differences can in general be attributed to both spectral and spatial flux shape bias in the calculation of the long term buildup of the poison concentration in the reflector elements.

TABLE XII-19. CONSOLIDATED RESULTS FOR OLD/IRRADIATED BERYLLIUM REFLECTOR ACTIVATION

Position	South Africa		Romania		Measured	
	Nickel	Cobalt	Nickel	Cobalt	Nickel	Cobalt
Discharged Activity (10^5 Bq/g)						
A5	5.11	4.26	2.67	6.22	4.60	3.56
		4.37				3.62
D2	4.85	3.84	2.23	6.19	3.81	3.72
		3.93				3.68

TABLE XII-20. CONSOLIDATED RESULTS FOR NEW/FRESH BERYLLIUM REFLECTOR ACTIVATION

Position	South Africa		Romania		Measured	
	Nickel	Cobalt	Nickel	Cobalt	Nickel	Cobalt
Discharged activity (10^5 Bq/g)						
A5	5.97	4.52	2.80	6.50	4.19	3.97
		4.88				4.21
D2	4.75	4.03	2.52	6.32	3.65	3.68
		4.38				3.71

These differences could be as a result of misinterpretation or even shortages of the benchmark specification data as well as the use of a different model approach in calculating the problem. The approaches used by both participants in accounting for calculating the beryllium isotopic evolution over the 45 years could also be a contributing factor. The reactivity results are summarized in Table XII-21.

The reactivity results of both participants for Scenario B2.3 (see Table XII-2) are lower than the measured values, with South African result showing a particularly large underestimation (almost 50%) for the partial replacement case, but good agreement for the full case. Good agreement is achieved for both replacement steps in the case of the Romanian results. In general, the effects of beryllium poisoning can be clearly observed in all the cases.

TABLE XII-21. CONSOLIDATED REACTIVITY RESULTS COMPARED TO MEASUREMENTS

Scenario	All old Beryllium reflectors	New D2 and F2 Beryllium reflectors	All new Beryllium reflectors
Critical bank (mm)	All rods : 624.0	Rods 1-4 & 6: 624.0 Rod 5: 604.5	Rods 1-4 & 6: 624.0 Rod 5: 516.7
Measured worth (\$)	–	0.15	0.55
South Africa Calculated worth (\$)	–	0.07	0.60
Romanian Calculated worth (\$)	–	0.13	0.62

XII-3.3. Conclusions

NECSA-1 and NECSA-2 spans four experiments: the first relates to multicycle depletion modelling, enumerated by Experiments 1–3 in this Annex; the second relates to the activation of beryllium reflector elements and the associated buildup of neutron poisons in the beryllium elements, given as Experiment 4 in this Annex.

The specification of the facility is quite detailed, and associated experimental data are available in various levels of granularity. However, no direct burnup measurement information on the fuel assemblies are provided, and depletion can only be indirectly evaluated via reactivity, Cu wire activation and control rod worth experiments. The benchmark also contains a series of intermediate code-to-code results, useful for confirming that the modelling is reasonable prior to engaging full modelling for recreating the experimental conditions.

The coverage from participants was not particularly wide, with only two participants for NECSA-1 and two for NECSA-2. Methodologies used by participants were generally consistent, with both deterministic and Monte Carlo methods used in synergy to model the experiments.

Certain aspects of the benchmark are well suited to code validation, such as the multicycle reactivity cases. The information provided is typical of what is available in a reactor operational modelling scenario, and thus the obtained margins can be considered relevant. However, the Cu wire activation experiments have large associated experimental uncertainties, and while very relevant for training purposes, might not provide sufficient detail for accurately establishing code margins or capabilities.

The SAFARI-1 benchmark presents a series of experiments to indirectly determine the accuracy of multicycle depletion analysis. In particular, the benchmark proposed the analysis of multicycle reactivity, Cu wire activation and control rod calibration as indirect measures of fuel depletion. The results presented in this Annex exhibit good agreement with experimental data. Multicycle results indicate that after an initial burn-in period (3–4 cycles) reactivity estimates settle to a stable level of less than 500 pcm, which is however strongly dependent on the approach used in processing plant data. Reactivity results obtained from deterministic and stochastic solution methods consistently show a notable standard deviation (also of the order of 500 pcm), which largely originates from the extensive in-core irradiation rig movements during operation, the details of which are not included in the benchmark specifications.

Cycle specific Cu wire activation profiles match experimental results well, and presented analyses generally show total activation errors per core position (over all cycles) to be between

10 and 15%. Control rod calibration experiments also agree well, but all the analyses show a slight overestimation of the control rod worth per rod in all cycles analysed.

The beryllium reflector poisoning in the SAFARI-1 reactor has been accounted for by the two participants using different approaches and methods. The effect of the beryllium reflector poisoning on reactivity and neutron flux or activity has also been accounted for through measurements and calculations. The South African and Romania participants calculated this benchmark and established comparisons to experimental measurements.

A comparison of results submitted by the two participants shows some notable differences. However, both submissions consistently quantify the order (or level) of the impact of the poison buildup on reactivity as well as spectral and spatial flux distribution. It can be concluded that these phenomena have to be taken into consideration when calculating the beryllium reflected reactors.

REFERENCES TO ANNEX XII

- [XII-1] INTERNATIONAL ATOMIC ENERGY AGENCY, Research Reactor Benchmarking Database: Facility Specification and Experimental Data, Technical Reports Series No. 480 (Rev. 1), IAEA, Vienna (in preparation).
- [XII-2] PRINSLOO, R., et al., Recent developments of the OSCAR calculational system, as applied to selected examples from IAEA research reactor benchmarks, Proc. 18th IGORR Conference, Sydney, Australia, 3–7 December (2017).
- [XII-3] LEPPÄNEN, J., Serpent – a Continuous-energy Monte Carlo Reactor Physics Burnup Calculation Code User’s Manual, VTT Technical Research Centre of Finland, 18 June 2015 (2015).
- [XII-4] X-5 MONTE CARLO TEAM, MCNP – A General Monte Carlo N-Particle Transport Code, Version 5, Los Alamos National Laboratory Report LA-UR-03-1987, Los Alamos, NM (2008).
- [XII-5] FENSIN, M., et al., The New MCNP6 Depletion Capability, Los Alamos National Laboratory Report LA-UR-12-22314, Los Alamos, NM (2012).
- [XII-6] VILLARINO, E., CONDOR-CITVAP-MCNP calculation line description, Proc. National Meeting of Reactor Physics and Thermal Hydraulics, Rio de Janeiro, Brazil, 11–16 August (2002).
- [XII-7] OAK RIDGE NATIONAL LABORATORY, SCALE: A Comprehensive Modeling and Simulation Suite for Nuclear Safety Analysis and Design, Oak Ridge National Laboratory Report ORNL/TM-2005/39, Version 6.1, Oak Ridge, TN (2011).
- [XII-8] PELOWITZ, D.B., MCNPX User’s Manual, Version 2.7.0, Los Alamos National Laboratory Report LA-CP-11-00438, Los Alamos, NM (2011).

ANNEX XIII

BENCHMARK CONSOLIDATED RESULTS AGAINST EXPERIMENTAL DATA FROM TINT

XIII-1. INTRODUCTION

The TINT benchmark analysis, for the Thai Research Reactor-1/Modification 1 (TRR-1/M1), including the reactor specification and experimental data, is documented in Ref. [XIII-1]. This benchmark is related to a multicycle depletion case. The operation history of over 35 years has been summarized to be used for numerical simulation. There are in total 19 core configurations for the benchmark and three fuel elements were selected to perform gamma ray spectrometry in order to evaluate the fuel burnup.

TRR-1/M1 is essentially a TRIGA Mark III research reactor designed and manufactured by General Atomics. Historically, this reactor was converted from an MTR type reactor in 1977. The nominal power of TRR-1/M1 is 1.3 MW thermal. The core of TRR-1/M1 is submerged in an open pool with a concrete biological shield. The cooling of the core is done by natural circulation of the pool water, which is in turn cooled and purified in external coolant circuits. The TRR-1/M1 experimental facilities include neutron beam tubes, a thermal column with graphite, one rotary specimen rack, a pneumatic transfer system, and several in-core and out-of-core irradiation positions.

TRR-1/M1 uses typical rod type TRIGA fuel elements (8.5 and 20 wt% TRIGA fuel moderator U-Zr-Hf). The core of TRR-1/M1 is arranged in six hexagonal rings, namely ring A, B, C, D, E, F and G (from inner to outer). Ring A is the location of the central thimble, which has been used as an irradiation facility. Rings B, C, D, E, F and G contain other core components (i.e. fuel elements, control rods, and irradiation facilities). Each position within the core is referred to by a labelled core position, as shown in Fig. XIII-1.

Detailed benchmark specification and experimental data can be found in Ref. [XIII-1].



FIG. XIII-1. Core position of TRR-1/M1. (courtesy of TINT, Thailand)

XIII-2. SUMMARY OF THE BENCHMARK SPECIFICATION AND CODES AND MODELS USED

XIII-2.1. Summary of the benchmark specification

TRR-1/M1 was first loaded with only 8.5 wt% fuel elements in 1977. The critical core configuration (it is referred to as core configuration No. 0 and is out of the specification of this benchmark) is an experimental core configuration for the purpose of determining the critical mass of TRR-1/M1 core. This is the core configuration which can achieve criticality with the least number of fuel elements. The operation and the pattern of these core configurations which belong to the benchmarks are provided in Table XIII-1 [XIII-1].

In the benchmark specification and the experimental data specification [XIII-1], the 19 core configurations are described and the detailed information on the measured data and the reactor specification allow the proper modelling of the benchmark.

TABLE XIII-1. OPERATION INFORMATION FOR TRR-1/M1

Core No.	BOC* date	EOC# date	Total MWd	Critical rod position (cm)				
				TR	SA	SH1	SH2	RR
1	07/11/1977	05/03/1980	61.23	17.5	17.6	17.6	17.6	17.2
2	14/04/1980	26/05/1982	76.28	18.1	18.1	18.1	18.1	15.4
3	10/06/1982	03/02/1984	86.97	19.1	19.1	19.1	19.1	18.4
4	04/04/1984	20/02/1985	47.29	17.6	17.6	17.6	17.6	21.7
5	29/03/1985	26/03/1987	119.84	16.7	16.7	16.7	16.7	17.9
6	14/05/1987	23/03/1988	62.91	19.6	19.6	19.6	19.6	18.0
7	27/05/1988	09/12/1989	111.03	18.6	18.6	18.6	18.6	18.6
8	12/12/1989	30/04/1990	27.22	22.9	22.9	22.9	22.9	18.0
9	18/06/1990	28/12/1990	45.37	19.1	19.1	19.1	19.1	15.8
10	07/09/1992	03/04/1995	169.79	17.9	17.9	17.9	17.9	17.9
11	13/05/1995	11/03/1997	132.61	19.1	19.1	19.1	19.1	16.9
12	02/04/1997	03/03/2000	219.28	18.6	18.6	18.6	18.6	18.9
13	15/08/2000	21/02/2003	225.36	18.8	18.8	18.8	18.8	18.3
14	17/03/2003	13/02/2005	191.44	20.0	20.0	20.0	20.0	20.1
15	11/03/2005	16/02/2007	202.60	21.4	21.4	21.4	21.4	19.3
16	21/03/2007	25/07/2008	98.25	22.9	22.9	22.9	22.9	22.9
17	31/07/2008	22/02/2010	133.24	19.4	19.3	19.3	19.6	19.3
18	08/03/2010	28/01/2011	94.49	19.0	19.0	19.0	19.0	18.6
19	28/01/2011	08/02/2012	76.48	18.8	18.8	18.8	18.8	18.8

* BOC: Beginning of cycle.

EOC: End of cycle.

XIII-2.2. Summary of the codes and nuclear data libraries used

Two different CPR participants presented their calculation results for comparison against the measurement results. An outline of the codes and nuclear data libraries used to perform the various calculations will be presented.

A detailed description of the codes is available in Ref. [XIII-1], and in this section only a summary of the codes and libraries used are presented in Table XIII-2. An outline of the codes, and nuclear data libraries used to perform the various calculations will be presented in the following sections.

TABLE XIII–2. CODES AND LIBRARIES USED BY THE PARTICIPANTS

Participant	Code (library)
Argentina	CONDOR 2.7.01 – CITVAP 3.9.04 (ENDF/B-VI)
Thailand	MVP (JENDL-3.3) MCNPX 2.6 (ENDF/B-VI)

XIII–2.2.1. Thailand

Two general purpose Monte Carlo codes for neutron and photon transport calculations were used for the analysis of the benchmark: MVP and MCNPX.

The MVP code (developed by the Japan Atomic Energy Agency, JAEA) has currently been adopted at TRR-1/M1 as the common tool for the reactor core analysis and fuel management calculation. The continuous cross-section library mainly processed from ENDF/B-VI was used. However, for a few isotopes, a continuous cross-section library processed from JENDL-3.3 is used to supplement those missing from ENDF/B-VI.

The MCNPX code (version 2.6) was used to perform the reactor core analysis and depletion calculation. The objective of introducing MCNPX for the fuel management calculation at TRR-1/M1 was to acquire additional Monte Carlo depletion calculation capability for comparison. A continuous cross-section library, mainly processed from the ENDF/B-VII.0 continuous cross-section library (70c), was used.

XIII–2.2.2. Argentina

INVAP’s calculation line was used for the analysis of the benchmark, and the deterministic codes CONDOR-CITVAP were selected for the analysis.

As a result, INVAP’s proposed scheme for the TRR-1/M1 benchmark was to develop a comparison between two different approaches:

- (a) CONDOR-CITVAP calculation (INVAP standard methodology);
- (b) CONDOR 2-D calculation, mainly to evaluate the CONDOR capabilities to perform follow-up simulations including fuel management without the core code CITVAP.

The Helios 190 group nuclear data library [XIII–2] was used for cell calculations. This library was selected because it has the zirconium and the hydrogen cross-sections for the H–Zr material, which were validated against experimental data in previous work [XIII–3].

XIII–2.3. Summary of the models used

XIII–2.3.1. Thailand

The modelling of the TRR-1/M1 core by MVP (Fig. XIII–2) and MCNPX (Fig. XIII–3) codes has been performed. Both figures show the first core configuration model of TRR-1/M1.

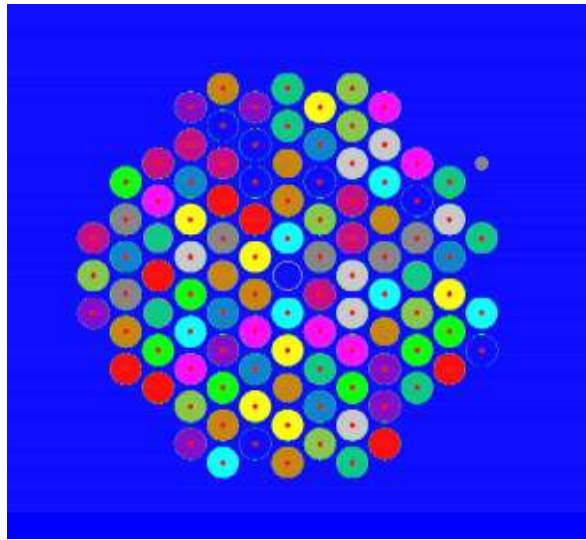


FIG. XIII-2. Core configuration 1 by MVP (Top view $z = 0$). (courtesy of TINT, Thailand)

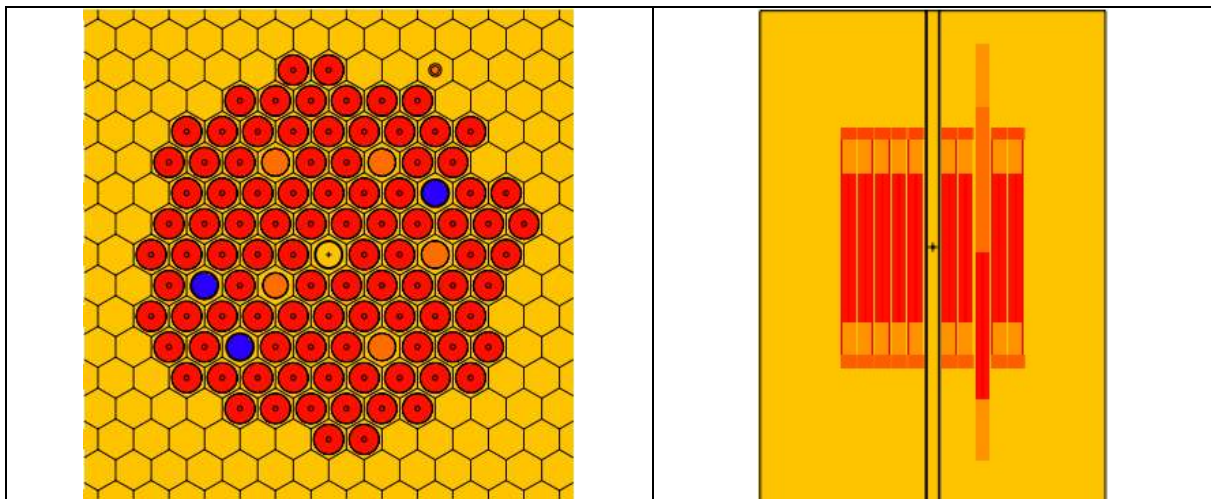


FIG. XIII-3. Core configuration 1 by MCNPX. (courtesy of TINT, Thailand)

To perform the benchmark calculation, 19 different core configurations are modelled in order to simulate the fuel utilization history. This is to match the irradiation history with the measured fuel elements. Burnup and control rod positions are modelled according to the benchmark specification, the depletion calculation was done at the nominal power of 1 MW. Each fuel element is depleted individually one fuel zone per fuel element.

XIII-2.3.2. Argentina

Different models were used for the CONDOR and CITVAP codes. For CONDOR, two different approaches were used: Approach A, a standard design methodology to generate homogenized cross-sections for the CITVAP code; and Approach B, a 2-D core model to perform a preliminary calculation of the benchmark.

The Helios 190 group nuclear data library was used by the CONDOR code and the condensation procedure considered three energy groups at core level, with the energy limits presented in Table XIII-2.

TABLE XIII-2. CONDENSATION ENERGY LIMITS FOR CITVAP CALCULATION

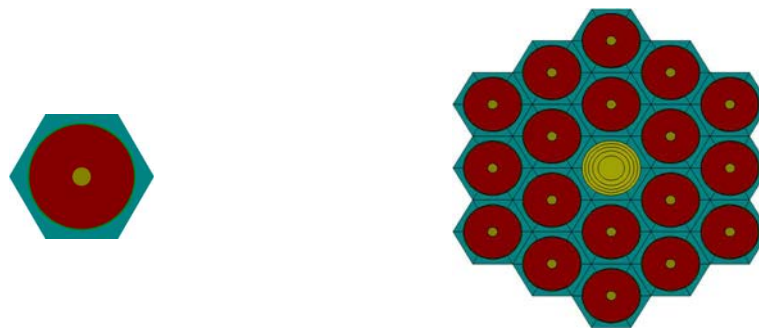
Group	Lower limit [MeV]	Upper limit [MeV]
1	0.821	20 (from library)
2	0.625E-6	0.821
3	0	0.625E-6

Approach A: CONDOR Models for homogenized cross-section generation):

Two different models were used:

- (i) Fuelled cell (where burnup dependent cross-sections were generated);
- (ii) Non-fuelled cell.

Figure XIII-4 shows these models.



i) Fuelled cell model

ii) Non-fuelled cell model

FIG. XIII-4. CONDOR core models. Fuelled cell and non-fuelled cell. (courtesy of INVAP, Argentina)

Approach A: CITVAP Models: A triangular-axial geometry model was used for the 3-D core model. The first and the last core configuration are given in Fig. XIII-5.

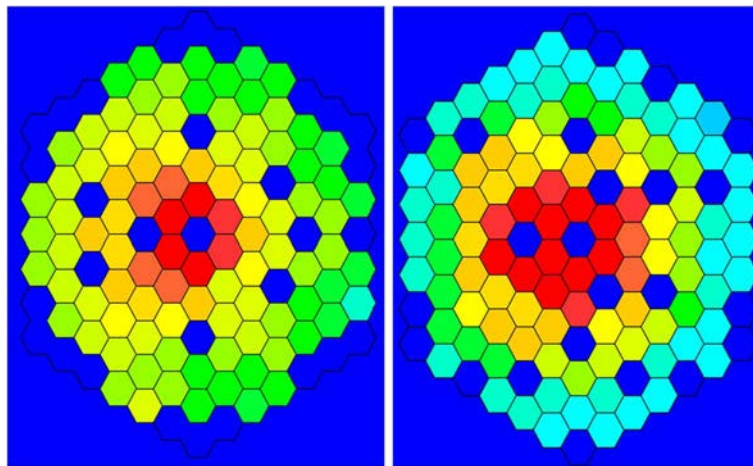


FIG. XIII-5. CITVAP core models in triangular-axial geometry. Core 01 (left) and Core 19 (right). (courtesy of INVAP, Argentina)

Approach B: CONDOR Core Models: 19 different 2-D core models were created and used for the verification of the benchmark. Figure XIII-6 shows the first and the last 2-D core model used in the analysis.

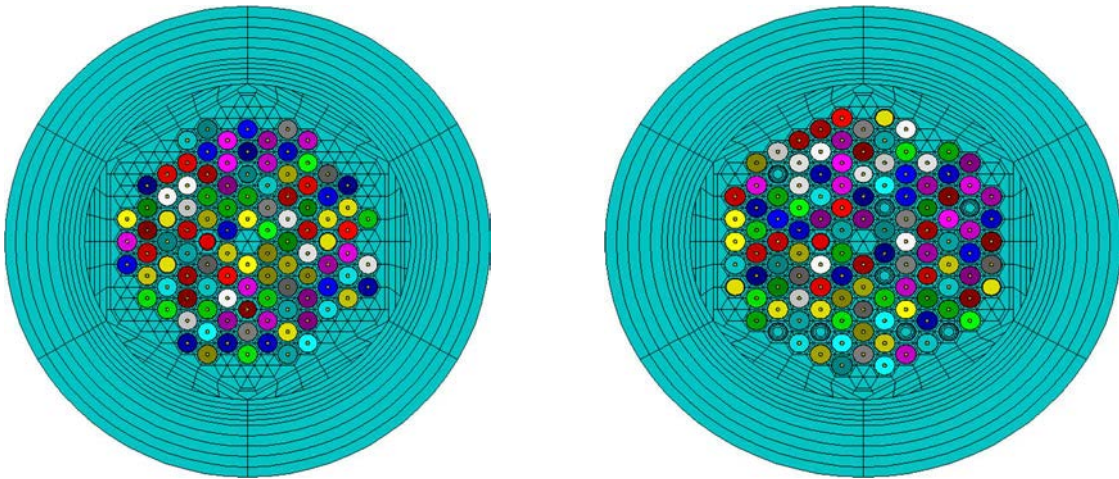


FIG. XIII-6. CONDOR core models. Core 01 (left) and Core 19 (right). (courtesy of INVAP, Argentina)

XIII-3. RESULTS

The results from the multicycle burnup calculations of both participants are presented and then compared and discussed in this section.

XIII-3.1. Results of the individual participant contributions

XIII-3.1.1. Thailand (THA) results

Two different Monte Carlo codes were used (MCNPX and MVP). The cycle dependent burnup for each of the measured fuel elements is provided along with the final burnup, which is compared with the experimental data.

Because the Monte Carlo models were built without different materials in the axial fuelled region (to allow axial dependent fuel depletion), it was not possible to compare the axial profile against the measurement.

The results are shown in Table XIII-3.

XIII-3.1.2. Argentina (ARG) results

Argentina results were obtained from a preliminary verification with CONDOR cell code level (Approach B: 2-D core model) and a CITVAP 3-D detailed model (Approach A).

The cycle dependent burnup for each of the measured fuel elements is provided for the CITVAP calculations with the final burnup, which is compared with the experimental data and the results from other participants in Table XIII-3.

The 3-D core model provides the axial burnup profile, which is compared with the measured data in Table XIII-4.

XIII-3.2. Comparison and discussion of the individual results

Table XIII-3 specifies the experimental burnup $100 (U-235(t=0) - U-235(t)) / U-235(t=0)$ as a percentage and all the participants calculated data with their relative difference $100 (C - E) / E$,

as a percentage, where C and E are the calculated and experimental values, respectively. The Argentina results for Approach A are named CITVAP and for Approach B are named CONDOR.

TABLE XIII-3. PARTICIPANTS' CALCULATION AND COMPARISON WITH EXPERIMENTAL RESULTS

Fuel element	Exp. burnup (%)	THAILAND				ARGENTINA			
		MVP (%)	Diff. (%)	MCNPX	Diff. (%)	CITVAP	Diff. (%)	CONDOR (2-D)	Diff. (%)
08558	32.0	37.5	17.2	34.0	6.2	35.4	10.7	38.0	18.6
08572	38.1	38.8	1.9	38.3	0.6	40.0	4.9	36.1	-5.3
08595	33.2	34.9	5.1	35.4	6.7	38.0	14.5	34.7	4.5

Figures XIII-7 and XIII-8 show the cycle dependent burnup per fuel element, calculated by the different codes and participants. Only the calculated information is given, allowing a comparison between the different codes. Additionally, the last cycle has the experimental data measured to compare with the calculated prediction.

Figure XIII-7 shows the fuel element 08558, where it can be seen that all the codes have a similar behaviour and a good agreement between THA-MVP and ARG-CONDOR, but both codes are overpredicting the fuel element burnup. The THA-MCNPX and ARG-CITVAP have similar calculated values, but there are differences in cycles 15 and 19 in the THA-MCNPX calculation with respect to the other codes.

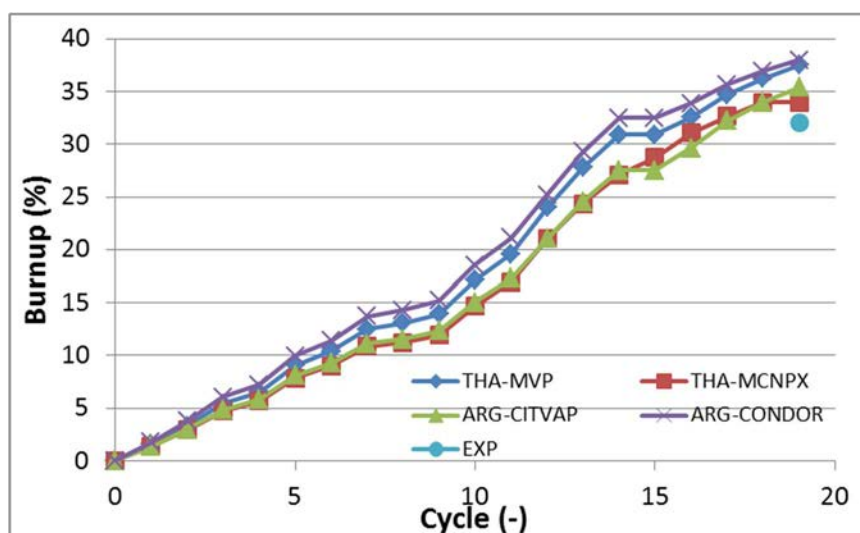


FIG. XIII-7. Fuel element 08558 cycle dependent calculated burnup and experimental value. (courtesy of INVAP, Argentina)

Figure XIII-8 shows the fuel element 08572, where it can be seen that all the codes have a similar behaviour and a good agreement between them.

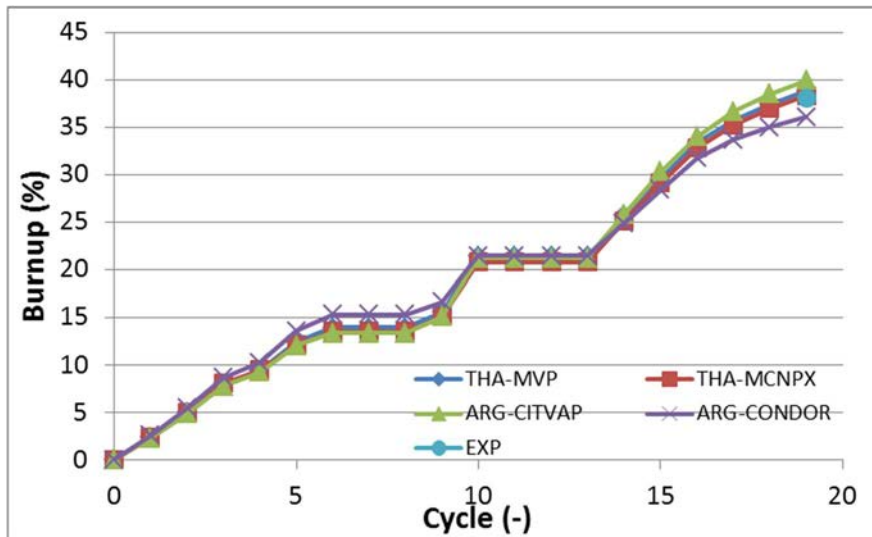


FIG. XIII-8. Fuel element 08572 cycle dependent calculated burnup and experimental value. (courtesy of INVAP, Argentina)

Figure XIII-9 shows the fuel element 08595, where it can be seen that all the codes have a similar behaviour and a good agreement between them. The ARG-CITVAP has a higher error than the other codes, and a significant increment can be observed in cycle 13.

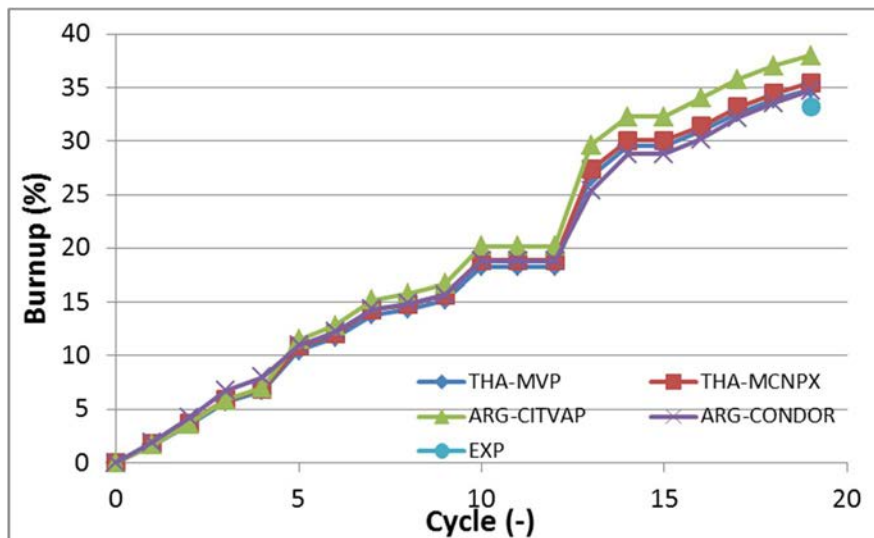


FIG. XIII-9. Fuel element 08595 cycle dependent calculated burnup and experimental value. (courtesy of INVAP, Argentina)

Axial ^{137}Cs measurements were made for five axial points. Only one participant (ARG) provided a comparison with this experimental data. Table XIII-4 shows the measured values, the calculated values, and their relative difference in % for each fuel element.

TABLE XIII-4. AXIAL BURNUP RATIO COMPARISON

Position	Exp (-)	ARG-CITVAP	Difference [%]
Fuel element 08558			
1 - Upper end	0.492	0.505	2.61
2 - Middle point between 1 & 3	0.691	0.757	9.51
3 - Center	0.981	1.000	1.95
4 - Middle point between 3 & 5	1.000	0.954	-4.59
5 - Lower end	0.844	0.737	-12.77
Fuel element 08572			
1 -Upper end	0.391	0.514	31.65
2 - Middle point between 1 & 3	0.861	0.765	-11.15
3 - Center	1.000	1.000	0.00
4 - Middle point between 3 & 5	0.904	0.948	4.90
5 - Lower end	0.754	0.720	-4.51
Fuel element 08595			
1 - Upper end	0.391	0.505	2.61
2 - Middle point between 1 & 3	0.861	0.757	9.51
3 - Center	1.000	1.000	1.95
4 - Middle point between 3 & 5	0.904	0.954	-4.59
5 - Lower end	0.754	0.737	-12.77

Unfortunately, only one participant and one methodology provided a comparison of the calculated axial dependence against experimental data. However, most of the difference is below or close to 10%, except a large difference in the top of the fuel element 08572, which needs a deeper analysis from both a modelling and experimental point of view, to properly understand this difference.

XIII-3.3. Conclusions

The TRR-1/M1 benchmark case, which is a multicycle depletion calculation problem, is proposed by Thailand. This benchmark case follows the operation history of TRR-1/M1 and gamma ray spectrometry (^{137}Cs measurements) was performed for selected three fuel elements to evaluate the fuel burnup (% ^{235}U depleted).

Four computer models from two CRP participants were used and the calculation results are discussed in this Annex. In general, the calculated values of all the codes agreed quite well with the measured values, and most of the calculated values overpredicted the experimental values. However, there are some discrepancies in some of the modelling codes that need further analysis. For example, the Monte Carlo codes do not have axial discretization to allow a proper 3-D burnup calculation and a comparison between the axial profiles provided.

REFERENCES TO ANNEX XIII

- [XIII-1] INTERNATIONAL ATOMIC ENERGY AGENCY, Research Reactor Benchmarking Database: Facility Specification and Experimental Data, Technical Reports Series No. 480 (Rev. 1), IAEA, Vienna (in preparation).
- [XIII-2] FERRI, A.A., et al., Helios Methods, Chapter IX: The library, Studsvik Scandpower (1997).

- [XIII-3] BOSCHETTI, F., MAZUFRI, C., VILLARINO, E., Conceptual design of U-Mo fuel with hydrogen, Proc. ISMTR 2013, 6th International Symposium on Material Testing Reactors, Bariloche, Río Negro, Argentina, 28-31 October (2013).

ANNEX XIV SUPPLEMENTARY FILES

The supplementary files for this publication can be found on the publication's individual web page at www.iaea.org/publications. These files contain individual participant reports (prepared and published as working documents).

These reports are individual benchmark contributions, submitted by participants to the data providers of each benchmark, who consolidated all the results leading to Annexes I–XIII. The reports include a level of detail and intermediate calculation steps and results beyond what is given in the benchmark consolidated results, and may be useful for readers interested in following closely the options taken and detailed procedure and calculation sequence that each participant adopted.

Benchmark name	Contributor	File name
ANSTO-1	Argentina	ANSTO-1 benchmark - results ARGENTINA.pdf
ANSTO-1	Australia	ANSTO-1 benchmark - results AUSTRALIA results.pdf
ANSTO-1	France	ANSTO-1 benchmark - results FRANCE.pdf
ANSTO-1	South Africa	ANSTO-1 benchmark - results SOUTH AFRICA.pdf
ANSTO-2	Argentina	ANSTO-2 benchmark - results ARGENTINA.pdf
ANSTO-2	Australia	ANSTO-2 benchmark - results AUSTRALIA results.pdf
ANSTO-2	France	ANSTO-2 benchmark - results FRANCE.pdf
ANSTO-3	Argentina	ANSTO-3 benchmark - results ARGENTINA.pdf
ANSTO-3	Australia	ANSTO-3 benchmark - results AUSTRALIA results.pdf
ATI-1, ATI-2	Thailand	ATI-1 ATI-2 benchmark - results THAILAND.pdf
EAEA-1	Argentina	EAEA-1 benchmark - results ARGENTINA.pdf
EAEA-1	Egypt	EAEA-1 benchmark - results EGYPT.pdf
EAEA-1	Israel	EAEA-1 benchmark - results ISRAEL.pdf
EAEA-1	South Africa	EAEA-1 benchmark - results SOUTH AFRICA.pdf
EAEA-2	Australia	EAEA-2 benchmark - results AUSTRALIA.pdf
EAEA-2	Egypt	EAEA-2 benchmark - results EGYPT.pdf
EAEA-2	Israel	EAEA-2 benchmark - results ISRAEL.pdf
INR-1	Romania	INR-1 benchmark - results ROMANIA.pdf
INR-1	South Africa	INR-1 benchmark - results SOUTH AFRICA.pdf
IPEN-MB-01	Argentina	IPEN-MB-01 benchmark - results ARGENTINA.pdf
IPEN-MB-01	Brazil	IPEN-MB-01 benchmark - results BRAZIL.pdf
IPEN-MB-01	South Africa	IPEN-MB-01 benchmark - results SOUTH AFRICA.pdf
IRR-1	South Africa	IRR-1 benchmark - results SOUTH AFRICA.pdf
JSI-1	Argentina	JSI-1 benchmark - results ARGENTINA.pdf
NECSA-1	Argentina	NECSA-1 benchmark - results ARGENTINA.pdf
NECSA-1	South Africa	NECSA-1 benchmark - results SOUTH AFRICA.pdf
NECSA-2	Romania	NECSA-2 benchmark - results ROMANIA.pdf
TRR1	Argentina	TRR1 benchmark - results ARGENTINA.pdf
TRR1	Thailand	TRR1 benchmark - results THAILAND.pdf

Note: Some benchmark consolidators did not submit an individual report for their own benchmark. Some participants submitted their results in presentations during meetings and in informal communications, and therefore also did not submit individual reports.

LIST OF ABBREVIATIONS

ATI	Atominstitut
ANSTO	Australian Nuclear Science and Technology Organisation
BOC	Beginning of cycle
CC	Central channel
CD-ROM	Compact disc read-only memory
CFY	Cumulative fission yield
CNS	Cold neutron source
COCONEUT	Core Conception Neutronic Tool
CPM	Collision probabilities method
CPU	Central processing unit
CRP	Coordinated research project
CSAS	Criticality safety analysis sequence
EAEA	Egyptian Atomic Energy Authority
EOC	End of cycle
ETR-2	Experimental Training Research Reactor – 2
FA	Fuel assembly
FE	Fuel element
HEADE	Heterogeneous Assembly Depletion
HEU	High enriched uranium
HPGe	High purity germanium
HTML	Hypertext markup language
ICSBEP	International criticality safety benchmark evaluation project
INR	Institute for Nuclear Research
INVAP	Investigaciones Aplicadas
IPEN	Instituto de Pesquisas Energéticas e Nucleares
IRPhE	International reactor physics experiment evaluation
IRR-1	Israel Research Reactor – 1
JSI	Jožef Stefan Institute
LEU	Low enriched uranium
MCNP	Monte Carlo N-Particle
MCNPX	Monte Carlo N-Particle eXtended
MGRAC	Multi-group reactor analysis code
MOC	Method of characteristics
MTR	Material testing reactor
NECSA	South African Nuclear Energy Corporation SOC Ltd.
OPAL	Open Pool Australian Lightwater
ORIGEN	Oak Ridge Isotope GENeration
ORNL	Oak Ridge National Laboratory
OSCAR-5	Overall System for Calculation of Reactors, Generation 5

PT	Pneumatic tube
RCC	Reference core configuration
RCM	Research coordination meeting
SAFARI-1	South African Fundamental Atomic Research Installation – 1
TINT	Thailand Institute of Nuclear Technology
TRIGA	Training, Research, Isotopes, General Atomics
TRR-1/M1	Thai Research Reactor – 1 / Modification 1
UKAEA	United Kingdom Atomic Energy Authority
WIMS	Winfrith Improved Multi-Group Scheme
WLUP	WIMS Library Update Project

CONTRIBUTORS TO DRAFTING AND REVIEW

Abdelrazek, I.D.	Egypt Atomic Energy Authority, Egypt
Albornoz, F.	INVAP SE, Argentina
Ambrožič, K.	Jožef Stefan Institute, Slovenia
Aviv, O.	Jožef Stefan Institute, Slovenia
Boschetti, F.	INVAP SE, Argentina
Botes, D.	Nuclear Energy Corporation of South Africa, South Africa
Bouret, C.	TechnicAtome, France
Braoudakis, G.	Australian Nuclear Science and Technology Organisation, Australia
Buznach, E.	Soreq Nuclear Research Center, Israel
Cagnazzo, M.	Technische Universität Wien, Austria
Champagnat, M.	TechnicAtome, France
Couybes, J.	TechnicAtome, France
Decroocq, M.	TechnicAtome, France
Diniz, R.	Instituto de Pesquisas Energéticas e Nucleares, Brazil
Domingos, D.B.	Instituto de Pesquisas Energéticas e Nucleares, Brazil
Dos Santos, A.	Instituto de Pesquisas Energéticas e Nucleares, Brazil
Ersez, T.	Australian Nuclear Science and Technology Organisation, Australia
Esposito, F.	Australian Nuclear Science and Technology Organisation, Australia
Estebe, F.	TechnicAtome, France
Farjallah, N.	International Atomic Energy Agency
Ferrari, I.	INVAP SE, Argentina
Ferraro, D.	INVAP SE, Argentina
Fuentes Solis, N.	International Atomic Energy Agency
Gandoin, N.	TechnicAtome, France
Gavoille, N.	TechnicAtome, France
Geupel, S.	International Atomic Energy Agency
Groenewald, S.A.	Nuclear Energy Corporation of South Africa, South Africa
Hall, R.	Australian Nuclear Science and Technology Organisation, Australia
Hazenshrung, N.	Jožef Stefan Institute, Slovenia
Kennedy, W.B.	International Atomic Energy Agency
Koubbi, J.	TechnicAtome, France
Krakovich, A.	Soreq Nuclear Research Center, Israel
Maitre, A.	INVAP SE, Argentina
Manificier, L.	TechnicAtome, France
Marshall, F.	International Atomic Energy Agency

Mashau, M.	Nuclear Energy Corporation of South Africa, South Africa
Matzkin, S.	INVAP SE, Argentina
Maul, L.	Australian Nuclear Science and Technology Organisation, Australia
Mavric, H.	International Atomic Energy Agency
Meier, H.	INVAP SE, Argentina
Mladin, M.	Institute for Nuclear Research, Romania
Mohamed, N.M.A.	Egypt Atomic Energy Authority, Egypt
Moloko, L.E.	Nuclear Energy Corporation of South Africa, South Africa
Muhammad Nor, A.W.	International Atomic Energy Agency
Mura, L.F.L.	Instituto de Pesquisas Energéticas e Nucleares, Brazil
Naseer, F.	International Atomic Energy Agency
Neder, I.	Soreq Nuclear Research Center, Israel
Pechrak, A.	Technische Universität Wien, Austria
Pessoa Barradas, N.	International Atomic Energy Agency
Prinsloo, R.H.	Nuclear Energy Corporation of South Africa, South Africa
Privas, E.	TechnicAtome, France
Radulović, V.	Jožef Stefan Institute, Slovenia
Ridikas, D.	International Atomic Energy Agency
Samiei Bermudez, M.D.	International Atomic Energy Agency
Santos, D.F.D.	Instituto de Pesquisas Energéticas e Nucleares, Brazil
Schlünz, B.	Nuclear Energy Corporation of South Africa, South Africa
Shokr, A.M.	International Atomic Energy Agency
Snoj, L.	Jožef Stefan Institute, Slovenia
Steinitz, U.	Soreq Nuclear Research Center, Israel
Tippayakul, C.	Institute of Nuclear Technology, Thailand
Tiyapun, K.	Institute of Nuclear Technology, Thailand
Van Heerden, F.A.	Nuclear Energy Corporation of South Africa, South Africa
Villa, M.	Technische Universität Wien, Austria
Villarino, E.	INVAP SE, Argentina
Wetchagarun, S.	Thailand Institute of Nuclear Technology, Thailand
Wong, L.	Australian Nuclear Science and Technology Organisation, Australia
Yakobi, S.	Soreq Nuclear Research Center, Israel
Zegarra, M.	INVAP SE, Argentina
Žerovnik, G.	Jožef Stefan Institute, Slovenia

Research Coordination Meetings

First Research Coordination Meeting: 13–17 April 2015
Second Research Coordination Meeting: 18–22 July 2016
Third Research Coordination Meeting: 27–31 August 2018

Technical Meetings

First Technical Meeting: 16–20 October 2017
Second Technical Meeting: 2–6 September 2019

Consultancy Meetings

Consultancy Meeting to Prepare for the Third RCM: 26–28 June 2018
Consultancy Meeting: 6–9 May 2019
Consultancy Meeting: 19–21 February 2020
Consultancy Meeting: 17–19 November 2020



IAEA

International Atomic Energy Agency

No. 26

ORDERING LOCALLY

IAEA priced publications may be purchased from the sources listed below or from major local booksellers.

Orders for unpriced publications should be made directly to the IAEA. The contact details are given at the end of this list.

NORTH AMERICA

Bernan / Rowman & Littlefield

15250 NBN Way, Blue Ridge Summit, PA 17214, USA

Telephone: +1 800 462 6420 • Fax: +1 800 338 4550

Email: orders@rowman.com • Web site: www.rowman.com/bernan

REST OF WORLD

Please contact your preferred local supplier, or our lead distributor:

Eurospan Group

Gray's Inn House

127 Clerkenwell Road

London EC1R 5DB

United Kingdom

Trade orders and enquiries:

Telephone: +44 (0)176 760 4972 • Fax: +44 (0)176 760 1640

Email: eurospan@turpin-distribution.com

Individual orders:

www.eurospanbookstore.com/iaea

For further information:

Telephone: +44 (0)207 240 0856 • Fax: +44 (0)207 379 0609

Email: info@eurospangroup.com • Web site: www.eurospangroup.com

Orders for both priced and unpriced publications may be addressed directly to:

Marketing and Sales Unit

International Atomic Energy Agency

Vienna International Centre, PO Box 100, 1400 Vienna, Austria

Telephone: +43 1 2600 22529 or 22530 • Fax: +43 1 26007 22529

Email: sales.publications@iaea.org • Web site: www.iaea.org/publications

**International Atomic Energy Agency
Vienna**